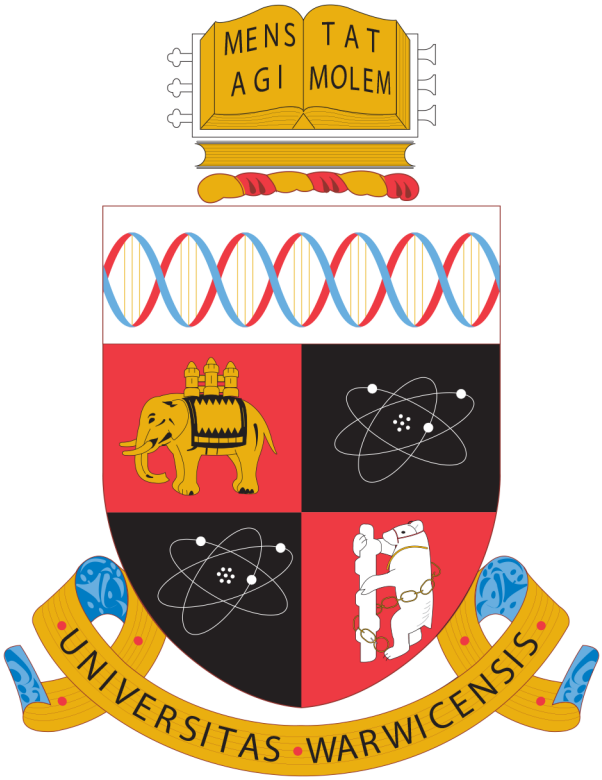

Advancing petroleomics methodologies and their application to crude and heavy fuel oils, asphaltenes, and the environment

Mary Joanna Thomas

A thesis submitted for the degree of
Analytical Science

Doctor of Philosophy

Molecular Analytical Sciences Centre for Doctoral Training
University of Warwick

June 2020

Table of Contents

Acknowledgements

First and foremost, I feel incredibly lucky to have undertaken my PhD under the supervision of such a proficient advisor: Professor Mark Barrow. Not only does Mark possess a wealth of knowledge and experience, making him an excellent guide and tutor, but he also continues to show the utmost patience, care, and sensitivity, in addressing any and all concerns imaginable for his group members. So, thank you Mark, and I hope that the end of my PhD journey is just the beginning of many more exciting and productive endeavours alongside the rest of our allies and friends!

My PhD position would not have existed without funding from my industry partner, Lubrizol Ltd, and so I am grateful to all those at Lubrizol who saw the potential of our projects and helped to secure funding, particularly Antonio Mastrangelo, who took that first leap of faith with us! I'd also like to thank my primary industrial supervisor, Shaun Carney, for all his guidance and input at each stage of the project, as well as Dave Growney, Chris Huener, Dave Asaerud, Corrine DeMuth, Mathew Robin, Paul Kirkman, Dave Morton, Julie Edgar, Alan Tatham, and all of the colleagues involved in Lubrizol University Contact, for their warm welcome on each visit and for keeping in touch throughout.

Some of the most exciting work carried out during my PhD was done in collaboration with Environment Canada, British Geological Survey, and The British Museum. I am grateful to have had input and encouragement throughout from the researchers working at these diverse institutions, in particular Dr John Headley, Kerry Peru, Dr Christopher Vane, Christopher Mussell, and Rebecca Stacey.

For their input and guidance through each stage of my PhD, I would like to thank my advisory committee members, Dr Simon Spencer and Professor Richard Walton. I would also like to thank the MAS CDT course leaders and administrators for their ongoing support throughout my time at the University

of Warwick, particularly Professor Steven Brown, Dr Nikola Chmel, Naomi Grew, and Christina Forbes. I'm also grateful to the Engineering and Physical Research Council for the funding which has not only allowed me to carry out the research contained within this thesis, but has enabled me to present my work at several conferences, some of which were in parts of the world I could hardly have hoped to visit otherwise while undertaking full time education.

I'm extremely grateful to Dr Diana Catalina Palacio Lozano, who has devoted a lot of time and effort to ensuring I could independently utilise the instrument and understand my observations, and has been an incredibly strong and inspirational role model throughout. I'm also grateful for all of the support (and patient communication of how to make use of their amazing software developments!) from Rémy Gavard and Hugh Jones, and to Professor Peter O'Connor, whose enthusiasm first inspired me to pursue a PhD in mass spectrometry. I'd also like to thank all of the wider ICR group, past and present, for making my PhD journey more bearable through conversation, adventure, laughter, and friendship: Anisha Haris, Dr Cookson Chiu, Dr Alina Theisen, Izaak Tyson-Hirst, Johanna Paris, Dr Christopher Wootton, Dr Yuko Lam, Tomos Morgan, Bryan Marzullo, Dr Federico Floris, Dr Frederik Lermyte, Dr Maartje van Agthoven, Sam Bisby, Molly Hayle, Latifa Alostad, Rory Downham, and Meng Li!

I would like to thank all of the teachers, tutors, and mentors that identified and encouraged me in my abilities, even in light of stretched resources in many cases. In particular, I thank the following for going beyond the call of duty required by their respective positions at the time: Jennifer Jackson and Denise Tandy of Southam Primary School; Nigel Chapman of Harbury Church of England Primary School; Mrs Owen of Southam College; Dr Melanie Britton, Professor Josephine Bunch, and Professor Richard Tuckett of the University of Birmingham.

I'd also like to thank my co-leaders and all of the former and current girls and young women from Southam 3rd Guide Unit, for keeping me active and

empowering me through the encouragement of others, and for reminding me each week that the most important lessons that you can learn (and teach!) are not those that you find between the covers of an academic journal.

Continuing at University for a postgraduate education is not easily done without the encouragement of a supportive family: thank you to my brothers Alfie and Harvey; aunties Julie and Jenny; cousins Cerys and Lucy; and Dad. A special thank you to my Great Great Aunt Mary, whose thirst for learning has not lessened in 93 years - and whose excitement at the prospect of a doctor in the family has upheld the belief that I could meet each challenge along the way. I am also grateful to Jade for fun and figure help, and for the support from the family that I chose for myself: Emily, Lisa, Kerrie, and all of my oldest friends.

Finally, thank you Mum and Grandma, for supporting and nurturing each endeavour that I have undertaken.

Vita

Mary Joanna Thomas AMRSC

Education

PhD Analytical Science

University of Warwick October 2016 - January 2020

Thesis title: Advancing petroleomics methodologies and their application to crude and heavy fuel oils, asphaltenes, and the environment

Supervisor: Professor Mark P. Barrow

MSc Molecular Analytical Science

Distinction

University of Warwick September 2015 - September 2016

MSci Chemistry

First Class Honours

University of Birmingham September 2009 - June 2015

Publications

* Findings included as part of thesis

Accepted

- KairosMS: A new solution for the processing of hyphenated ultrahigh resolution mass spectrometry data. Gavard, R.; Palacio Lozano, D. C.; Jones, H. E.; **Thomas, M. J.**; Rossell, D.; Spencer, S. E. F.; Barrow, M. P., *Anal. Chem.*, 2020.
- Petroleomics: Tools, Challenges, and Developments. Palacio Lozano, D. C.; **Thomas, M. J.**; Jones, H. E.; Barrow, M. P. *Annu. Rev. Anal. Chem.* **2020**, 13, 405–430.
- Characterization of bio-crude components derived from pyrolysis of soft wood and its esterified product by ultrahigh resolution mass spectrometry and

spectroscopic techniques. Palacio Lozano, D. C.; Ramírez, C. X.; Sarmiento Chaparro, J. A.; **Thomas, M. J.**; Gavard, R.; Jones, H. E.; Hernández, R. C.; Mejía-Ospino, E.; Barrow, M.P. *Fuel* **2020**, 259, 116085.

- Pushing the analytical limits: new insights into complex mixtures using mass spectra segments of constant ultrahigh resolving power. Palacio Lozano, D. C.; Gavard, R.; Arenas-Diaz, J. P.; **Thomas, M. J.**; Stranz, D. D.; Mejía-Ospino, E.; Guzman, A.; Spencer, S. E. F.; Rossell, D.; Barrow, M. P. *Chemical Science* **2019,** 10 (29), 6966-6978.
- *Characterization of oil sands naphthenic acids by negative-ion electrospray ionization mass spectrometry: Influence of acidic versus basic transfer solvent. Peru, K. M.; **Thomas, M. J.**; Palacio Lozano, D. C.; McMartin, D. W.; Headley, J. V.; Barrow, M. P. *Chemosphere* **2019,** 222, 1017-1024.
- *Petroleomic depth profiling of Staten Island salt marsh soil: 2 omega detection FTICR MS offers a new solution for the analysis of environmental contaminants. **Thomas, M. J.**; Collinge, E.; Witt, M.; Lozano, D. C. P.; Vane, C. H.; Moss-Hayes, V.; Barrow, M. P. *Science of the Total Environment* **2019,** 662, 852-862.

Manuscripts in Preparation

- *Comprehensive analysis of multiple asphaltene fractions combining statistical analyses and novel visualization tools. **Thomas, M. J.**; Jones, H. E.; Palacio Lozano, D. C.; Gavard, R.; Carney, S.; Barrow, M. P.
- *Solvent and Flow Rate Effects on the Observed Crude Oil Profile and the Relative Intensities of Radical and Protonated Species in APPI Experiments. **Thomas, M. J.;** Chan, H.; Palacio Lozano, D. C.; Barrow, M. P.

Awards

- Analytical Chemistry Trust Fund Overseas Travel Grant (Royal Society of Chemistry, 2019)
- John Beynon Travel Grant (British Mass Spectrometry Society, 2019)
- Nico Nibbering Student Travel Award (International Mass Spectrometry Foundation, 2018)
- Student Travel Award (American Mass Spectrometry Society, 2018)

- Early Career Researcher Bursary (Hyphenated Techniques in Chromatography, 2018)
- Allen Murray Centenary Scholarship (University of Birmingham, 2012-2015)
- Winner of student poster poster prize (Lubrizol University Contacts Meeting, Derby, UK, 2019)
- Winner of Barber Prize for best student talk (39th British Mass Spectrometry Society Annual Meeting, Cambridge, UK, 2018)

Presentations

Oral presentations

- UN World Cities Day Conference, University of Warwick (October 2019).
- Energy Forum 2019, University of Warwick (May 2019).
- 39th BMSS Annual Meeting, Cambridge, UK (September 2018)
- 22nd International Mass Spectrometry Conference, Florence, Italy (August 2018).
- 15th International Symposium on Hyphenated Techniques in Chromatography and Separation Technology, Cardiff, UK (January 2018).
- 7th International Symposium on Energy, Manchester, UK (August 2017)

Poster presentations

- #EnvChem2019: Advances in Environmental Chemistry, London, UK (October 2019).
- 40th BMSS Annual Meeting, Manchester, UK (September 2019).
- 20th International Conference on Petroleum Phase Behavior and Fouling (PetroPhase), Kanazawa, Japan (June 2019).
- Advances in Hyphenated Mass Spectrometry (BMSS Dai Games Meeting), London, UK (April 2019).
- RSC Analytical Research Forum 2018, London, UK (June 2018).
- 66th ASMS Conference on Mass Spectrometry and Allied Topics, San Diego, CA, USA (June 2018).
- 38th BMSS Annual Meeting, Manchester, UK (September 2017).

Declaration

I herby declare that, except where specifically referenced to other sources, the thesis titled "Advancing petroleomics methodologies and their application to crude and heavy fuel oils, asphaltenes, and the environment" has been composed by myself and and has not been submitted in whole or in part for any other degree, diploma, or qualification. The work presented (including data generated and data analysis) was carried out by the author except in the cases outlined below.

List of data and figures provided and experimental procedures and analyses carried out by collaborators, co-authors, and courtesy of others:

- Figures 1.1 and 1.2 were created with assistance from, and are courtesy of, Jade Anne Allsopp. Figure 1.2 is adapted with permission from Boduszynski MM, Energy & Fuels 1987; 1: 2-11 and is copyright 1987 American Chemical Society. Figure 1.3 contains schematic images courtesy of Bruker Daltonik GmbH and Thermo Fisher Scientific. Figure 1.4 is courtesy of RSC Analytical Methods Committee is reproduced with permission of the original authors.

- Bulk measurements of heavy fuel oils and lubricant base oils, benchtop oxidation and engine tests and liquid phase sampling, data, photographs and figures shown in Table 2.1, Figures 2.1, 4.1, and 4.2 are courtesy of Lubrizol Ltd.

- The extraction procedure, Orbitrap MS analysis, and data and illustrations shown in Figures 6.2a, 6.2b, 6.3a, 6.10a, and part of Figures 6.9, 6.10, and 6.12 are courtesy of Environment Canada. Chapter 6 represents an adaptation of the publication titled "Characterization of oil sands naphthenic acids by negative-ion electrospray ionization mass spectrometry: Influence of acidic versus basic transfer solvent", prepared

alongside co-authors Kerry M. Peru, Diana Catalina Palacio Lozano, Dena W. McMartin, John V. Headley, and Mark P. Barrow.

- The sampling procedure, Rock-Eval(6) pyrolysis, and data and illustrations shown in Figures 7.1 and 7.2 are courtesy of the British Geological Survey. Chapter 7 represents an adaptation of the publication titled "Petroleomic depth profiling of Staten Island salt marsh soil: 2ω detection FTICR MS offers a new solution for the analysis of environmental contaminants", prepared alongside co-authors Emma Collinge, Matthias Witt, Diana Catalina Palacio Lozano, Christopher H. Vane, Vicky Moss-Hayes, and Mark P. Barrow.

Mary Joanna Thomas
June 2020

Abstract

The work presented herein describes advancing analytical procedures utilising, and associated with, ultra-high resolution Fourier transform ion cyclotron resonance mass spectrometry (FTICR MS), applied to characterising ultra-complex petroleum-related samples.

A proof-of-concept FTICR MS characterisation of marine heavy fuel oils (HFOs) is initially performed. Building upon this, the asphaltene fractions of eight HFOs, including one that may have undergone desulfurization via an oxidation process, were studied. Infra-red multi photon dissociation (IRMPD) fragmentation was utilised for structural insight. Statistical analyses and novel visualisation modes provide a comprehensive, simplified, means of comparison.

The impact of oxidation on lubricant base oils was explored through the application of both direct infusion (DI) and gas chromatography (GC) FTICR MS. The effectiveness of antioxidant additive packages is demonstrated, with the semi-quantitative analysis indicating the extent to which benchtop oxidation procedures may provide a robust alternative to full engine tests.

The operating parameters of FTICR MS vary widely, with the impact on the relative spectral intensity of analyte species poorly understood. The influence of solvent system and flow rate on the observed profile and the ion-type ratio in positive-ion atmospheric pressure ionization (APPI) analyses is demonstrated. Furthermore, the O_2/O_4 class relative intensity ratio, proposed as a means by which to monitor the presence of anthropogenic compounds in the environment is found to invert at low pH in negative-ion electrospray (ESI) analyses.

The emerging role of petroleomics in environmental research is demonstrated further, with soil extracts characterised using DI and GC-FTICR MS. Differing relative contributions from a range of anthropogenic contaminants, and the isomeric complexity underlying individual assignments, are observed between sampling depths.

Finally, key findings are summarized and future research directions, with respect to advancing petroleomics methodologies and enhancing understanding of complex samples.

List of Abbreviations

ACN	Acetonitrile
API	American Petroleum Institute
APCI	Atmospheric pressure chemical ionization
APLI	Atmospheric pressure laser ionization
APPI	Atmospheric pressure photoionization
ASAP	Atmospheric solid analysis probe
ASTM	American Society for Testing and Materials
AUC	Area under curve
CCS	Collision cross section
CID	Collision induced dissociation
Da	Dalton
DBE	Double bond equivalents
DCM	Dichloromethane
DI	Direct infusion
DoE	Design of experiments
DOM	Dissolved organic matter
DWH	Deepwater Horizon
eFT	Enhanced Fourier transform
EI	Electron ionization
EIC	Extracted ion chromatogram
ESI	Electrospray ionization
FD	Field desorption
FTICR	Fourier transform ion cyclotron resonance
FWHM	Full width at half maximum height
GC	Gas chromatography
GC X GC	Two dimensional gas chromatography
HCA	Hierarchical clustering analysis
HFO	Heavy fuel oil
HPLC	High pressure liquid chromatography
IMMS	Ion mobility mass spectrometry

IMO	International maritime organisation
IR	Infra-red
IRMPD	Infra-red multiple photon dissociation
ISD	In-source dissociation
KMD	Kendrick mass defect
kν	Kinematic viscosity
kV	Kilovolt
LC	Liquid chromatography
LDI	Laser desorption ionization
LTP	Low temperature plasma
m/z	Mass-to-charge ratio
MALDI	Matrix assisted laser dissociation
MS	Mass spectrometry
MS/MS	Tandem mass spectrometry
MW	Megaword
M_w	Molecular weight
NA	Naphthenic acid
NAFC	Naphthenic acid fraction compound
nESI	Nano electrospray ionization
NMR	Nuclear magnetic resonance
NOM	Natural organic matter
NY/NJ	New York/New Jersey
OCULAR	Operation at constant ultrahigh resolution
OSPW	Oil sands process-affected water
PAH	Polycyclic aromatic hydrocarbon
PASH	Sulfur polycyclic aromatic hydrocarbon
PAV	Pressure ageing vessel
PCA	Principal component analysis
PI	Production index
PLS	Partial least squares
ppm	Parts-per-million
RC	Residual carbon
R/P	Radical-to-protonated species ratio

S1	Free hydrocarbons
S2	Bound (polymeric) hydrocarbons
SARA	Saturates, aromatics, resins, asphaltenes
SFC	Supercritical fluid chromatography
S/N	Signal-to-noise ratio
T	Tesla
TA	Thermal analysis
TAN	Total acid number
TIC	Total ion chromatogram
TIMS	Trapped ion mobility spectrometry
TOC	Total organic carbon
TOF	Time-of-flight
TPEO	Trunk piston engine oil
WAF	Water accommodated fraction
Z	Hydrogen deficiency
ZDDP	Zinc dialklyldithiophosphate

List of Tables

List of Figures

1. Introduction

1.1 Petroleum

1.1.1 Demand and Importance

Petroleum, a fossil fuel largely comprising hydrocarbons, is formed over geological time periods under extremes of temperature and pressure, and is one of nature's most complex mixtures, with an estimated 10^{16} molecules in a single oil droplet and 60 trillion isomers possible for a C_{40} alkane (Rahimi et al., 2019). Though vital for the supply of energy and materials globally (Figure 1.1), petroleum remains poorly understood on the molecular level. Its composition and properties are known to vary depending on factors including geological origin, thermal maturity, and biodegradation (Hunt, 1995; Tissot and Welte, 1984). Crude oils are fractionated into cuts ranging from gas condensates non-distillable vacuum residue, and although retaining significant economic importance, the complexity increases with boiling point (Boduszynski, 1987) (Figure 1.2). Despite the shift towards the generation of fuels from renewable sources, oil demand for both energy and manufacturing purposes continues to grow by more than 1 % per annum (Tryggestad et al., 2019).

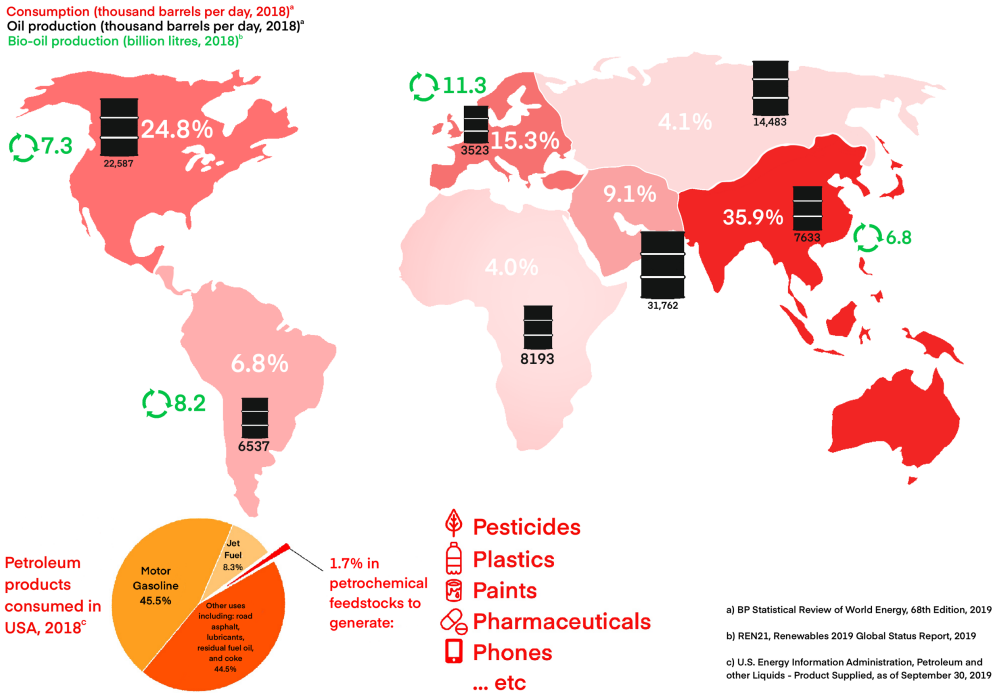

Figure 1.1 – Global production and consumption of petroleum in 2018, with end use in the USA summarized. Image courtesy of Jade Anne Allsopp.

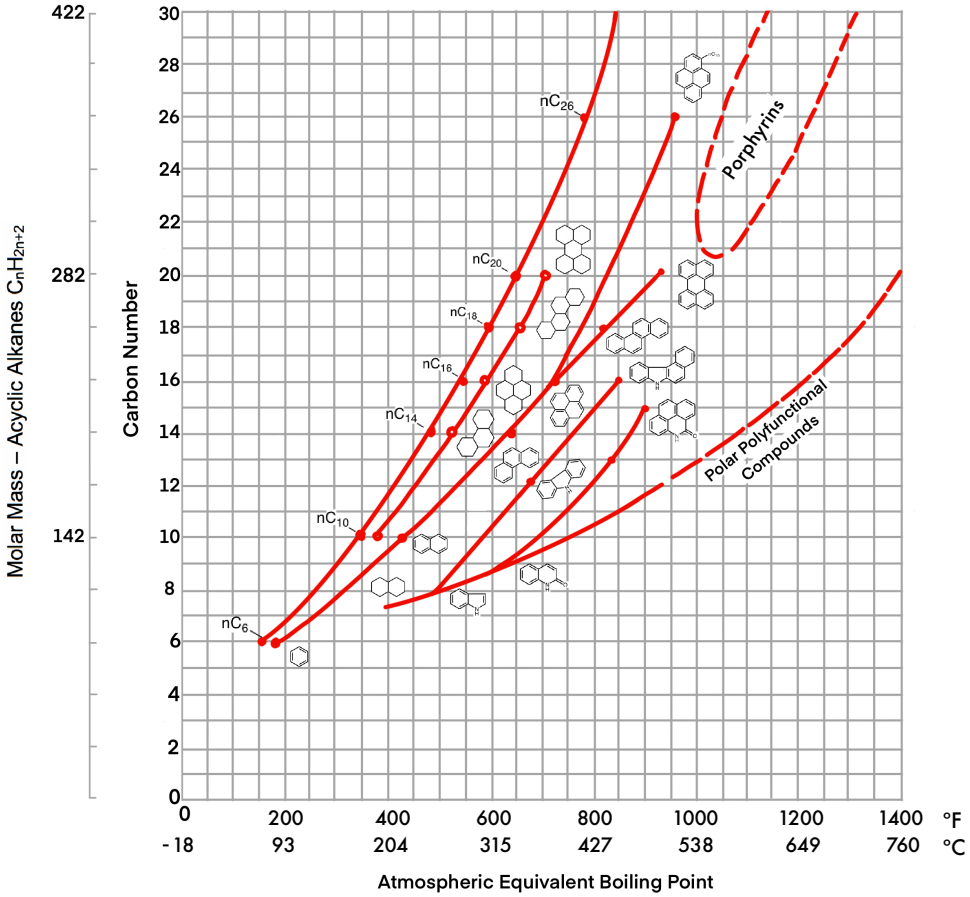

Figure 1.2 Boduszynski curve illustrating increase in molecular complexity with increasing boiling point. Adapted with permission from Boduszynski MM. Composition of Heavy Petroleums 1. Molecular-Weight, Hydrogen Deficiency, and Heteroatom Concentration as a Function of Atmospheric Equivalent Boiling-Point up to 1400 Degrees F (760 Degrees C). Energy & Fuels 1987; 1: 2-11. Copyright 1987 American Chemical Society. Adapted image courtesy of Jade Anne Allsopp.

1.1.2 Scarcity of Conventional Sources - Challenges of Unconventional Sources

With conventional crude oil reserves becoming depleted, production is shifting to heavier unconventional sources (Murray and King, 2012), the resources of which stand at more than double those of light crude oil (Hart, 2014), including heavy oils, oil sands bitumen, and biooils (Hirsch et al., 2006), as well as increased exploration using hydraulic fracturing. The American Petroleum Institute (API) gravity is an inverse measure of how heavy a petroleum liquid is compared to water, with API in excess of 31.1° indicative of lighter oils with higher market value. Compared to conventional oils, which are lighter and lower in sulfur-containing compounds (sweet), heavier oils may be higher in sulfur (sour, defined as those determined to have S in excess of 0.5 %), as well as other

heteroatoms including N, O and metals (Boduszynski, 1987), which can lead to a higher instance of catalyst deactivation and corrosion (Javadli and de Klerk, 2012; Prado et al., 2017). Heavier oils typically have a greater asphaltene content, defined as the fraction insoluble in n-alkanes but soluble in toluene (Mullins, 2008). Due to pi-pi interactions between multiple fused aromatic rings, asphaltenes aggregate readily, forming floccules when unstable in solution (Wiehe and Kennedy, 2000) which can lead to pipeline plugging (Becker, 1997). Asphaltenes may comprise a single polyaromatic hydrocarbon (PAH) core substituted by alkyl chains, known as island type, or multiple PAHs connected by alkyl linkers, known as archipelago type. The molecular architecture of asphaltene molecules continues to be debated with evidence for both island (Tang et al., 2015) and archipelago motifs (Gray, 2003; Rueda-Velasquez et al., 2013) recently presented. Biooils are an emerging unconventional oil source, which due to a high oxygen content present problems with stability and corrosivity, and often require upgrading to improve calorific load (Kanaujia et al., 2013).

Compared to conventional crude oil, heavy crude oils have higher viscosity and lower API gravity, typically below 20, meaning that they present lower market value prior to processing. In addition, they usually have a higher content of heteroatoms such as N, O, S, and metals, and contain a greater proportion of asphaltene molecules (Boduszynski, 1987). Although recovery of heavy oils can be challenging, often necessitating expensive enhanced recovery processes (Fink, 2016), some reservoirs show remarkably high recovery efficiency due to a large proportion of gas remaining in the reservoir (Tang and Firoozabadi, 2003).

Bitumen is a highly viscous and complex material, mostly generated as a residual fraction of crude oil (Handle et al., 2017; Le Guern et al., 2010), but that can also occur naturally in deposits. Production of petroleum from oil sands bitumen requires large quantities of water, typically 2-4 barrels to produce one barrel of synthetic crude oil (Barrow et al., 2016). Oil sands process-affected water (OSPW), a complex mixture which has been shown to be toxic to aquatic organisms (Marentette et al., 2015), cannot be released into adjacent natural waters and so is stored in large tailings ponds (Martin, 2015). Nevertheless, bitumen represents an important source of unconventional oil with reserves estimated at 1.7-2.5 trillion barrels in the Athabasca region of Alberta, Canada, alone (Burrowes et al., 2009; Clemente et al., 2003).

With the shift in production away from conventional petroleum sources, higher sulfur sour crude oil, is becoming more ubiquitous. Sour crude presents a range of problems, including limiting the quality and quantity of coke that can be used for carbon products such as graphite and electrodes (Zhao et al., 2018). In addition, the residual fractions, used for purposes such as marine heavy fuel oils (HFOs), far exceed tightening restrictions on sulfur content. The International Maritime Organization (IMO) 2020 legislation limits S content in HFOs to 0.5 % in order to reduce sulfur oxide emissions from ships (Halff et al., 2019). To minimize the downstream disadvantages of high sulfur oils, pretreatment using methods such as catalytic hydrotreating processes have become more widespread (Fink, 2016).

1.1.3 Analyzing Petroleum: Requirements

Characterization of petroleum at the molecular level, requires analytical instrumentation capable of separating and identifying thousands of components in a single experiment. Ultra-high resolution mass spectrometry is capable of meeting this requirement, and is growing field of research known as petroleomics, whereby multiple species are detected and resolved at each nominal mass unit. Such techniques offer superior resolving power and mass accuracy, defined as shown in Equations 1.1 and 1.2 respectively, where m is the mass-to-charge ratio (m/z) of a given peak, Δm is its full width at half maximum height (FWHM), $m_{measured}$ is its detected m/z and $m_{theoretical}$ is that of the molecular assignment. Mass errors are typically sub parts-per-million (ppm).

$$Resolving\ power = \frac{m}{\Delta m} \tag{1.1}$$

$$Mass\ error = \left(\frac{m_{measured} - m_{theoretical}}{m_{theoretical}}\right) \times 10^6 \tag{1.2}$$

The development of ultra-high resolution mass analyzers (Comisarow and Marshall, 1974; Makarov, 2000) and their advancements (Boldin and Nikolaev, 2011; Shaw et al., 2016) has led to increasingly successful compositional analysis of petroleum samples. Important milestones in petroleomics capabilities included the successful resolution of the 3.4 mDa mass split between SH_4 and C_3 (Marshall and Rodgers, 2004), with capabilities and novel approaches improving to yield a recent resolving power of 3 million across a wide mass range, such that the resolution of the 0.39 mDa mass split, lower than the mass of an electron, is achievable (Palacio Lozano et al., 2019).

After thousands of individual peaks have been resolved in a single mass spectrum, petroleomics data may be processed to improve resolution, signal-to-noise, mass accuracy, and distinction of real peaks from noise. To improve signal to noise and resolution a phase correction may be applied across the full spectrum (Cho et al., 2014a), and real peaks may be differentiated from noise by pre-processing of replicate data sets (Gavard et al., 2017). With an increasing prevalence of hyphenated methods and increasing data set size, algorithms designed to handle such data continue to be developed and employed in the field (Palacio Lozano et al., 2019; Schwemer et al., 2015).

Converting many thousands of unique molecular compositions into a readily interpretable format typically follows categorization of molecules based on three features:

- Carbon number, a count of carbon atoms in a molecule, indicating the degree of alkylation.
- Number of rings and double bonds, or double bond equivalents (DBE). The DBE value indicates the degree of aromaticity, or condensation, of a molecule.
- Heteroatom class, summarizing the number of atoms that are neither carbon nor hydrogen, aiding understanding of chemical properties.

Data then need to be visualized in a graphical format that summarizes compositional information and makes comparison between samples more feasible. Example representations (Hughey et al., 2002; Stanford et al., 2006) that are yielded by these features include carbon number distribution, plots of DBE against carbon number, compound class distributions, and van Krevelen diagrams (Kim et al., 2003; van Krevelen, 1950). In a plot of DBE against carbon number a whole compound class may be broken down into its component assignments, with each coordinate simultaneously displaying the degree of alkylation and aromaticity of each molecular formulae. Compound class distributions summarize the relative contributions to mass spectral intensity of heteroatom class detected. Van Krevelen diagrams may be used to visualize, for example, the O/C and H/C ratios of many molecular assignment simultaneously, summarising the degree of oxidation or indicating the types of molecular species present in a complex mixture by the coordinate regions occupied (Rivas-Ubach et al., 2018).

Comparisons between complex data sets are necessary for understanding and predicting differences in bulk properties and structure-function relationships (Marshall and Rodgers, 2004; Mullins, 2007), and for distinguishing between oils from diverse geographical locations or exposed to different conditions (Hunt, 1995; Marshall and Rodgers, 2008). While comparisons may be drawn between a limited number of samples by visualizing multiple compound class distributions on a single chart (Hughey et al., 2002), profiles may be compared more succinctly in a single graphic by employing statistical methods such as principal component analysis (PCA) and hierarchical clustering analysis (HCA) (Hur et al., 2010), partial least squares regression (Lozano et al., 2017) or volcano plots (Hur et al., 2018; Li, 2012).

While petroleomics has demonstrated an unrivalled capability in determining the molecular composition of petroleum, the current challenge now falls to characterizing structural differences between components. Coupling chromatographic methods such as liquid chromatography (LC) or gas chromatography (GC) offers a prior separation step and can provide an indication of the isomeric complexity (Barrow et al., 2014; Hawkes et al., 2018; Thomas et al., 2019). Utilizing hyphenated methods, whereby, for instance, a chromatographic separation is applied prior to mass spectrometry analysis, the multiple isomeric structures underlying each of the many thousands of molecular assignments has been demonstrated. A lack of suitable standards and matrix interferences mean that confirming or discounting the presence of particular structures, or comparing the overall isomeric complexity between samples is, at present, a great difficulty, and presents the next grand challenge for petroleomics (Hertkorn et al., 2007).

1.1.4 Challenges of Analysis

The complexity of petroleum samples has meant that, until recently, comprehensive compositional analysis on the molecular level was impossible and study was limited to determining bulk or average properties. General parameters still widely used to determine the value of crude oil and petroleum products include API gravity, density, and viscosity (Speight, 2006). Other bulk measurements such as aromatic carbon content can be determined by nuclear magnetic resonance (NMR) (Silva et al., 2011), and recently this method has been used to successfully estimate the proportions of saturate, aromatic, resin and asphaltene (SARA) fractions (Verşan Kök et al., 2019). GC, and two dimensional GCXGC, methods are able to obtain detailed molecular-level compositional

information, however characterization is typically limited to the polar and more volatile species, broadly below 300 Da (Zhu et al., 2011).

Petroleomics allows unique compositional profiles, or fingerprints, to be obtained and compared (Marshall and Rodgers, 2004). This chemical fingerprinting yields an understanding of petroleum properties and behavior, the longstanding applications of which include the characterization of residual cuts, asphaltenes, and naphthenic acids (NAs) in crude oils and OSPW (Niyonsaba et al., 2019).

1.2 Petroleomics

1.2.1 Mass Spectrometry Instrumentation

Sector instruments (Dempster, 1918) scan ions as they are able to progress through a bend in a magnetic or electric field dependent upon their intrinsic properties, such as momentum-to-charge or m/z. The compositional information obtained for petroleum samples using these early instruments was limited in large part by the dynamic range attainable (Burgoyne and Hieftje, 1996). Early studies of petroleum were typically performed using sector instruments and GC coupled to evolving mass spectrometry instrumentation, including a study hypothesizing that isoprenoids in crude oil could be used for fingerprinting biogenetic origin (Koons and Pancirov, 1970), and characterization of the nitrogen-containing compounds of a shale oil (Simoneit et al., 1970). GC-MS experiments have advanced with higher resolution instrumentation recently used for the study of gas condensate derived from Arabian oil (Kondyli and Schrader, 2019).

The principles of cyclotron resonance were first introduced in the early 1930s (Lawrence and Livingston, 1932), with the first mass spectrometer (Hipple et al., 1949) and subsequent developments (Baldeschwieler, 1968; Goode et al., 1970; Wobschall, 1965) allowing ICR MS to become commercialized and develop as a prominent analytical technique (Wilkins, 2016). The invention of ion trap mass analyzers (Paul and Steinwedel, 1960) lead to the development of Fourier transform ion cyclotron resonance (FTICR) (Comisarow and Marshall, 1974) and Orbitrap (Makarov, 2000) instrumentation. The frequency of ion motion (ω) in rad s^{-1} may be calculated as shown in Equations 1.3, for ICR, and 1.4, for Orbitrap, where q is the ion charge, B is the strength of the magnetic field, m is the ion mass, and k is the axial restoring force determined by the shape of the trapping

electrodes and applied potential. In ICR the frequency of cyclotron motion is detected, whereas in Orbitrap the frequency of axial oscillations of trapped ions orbit as they orbit central electrode is detected, in both cases as an image current. A Fourier transform is then applied to convert the time domain to frequency, before calibration to calculate *m*/*z*.

$$\omega = \frac{qB}{m} \tag{1.3}$$

$$\omega = \sqrt{\frac{kq}{m}} \tag{1.4}$$

Fourier transform mass spectrometry continues to evolve, for instance through increasing magnetic field strength and developments in cell design, including the invention of the ParaCell (Boldin and Nikolaev, 2011) in FTICR instrumentation, as well as the introduction of the compact, high field, Orbitrap Elite hybrid ion-trap analyzer (Eliuk and Makarov, 2015).

Complementary to hardware developments, data processing algorithms have been developed to enhance performance further, specifically phase correction (Qi et al., 2011; Xian et al., 2010) to increase resolution, and apodization and zero filling to improve peak shape and therefore mass accuracy, for FTICR data. In combination with additional filtering, such processing is termed enhanced FT (eFT) for Orbitrap data (Michalski et al., 2012).

Modern FTICR instrumentation offers unrivalled resolving power and mass accuracy for the analysis of complex samples, including petroleum (Guan et al., 1996; Hsu et al., 2011). An ICR cell typically comprises six electrodes: two excitation and two detection electrodes, plus two trapping plates at each end of the cell designed to constrain axial ion motion. A range of radiofrequencies are swept in order to excite ions of a range of *m*/*z* into an orbiting radius, with larger radii allowing both efficient detection and more coherent motion of individual ion clouds. The cyclotron motion of ions as they pass the detection plates, the frequency of which is proportional to magnetic field strength of the instrument and inversely proportional to *m*/*z* (Equation 1.3), induces an image current for detection. The time domain detected current is converted by fast Fourier transform to the frequency domain, and a calibration equation is then applied that converts frequency data into *m*/*z* (Marshall et al., 1998).

Increasing magnetic field strength to 21 T (Shaw et al., 2016; Smith et al., 2018), permits a larger number of ions to be stored in the ICR cell before peak coalescence occurs, enabling a greater ion population component of complex mixtures to be measured with high sensitivity, resolving power, and mass accuracy over a wide *m*/*z* range. The Infinity Cell (Caravatti and Allemann, 1991) represented a significant development with cylindrical, rather than cubic, Penning trap geometry, and segmented trapping plates that simulated an infinitely long cell, which minimized ion losses during excitation. Developed more recently, the dynamically harmonized ParaCell (Boldin and Nikolaev, 2011; Kostyukevich et al., 2012; Nikolaev et al., 2012) reduces the dephasing of ion clouds, affording a longer time domain signal even at lower magnetic fields (Popov et al., 2014; Qi et al., 2012b). Quadrupolar detection (Pan et al., 1988; Schweikhard, 1991) has also been implemented in the recently developed 2xR instrument which detects an ion cyclotron frequency twice as often as a standard xR instrument. This allows double the resolving in the same acquisition time, or the same resolving in half the acquisition time, of an instrument operating with the same magnetic field strength. These attributes make 2xR instruments particularly well suited to the study of complex petroleum-related samples, offering high performance even at lower magnetic fields (Cho et al., 2017), with the latter permitting faster experiments such as coupling to chromatography runs, where the more rapid scan rate affords highly resolved ion chromatograms (Kim et al., 2019; Thomas et al., 2019).

Orbitrap instrumentation is also widely applied to the analysis of complex petroleum-related samples (Nyadong et al., 2018; Peru et al., 2019; Schmidt et al., 2018), owing to its lower entry cost, smaller size, and less demand on user expertise for efficient operation (Eliuk and Makarov, 2015). Although the resolving power cannot routinely meet that of FTICR instrumentation, a resolving power of 840,000 at *m*/*z* 400 has been reported (Schmidt et al., 2018) on a modified MegaOrbitrap instrument (Denisov et al., 2012). Petroleomics studies involving a prior separation step, such as high pressure liquid chromatography (HPLC), coupled to Orbitrap instrumentation, have also been successfully applied to OSPW (Sun et al., 2017). Schematics of ICR and Orbitrap analyzers are shown in Figure 1.3.

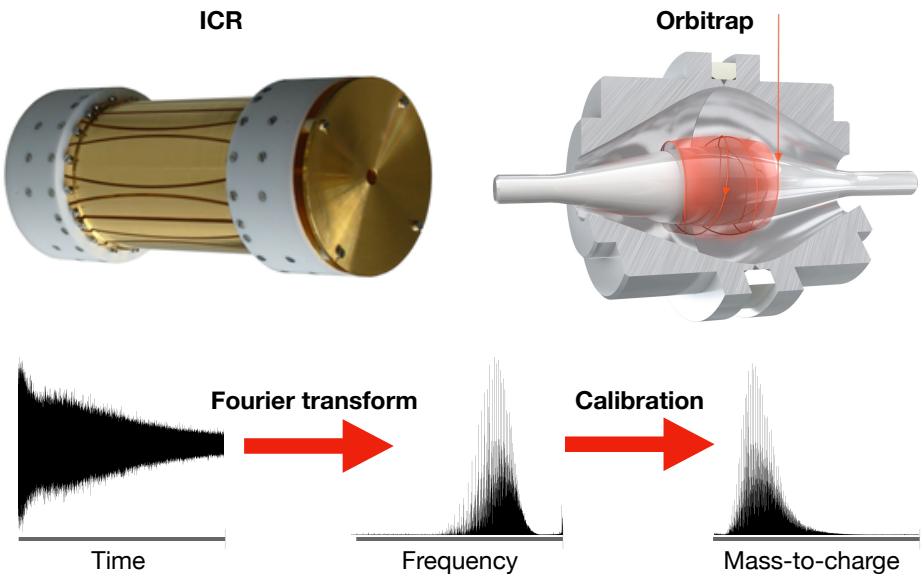

Figure 1.3 – FT mass analyzers compared. An orbiting motion is established in both. In an ICR cell the cyclotron motion of ions is measured, while in an Orbitrap cell it is their axial, oscillating, motion that is measured as ions orbit a central electrode. In both cases the time domain signal is Fourier transformed into the frequency domain, before a calibration is applied to convert to mass-to-charge ratio. Schematics courtesy of Bruker Daltonik GmbH and Thermo Fisher Scientific.

1.2.2 Ionization

The first MS analysis of petroleum was carried out using electron ionization (EI) at 70 eV (Van Meter et al., 1951), and EI-MS became the basis of many ASTM quantification methods (Drews, 1998). Although EI is non-selective and so can access a wide range of petroleum components, the technique causes extensive fragmentation, further complicating spectra, and is also limited to more volatile species that can be vaporized prior to ionization. Nevertheless, lower voltage EI (5-15 V) mass spectra were successfully acquired for olefin and aromatic parent ions in the gasoline boiling point range (Lumpkin, 1958). Field desorption (FD) was able to preserve parent ions more successfully, allowing the relative concentrations and mass ranges for constituents of waxes, such as n- and iso-paraffins to be determined (Mead, 1968). A recent summary of the wide array of ionization methods, prior separation techniques, and mass spectrometry methods that have been developed is presented in Figure 1.4.

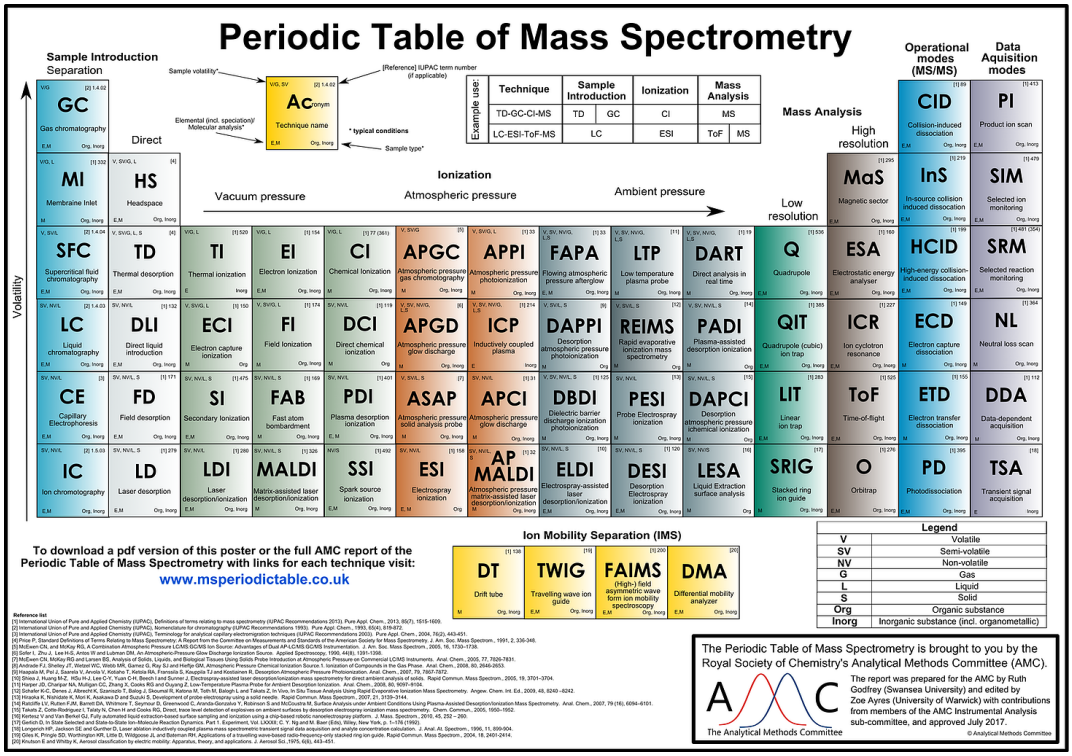

Figure 1.4 – Periodic Table of Mass Spectrometry and associated techniques. Image courtesy of RSC Analytical Methods Committee and reproduced with permission of the original authors. Further details can be found at https://www.msperiodictable.co.uk

The development of softer ionization methods beginning with electrospray ionization (ESI) (Fenn et al., 1989; Yamashita and Fenn, 1984), allowed fragmentation of ions within the source to be avoided: facilitating the characterization of large, intact, molecular species. However, ESI is more selective towards polar protic species with ionization taking place in the solution phase before gas-phase ions are produced following solvent evaporation. In atmospheric pressure chemical ionization (APCI) (Harrison, 1992) desolvation takes place prior to ionization at a corona discharge electrode (at 3-5 kV) (Byrdwell, 2001). APCI allows characterization of both polar and relatively less polar species than ESI, and has been successfully applied to the analysis of a range of petroleum related substances (Barrow et al., 2014; Kim and Kim, 2010; Tose et al., 2015), including those that may have low volatility or be present in low concentrations (RosellMele et al., 1996). Atmospheric pressure laser ionization (APLI) is a method whereby a laser beam intercepts the vapor stream of solvent and analyte molecules close to the sampling orifice (Constapel et al., 2005; Schrader et al., 2008), and while the technique is selective towards non-polar aromatic compounds and those containing sulfur, with prior GC separation allowing PAH isomers to be separated and characterized (Benigni et al., 2016), it

has also been demonstrated to be able to access species in all SARA fractions (Gaspar et al., 2012).

Although ESI was eventually applied successfully to the study petroleum samples (Zhan and Fenn, 2000) and has since had been used to selectively characterize the more polar components, particularly acidic (Qian et al., 2001), basic (Stanford et al., 2007), and nitrogen-containing compounds (Klein et al., 2006b), there is a requirement to move beyond ESI for full compositional analysis

Matrix-assisted laser desorption ionization (MALDI) (Karas et al., 1987) is a technique developed for the analysis of non-volatile and thermally labile compounds, with the matrix and analyte mixture simultaneously desorbed and ionized in the gas phase following irradiation (Bae and Kim, 2015; Zenobi and Knochenmuss, 1998). Petroleum-related samples are often suitable for analysis by laser desorption ionization (LDI) without a matrix, which allows solid phase and low volatility samples to be characterized (Cho et al., 2013; Cho et al., 2014b; Lozano et al., 2016).

While FD has been successfully coupled to FTICR MS and applied to the study of non-polar hydrocarbons (Schaub et al., 2003), atmospheric pressure photoionization (APPI) is a more recently developed ionization method (Robb et al., 2000; Syage et al., 2000) regularly used for petroleum analysis. The technique utilizes a krypton or argon lamp to emit photons of specific energy capable of ionizing analyte molecules directly, or more extensively with the aid of an included dopant such as toluene. APPI offers greater sensitivity and the highest ionization efficiency for petroleum-related samples (Sama et al., 2018), accesses the broadest range of components due to a lower reliance on ion-molecule chemistry, and is also less susceptible to ion suppression than ESI and APCI (Annesley, 2003; Hanold et al., 2004).

Given that ESI, APPI, and APCI can all be operated at atmospheric pressure, an ion source based on each can be constructed such that they can be coupled interchangeably to MS instrumentation. It is therefore these three ionization techniques that are routinely utilized throughout this thesis. The key similarities and differences in source design and ionization between ESI, APPI, and APCI are illustrated schematically Figure 1.5.

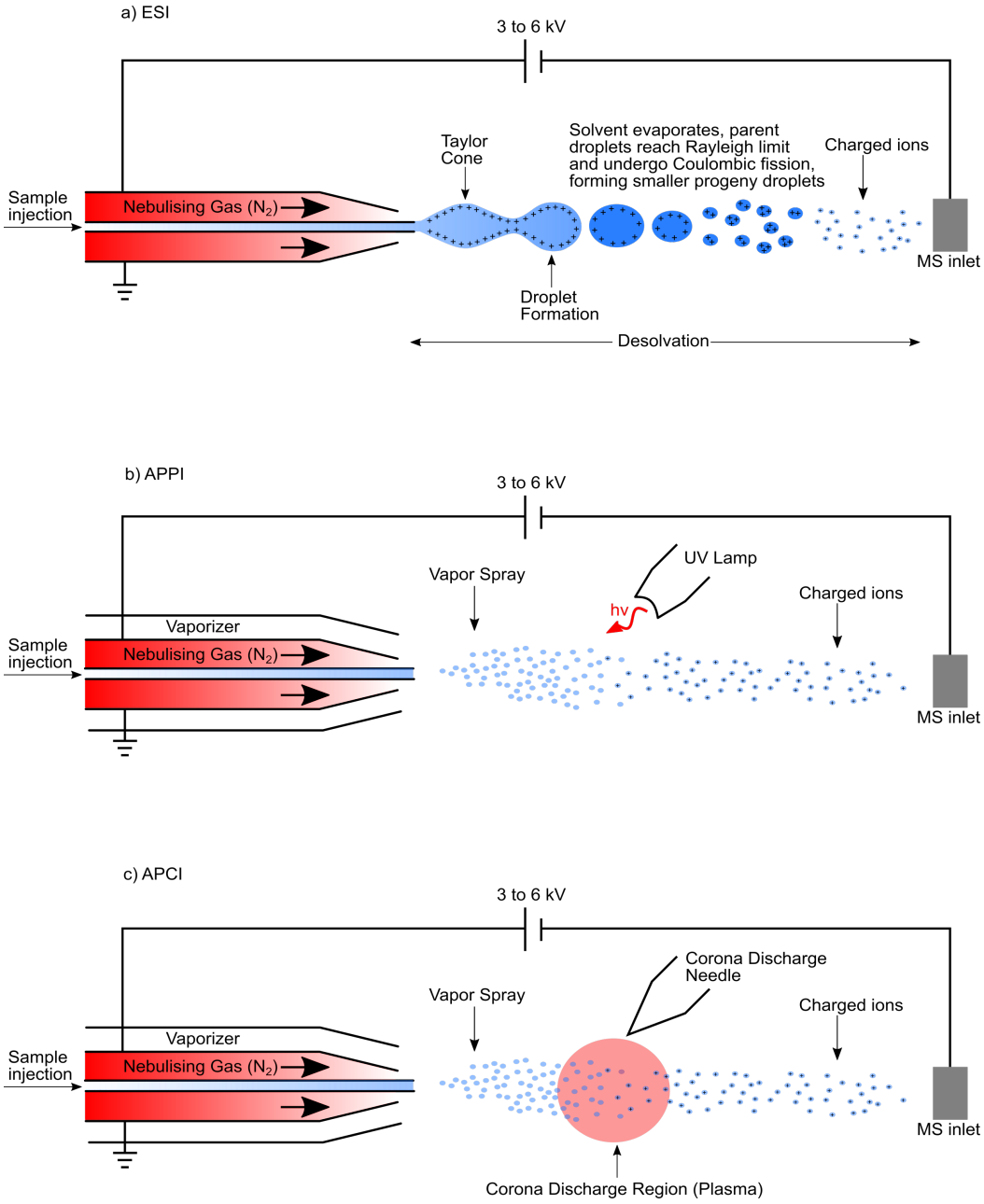

Figure 1.5 Schematics illustrating a) ESI, b) APPI, and c) APCI ionization.

In ESI the transfer of analytes from solution to gas phase molecular ions is a desolvation process, in which, for example when operated in positive-ion mode, a protic solvent can act as a source of H^+ to form $[M + H]^+$ species where a site suitable for pronation exists in the analyte. ESI therefore provides the most efficient ionization of, and is selective towards, the more polar protic constituents of petroleum, particularly acidic and basic species when operated in negative-ion and positive-ion mode respectively. This contrasts with APPI and APCI, which although are soft ionization techniques are less soft than ESI, as a vaporizer is

used such that ionization occurs in the gas-phase. Furthermore, less polar species are accessed as a result of photoionization and chemical ionization processes.

APPI is capable of directly ionizing species with an ionization potential lower than the photon energy of the UV lamp, typically 10.0 or 10.6 eV. The constituents of petroleum samples most efficiently ionized in this manner are those containing highly conjugated moieties such as polycyclic aromatic hydrocarbons (PAHs). Analytes with higher ionization potentials can be accessed through use of a dopant (D), such as toluene, for primary ion formation before undergoing charge transfer to form radical ions and protonated species. APPI therefore provides the most extensive coverage of petroleum compositional space, including non-polar and less polar components. The mechanism for dopant-assisted APPI is shown in Equation scheme 1.5 (Hanold et al., 2004).

$$\begin{aligned} &D + h\nu \rightarrow D^{+\cdot} \\ &D^{+\cdot} + M \rightarrow D + M^{+\cdot} \\ &D^{+\cdot} + M \rightarrow [D - H]^{\cdot} + [M + H]^{+} \end{aligned} \qquad (1.5)$$

In APCI the high voltage used at the corona discharge forms a plasma in which reactive species can be formed from molecules present in the atmosphere and nebulizing gas. These can then form analyte ions through charge exchange, via electron capture and proton transfer, to form both radical ions and pronated species respectively. The mechanisms of ion formation in APCI are shown in Equation scheme 1.6 (Herrera et al., 2008). In APCI the efficiency of analyte ion formation depends upon these ion-molecule chemistries, although a greater range of species, including less polar analytes, may be accessed compared to ESI.

$$\begin{aligned} &e^{-} + N_2 \rightarrow 2e^{-} + {N_2}^{+\cdot} \\ &{N_2}^{+\cdot} + M \rightarrow N_2 + M^{+\cdot} \\ &{N_2}^{+\cdot} + H_2O \rightarrow N_2 + {H_2O}^{+\cdot} \\ &{H_2O}^{+\cdot} + H_2O \rightarrow OH^{\cdot} + {H_3O}^{+\cdot} \\ &{H_3O}^{+\cdot} + M \rightarrow H_2O + [M + H]^{+} \end{aligned} \qquad (1.6)$$

The differences in preferential ionization offered by ESI, APPI, and APCI (Huba et al., 2016) can be utilized to obtain complementary compositional information for a single sample, and when operated in positive-ion or negative-ion mode can further enhance selectivity towards basic or acidic species respectively (Barrow et al., 2010). The wider range of ionization methods and prior separation

techniques that can be coupled to mass spectrometry is now expansive, with a recent summary of methodologies illustrated in Figure 1.4 (Analytical Methods Comm, 2017).

With tightening restrictions on sulfur content for a range of petroleum products, including diesels and HFOs (Halff et al., 2019) the characterization of sulfur-containing groups is increasing important, particularly thiophenic groups known to be resistant to many desulfurization processes owing to steric hindrance (Houda et al., 2018; Vetere et al., 2017). ESI does not provide efficient coverage of many sulfur-containing molecules without derivatization (Purcell et al., 2007a), instead preferentially ionizing nitrogen containing species such as pyridines, that protonate readily in positive mode, or pyrroles, that deprotonate readily in negative mode (Huba et al., 2016; Purcell et al., 2007b). APPI provides the most efficient access to the widest range of compounds, including sulfur-containing PAHs, whose aromatic structures can stabilize a radical species more readily (Creary et al., 1989), and is therefore the most appropriate technique for their characterisation.

The compositional analysis of petroleum samples is inherently challenging, with no single ionization method capable of providing full compositional coverage. Furthermore, techniques such as ESI, APPI, and APCI are unsuitable for solid substances and such samples require further work-up, including dissolution, filtration, and dilution, prior to analysis. New ambient ionization techniques continue to be developed (Bouslimani et al., 2014; Cody et al., 2005; Wu et al., 2010) and used in the study of petroleum-related samples (Ren et al., 2016; Romao et al., 2016), which facilitate direct analysis without prior sample preparation, with an increasing number capable of analyzing solid samples. Those most applicable to petroleum include low temperature plasma (LTP), which desorbs and ionizes surface molecules under ambient conditions (Harper et al., 2008) and the atmospheric solid analysis probe (ASAP) which facilitates solvent-free ionization of solid samples (McEwen et al., 2005). LTP has allowed direct characterization of crude oils without prior sample preparation or dilution (Benassi et al., 2013), while ASAP ionization has demonstrated the ability to study PAHs in complex matrices, including oils, without prior sample preparation (Carrizo et al., 2015), as well as direct characterization of crude oil and a paraffinic fraction (Tose et al., 2017). Ambient ionization methods may be particularly useful for petroleum samples that fail to ionize by traditional methods or are unstable in solution, giving scope to accessing greater compositional detail where

these ionization methods are used in combination with ultra-high resolution mass spectrometry.

1.2.3 Separation

Applying prior separation methods allows the preferential ionization of major classes of whole oils to be overcome and for different compound types to be characterized (Rodgers et al., 2019). Petroleum compounds are most commonly separated based on solubility and polarity into SARA fractions (Akbarzadeh et al., 2007). Asphaltene deposition is a major problem in the field, with the classical physical model of petroleum defining asphaltenes as solute, resins as dispersants, aromatics as solvent, and saturates as destabilizing non-solvent (Wiehe, 2008). The SARA fractions can be isolated from one another, with the asphaltene fraction isolated first due to its insolubility in n-alkanes (Sheu and Storm, 1995), followed by chromatographic separation using solvents of particular polarity to elute the remaining fractions (Akbarzadeh et al., 2007; Raki et al., 2000). The characterization of each fraction reveals differences in heteroatom content and the molecular weight of the species identified (Shi et al., 2010). Studying each separately has allowed access to a wider range of compositions than when studying the unfractionated sample, which is typically dominated by species sorted into the aromatic fraction (Cho et al., 2012b).

Chromatographic separation techniques, GC and LC, can be applied to separate the constituents of petroleum-related samples. In such techniques the sample is solute in an injected mobile phase; a carrier gas such as helium in GC, or a solvent system in LC. Analytes equilibrate between the mobile phase and the column stationary phase, with the equilibrium constant determined by their physical and chemical properties. Separation is afforded as species elute at differing retention times from the column. The stationary phase can be selected to best suit the sample type, for example GC separation of less polar species using polysiloxane, or of more polar species using stable ionic liquids (Berthod et al., 2018).

GC techniques are limited by boiling point and therefore provide access only to the lower molecular weight species present in petroleum, and therefore thorough analyses are restricted to cuts such as gas condensate (Kondyli and Schrader, 2019). GC is a widely used standard method in the petroleum industry, and has also been used for determining petroleum origins, thermal maturity, and reservoir alteration processes through analysis of biomarkers (Barman et al., 2000; Hsu et al., 2003). LC, while typically offering less efficient separation, is not

limited by boiling point, and as such HPLC has been used for hydrocarbon type analysis of heavier petroleum samples (Ali and Hassan, 2002), although attaining clean separations is more challenging than for light and middle distillates (Barman et al., 2000). Prior separation using HPLC has improved compositional coverage when combined with ultra-high resolution mass spectrometry and other analytical techniques (Kim et al., 2015).

Two dimensional GC experiments, whereby a modulator traps, focuses, and injects small fractions from one column into another (Liu and Phillips, 1991), provide enhanced coverage of low boiling point and polar petroleum samples. Although GCXGC is limited by boiling point and so cannot be applied to heavier petroleum samples, the technique has demonstrated the ability to separate the components of a complex mixture by a combination of physical and chemical properties on the two independent columns, for example separation of alkanes from aromatic compounds, sequentially grouped by ring numbers (Marriott et al., 2004). GCXGC can access aliphatic, saturated cyclic, and one-ring aromatic compounds, and so can provide information complementary to APPI experiments (Cho et al., 2012a). Coupling GCXGC to lower resolution mass spectrometry techniques can enhance performance beyond that offered by comparable direct infusion, with the C_3 and SH_4 mass split of 3.4 mDa resolved in such experiments (Bowman et al., 2018; Byer et al., 2016).

1.2.4 Hyphenating ultra-high resolution MS

MS in isolation is not capable of separating species with the same molecular weight but differing structures, and so cannot provide information on the range of isomers present. Hyphenating GC and LC to ultra-high resolution mass spectrometry adds an extra dimension of separation, improves dynamic range and provides insight into the isomeric complexity of samples, with multiple individual molecular structures underlying each molecular composition assigned in the mass spectra of petroleum-related samples (Barrow et al., 2014; Kondyli and Schrader, 2019). Early studies of petroleum samples by GC-FTICR MS benefited from sensitivity an order of magnitude lower than GC coupled to a commercial quadrupole mass spectrometer (GC-QMS), but slow scan rates restricted the resolution of chromatographic peaks, which may possess a retention time FWHM of less than 1 s (Szulejko and Solouki, 2002). The recent development of quadrupolar (2ω) detection in FTICR instrumentation (Cho et al., 2017) has allowed equivalent mass resolution and sensitivity in half the scan time, improving the feasibility of coupling FTICR MS to prior chromatographic

separation and affording fully resolving ion chromatograms (Thomas et al., 2019). Supercritical fluid chromatography (SFC) MS is well suited to the separation and analysis of petroleum samples (Crepier et al., 2018; Ratsameepakai et al., 2015) due to the use of non-polar CO_2 mobile phase (Pilarova et al., 2019; West, 2018), and a future challenge for petroleomics is hyphenating this method to FTICR MS.

Thermal analysis (TA) investigates the properties of materials as a function of temperature, and the gases evolved from crude oils have been successfully analyzed by mass spectrometry in a number of studies (Geissler et al., 2009). The qualitative compositional information obtained can be then compared to quantitative thermogravimetric (Tiwari and Deo, 2012) and calorimetric data. Coupling TA to ultra-high resolution MS increases compositional coverage and identifies strong correlations to physiochemical properties, such as between average DBE and API gravity, as well as suggesting the presence of archipelago type asphaltenes (Ruger et al., 2017).

In this work the rapid scan rate made possible when using 2ω detection on newly developed 2xR instrumentation is employed such that GC can be hyphenated to FTICR MS. The extra dimension of separation affords information complementary to direct infusion analyses, including improved detection of lower abundance species, visualization and comparison of isomeric complexity between samples, and a semi-quantitative assessment of contributions from compound classes of interest.

1.2.5 Ion Mobility-Mass Spectrometry

Ion mobility-mass spectrometry (IMMS) separates ions by their ability to move in a carrier gas under the influence of an electric field (Kanu et al., 2008). The size, shape and m/z of an ion determine its collisional cross section (CCS), which in turn define its mobility. A recent advancement is known as trapped ion mobility mass spectrometry (TIMS), in which ions are held stationary in a moving column of gas, permitting analyzers to become smaller, more versatile, and a higher performance alternative with the effective length of the drift cell becoming user-defined (Ridgeway et al., 2018). IMMS, and the more recently developed TIMS, has been successfully applied to the study of light, medium, and heavy crude oils (Fernandez-Lima et al., 2009), and dissolved organic matter (DOM) (Leyva et al., 2019). IMMS has been proposed as a complementary technique for the elucidation of structural properties of the molecular components of crude oils (Ahmed et al., 2014; Ahmed et al., 2011). The prior separation step afforded by ion mobility

increases the overall spectral peak capacity and provides information on isomeric complexity and CCS, with successful application to the study of NAs (Lalli et al., 2015), and crude oil contaminants and fuel additives (Santos et al., 2015). Ion mobility separation followed by ESI allowed for partial speciation of nitrogen-containing molecules (Farenc et al., 2016), although a full characterization of isomeric species continues to present a challenge.

1.2.6 Data Handling

While FTICR MS generates ultra-high resolution mass spectra, particularly for petroleum-related samples, they are often extremely complex and many peaks may not be fully resolved, particularly for heavier fractions or at the higher *m*/*z* ranges. To improve resolution and peak shape further, phasing and apodization may be applied (Qi et al., 2013). Apodization is a signal processing method that can improve spectra by suppressing the overlapping sidebands of neighboring peaks by suppressing the extreme ends of the transient signal (Zhang et al., 2014). Phasing of mass spectra has been demonstrated to improve the signal-to-noise across broadband spectra by values exceeding the theoretical minimum $\sqrt{2}$, increasing the resolving power by a factor of $\sqrt{3}$ to 2, and has been successfully applied to petroleum samples (Qi and O'Connor, 2014; Qi et al., 2012a; Qi et al., 2013). Although petroleum spectra are inherently complex, simplistic signal-to-noise thresholds are typically applied during peak picking, which results in either low intensity peaks being discounted as noise, or a large amount of noise included to ensure that data points are not missed, which can lead to false assignments. Recently developed pre-processing algorithm Themis distinguishes peaks reliably observed across replicates, improving the accuracy of assignments and inclusion of low intensity peaks (Gavard et al., 2017).

Petroleum samples predominantly comprise hydrocarbon systems, sometimes containing heteroatoms, that may be separated by differences in alkyl substitution, and so differing in mass by CH_2 (14.01565 Da), or differences in number of double bond equivalents (DBE), and so differing in mass by H_2 (2.01565 Da). Searching for homologous series separated by repeat units of CH_2 (14.01565 Da) or H_2 (2.01565 Da) allows calibration and assignment of entire data sets. The repeat unit is illustrated in mass spectrum shown in Figure 1.6. Conversion to the Kendrick mass scale (Kendrick, 1963) may be achieved by multiplying the IUPAC mass of each species by 14.00000/14.01565, effectively converting CH_2 units to exactly 14.00000 Da. Therefore, each homologous series, comprising species only differing by their degree of alkylation, or carbon number,

all possessing the same DBE and belonging to the same heteroatom class, will have a uniform Kendrick mass defect (KMD), which can be obtained by subtracting the exact Kendrick mass from the nominal Kendrick mass. Identification of the entire homologous series by KMD is then possible, eliminating the need for the time-consuming process of making compositional ssignments peak-by-peak (Hsu et al., 1992). The numerous assignments detected in a single petroleum sample may be represented in a number of ways. KMD plots (Hughey et al., 2001), allow the compact display of multiple assignments, with vertical separation between homologous series.

Once data has been calibrated, many thousands of assignments may be made in a single petroleomics spectrum, typically comprising elemental compositions of $C_cH_{2c+z}N_nO_oS_sP_p$ where Z is a negative integer known as the hydrogen deficiency, which is constant across a given homologous series. Assignments may then be categorized according to carbon number, heteroatom class (including ion type), and DBE. For an overview of composition, the relative contribution from each heteroatom class to spectral intensity may be represented as a compound class bar chart (Hughey et al., 2002). Each compound class may then be represented by its component DBE distribution (Hughey et al., 2002) or be broken down into a plot of DBE against carbon number (Barrow et al., 2009; Stanford et al., 2006) (Figure 1.6).

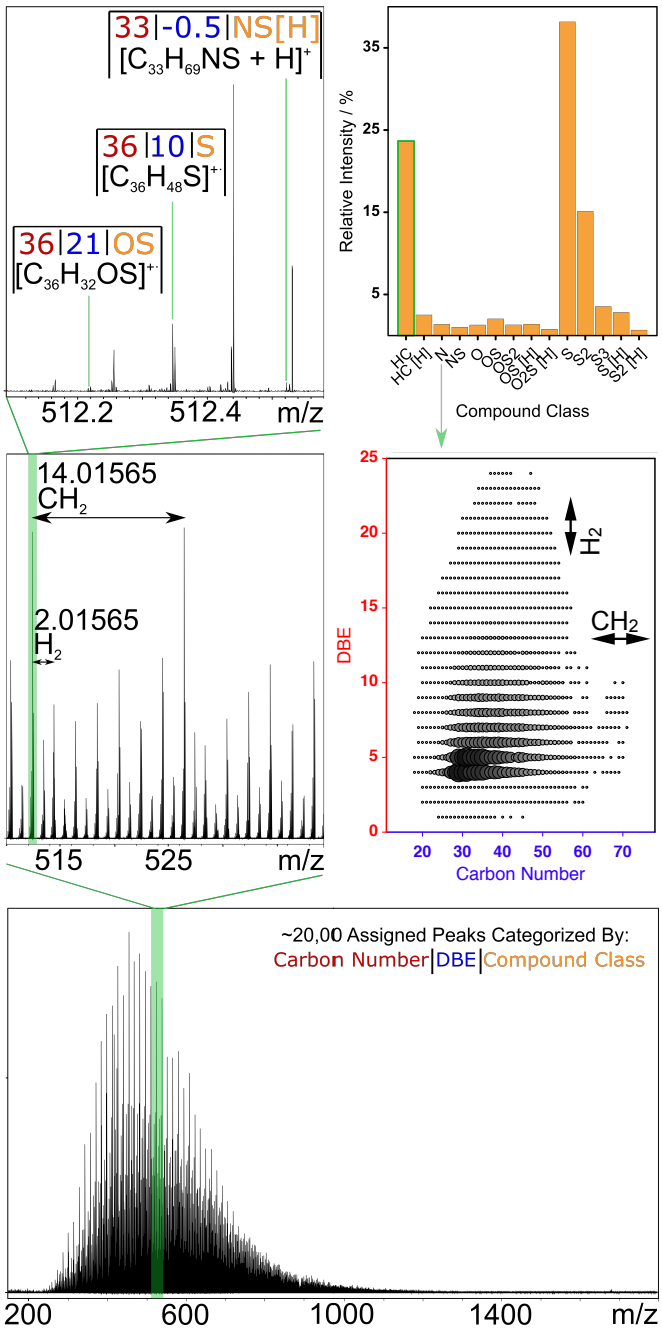

Figure 1.6 – Sequential zooms of a FTICR mass spectrum of crude oil showing the CH_2 and H_2 repeat units, used for assignment of homologous series. The same separation may be visualized in a plot of DBE against carbon number for a selected compound class.

Compositional analysis was once widely performed using in-house scripts (Hughey et al., 2002) and individual data analysis methods (Barrow et al., 2003). More recently, commercially available software packages including PetroOrg (Florida State University, Tallahassee, FL) (Klitzke et al., 2012) and Composer (Sierra Analytics, Modesto, CA) (Barrow et al., 2010; Zhurov et al., 2013b) have

been developed. Composer continues to offer several advantageous features, such as including differentiating analyte peaks from noise and sequential element range passes, allowing assignment of most likely formulae prior to moving on to less likely, but theoretically possible, assignments with more diverse heteroatom content.

Where oxygen containing species are of significant interest, for example in natural organic matter (NOM), DOM, and bio-oils, van Krevelen (van Krevelen, 1950) plots may be used to compare the ratio of H/C against O/C simultaneously for all assignments, with the coordinate location of points known to be characteristic of differing biogeochemical compound classes such as lignin, fatty acids, and carbohydrates (Kim et al., 2003; Rivas-Ubach et al., 2018). The diagenetic history of compounds (Reuter and Perdue, 1984), as well as an understanding of how petroleum-related samples age (Handle et al., 2017; Reuter and Perdue, 1984), can be elucidated as reactions that lead to characteristic losses or gains of C, H, O, or N atoms yield unique trajectories and changes in the coordinates of higher point density on the van Krevelen plot. Visualization approaches for comparing multiple large data sets continue to be developed and adapted to more appropriately represent research findings.

1.2.7 Statistical Approaches

Statistical interpretation methods (Cho et al., 2015; Hur et al., 2010) can be used to compare detailed petroleomics compositional information more rapidly. Heat maps have been used to compare similar classes of compounds simultaneously, and are a promising means by which to identify trends such as the degree of oxidation (Barrow et al., 2009). Volcano plots, previously developed for application to microarrays (Cui and Churchill, 2003; Li, 2012; Mariani et al., 2002), are generated by plotting statistical significance against degree of change, and have recently been applied to the comparison of crude oil composition (Hur et al., 2018). In the research presented herein, two forms of unsupervised multivariate analysis, whereby no assumptions are drawn from group classifications, are employed. HCA is used to group samples by their relative similarities (Ward, 1963), while PCA allows for visual interpretation of the variance (Bell and Blais, 2019) and identification of variables that may underly observed differences. In addition, design of experiments (DoE) is utilized to determine which sample preparation and procedural factors have the most significant effect on the results observed.

HCA has been used in GC-MS studies of oils and source-rocks (Alves et al., 2018; Bao et al., 2017; Ekpo et al., 2018) as well as in APPI-FTICR MS studies to group oils based on well and geographical origin (Chiaberge et al., 2013). In HCA a hierarchical dendrogram is generated, which at increasing height represents greater distance between the sample clusters. A range of clustering approaches may be used, including agglomerative clustering which treats each sample as an individual cluster and successively pairs similar samples until all data is merged. The inverse of this approach is divisive clustering, which treats all data as a single cluster and splits them iteratively until each sample is in an individual cluster. A cophenetic correlation coefficient defines the efficiency of the clustering and how adequately the hierarchical structure imposed by the dendrogram represents the distances in the original data, with values closer to 1 indicating the most efficient clustering (Saraçli et al., 2013; Sokal and Rohlf, 1962).

PCA (Hotelling, 1933) separates samples based on variability and has been successfully applied to differentiating tailings ponds water from river and lake waters in the Athabasca oil sands region (Headley et al., 2011), classifying oil spills (Ismail et al., 2016), and identifying their source (Corilo et al., 2013). PCA combines the original variables into principal components, in order to compress and simplify the description of the data and extract the most important information (Abdi and Williams, 2010). A sufficient proportion of the total variance, for instance greater than 70 % (Kafer et al., 2019), should be explained within the first two principal components in order for the PCA to be considered successful.

In DoE experimental parameters can be adjusted simultaneously in a systematic manner such that those that have the statistically significant impact on a selected response factor can be identified (Weissman and Anderson, 2015). In addition to the information that may be obtained directly from a DoE analysis, non-linear responses may be indicated and direct further investigation. A minimum and maximum of each parameter, such as sample concentration or injection flow rate, is investigated, while the response factor at the DoE centerpoint is that generated at the average value for all parameters. The direction and magnitude of the effect is represented by the straight line drawn between the response factor observed at the minimum and maximum parameters, while a non-linear response is indicated by a centerpoint that does not sit on a straight line between these values. A full factorial DoE ensures that no aliasing, whereby effects may be confounded with one another such that their individual or interactive impact on the response factor

cannot be resolved, takes place. Petroleomics researchers have previously used DoE to optimize experimental procedures, with heteroatom class intensity as a response factor to determine which parameters had the most significant effect (Guillemant et al., 2019).

1.3 Example Applications

1.3.1 Heavy Petroleum

Heavy petroleum and residual fractions of crude oil tend to have higher viscosity and high boiling points making them unsuitable for study by GC (Cho et al., 2015; Zhu et al., 2011). In addition, the relative proportions of heteroatoms such as S, N, O, and metals increases with boiling point (Boduszynski, 1987). Heavier petroleum fractions also tend to have higher asphaltene content which is known to cause problems with transportation and storage due to flocculation above a critical concentration (Akbarzadeh et al., 2007), under extreme conditions of temperature and pressure (Buckley et al., 2007; Hammami et al., 2000), when part of an incompatible blend or when self-incompatible (Durand et al., 2010; Wiehe and Kennedy, 2000), leading to fouling and deposition (Mullins, 2008). Asphaltene instability can cause scraper ring clogging, leading to high lubricant oil consumption, or undesirable black paint formation on cooler engine parts in marine applications (Vermeire, 2012). A minimum of approximately 100 ions is required for a signal to be detected and spectral peak generated, but due to limitations on the maximum number of ions that a modern ICR cell can accommodate (Nikolaev et al., 2016), the greater complexity of heavier oils can make acquisition of a single mass spectrum across the full mass range, known as a broadband mass spectrum, impossible. Stitching together small mass range segments can improve characterization by increasing the number of species resolved (Gaspar and Schrader, 2012; Krajewski et al., 2017), and facilitate analysis of samples previously inaccessible due to their complexity, with a record-breaking 244,779 individual molecular formulae identified using the recently developed operation at constant ultra-high resolution (OCULAR) method (Palacio Lozano et al., 2019).

Asphaltenes, the fraction of petroleum insoluble in n-alkane solvents (Sheu and Storm, 1995), may be observed at lower abundance, or not detected, in whole oil spectra, but can be isolated by their solubility. With the more efficiently ionized, n-alkane soluble, maltene species removed from the sample, asphaltene mass spectra tend to be more complicated than the corresponding whole crude or

heavy oil spectrum (Cho et al., 2012c) with many more peaks observed at a single nominal mass unit. Asphaltenes also tend to have higher heteroatom content (Wiehe, 2008) and DBE (Klein et al., 2006a) than the whole oil or other SAR fractions. Both island and archipelago structures, defined as a single PAH core substituted with alkyl chains or multiple PAHs bridged by alkyl linkers, respectively, have been postulated (Gray, 2003; Mullins, 2008; Mullins, 2011) and studies into the relative stability and probable occurrence of each continues (Alvarez-Ramirez and Ruiz-Morales, 2013; Schuler et al., 2015). Example island and archipelago structures possible for asphaltene species possessing the same molecular formula, and therefore the same DBE, are shown in Figure 1.7.

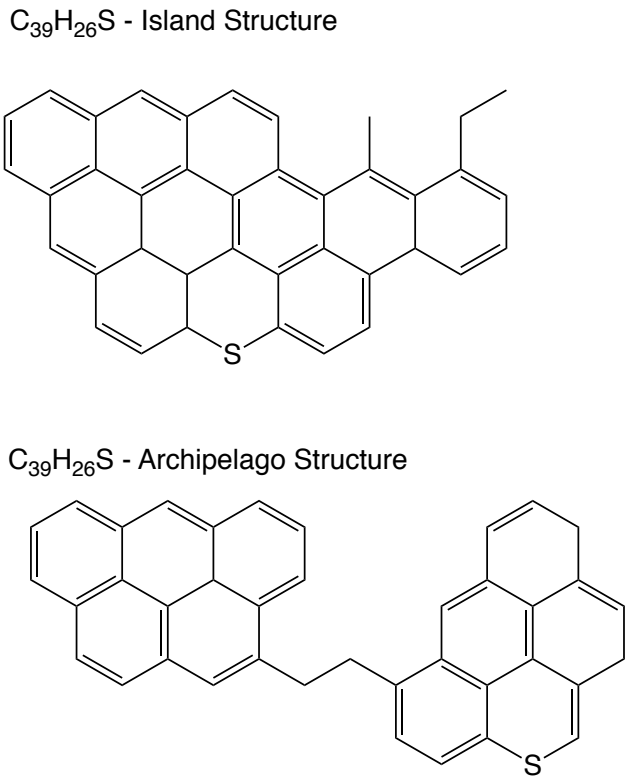

Figure 1.7 – Possible island and archipelago structures for an example asphaltene species of molecular formula $C_{39}H_{26}S$, possessing a DBE of 27.

Tandem mass spectrometry (MS/MS) methods, whereby a range of precursor ions can be selected based on *m*/*z*, and a mass spectrum of the fragment species generated is produced, can be utilized for structure elucidation. Quadrupolar isolation is typically used for precursor selection, while a range of fragmentation methods including collision induced dissociation (CID) (Jennings, 1968; McLafferty and Bryce, 1967; Tang et al., 2015), high-energy collision dissociation (Nyadong et al., 2018), electron capture dissociation (ECD), and infra-red multi

photon dissociation (IRMPD) can be used for fragmentation. ECD has been demonstrated to provide extensive structural characterisation in proteomics applications, however the technique relies upon precursor ions possessing multiple positive charges such that they can be detected subsequent to electron capture (Zhurov et al., 2013a), and therefore the technique is unsuitable for petroleomics whereby most analyte species observed are singly charged. Collision induced dissociation is used widely, however the technique has several drawbacks including lower *m*/*z* fragments failing to reach the detector (Little et al., 1994; Payne and Glish, 2001). IRMPD, which allows low *m*/*z* fragments to be retained due to fragmentation taking place in the analyzer cell, has previously been used to differentiate between and determine whether island or archipelago structures predominate in a sample (Chacon-Patino et al., 2017).

1.3.2 Corrosion

The characterization of NAs within crude oil samples has become vital as corrosion of refinery equipment leads to increased operating costs, particularly as production shifts to unconventional oils that tend to have a greater acid content (Slavcheva et al., 1999). While a high total acid number (TAN), defined numerically as the milligrams of potassium hydroxide required to neutralize one gram crude oil, may implicate a higher NA content, several deficiencies with using this measure have been identified. The standard methods may yield TAN values varying by up to 80 %, and differences in observed corrosivity at equivalent TAN have been observed, due to the varying molecular properties of the NAs present (Slavcheva et al., 1999; Turnbull et al., 1998).

NAs are defined as carboxylic acids that contain one or more saturated ring structures with the empirical formula $C_nH_{2n+z}O_2$ (Dzidic et al., 1988; Fan, 1991; Hsu et al., 2000), while oxy-NAs or NA fraction compounds (NAFCs) may have higher oxygen content (Peru et al., 2019). Selective observation and molecular characterization of NAs in whole crudes oils (Barrow et al., 2003) as well as in environmental samples such as OSPW (Headley et al., 2009) is typically afforded through ESI analysis. SFC has been successfully coupled with Orbitrap MS for examining the isomeric complexity of molecular species in OSPW (Pereira and Martin, 2015). The use of comprehensive GCXGC-MS has facilitated the identification of individual acids (Rowland et al., 2011), while HPLC coupled to time-of-flight (TOF) MS has been demonstrated as a viable method for the quantitation of total oxy-NAs, or qualitative identification of particular NA compounds of interest (Hindle et al., 2013). When studying NAFCs for

environmental monitoring purposes, particularly where comparison of relative contributions to spectral intensity is used as a semi-quantitative measure, consideration of sampling handling factors including solvent (Headley et al., 2007) and mobile phase pH (Peru et al., 2019) is imperative.

1.3.3 Petroleum in the Environment

Petroleomics research plays a key role in assessing the historical and ongoing impact of petroleum on the environment, including water (Headley et al., 2013; Headley et al., 2016), and soil quality (Thomas et al., 2019). Petroleomics methodologies have also been employed in studies evaluating the impact of the petroleum industry on wildlife and assessing the prospect of ultimate remediation (Marentette et al., 2015). Oil sources may identified by combining mass spectrometry data with statistical approaches (Chiaberge et al., 2013; Stout et al., 2001), such that this approach has been successfully applied to fingerprinting spill origins and comparing natural and anthropogenic substances (Corilo et al., 2013; Islam et al., 2016; Krajewski et al., 2018). Furthermore, an understanding of the longer-term impacts of spills is made possible by monitoring contamination sites over extended periods or by exposing petroleum-related samples to stimulated environmental conditions (Aeppli et al., 2012; Chen et al., 2016; Griffiths et al., 2014; Handle et al., 2017; Islam et al., 2016; Yim et al., 2012).

The explosion at the Deepwater Horizon (DWH) rig, which resulted in the release of 5.3×10^8 kg of oil from the Macondo Well into the Gulf of Mexico, was the largest accidental spill in history (Aeppli et al., 2012), with more than 2100 km of shoreline affected (Beyer et al., 2016). Although GC studies have monitored the transportation and fate of compounds such biomarkers and PAHs (Allan et al., 2012; Natter et al., 2012), petroleomics methodologies are able to target a wider range of spilt compounds and their weathered products in the aftermath (Aeppli et al., 2012; Chen et al., 2016; Ruddy et al., 2014). A recent longitudinal study determined the molecular transformation of DWH contaminants over the course of 4 years, with contributions from hydrocarbon classes not detected after 43 months with a corresponding increase in oxygen-containing compounds observed (Chen et al., 2016).

As oil ages in the environment irradiation by sunlight, exposure to oxygen, and microbial degradation, can cause result in compositional changes. In addition to investigating the effects of weathering on petroleum-related contaminants from

oil spill events (Islam et al., 2013; Lemkau et al., 2014; Thomas et al., 2019; Yim et al., 2012), simulated ageing experiments can improve molecular-level understanding of the ageing process in controlled laboratory conditions. Subjecting bitumen to a pressure ageing vessel (PAV) procedure improved understanding of the factors leading to embrittlement and subsequent material failure, which may include reduction of condensed compounds to alicyclic and chain structures (Handle et al., 2017). Exposing crude oil to stimulated sunlight caused changes in the heteroatom class distribution and an increase DBE and carbon number to be observed, with low DBE sulfur-containing compounds found to be the most susceptible to transformation, potentially becoming more water soluble and acidic as a result (Griffiths et al., 2014). TIMS-FTICR MS analysis of the water-accommodated fraction (WAF) of crude oil revealed an increase in carbon number, CCS, and isomeric complexity, with more oxygenated species detected, as a function of the time the WAF was exposed to stimulated sunlight (Benigni et al., 2017).

For oil spill events occurring at sea, the application of dispersants, for example Corexit 9500, may be used to mitigate the short term impact; enabling the rapid diffusion of slicks and thereby limiting shoreline contamination (Prince, 2015). However, it has recently been suggested that Corexit 9500 increases the toxicity of spilt oil (Rico-Martínez et al., 2013), and CID-FTICR MS experiments have demonstrated the need to monitor compounds that may be Corexit-derived transformation products, particularly sulfur-containing species, in the environment (Seidel et al., 2016). In addition, a recent study using a range of analytical techniques, including FTICR MS analysis of DOM, has demonstrated that the use of Corexit 9500 impairs the activity of oil-degrading microorganisms in WAFs, used to simulate deepwater plumes (Kleindienst et al., 2015).

Bioremediation, defined as the use of microorganisms to convert organic pollutants to biomass, water and innocuous gases, is a process that can be utilized as it occurs naturally, or accelerated through the use of hydrophobic fertilizers (Ron and Rosenberg, 2014), without adversely affecting the environment. Although representing a low cost and economically viable means by which to improve the quality of contaminated soils, the low efficiency and sensitivity of microbial communities present some drawbacks to bioremediation (Lim et al., 2016). Petroleomic analyses continue to be applied to the study of hydrophobic soil extracts (Thomas et al., 2019) and OSPW (Peru et al., 2019), and so may

become more widely used to assess the efficacy of bioremediation processes at sites of anthropogenic contamination (Leshuk et al., 2018; Quagraine et al., 2005).

1.4 Aims of Thesis

Given the current state of the art in petroleomics methodologies and challenges identified by industrial and collaborative partners, the aims of the research presented in this thesis can be summarized as follows.

Provide a detailed, molecular-level, comparison between marine HFOs and their asphaltene fractions, such that bulk properties and characteristics, including asphaltene handling issues and differing responsiveness to additive chemistries, can be better understood and addressed.

Based on the demands of generating multiple complex data sets, develop novel means of visualization and apply statistical approaches to their representation and comparison to more rapidly identify and succinctly describe compositional features linked to observed differences in bulk properties and behaviors.

Through means of compositional analysis, also track changes in composition of lubricant base oils as they are oxidized, determining the efficacy of additive packages and exacerbation of oxidative processes in the presence of biofuel, and compare results from an expensive engine test to a bench top procedure.

To also determine the effect of the analytical procedure, including sample solvent system, pH, and injection flow rate, upon the observed compositional profile, as well as explore the improved capabilities offered by newly developed instrumentation for hyphenated GC-FTICR MS analyses, and to utilize advanced petroleomics methodologies for molecular-level profiling of environmental samples.

1.5 References

Abdi H, Williams LJ. Principal component analysis. Wiley Interdisciplinary Reviews: Computational Statistics 2010; 2: 433-459.

Aeppli C, Carmichael CA, Nelson RK, Lemkau KL, Graham WM, Redmond MC, et al. Oil Weathering after the Deepwater Horizon Disaster Led to the Formation of Oxygenated Residues. Environmental Science & Technology 2012; 46: 8799-8807.

Ahmed A, Cho Y, Giles K, Riches E, Lee JW, Kim HI, et al. Elucidating Molecular Structures of Nonalkylated and Short-Chain Alkyl (n < 5, (CH2)(n)) Aromatic Compounds in Crude Oils by a Combination of Ion Mobility and Ultrahigh-Resolution Mass Spectrometries and Theoretical Collisional Cross-Section Calculations. Analytical Chemistry 2014; 86: 3300-3307.

Ahmed A, Cho YJ, No MH, Koh J, Tomczyk N, Giles K, et al. Application of the Mason-Schamp Equation and Ion Mobility Mass Spectrometry To Identify Structurally Related Compounds in Crude Oil. Analytical Chemistry 2011; 83: 77-83.

Akbarzadeh K, Hammami A, Kharrat A, Zhang D, Allenson S, Creek J, et al. Asphaltenes - Problematic but Rich in Potential. Oilfield Review 2007; 19: 22-43.

Ali MA, Hassan A. Hydrocarbon Group Types Analysis of Petroleum Products: A Comparative Evaluation of HPLC And TLC Analytical Performance. Petroleum Science and Technology 2002; 20: 751-762.

Allan SE, Smith BW, Anderson KA. Impact of the Deepwater Horizon Oil Spill on Bioavailable Polycyclic Aromatic Hydrocarbons in Gulf of Mexico Coastal Waters. Environmental Science & Technology 2012; 46: 2033-2039.

Alvarez-Ramirez F, Ruiz-Morales Y. Island versus Archipelago Architecture for Asphaltenes: Polycyclic Aromatic Hydrocarbon Dimer Theoretical Studies. Energy & Fuels 2013; 27: 1791-1808.

Alves JC, Araujo RGO, de Souza ES, Soares SAR, Cerqueira JR, Garcia KS, et al. Geochemical Correlations Between Petroleum Samples from the Potiguar Basin and Definition of their Possible Generating Rocks. Quimica Nova 2018; 41: 417-428.

Analytical Methods Comm A. A 'Periodic Table' of mass spectrometry instrumentation and acronyms. Analytical Methods 2017; 9: 5086-5090.

Annesley TM. Ion suppression in mass spectrometry. Clinical Chemistry 2003; 49: 1041-1044.

Bae YJ, Kim MS. A Thermal Mechanism of Ion Formation in MALDI. Annual Review of Analytical Chemistry, Vol 8 2015; 8: 41-60.

Baldeschwieler JD. Ion Cyclotron Resonance Spectroscopy. Science 1968; 159: 263.

Bao XH, Ji YB, Hu Y, Zong Y. Geochemical characteristics, origins, and model of lacustrine source rocks in the Zhu 1 depression, eastern Pearl River Mouth Basin, South China Sea. Aapg Bulletin 2017; 101: 1543-1564.

Barman B, Cebolla V, Membrado L. Chromatographic Techniques for Petroleum and Related Products. Critical Reviews in Analytical Chemistry 2000; 30: 75-120.

Barrow M, Headley J, Peru K, Derrick P. Data Visualization for the Characterization of Naphthenic Acids within Petroleum Samples. Energy & Fuels 2009; 23: 2592-2599.

Barrow M, Witt M, Headley J, Peru K. Athabasca Oil Sands Process Water: Characterization by Atmospheric Pressure Photoionization and Electrospray Ionization Fourier Transform Ion Cyclotron Resonance Mass Spectrometry. Analytical Chemistry 2010; 82: 3727-3735.

Barrow MP, McDonnell LA, Feng XD, Walker J, Derrick PJ. Determination of the nature of naphthenic acids present in crude oils using nanospray Fourier transform ion cyclotron resonance mass spectrometry: The continued battle against corrosion. Analytical Chemistry 2003; 75: 860-866.

Barrow MP, Peru KM, Headley JV. An Added Dimension: GC Atmospheric Pressure Chemical Ionization FTICR MS and the Athabasca Oil Sands. Analytical Chemistry 2014; 86: 8281-8288.

Barrow MP, Peru KM, McMartin DW, Headley JV. Effects of Extraction pH on the Fourier Transform Ion Cyclotron Resonance Mass Spectrometry Profiles of Athabasca Oil Sands Process Water. Energy & Fuels 2016; 30: 3615-3621.

Becker JR. *Crude Oil Waxes, Emulsions, and Asphaltene*. Tulsa, OK: Pennwell Books, 1997.

Bell M, Blais JM. "-Omics" workflow for paleolimnological and geological archives: A review. Science of the Total Environment 2019; 672: 438-455.

Benassi M, Berisha A, Romao W, Babayev E, Rompp A, Spengler B. Petroleum crude oil analysis using low-temperature plasma mass spectrometry. Rapid Communications in Mass Spectrometry 2013; 27: 825-834.

Benigni P, DeBord J, Thompson C, Gardinali P, Fernandez-Lima F. Increasing Polyaromatic Hydrocarbon (PAH) Molecular Coverage during Fossil Oil Analysis by Combining Gas Chromatography and Atmospheric-Pressure Laser Ionization Fourier Transform Ion Cyclotron Resonance Mass Spectrometry (FT-ICR MS). Energy & Fuels 2016; 30: 196-203.

Benigni P, Sandoval K, Thompson CJ, Ridgeway ME, Park MA, Gardinali P, et al. Analysis of Photoirradiated Water Accommodated Fractions of Crude Oils Using Tandem TIMS and FT-ICR MS. Environmental Science & Technology 2017; 51: 5978-5988.

Berthod A, Ruiz-Angel MJ, Carda-Broch S. Recent advances on ionic liquid uses in separation techniques. Journal of Chromatography A 2018; 1559: 2-16.

Beyer J, Trannum HC, Bakke T, Hodson PV, Collier TK. Environmental effects of the Deepwater Horizon oil spill: A review. Marine Pollution Bulletin 2016; 110: 28-51.

Boduszynski MM. Composition of Heavy Petroleums 1. Molecular-Weight, Hydrogen Deficiency, and Heteroatom Concentration as a Function of Atmospheric Equivalent Boiling-Point Up To 1400-Degrees-F (760-Degrees-C). Energy & Fuels 1987; 1: 2-11.

Boldin IA, Nikolaev EN. Fourier transform ion cyclotron resonance cell with dynamic harmonization of the electric field in the whole volume by shaping of the excitation and detection electrode assembly. Rapid Communications in Mass Spectrometry 2011; 25: 122-126.

Bouslimani A, Sanchez LM, Garg N, Dorrestein PC. Mass spectrometry of natural products: current, emerging and future technologies. Natural Product Reports 2014; 31: 718-729.

Bowman DT, Jobst KJ, Ortiz X, Reiner EJ, Warren LA, McCarry BE, et al. Improved coverage of naphthenic acid fraction compounds by comprehensive two-dimensional gas chromatography coupled with high resolution mass spectrometry. Journal of Chromatography A 2018; 1536: 88-95.

Buckley JS, Wang J, Creek J. Solubility of the Least-Soluble Asphaltenes, 2007, pp. 401-437.

Burgoyne TW, Hieftje GM. An introduction to ion optics for the mass spectrograph. Mass Spectrometry Reviews 1996; 15: 241-259.

Burrowes A, Marsh R, Evans C, Teare M, Ramos S, Rahnama F, et al. Alberta's Energy Reserves 2008 and Supply/Demand Outlook 2009–2018. Energy Resources Conservation Board, Government of Alberta , Calgary, Alberta, Canada, 2009, pp. pp. 220.

Byer JD, Siek K, Jobst K. M Distinguishing the C-3 vs SH4 Mass Split by Comprehensive Two-Dimensional Gas Chromatography-High Resolution Time-of-Flight Mass Spectrometry. Analytical Chemistry 2016; 88: 6101-6104.

Byrdwell WC. Atmospheric pressure chemical ionization mass spectrometry for analysis of lipids. Lipids 2001; 36: 327-346.

Caravatti P, Allemann M. The Infinity Cell - A New Trapped-Ion Cell with Radiofrequency Covered Trapping Electrodes for Fourier-Transform Ion-Cyclotron Resonance Mass-Spectrometry. Organic Mass Spectrometry 1991; 26: 514-518.

Carrizo D, Domeno C, Nerin I, Alfaro P, Nerin C. Atmospheric pressure solid analysis probe coupled to quadrupole-time of flight mass spectrometry as a tool for screening and semi-quantitative approach of polycyclic aromatic hydrocarbons, nitro-polycyclic aromatic hydrocarbons and oxo-polycyclic aromatic hydrocarbons in complex matrices. Talanta 2015; 131: 175-184.

Chacon-Patino M, Rowland S, Rodgers R. Advances in Asphaltene Petroleomics. Part 1: Asphaltenes Are Composed of Abundant Island and Archipelago Structural Motifs. Energy & Fuels 2017; 31: 13509-13518.

Chen H, Hou AX, Corilo YE, Lin QX, Lu J, Mendelssohn IK, et al. 4 Years after the Deepwater Horizon Spill: Molecular Transformation of Macondo Well Oil in Louisiana Salt Marsh Sediments Revealed by FT-ICR Mass Spectrometry. Environmental Science & Technology 2016; 50: 9061-9069.

Chiaberge S, Fiorani T, Savoini A, Bionda A, Ramello S, Pastori M, et al. Classification of crude oil samples through statistical analysis of APPI FTICR mass spectra. Fuel Processing Technology 2013; 106: 181-185.

Cho E, Witt M, Hur M, Jung MJ, Kim S. Application of FT-ICR MS Equipped with Quadrupole Detection for Analysis of Crude Oil. Analytical Chemistry 2017; 89: 12101-12107.

Cho Y, Ahmed A, Islam A, Kim S. Developments in FT-ICR MS Instrumentation, Ionization Techniques, and Data Interpretation Methods for Petroleomics. Mass Spectrometry Reviews 2015; 34: 248-263.

Cho Y, Islam A, Ahmed A, Kim S. Application of comprehensive 2D GC-MS and APPI FT-ICR MS for more complete understanding of chemicals in diesel fuel. Vol 3, 2012a.

Cho Y, Jin J, Witt M, Birdwell J, Na J, Roh N, et al. Comparing Laser Desorption Ionization and Atmospheric Pressure Photoionization Coupled to Fourier Transform Ion Cyclotron Resonance Mass Spectrometry To Characterize Shale Oils at the Molecular Level. Energy & Fuels 2013; 27: 1830-1837.

Cho Y, Na J, Nho N, Kim S. Application of Saturates, Aromatics, Resins, and Asphaltenes Crude Oil Fractionation for Detailed Chemical Characterization of Heavy Crude Oils by Fourier Transform Ion Cyclotron

Resonance Mass Spectrometry Equipped with Atmospheric Pressure Photoionization. Energy & Fuels 2012b; 26: 2558-2565.

Cho Y, Qi YL, O'Connor PB, Barrow MP, Kim S. Application of Phase Correction to Improve the Interpretation of Crude Oil Spectra Obtained Using 7 T Fourier Transform Ion Cyclotron Resonance Mass Spectrometry. Journal of the American Society for Mass Spectrometry 2014a; 25: 154-157.

Cho Y, Witt M, Jin JM, Kim YH, Nho NS, Kim S. Evaluation of Laser Desorption Ionization Coupled to Fourier Transform Ion Cyclotron Resonance Mass Spectrometry To Study Metalloporphyrin Complexes. Energy & Fuels 2014b; 28: 6699-6706.

Cho YJ, Na JG, Nho NS, Kim S. Application of Saturates, Aromatics, Resins, and Asphaltenes Crude Oil Fractionation for Detailed Chemical Characterization of Heavy Crude Oils by Fourier Transform Ion Cyclotron Resonance Mass Spectrometry Equipped with Atmospheric Pressure Photoionization. Energy & Fuels 2012c; 26: 2558-2565.

Clemente JS, Prasad NGN, MacKinnon MD, Fedorak PM. A statistical comparison of naphthenic acids characterized by gas chromatography-mass spectrometry. Chemosphere 2003; 50: 1265-1274.

Cody RB, Laramee JA, Durst HD. Versatile new ion source for the analysis of materials in open air under ambient conditions. Analytical Chemistry 2005; 77: 2297-2302.

Comisarow MB, Marshall AG. Fourier-Transform Ion-Cyclotron Resonance Spectroscopy. Chemical Physics Letters 1974; 25: 282-283.

Constapel M, Schellentrager M, Schmitz OJ, Gab S, Brockmann KJ, Giese R, et al. Atmospheric-pressure laser ionization: a novel ionization method for liquid chromatography/mass spectrometry. Rapid Communications in Mass Spectrometry 2005; 19: 326-336.

Corilo YE, Podgorski DC, McKenna AM, Lemkau KL, Reddy CM, Marshall AG, et al. Oil Spill Source Identification by Principal Component Analysis of Electrospray Ionization Fourier Transform Ion Cyclotron Resonance Mass Spectra. Analytical Chemistry 2013; 85: 9064-9069.

Creary X, Mehrsheikhmohammadi ME, McDonald S. A Comparison of the Radical-Stabilizing Ability of Aromatic-Groups - Gamma-Values for Aromatic-Groups. Journal of Organic Chemistry 1989; 54: 2904-2910.

Crepier J, Le Masle A, Charon N, Albrieux F, Duchene P, Heinisch S. Ultra-high performance supercritical fluid chromatography hyphenated to atmospheric pressure chemical ionization high resolution mass spectrometry for the characterization of fast pyrolysis bio-oils. Journal of

Chromatography B-Analytical Technologies in the Biomedical and Life Sciences 2018; 1086: 38-46.

Cui XQ, Churchill GA. Statistical tests for differential expression in cDNA microarray experiments. Genome Biology 2003; 4.

Dempster AJ. A new Method of Positive Ray Analysis. Physical Review 1918; 11: 316-325.

Denisov E, Damoc E, Lange O, Makarov A. Orbitrap mass spectrometry with resolving powers above 1,000,000. International Journal of Mass Spectrometry 2012; 325: 80-85.

Drews A. Standard Test Method for Aromatic Types Analysis of Gas-Oil Aromatic Fractions by High Ionizing Voltage Mass Spectrometry

Manual on Hydrocarbon Analysis, 6th Edition. West Conshohocken, PA: ASTM International, 1998.

Durand E, Clemancey M, Lancelin JM, Verstraete J, Espinat D, Quoineaud AA. Effect of Chemical Composition on Asphaltenes Aggregation. Energy & Fuels 2010; 24: 1051-1062.

Dzidic I, Somerville AC, Raia JC, Hart HV. Determination of Naphthenic Acids in California Crudes and Refinery Wastewaters by Fluoride-Ion Chemical Ionization Mass-Spectrometry. Analytical Chemistry 1988; 60: 1318-1323.

Ekpo BO, Essien N, Neji PA, Etsenake RO. Geochemical fingerprinting of western offshore Niger Delta oils. Journal of Petroleum Science and Engineering 2018; 160: 452-464.

Eliuk S, Makarov A. Evolution of Orbitrap Mass Spectrometry Instrumentation. Annual Review of Analytical Chemistry, Vol 8 2015; 8: 61-80.

Fan TP. Characterization of Naphthenic Acids in Petroleum by Fast-Atom-Bombardment Mass-Spectrometry. Energy & Fuels 1991; 5: 371-375.

Farenc M, Corilo YE, Lalli PM, Riches E, Rodgers RP, Afonso C, et al. Comparison of Atmospheric Pressure Ionization for the Analysis of Heavy Petroleum Fractions with Ion Mobility-Mass Spectrometry. Energy & Fuels 2016; 30: 8896-8903.

Fenn JB, Mann M, Meng CK, Wong SF, Whitehouse CM. Electrospray Ionization for Mass-Spectrometry of Large Biomolecules. Science 1989; 246: 64-71.

Fernandez-Lima FA, Becker C, McKenna AM, Rodgers RP, Marshall AG, Russell DH. Petroleum Crude Oil Characterization by IMS-MS and FTICR MS. Analytical Chemistry 2009; 81: 9941-9947.

Fink J. Chapter 11 - Processes. In: Fink J, editor. Guide to the Practical Use of Chemicals in Refineries and Pipelines. Gulf Professional Publishing, Boston, 2016, pp. 185-223.

Gaspar A, Schrader W. Expanding the data depth for the analysis of complex crude oil samples by Fourier transform ion cyclotron resonance mass spectrometry using the spectral stitching method. Rapid Communications in Mass Spectrometry 2012; 26: 1047-1052.

Gaspar A, Zellermann E, Lababidi S, Reece J, Schrader W. Characterization of Saturates, Aromatics, Resins, and Asphaltenes Heavy Crude Oil Fractions by Atmospheric Pressure Laser Ionization Fourier Transform Ion Cyclotron Resonance Mass Spectrometry. Energy & Fuels 2012; 26: 3481-3487.

Gavard R, Rossell D, Spencer SEF, Barrow MP. Themis: Batch Preprocessing for Ultrahigh-Resolution Mass Spectra of Complex Mixtures. Analytical Chemistry 2017; 89: 11383-11390.

Geissler R, Saraji-Bozorgzad M, Streibel T, Kaisersberger E, Denner T, Zimmermann R. Investigation of different crude oils applying thermal analysis/mass spectrometry with soft photoionisation. Journal of Thermal Analysis and Calorimetry 2009; 96: 813-820.

Goode GC, O'Malley RM, Ferrer-Correia AJ, Jennings KR. Ion Cyclotron Resonance Mass Spectrometry. Nature 1970; 227: 1093-1097.

Gray MR. Consistency of asphaltene chemical structures with pyrolysis and coking behavior. Energy & Fuels 2003; 17: 1566-1569.

Griffiths M, Da Campo R, O'Connor P, Barrow M. Throwing Light on Petroleum: Simulated Exposure of Crude Oil to Sunlight and Characterization Using Atmospheric Pressure Photoionization Fourier Transform Ion Cyclotron Resonance Mass Spectrometry. Analytical Chemistry 2014; 86: 527-534.

Guan SH, Marshall AG, Scheppele SE. Resolution and chemical formula identification of aromatic hydrocarbons and aromatic compounds containing sulfur, nitrogen, or oxygen in petroleum distillates and refinery streams. Analytical Chemistry 1996; 68: 46-71.

Guillemant J, Albrieux F, de Oliveira LP, Lacoue-Negre M, Duponchel L, Joly JF. Insights from Nitrogen Compounds in Gas Oils Highlighted by High-Resolution Fourier Transform Mass Spectrometry. Analytical Chemistry 2019; 91: 12644-12652.

Halff A, Younes L, Boersma T. The likely implications of the new IMO standards on the shipping industry. Energy Policy 2019; 126: 277-286.

Hammami A, Phelps CH, Monger-McClure T, Little TM. Asphaltene Precipitation from Live Oils: An Experimental Investigation of Onset Conditions and Reversibility. Energy & Fuels 2000; 14: 14-18.

Handle F, Harir M, Fussl J, Kosyun AN, Grossegger D, Hertkorn N, et al. Tracking Aging of Bitumen and Its Saturate, Aromatic, Resin, and Asphaltene Fractions Using High-Field Fourier Transform Ion Cyclotron Resonance Mass Spectrometry. Energy & Fuels 2017; 31: 4771-4779.

Hanold KA, Fischer SM, Cormia PH, Miller CE, Syage JA. Atmospheric pressure photoionization. 1. General properties for LC/MS. Analytical Chemistry 2004; 76: 2842-2851.

Harper JD, Charipar NA, Mulligan CC, Zhang XR, Cooks RG, Ouyang Z. Low-Temperature Plasma Probe for Ambient Desorption Ionization. Analytical Chemistry 2008; 80: 9097-9104.

Harrison AG. *Chemical Ionization Mass Spectrometry*: Taylor & Francis, 1992.

Hart A. A review of technologies for transporting heavy crude oil and bitumen via pipelines. Journal of Petroleum Exploration and Production Technology 2014; 4: 327-336.

Hawkes J, Patriarca C, J. R. Sjöberg P, Tranvik L, Bergquist J. Extreme isomeric complexity of dissolved organic matter found across aquatic environments: Extreme isomeric complexity of DOM. Limnology and Oceanography Letters 2018; 3.

Headley J, Barrow M, Peru K, Fahlman B, Frank R, Bickerton G, et al. Preliminary fingerprinting of Athabasca oil sands polar organics in environmental samples using electrospray ionization Fourier transform ion cyclotron resonance mass spectrometry. Rapid Communications in Mass Spectrometry 2011; 25: 1899-1909.

Headley J, Peru K, Barrow M. Mass Spectrometric Characterization of Naphthenic Acids in Environmental Samples: A RevieW. Mass Spectrometry Reviews 2009; 28: 121-134.

Headley J, Peru K, Barrow M, Derrick P. Characterization of naphthenic acids from Athabasca oil sands using electrospray ionization: The significant influence of solvents. Analytical Chemistry 2007; 79: 6222-6229.

Headley J, Peru K, Mohamed M, Frank R, Martin J, Hazewinkel R, et al. Chemical fingerprinting of naphthenic acids and oil sands process watersA review of analytical methods for environmental samples. Journal of Environmental Science and Health Part a-Toxic/hazardous Substances & Environmental Engineering 2013; 48: 1145-1163.

Headley JV, Peru KM, Barrow MP. Advances in mass spectrometric characterization of naphthenic acids fraction compounds in oil sands environmental samples and crude oil-A review. Mass Spectrometry Reviews 2016; 35: 311-328.

Herrera LC, Grossert JS, Ramaley L. Quantitative Aspects of and Ionization Mechanisms in Positive-Ion Atmospheric Pressure Chemical Ionization Mass Spectrometry. Journal of the American Society for Mass Spectrometry 2008; 19: 1926-1941.

Hertkorn N, Ruecker C, Meringer M, Gugisch R, Frommberger M, Perdue EM, et al. High-precision frequency measurements: indispensable tools at the core of the molecular-level analysis of complex systems. Analytical and Bioanalytical Chemistry 2007; 389: 1311-1327.

Hindle R, Noestheden M, Peru K, Headley J. Quantitative analysis of naphthenic acids in water by liquid chromatography–accurate mass time-of-flight mass spectrometry. Journal of Chromatography A 2013; 1286: 166-174.

Hipple JA, Sommer H, Thomas HA. A Precise Method of Determining the Faraday by Magnetic Resonance. Physical Review 1949; 76: 1877-1878.

Hirsch RL, Bezdek R, Wendling R. Peaking of world oil production and its mitigation. Aiche Journal 2006; 52: 2-8.

Hotelling H. Analysis of a complex of statistical variables into principal components. Journal of Educational Psychology 1933; 24: 417-441.

Houda S, Lancelot C, Blanchard P, Poinel L, Lamonier C. Oxidative Desulfurization of Heavy Oils with High Sulfur Content: A Review. Catalysts 2018; 8.

Hsu C, Hendrickson C, Rodgers R, McKenna A, Marshall A. Petroleomics: advanced molecular probe for petroleum heavy ends. Journal of Mass Spectrometry 2011; 46: 337-343.

Hsu C, Walters C, H. Isaksen G, E. Schaps M, Peters K. Biomarker Analysis in Petroleum Exploration, 2003, pp. 223-245.

Hsu CS, Dechert GJ, Robbins WK, Fukuda EK. Naphthenic acids in crude oils characterized by mass spectrometry. Energy & Fuels 2000; 14: 217-223.

Hsu CS, Qian KN, Chen YNC. An Innovative Approach to Data-Analysis in Hydrocarbon Characterization by Online Liquid-Chromatography Mass-Spectrometry. Analytica Chimica Acta 1992; 264: 79-89.

Huba AK, Huba K, Gardinali PR. Understanding the atmospheric pressure ionization of petroleum components: The effects of size, structure, and presence of heteroatoms. Science of the Total Environment 2016; 568: 1018-1025.

Hughey C, Hendrickson C, Rodgers R, Marshall A, Qian K. Kendrick mass defect spectrum: A compact visual analysis for ultrahigh-resolution broadband mass spectra. Analytical Chemistry 2001; 73: 4676-4681.

Hughey CA, Rodgers RP, Marshall AG, Qian KN, Robbins WK. Identification of acidic NSO compounds in crude oils of different geochemical origins by negative ion electrospray Fourier transform ion cyclotron resonance mass spectrometry. Organic Geochemistry 2002; 33: 743-759.

Hunt JM. Petroleum Geochemistry and Geology. New York: W. H. Freeman, 1995.

Hur M, Ware RL, Park J, McKenna AM, Rodgers RP, Nikolau BJ, et al. Statistically Significant Differences in Composition of Petroleum Crude Oils Revealed by Volcano Plots Generated from Ultrahigh Resolution Fourier Transform Ion Cyclotron Resonance Mass Spectra. Energy & Fuels 2018; 32: 1206-1212.

Hur M, Yeo I, Park E, Kim Y, Yoo J, Kim E, et al. Combination of Statistical Methods and Fourier Transform Ion Cyclotron Resonance Mass Spectrometry for More Comprehensive, Molecular-Level Interpretations of Petroleum Samples. Analytical Chemistry 2010; 82: 211-218.

Islam A, Ahmed A, Hur M, Thorn K, Kim S. Molecular-level evidence provided by ultrahigh resolution mass spectrometry for oil-derived doc in groundwater at Bemidji, Minnesota. Journal of Hazardous Materials 2016; 320: 123-132.

Islam A, Cho Y, Yim UH, Shim WJ, Kim YH, Kim S. The comparison of naturally weathered oil and artificially photo-degraded oil at the molecular level by a combination of SARA fractionation and FT-ICR MS. Journal of Hazardous Materials 2013; 263: 404-411.

Ismail A, Toriman ME, Juahir H, Kassim AM, Zain SM, Ahmad WKW, et al. Chemometric techniques in oil classification from oil spill fingerprinting. Marine Pollution Bulletin 2016; 111: 339-346.

Javadli R, de Klerk A. Desulfurization of heavy oil. Applied Petrochemical Research 2012; 1: 3-19.

Jennings KR. Collision-induced decompositions of aromatic molecular ions. International Journal of Mass Spectrometry and Ion Physics 1968; 1: 227-235.

Kafer U, Groger T, Ruger CP, Czech H, Saraji-Bozorgzad M, Wilharm T, et al. Direct inlet probe - High-resolution time-of-flight mass spectrometry as fast technique for the chemical description of complex high-boiling samples. Talanta 2019; 202: 308-316.

Kanaujia PK, Sharma YK, Agrawal UC, Garg MO. Analytical approaches to characterizing pyrolysis oil from biomass. Trac-Trends in Analytical Chemistry 2013; 42: 125-136.

Kanu AB, Dwivedi P, Tam M, Matz L, Hill HH. Ion mobility-mass spectrometry. Journal of Mass Spectrometry 2008; 43: 1-22.

Karas M, Bachmann D, Bahr U, Hillenkamp F. Matrix-Assisted Ultraviolet-Laser Desorption of Nonvolatile Compounds. International Journal of Mass Spectrometry and Ion Processes 1987; 78: 53-68.

Kendrick E. A Mass Scale Based on CH2 = 14.0000 for High Resolution Mass Spectrometry of Organic Compounds. Analytical Chemistry 1963; 35: 2146-2154.

Kim D, Jin JM, Cho Y, Kim EH, Cheong HK, Kim YH, et al. Combination of ring type HPLC separation, ultrahigh-resolution mass spectrometry, and high field NMR for comprehensive characterization of crude oil compositions. Fuel 2015; 157: 48-55.

Kim D, Kim S, Son S, Jung M-J, Kim S. Application of Online Liquid Chromatography 7 T FT-ICR Mass Spectrometer Equipped with Quadrupolar Detection for Analysis of Natural Organic Matter. Analytical Chemistry 2019; 91: 7690-7697.

Kim S, Kramer RW, Hatcher PG. Graphical method for analysis of ultrahigh-resolution broadband mass spectra of natural organic matter, the van Krevelen diagram. Analytical Chemistry 2003; 75: 5336-5344.

Kim YH, Kim S. Improved Abundance Sensitivity of Molecular Ions in Positive-Ion APCI MS Analysis of Petroleum in Toluene. Journal of the American Society for Mass Spectrometry 2010; 21: 386-392.

Klein GC, Kim S, Rodgers RP, Marshall AG, Yen A. Mass spectral analysis of asphaltenes. II. Detailed compositional comparison of asphaltenes deposit to its crude oil counterpart for two geographically different crude oils by ESI FT-ICR MS. Energy & Fuels 2006a; 20: 1973-1979.

Klein GC, Rodgers RP, Marshall AG. Identification of hydrotreatment-resistant heteroatomic species in a crude oil distillation cut by electrospray ionization FT-ICR mass spectrometry. Fuel 2006b; 85: 2071-2080.

Kleindienst S, Seidel M, Ziervogel K, Grim S, Loftis K, Harrison S, et al. Chemical dispersants can suppress the activity of natural oil-degrading microorganisms. Proceedings of the National Academy of Sciences 2015; 112: 14900.

Klitzke CF, Corilo YE, Siek K, Binkley J, Patrick J, Eberlin MN. Petroleomics by Ultrahigh-Resolution Time-of-Flight Mass Spectrometry. Energy & Fuels 2012; 26: 5787-5794.

Kondyli A, Schrader W. High-resolution GC/MS studies of a light crude oil fraction. Journal of Mass Spectrometry 2019; 54: 47-54.

Koons CB, Pancirov RJ. Isoprenoid Isoparaffins in Crude Oils From C5 To C21 - Analyses and Significance to Origin of Petroleum - Petr. Abstracts of Papers of the American Chemical Society 1970: 4.

Kostyukevich YI, Vladimirov GN, Nikolaev EN. Dynamically Harmonized FT-ICR Cell with Specially Shaped Electrodes for Compensation of Inhomogeneity of the Magnetic Field. Computer Simulations of the Electric Field and Ion Motion Dynamics. Journal of the American Society for Mass Spectrometry 2012; 23: 2198-2207.

Krajewski LC, Lobodin VV, Johansen C, Bartges TE, Maksimova EV, MacDonald IR, et al. Linking Natural Oil Seeps from the Gulf of Mexico to Their Origin by Use of Fourier Transform Ion Cyclotron Resonance Mass Spectrometry. Environmental Science & Technology 2018; 52: 1365-1374.

Krajewski LC, Rodgers RP, Marshall AG. 126 264 Assigned Chemical Formulas from an Atmospheric Pressure Photoionization 9.4 T Fourier Transform Positive Ion Cyclotron Resonance Mass Spectrum. Analytical Chemistry 2017; 89: 11318-11324.

Lalli PM, Corilo YE, Rowland SM, Marshall AG, Rodgers RP. Isomeric Separation and Structural Characterization of Acids in Petroleum by Ion Mobility Mass Spectrometry. Energy & Fuels 2015; 29: 3626-3633.

Lawrence EO, Livingston MS. The Production of High Speed Light Ions Without the Use of High Voltages. Physical Review 1932; 40: 19-35.

Le Guern M, Chailleux E, Farcas F, Dreessen S, Mabille I. Physico-chemical analysis of five hard bitumens: Identification of chemical species and molecular organization before and after artificial aging. Fuel 2010; 89: 3330-3339.

Lemkau KL, McKenna AM, Podgorski DC, Rodgers RP, Reddy CM. Molecular Evidence of Heavy-Oil Weathering Following the M/V Cosco Busan Spill: Insights from Fourier Transform Ion Cyclotron Resonance Mass Spectrometry. Environmental Science & Technology 2014; 48: 3760-3767.

Leshuk T, Peru KM, Livera DD, Tripp A, Bardo P, Headley JV, et al. Petroleomic analysis of the treatment of naphthenic organics in oil sands process-affected water with buoyant photocatalysts. Water Research 2018; 141: 297-306.

Leyva D, Tose LV, Porter J, Wolff J, Jaffé R, Fernandez-Lima F. Understanding the structural complexity of dissolved organic matter: isomeric diversity. Faraday Discussions 2019.

Li W. Volcano Plots in Analyzing Differential Expressions with MRNA Microarrays. Journal of Bioinformatics and Computational Biology 2012; 10.

Lim MW, Lau EV, Poh PE. A comprehensive guide of remediation technologies for oil contaminated soil — Present works and future directions. Marine Pollution Bulletin 2016; 109: 14-45.

Little DP, Speir JP, Senko MW, Oconnor PB, McLafferty FW. Infrared Multiphoton Dissociation of Large Multiply-Charged Ions for Biomolecule Sequencing. Analytical Chemistry 1994; 66: 2809-2815.

Liu ZY, Phillips JB. Comprehensive 2-Dimensional Gas-Chromatography Using an On-Column Thermal Modulator Interface. Journal of Chromatographic Science 1991; 29: 227-231.

Lozano DCP, Orrego-Ruiz JA, Barrow MP, Hernandez RC, Mejia-Ospino E. Analysis of the molecular weight distribution of vacuum residues and their molecular distillation fractions by laser desorption ionization mass spectrometry. Fuel 2016; 171: 247-252.

Lozano DCP, Orrego-Ruiz JA, Hernandez RC, Guerrero JE, Mejia-Ospino E. APPI(+)-FTICR mass spectrometry coupled to partial least squares with genetic algorithm variable selection for prediction of API gravity and CCR of crude oil and vacuum residues. Fuel 2017; 193: 39-44.

Lumpkin HE. Low Voltage Techniques in High Molecular Weight Mass Spectrometry. Analytical Chemistry 1958; 30: 321-325.

Makarov A. Electrostatic axially harmonic orbital trapping: A high-performance technique of mass analysis. Analytical Chemistry 2000; 72: 1156-1162.

Marentette JR, Frank RA, Bartlett AJ, Gillis PL, Hewitt LM, Peru KM, et al. Toxicity of naphthenic acid fraction components extracted from fresh and aged oil sands process-affected waters, and commercial naphthenic acid mixtures, to fathead minnow (Pimephales promelas) embryos. Aquatic Toxicology 2015; 164: 108-117.

Mariani TJ, Budhraja V, Mecham BH, Gu CC, Watson MA, Sadovsky Y. A variable fold-change threshold determines significance for expression microarrays. Faseb Journal 2002; 16: 321-+.

Marriott PJ, Massil T, Hugel H. Molecular structure retention relationships in comprehensive two-dimensional gas chromatography. Journal of Separation Science 2004; 27: 1273-1284.

Marshall A, Hendrickson C, Jackson G. Fourier transform ion cyclotron resonance mass spectrometry: A primer. Mass Spectrometry Reviews 1998; 17: 1-35.

Marshall A, Rodgers R. Petroleomics: The next grand challenge for chemical analysis. Accounts of Chemical Research 2004; 37: 53-59.

Marshall A, Rodgers R. Petroleomics: Chemistry of the underworld. Proceedings of the National Academy of Sciences of the United States of America 2008; 105: 18090-18095.

Martin JW. The Challenge: Safe release and reintegration of oil sands process-affected water. Environmental Toxicology and Chemistry 2015; 34: 2682-2682.

McEwen CN, McKay RG, Larsen BS. Analysis of solids, liquids, and biological tissues using solids probe introduction at atmospheric pressure on commercial LC/MS instruments. Analytical Chemistry 2005; 77: 7826-7831.

McLafferty FW, Bryce TA. Metastable-ion characteristics: characterization of isomeric molecules. Chemical Communications (London) 1967: 1215-1217.

Mead WL. Field ionization mass spectrometry of heavy petroleum fractions. Waxes. Analytical Chemistry 1968; 40: 743-747.

Michalski A, Damoc E, Lange O, Denisov E, Nolting D, Muller M, et al. Ultra High Resolution Linear Ion Trap Orbitrap Mass Spectrometer (Orbitrap Elite) Facilitates Top Down LC MS/MS and Versatile Peptide Fragmentation Modes. Molecular & Cellular Proteomics 2012; 11.

Mullins OC. Petroleomics and Structure–Function Relations of Crude Oils and Asphaltenes. In: Mullins OC, Sheu EY, Hammami A, Marshall AG, editors. Asphaltenes, Heavy Oils, and Petroleomics. Springer New York, New York, NY, 2007, pp. 1-16.

Mullins OC. Review of the molecular structure and aggregation of asphaltenes and petroleomics. Spe Journal 2008; 13: 48-57.

Mullins OC. The Asphaltenes. In: Cooks RG, Yeung ES, editors. Annual Review of Analytical Chemistry, Vol 4. 4, 2011, pp. 393-418.

Murray J, King D. Oil's tipping point has passed. Nature 2012; 481: 433.

Natter M, Keevan J, Wang Y, Keimowitz AR, Okeke BC, Son A, et al. Level and Degradation of Deepwater Horizon Spilled Oil in Coastal Marsh Sediments and Pore-Water. Environmental Science & Technology 2012; 46: 5744-5755.

Nikolaev EN, Jertz R, Grigoryev A, Baykut G. Fine Structure in Isotopic Peak Distributions Measured Using a Dynamically Harmonized Fourier Transform Ion Cyclotron Resonance Cell at 7 T. Analytical Chemistry 2012; 84: 2275-2283.

Nikolaev EN, Kostyukevich YI, Vladimirov GN. Fourier transform ion cyclotron resonance (FT ICR) mass spectrometry: Theory and simulations. Mass Spectrometry Reviews 2016; 35: 219-258.

Niyonsaba E, Manheim JM, Yerabolu R, Kenttämaa HI. Recent Advances in Petroleum Analysis by Mass Spectrometry. Analytical Chemistry 2019; 91: 156-177.

Nyadong L, Lai JF, Thompsen C, LaFrancois CJ, Cai XH, Song CX, et al. High-Field Orbitrap Mass Spectrometry and Tandem Mass Spectrometry for Molecular Characterization of Asphaltenes. Energy & Fuels 2018; 32: 294-305.

Palacio Lozano DC, Gavard R, Arenas-Diaz JP, Thomas MJ, Stranz DD, Mejía-Ospino E, et al. Pushing the analytical limits: new insights into complex mixtures using mass spectra segments of constant ultrahigh resolving power. Chemical Science 2019.

Palacio Lozano DC, Ramírez CX, Sarmiento Chaparro JA, Thomas MJ, Gavard R, Jones HE, et al. Characterization of bio-crude components derived from pyrolysis of soft wood and its esterified product by ultrahigh resolution mass spectrometry and spectroscopic techniques. Fuel 2020; 259: 116085.

Pan Y, Ridge DP, Rockwood AL. Harmonic Signal Enhancement in Ion-Cyclotron Resonance Mass-Spectrometry using Multiple Electrode Detection. International Journal of Mass Spectrometry and Ion Processes 1988; 84: 293-304.

Paul W, Steinwedel HS. Apparatus for separating charged particles of different specific charges, USA, 1960.

Payne AH, Glish GL. Thermally assisted infrared multiphoton photodissociation in a quadrupole ion trap. Analytical Chemistry 2001; 73: 3542-3548.

Pereira AS, Martin JW. Exploring the complexity of oil sands process-affected water by high efficiency supercritical fluid chromatography/orbitrap mass spectrometry. Rapid Communications in Mass Spectrometry 2015; 29: 735-744.

Peru KM, Thomas MJ, Palacio Lozano DC, McMartin DW, Headley JV, Barrow MP. Characterization of oil sands naphthenic acids by negative-ion electrospray ionization mass spectrometry: Influence of acidic versus basic transfer solvent. Chemosphere 2019; 222: 1017-1024.

Pilarova V, Plachka K, Khalikova MA, Svec F, Novakova L. Recent developments in supercritical fluid chromatography - mass spectrometry: Is it a viable option for analysis of complex samples? Trac-Trends in Analytical Chemistry 2019; 112: 212-225.

Popov IA, Nagornov K, Vladimirov GN, Kostyukevich YI, Nikolaev EN. Twelve Million Resolving Power on 4.7 T Fourier Transform Ion Cyclotron Resonance Instrument with Dynamically Harmonized Cell-Observation of Fine Structure in Peptide Mass Spectra. Journal of the American Society for Mass Spectrometry 2014; 25: 790-799.

Prado GHC, Rao Y, de Klerk A. Nitrogen Removal from Oil: A Review. Energy & Fuels 2017; 31: 14-36.

Prince RC. Oil Spill Dispersants: Boon or Bane? Environmental Science & Technology 2015; 49: 6376-6384.

Purcell JM, Juyal P, Kim DG, Rodgers RP, Hendrickson CL, Marshall AG. Sulfur speciation in petroleum: Atmospheric pressure photoionization or chemical derivatization and electrospray ionization fourier transform ion cyclotron resonance mass spectrometry. Energy & Fuels 2007a; 21: 2869-2874.

Purcell JM, Rodgers RP, Hendrickson CL, Marshall AG. Speciation of nitrogen containing aromatics by atmospheric pressure photoionization or electrospray ionization Fourier transform ion cyclotron resonance mass spectrometry. Journal of the American Society for Mass Spectrometry 2007b; 18: 1265-1273.

Qi Y, O'Connor P. Data processing in Fourier transform ion cyclotron resonance mass spectrometry. Mass Spectrometry Reviews 2014; 33: 333-352.

Qi YL, Barrow MP, Li HL, Meier JE, Van Orden SL, Thompson CJ, et al. Absorption-Mode: The Next Generation of Fourier Transform Mass Spectra. Analytical Chemistry 2012a; 84: 2923-2929.

Qi YL, Li HL, Wills RH, Perez-Hurtado P, Yu X, Kilgour DPA, et al. Absorption-Mode Fourier Transform Mass Spectrometry: The Effects of Apodization and Phasing on Modified Protein Spectra. Journal of the American Society for Mass Spectrometry 2013; 24: 828-834.

Qi YL, Thompson CJ, Van Orden SL, O'Connor PB. Phase Correction of Fourier Transform Ion Cyclotron Resonance Mass Spectra Using MatLab. Journal of the American Society for Mass Spectrometry 2011; 22: 138-147.

Qi YL, Witt M, Jertz R, Baykut G, Barrow MP, Nikolaev EN, et al. Absorption-mode spectra on the dynamically harmonized Fourier transform ion cyclotron resonance cell. Rapid Communications in Mass Spectrometry 2012b; 26: 2021-2026.

Qian K, Robbins W, Hughey C, Cooper H, Rodgers R, Marshall A. Resolution and identification of elemental compositions for more than 3000 crude acids in heavy petroleum by negative-ion microelectrospray high-field Fourier

transform ion cyclotron resonance mass spectrometry. Energy & Fuels 2001; 15: 1505-1511.

Quagraine EK, Peterson HG, Headley JV. In Situ Bioremediation of Naphthenic Acids Contaminated Tailing Pond Waters in the Athabasca Oil Sands Region—Demonstrated Field Studies and Plausible Options: A Review. Journal of Environmental Science and Health, Part A 2005; 40: 685-722.

Rahimi P, Ovalles C, Zhang Y, Adams JJ. Chemistry Solutions to Challenges in the Petroleum Industry: American Chemical Society, 2019.

Raki L, Masson JF, Collins P. Rapid bulk fractionation of maltenes into saturates, aromatics, and resins by flash chromatography. Energy & Fuels 2000; 14: 160-163.

Ratsameepakai W, Hemiman JM, Jenkins TJ, Langley GJ. Evaluation of Ultrahigh-Performance Supercritical Fluid Chromatography-Mass Spectrometry as an Alternative Approach for the Analysis of Fatty Acid Methyl Esters in Aviation Turbine Fuel. Energy & Fuels 2015; 29: 2485-2492.

Ren LM, Han YH, Zhang YH, Zhang YF, Meng XH, Shi Q. Spray Injection Direct Analysis in Real Time (DART) Ionization for Petroleum Analysis. Energy & Fuels 2016; 30: 4486-4493.

Reuter JH, Perdue EM. A chemical structural model of early diagenesis of sedimentary humus (proto-kerogens). Mitt. Geol.-Palaont. Inst., Univ. Hamburg 1984; 56: 249-262.

Rico-Martínez R, Snell TW, Shearer TL. Synergistic toxicity of Macondo crude oil and dispersant Corexit 9500A® to the Brachionus plicatilis species complex (Rotifera). Environmental Pollution 2013; 173: 5-10.

Ridgeway ME, Lubeck M, Jordens J, Mann M, Park MA. Trapped ion mobility spectrometry: A short review. International Journal of Mass Spectrometry 2018; 425: 22-35.

Rivas-Ubach A, Liu YN, Bianchi TS, Tolic N, Jansson C, Pasa-Tolic L. Moving beyond the van Krevelen Diagram: A New Stoichiometric Approach for Compound Classification in Organisms. Analytical Chemistry 2018; 90: 6152-6160.

Robb DB, Covey TR, Bruins AP. Atmospheric pressure photoionisation: An ionization method for liquid chromatography-mass spectrometry. Analytical Chemistry 2000; 72: 3653-3659.

Rodgers RP, Mapolelo Mmilili M, Robbins WK, Chacón-Patiño ML, Putman JC, Niles SF, et al. Combating selective ionization in the high resolution mass spectral characterization of complex mixtures. Faraday Discussions 2019.

Romao W, Tose LV, Vaz BG, Sama SG, Lobinski R, Giusti P, et al. Petroleomics by Direct Analysis in Real Time-Mass Spectrometry. Journal of the American Society for Mass Spectrometry 2016; 27: 182-185.

Ron EZ, Rosenberg E. Enhanced bioremediation of oil spills in the sea. Current Opinion in Biotechnology 2014; 27: 191-194.

RosellMele A, Carter JF, Maxwell JR. High-performance liquid chromatography mass spectrometry of porphyrins by using an atmospheric pressure interface. Journal of the American Society for Mass Spectrometry 1996; 7: 965-971.

Rowland SJ, West CE, Scarlett AG, Jones D. Identification of individual acids in a commercial sample of naphthenic acids from petroleum by two-dimensional comprehensive gas chromatography/mass spectrometry. Rapid Communications in Mass Spectrometry 2011; 25: 1741-1751.

Ruddy B, Huettel M, Kostka J, Lobodin V, Bythell B, McKenna A, et al. Targeted Petroleomics: Analytical Investigation of Macondo Well Oil Oxidation Products from Pensacola Beach. Energy & Fuels 2014; 28: 4043-4050.

Rueda-Velasquez RI, Freund H, Qian KN, Olmstead WN, Gray MR. Characterization of Asphaltene Building Blocks by Cracking under Favorable Hydrogenation Conditions. Energy & Fuels 2013; 27: 1817-1829.

Ruger CP, Neumann A, Sklorz M, Schwemer T, Zimmermann R. Thermal Analysis Coupled to Ultrahigh Resolution Mass Spectrometry with Collision Induced Dissociation for Complex Petroleum Samples: Heavy Oil Composition and Asphaltene Precipitation Effects. Energy & Fuels 2017; 31: 13144-13158.

Sama SG, Farenc M, Barrere-Mangote C, Lobinski R, Afonso C, Bouyssiere B, et al. Molecular Fingerprints and Speciation of Crude Oils and Heavy Fractions Revealed by Molecular and Elemental Mass Spectrometry: Keystone between Petroleomics, Metallopetroleomics, and Petrointeractomics. Energy & Fuels 2018; 32: 4593-4605.

Santos J, Galaverna R, Pudenzi M, Schmidt E, Sanders N, Kurulugama R, et al. Petroleomics by ion mobility mass spectrometry: resolution and characterization of contaminants and additives in crude oils and petrofuels. Analytical Methods 2015; 7: 4450-4463.

Saraçli S, Doğan N, Doğan İ. Comparison of hierarchical cluster analysis methods by cophenetic correlation. Journal of Inequalities and Applications 2013; 2013: 203.

Schaub TM, Hendrickson CL, Qian KN, Quinn JP, Marshall AG. High-resolution field desorption/ionization Fourier transform ion cyclotron resonance

mass analysis of nonpolar molecules. Analytical Chemistry 2003; 75: 2172-2176.

Schmidt EM, Pudenzi MA, Santos JM, Angolini CFF, Pereira RCL, Rocha YS, et al. Petroleomics via Orbitrap mass spectrometry with resolving power above 1 000 000 at m/z 200. Rsc Advances 2018; 8: 6183-6191.

Schrader W, Panda SK, Brockmann KJ, Benter T. Characterization of non-polar aromatic hydrocarbons in crude oil using atmospheric pressure laser ionization and Fourier transform ion cyclotron resonance mass spectrometry (APLI FT-ICR MS). Analyst 2008; 133: 867-869.

Schuler B, Meyer G, Pena D, Mullins OC, Gross L. Unraveling the Molecular Structures of Asphaltenes by Atomic Force Microscopy. Journal of the American Chemical Society 2015; 137: 9870-9876.

Schweikhard L. Theory of Quadrupole Detection Fourier Transform Ion Cyclotron-Resonance. International Journal of Mass Spectrometry and Ion Processes 1991; 107: 281-292.

Schwemer T, Ruger CP, Sklorz M, Zimmermann R. Gas Chromatography Coupled to Atmospheric Pressure Chemical Ionization FT-ICR Mass Spectrometry for Improvement of Data Reliability. Analytical Chemistry 2015; 87: 11957-11961.

Seidel M, Kleindienst S, Dittmar T, Joye SB, Medeiros PM. Biodegradation of crude oil and dispersants in deep seawater from the Gulf of Mexico: Insights from ultra-high resolution mass spectrometry. Deep Sea Research Part II: Topical Studies in Oceanography 2016; 129: 108-118.

Shaw J, Lin T, Leach F, Tolmachev A, Tolic N, Robinson E, et al. 21 Tesla Fourier Transform Ion Cyclotron Resonance Mass Spectrometer Greatly Expands Mass Spectrometry Toolbox. Journal of the American Society For Mass Spectrometry 2016; 27: 1929-1936.

Sheu EY, Storm DA. Colloidal Properties of Asphaltenes in Organic Solvents. In: Sheu EY, Mullins OC, editors. Asphaltenes: Fundamentals and Applications. Springer US, Boston, MA, 1995, pp. 1-52.

Shi Q, Hou DJ, Chung KH, Xu CM, Zhao SQ, Zhang YH. Characterization of Heteroatom Compounds in a Crude Oil and Its Saturates, Aromatics, Resins, and Asphaltenes (SARA) and Non-basic Nitrogen Fractions Analyzed by Negative-Ion Electrospray Ionization Fourier Transform Ion Cyclotron Resonance Mass Spectrometry. Energy & Fuels 2010; 24: 2545-2553.

Silva SL, Silva AMS, Ribeiro JC, Martins FG, Da Silva FA, Silva CM. Chromatographic and spectroscopic analysis of heavy crude oil mixtures

with emphasis in nuclear magnetic resonance spectroscopy: A review. Analytica Chimica Acta 2011; 707: 18-37.

Simoneit BR, Schnoes HK, Haug P, Burlingame AL. Nitrogenous Compounds of Colorado Green-River Formation Oil Shale - A Preliminary Analysis By Mass Spectrometry. Nature 1970; 226: 75.

Slavcheva E, Shone B, Turnbull A. Review of naphthenic acid corrosion in oil refining. British Corrosion Journal 1999; 34: 125-131.

Smith DF, Podgorski DC, Rodgers RP, Blakney GT, Hendrickson CL. 21 Tesla FT-ICR Mass Spectrometer for Ultrahigh-Resolution Analysis of Complex Organic Mixtures. Analytical Chemistry 2018; 90: 2041-2047.

Sokal R, Rohlf F. Sokal RR, Rohlf FJ. The comparison of dendrograms by objective methods. Taxon 11: 33-40. Taxon 1962; 11: 33-40.

Speight JG. The Chemistry and Technology of Petroleum: CRC Press: New York, NY, USA, 2006.

Stanford LA, Kim S, Klein GC, Smith DF, Rodgers RP, Marshall AG. Identification of water-soluble heavy crude oil organic-acids, bases, and neutrals by electrospray ionization and field desorption ionization Fourier transform ion cyclotron resonance mass spectrometry. Environmental Science & Technology 2007; 41: 2696-2702.

Stanford LA, Kim S, Rodgers RP, Marshall AG. Characterization of compositional changes in vacuum gas oil distillation cuts by electrospray ionization Fourier transform-ion cyclotron resonance (FT-ICR) mass spectrometry. Energy & Fuels 2006; 20: 1664-1673.

Stout SA, Uhler AD, McCarthy KJ. A Strategy and Methodology for Defensibly Correlating Spilled Oil to Source Candidates. Environmental Forensics 2001; 2: 87-98.

Sun C, Shotyk W, Cuss C, Donner M, Fennell J, Javed M, et al. Characterization of Naphthenic Acids and Other Dissolved Organics in Natural Water from the Athabasca Oil Sands Region, Canada. Environmental Science & Technology 2017; 51: 9524-9532.

Syage JA, Evans MD, Hanold KA. Photoionization mass spectrometry. American Laboratory 2000; 32: 24-+.

Szulejko JE, Solouki T. Potential analytical applications of interfacing a GC to an FT-ICR MS: Fingerprinting complex sample matrixes. Analytical Chemistry 2002; 74: 3434-3442.

Tang GQ, Firoozabadi A. Gas- and liquid-phase relative permeabilities for cold production from heavy-oil reservoirs. Spe Reservoir Evaluation & Engineering 2003; 6: 70-80.

Tang WJ, Hurt MR, Sheng HM, Riedeman JS, Borton DJ, Slater P, et al. Structural Comparison of Asphaltenes of Different Origins Using Multi-stage Tandem Mass Spectrometry. Energy & Fuels 2015; 29: 1309-1314.

Thomas MJ, Collinge E, Witt M, Lozano DCP, Vane CH, Moss-Hayes V, et al. Petroleomic depth profiling of Staten Island salt marsh soil: 2 omega detection FTICR MS offers a new solution for the analysis of environmental contaminants. Science of the Total Environment 2019; 662: 852-862.

Tissot PB, Welte DH. Petroleum formation and occurrence. Berlin: Springer-Varlag, 1984.

Tiwari P, Deo M. Compositional and kinetic analysis of oil shale pyrolysis using TGA-MS. Fuel 2012; 94: 333-341.

Tose L, Murgu M, Vaz B, Romo W. Application of Atmospheric Solids Analysis Probe Mass Spectrometry (ASAP-MS) in Petroleomics: Analysis of Condensed Aromatics Standards, Crude Oil, and Paraffinic Fraction. Journal of the American Society for Mass Spectrometry 2017; 28: 2401-2407.

Tose LV, Cardoso FMR, Fleming FP, Vicente MA, Silva SRC, Aquije G, et al. Analyzes of hydrocarbons by atmosphere pressure chemical ionization FT-ICR mass spectrometry using isooctane as ionizing reagent. Fuel 2015; 153: 346-354.

Tryggestad C, Sharma N, Rolser O, Smeets B, van de Staaij J. McKinsey Energy Insights' Global Energy Perspective. McKinsey Solutions Sprl, 2019.

Turnbull A, Slavcheva E, Shone B. Factors Controlling Naphthenic Acid Corrosion. CORROSION 1998; 54: 922-930.

van Krevelen DW. Graphical-statistical method for the study of structure and reaction processes of coal. Fuel 1950; 29: 269-284.

Van Meter R, Bailey CW, Brodie EC. (Determination of Nitrogen in Shale Oil and Petroleum)Evaluation of Dumas Procedures by Mass Spectrometry. Analytical Chemistry 1951; 23: 1638-1639.

Vermeire MB. Everything You Need to Know About Marine Fuels. Chevron Global Marine Products, 2012.

Verşan Kök M, Varfolomeev MA, Nurgaliev DK. Determination of SARA fractions of crude oils by NMR technique. Journal of Petroleum Science and Engineering 2019; 179: 1-6.

Vetere A, Profrock D, Schrader W. Quantitative and Qualitative Analysis of Three Classes of Sulfur Compounds in Crude Oil. Angewandte Chemie-International Edition 2017; 56: 10933-10937.

Ward JH. Hierarchical Grouping to Optimize an Objective Function. Journal of the American Statistical Association 1963; 58: 236-&.

Weissman SA, Anderson NG. Design of Experiments (DoE) and Process Optimization. A Review of Recent Publications. Organic Process Research & Development 2015; 19: 1605-1633.

West C. Current trends in supercritical fluid chromatography. Analytical and Bioanalytical Chemistry 2018; 410: 6441-6457.

Wiehe IA. Process Chemistry of Petroleum Macromolecules. FL: CRC Press: Boca Raton, 2008.

Wiehe IA, Kennedy RJ. The oil compatibility model and crude oil incompatibility. Energy & Fuels 2000; 14: 56-59.

Wilkins CL. A History of Ion Cyclotron Resonance (ICR) and Fourier Transform (FTICR) Mass Spectrometry. In: Gross ML, Caprioli RM, editors. The Encyclopedia of Mass Spectrometry. Elsevier, Boston, 2016, pp. 61-67.

Wobschall D. Ion Cyclotron Resonance Spectrometer. Review of Scientific Instruments 1965; 36: 466-475.

Wu CP, Qian KN, Nefliu M, Cooks RG. Ambient Analysis of Saturated Hydrocarbons Using Discharge-Induced Oxidation in Desorption Electrospray Ionization. Journal of the American Society for Mass Spectrometry 2010; 21: 261-267.

Xian F, Hendrickson CL, Blakney GT, Beu SC, Marshall AG. Automated Broadband Phase Correction of Fourier Transform Ion Cyclotron Resonance Mass Spectra. Analytical Chemistry 2010; 82: 8807-8812.

Yamashita M, Fenn JB. Electrospray Ion-Source - Another Variation on the Free-Jet Theme. Journal of Physical Chemistry 1984; 88: 4451-4459.

Yim UH, Kim M, Ha SY, Kim S, Shim WJ. Oil Spill Environmental Forensics: the Hebei Spirit Oil Spill Case. Environmental Science & Technology 2012; 46: 6431-6437.

Zenobi R, Knochenmuss R. Ion formation in MALDI mass spectrometry. Mass Spectrometry Reviews 1998; 17: 337-366.

Zhan DL, Fenn JB. Electrospray mass spectrometry of fossil fuels. International Journal of Mass Spectrometry 2000; 194: 197-208.

Zhang LZ, Zhang YH, Zhao SQ, Chung KH, Xu CM, Shi Q. Effect of apodization on FT-ICR mass spectrometry analysis of petroleum. International Journal of Mass Spectrometry 2014; 373: 27-33.

Zhao PJ, Ma C, Wang JT, Qiao WM, Ling LC. Almost total desulfurization of high-sulfur petroleum coke by Na2CO3-promoted calcination combined with

ultrasonic-assisted chemical oxidation. New Carbon Materials 2018; 33: 587-594.

Zhu XC, Shi QA, Zhang YH, Pan N, Xu CM, Chung KH, et al. Characterization of Nitrogen Compounds in Coker Heavy Gas Oil and Its Subfractions by Liquid Chromatographic Separation Followed by Fourier Transform Ion Cyclotron Resonance Mass Spectrometry. Energy & Fuels 2011; 25: 281-287.

Zhurov KO, Fornelli L, Wodrich MD, Laskay UA, Tsybin YO. Principles of electron capture and transfer dissociation mass spectrometry applied to peptide and protein structure analysis. Chemical Society Reviews 2013a; 42: 5014-5030.

Zhurov KO, Kozhinov AN, Tsybin YO. Evaluation of High-Field Orbitrap Fourier Transform Mass Spectrometer for Petroleomics. Energy & Fuels 2013b; 27: 2974-2983.

2. Industrial HFO Study: Proof of Concept

2.1 Introduction

Heavy fuel oil (HFO) is a residual fraction of crude oil used in marine engines. It is a particularly complex, heavy, and non-volatile mixture. The composition of crude oils, as well as refining processes, vary across the globe (Speight, 1997) and this variation is paralleled in the differences between the composition of HFOs. HFOs typically have an asphaltene content of 3-10 %, (Goldstein and Siegmund, 1976) further contributing to compositional complexity and compounding difficulties in analysis.

GC and low resolution MS are routinely used to characterise light, volatile petroleum fractions (Rodgers and McKenna, 2011) but these methods are unsuitable for the study of HFO. Ultra-high resolution mass spectrometry, specifically Fourier transform ion cyclotron resonance mass spectrometry (FTICR MS), can provide a more accurate determination of molecular composition for petroleum heavy ends (Hsu et al., 2011a). FTICR MS has demonstrated an ability to analyse not only asphaltene rich samples (Cho et al., 2013) but asphaltene fractions directly (Rodgers et al., 2006), however previous studies that used FTICR MS to analyse HFO samples by direct infusion have removed the asphaltenes during sample preparation (Elbaz et al., 2015).

Although the work presented in this chapter represents one of the earliest detailed compositional analyses of HFOs, such research has since become topical, with chemical characterisation of increasing interest (Guillemant et al., 2019; Jameel et al., 2016; Uhler et al., 2016). Furthermore, during the research period the International Maritime Organization (IMO) introduced restrictions on sulfur content in HFOs to limit harmful emissions associated with the shipping industry (Halff et al., 2019). In this proof-of-concept study, FTICR MS is applied to the study of HFOs with the aim of improving understanding of their differences in observed bulk properties, behaviours, and responsiveness to additive chemistries, and the range of techniques explored used to inform the best approaches for further study.

As an ultra-high resolution technique, FTICR MS can identify multiple peaks at the same nominal mass with sub-ppm mass errors (Hsu et al., 2011a). The technique can be coupled to complementary ionisation techniques, including

atmospheric pressure photoionization (APPI) and electrospray ionization (ESI). APPI can access a wide range of compounds, including non-polar, conjugated systems, and produces both protonated and radical species, increasing spectral complexity (Cho et al., 2015). ESI selectively accesses more polar species, and operated in positive or negative mode accesses a basic or acidic components respectively (Qian et al., 2001). Both APPI and ESI analyses are performed in this work to explore the complementarity between these techniques and their applicability to HFO samples. Caution must be exercised when comparing compositional profiles obtained by FTICR MS, as signal suppression (Marshall and Rodgers, 2008) and solvent effects (Headley et al., 2007) are known to influence spectral profiles. The data for each individual HFO whole sample and fractions were obtained using experimental procedures, including sample preparation and instrument parameters, that were as identical as possible, such that comparisons of relative class contributions can be considered robust.

FTICR MS is a state of the art technique and capable of accessing many thousands of molecular formulae in a single crude or heavy oil spectra, (Qian et al., 2001) as well as enhanced compositional coverage when petroleum is fractionated into its component saturates, aromatics, resins and asphaltenes (SARA) (Cho et al., 2012; Shi et al., 2010). Given that separating whole oil samples into SARA fractions has been shown to widen the compositional space accessible by FTICR (Cho et al., 2012), isolating the n-alkane insoluble fraction of an oil sample can yield information linked to asphaltene handling issues.

Lubricant trunk piston engine oils (TPEOs) used in marine diesel engines can easily become contaminated by HFO, because of leakage from fuel pumps or due to unburnt HFO washing down cylinder walls into the sump (Vermeire, 2012). Dissolution in lubricant oils can lead to HFO instability (Chen et al., 2016) which may be exacerbated by extreme engine conditions, causing asphaltene molecules to aggregate and form floccules before precipitating out of solution. The precipitates may deposit and create an undesirable black paint effect on cooler engine parts, such as the cambox and crankcase (Figure 2.1).

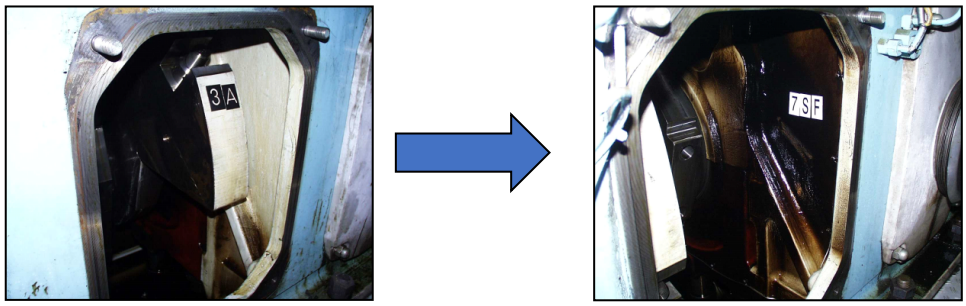

Figure 2.1 Undesirable 'black paint' formation following HFO contamination of crankcase. Photographs courtesy of Lubrizol Ltd.

The deposits can also cause a multitude of further problems, including oil scraper ring clogging resulting in high lubricant oil consumption (Vermeire, 2012). Detergents and dispersants to inhibit asphaltene aggregation and deposition (Kabel et al., 2015; Wiehe and Jermansen, 2003) are manufactured by Lubrizol for inclusion in TPEOs to prevent the formation of black paint, however the performance of TPEOs is found to be HFO dependant due to global variations in HFO composition.

In this work, HFO samples A-D were provided by Lubrizol with the aim of learning more about their composition to aid in understanding the differences in bulk properties and behaviour, particularly with respect to their interactions with additives. The results of their bulk analyses are provided in Table 2.1.

Table 2.1 Summary of results of bulk analyses for HFOs A-D

HFO	**S** / %	**Asphaltene** / %	**kV_{40}** / **$mm^2 s^{-1}$**	**kV_{50}** / **$mm^2 s^{-1}$**	**TAN** / **mg KOH g^{-1}**
A	2.543	2.9	No data	173.8	0.17
B	2.6808	6.0	854.6	494.6	No data
C	2.76	3.6	No data	69.81	2.23
D	2.1721	4.9	776.39	No data	No data

HFO A, which has a low asphaltene content, low total acid number (TAN), and relatively low viscosity, was selected as a high value, mild HFO, with no apparent asphaltene handling issues. HFO B was a more challenging oil which presented some asphaltene handling issues but was responsive to additive chemistry, while

HFO D appeared to be a milder version of HFO B, despite the higher bulk asphaltene content as displayed in Table 2.1. Although HFO C has a relatively low asphaltene content compared to HFOs B and D, its relatively high TAN is indicative of a lower value oil that may cause corrosion of metal surfaces.2.2

2.2 Materials and methods

HFO samples A-D were provided by Lubrizol (Lubrizol Ltd, Derby, UK). Mass spectra were acquired using a 12 T solariX Fourier transform ion cyclotron resonance (FTICR) mass spectrometer (Bruker Daltonik GmbH, Bremen, Germany), coupled to an Apollo II ESI source or APPI II source. Nitrogen was used as the drying gas at a temperature of 220 °C in ESI experiments and at 250 °C in APPI experiments, at a flow rate of 4 L min^{-1}. The nebulizing gas was nitrogen and was maintained at a pressure of 1.2 bar. In APPI experiments a krypton lamp was used to produce photons with energy 10.0 and 10.6 eV. Samples were introduced using a syringe pump at a rate of 210 μL h^{-1} with activation of in-source dissociation (ISD) at 40-60 V during ESI experiments only. After acquiring spectra, the data were zero-filled once and apodized using a Sine-Bell function prior to applying a fast Fourier transform. For apodized data, the resolving power at *m*/*z* 400 was typically 500,000 to 850,000, varying with ionization mode and sample. The spectra were internally calibrated using homologous series and analysed using DataAnalysis 4.2 (Bruker Daltonik GmbH, Bremen, Germany), prior to the data being imported into Composer 1.5.4 (Sierra Analytics, Modesto, CA, USA) for compositional analysis. Inkscape, Origin Pro 2016 (OriginLab Corporation, Northampton, Massachusetts, USA) and Aabel NG2 v.5.2 (Gigawiz Ltd. Co., Tulsa, Oklahoma, USA) were used for data visualization.

2.2.1 (+) APPI – non-protic solvent

HFO samples A-D were dissolved 0.05 mg mL^{-1} in toluene (Fisher Scientific, Hemel Hempstead, Hertfordshire, United Kingdom). 4 MW data sets were acquired in the detection range *m*/*z* 129-3000 for 150 scans.

2.2.2 (+) APPI – protic solvent

HFO samples A-D were dissolved 0.05 mg mL^{-1} in a 50:50 mixture of toluene and propan-2-ol (Fisher Scientific, Hemel Hempstead, Hertfordshire, United

Kingdom). 8 MW data sets were acquired in the detection range *m*/*z* 129-3000 for 300 scans.

2.2.3 (+/-) ESI

HFO samples A-D were dissolved 0.33 mg mL^{-1} in a 20:80 mixture of toluene and propan-2-ol (Fisher Scientific, Hemel Hempstead, Hertfordshire, United Kingdom). NH_4OH or HCOOH (Sigma-Aldrich Company Ltd., Gillingham, Dorset, United Kingdom) were added at 0.05 % for negative or positive mode experiments respectively. 4 MW data sets were acquired in the detection range *m*/*z* 147-3000 for 400 scans.

HFO C was also dissolved 0.05 mg mL^{-1} in 20:80 mixture of toluene and propan-2-ol (Fisher Scientific, Hemel Hempstead, Hertfordshire, United Kingdom) with 0.05 % HCOOH (Sigma-Aldrich Company Ltd., Gillingham, Dorset, United Kingdom) added. 4 MW data sets were collected for 300 scans. Data were recorded in the detection range *m*/*z* 147-3000 and in an isolated region *m*/*z* 368-432. Collision induced dissociation (CID) was then activated at 50 V with argon used as the collision gas, with a spectrum recorded in the detection range *m*/*z* 147-3000.

2.2.4 SAR/A Preliminary Method and (+) ESI Procedure

10 mg of HFO samples A-D were each placed on Whatman No. 1 filter paper (Sigma-Aldrich Company Ltd., Gillingham, Dorset, United Kingdom) and washed repeatedly in n-pentane (Acros Organics, Thermo Fisher Scientific, Loughborough, Leicestershire, UK) during a 48 h period until the filtrate ran clear. The pentane soluble fraction (maltene) and insoluble fraction (asphaltene) for each HFO were dissolved at 0.1 mg mL^{-1} in 20:80 mixture of toluene (Honeywell Speciality Chemicals, Seelze, Hanover, Germany) and propan-2-ol (Fisher Scientific, Hemel Hempstead, Hertfordshire, United Kingdom) with 0.5 % HCOOH (Sigma-Aldrich Company Ltd., Gillingham, Dorset, United Kingdom) added. 4 MW data sets were acquired in the detection range *m*/*z* 147-3000 for 400 scans.

2.2.5 SAR/A ASTM D3279 Method and (+) ESI Procedure

HFO samples A-D were dissolved in n-heptane (Fisher Scientific, Hemel Hempstead, Hertfordshire, United Kingdom) with a reflux and filtration experimental procedure carried out as described in ASTM D3279-07. The maltenes and asphaltene fractions obtained were dissolved at 0.05 mg mL^{-1} in a 20:80 mixture of toluene (Honeywell Speciality Chemicals, Seelze, Hanover, Germany) and propanol (Fisher Scientific, Hemel Hempstead, Hertfordshire, United Kingdom) with 0.5 % HCOOH added. 4 MW data sets were acquired in the detection range *m/z* 221-3000 for 400 scans.

2.3 Results and Discussion

2.3.1 Whole HFOs

2.3.1.1 (+) APPI

HFO samples A-D were initially dissolved in toluene only. The compound class distribution obtained after running each sample in triplicate is shown in Figure 2.2.

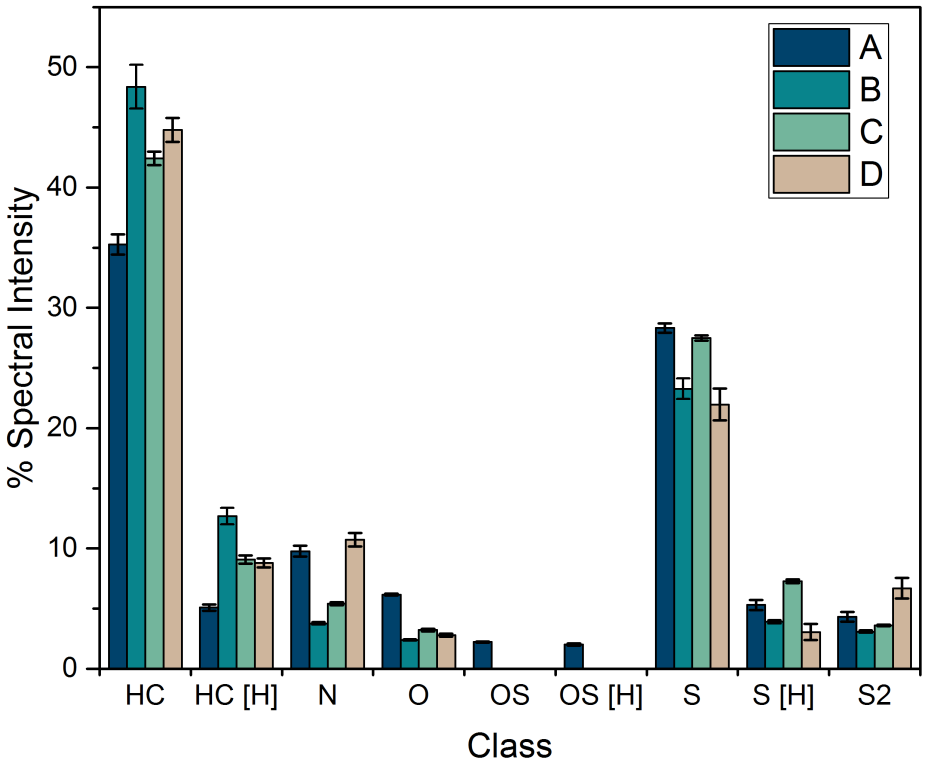

Figure 2.2 Compound class distribution from (+) APPI analysis of HFOs A-D dissolved in toluene solvent

The major classes identified by (+) APPI are HC and S radical classes in all cases. HFO C had a strong contribution from S and S[H] classes, while A had stronger contributions from all heteroatom containing classes including strong contributions from the O containing classes. Correspondingly, A had a lower contribution from HC and HC[H] classes compared to the other HFOs. Figure 2.2 demonstrates that there was little deviation in the relative class contributions between the triplicate runs of the same sample, particularly when considering minor contributions from heteroatom classes. It is imperative that comparisons between relative heteroatom class contributions are reliable when considering the potential interactions between asphaltenes and other reactive species with manufactured additives used to stabilise HFOs.

Figure 2.2 generally shows limited compositional differences between the HFOs, which may be due to poor ionization of many species with lower aromaticity in toluene solvent, resulting in few heteroatom-containing classes being identified in (+) APPI analysis. The N[H] compound class is routinely identified in (+) APPI data (Huba et al., 2016), but is not seen in these initial results. To improve access to HFO compositional space, the samples were dissolved instead in 50:50 toluene:propan-2-ol before acquiring (+) APPI spectra. The more protic solvent mixture was used to aid the ionisation of more functionalities, particularly heteroatom containing molecules. Adjusting solvent mixtures has previously been shown to alter the contribution that molecular classes make to spectral intensity in other petroleum related samples (Headley et al., 2007).

Due to the expected increase in spectral complexity, 300 scans of 8 MW datasets were acquired, with the spectra shown in Figure 2.3.

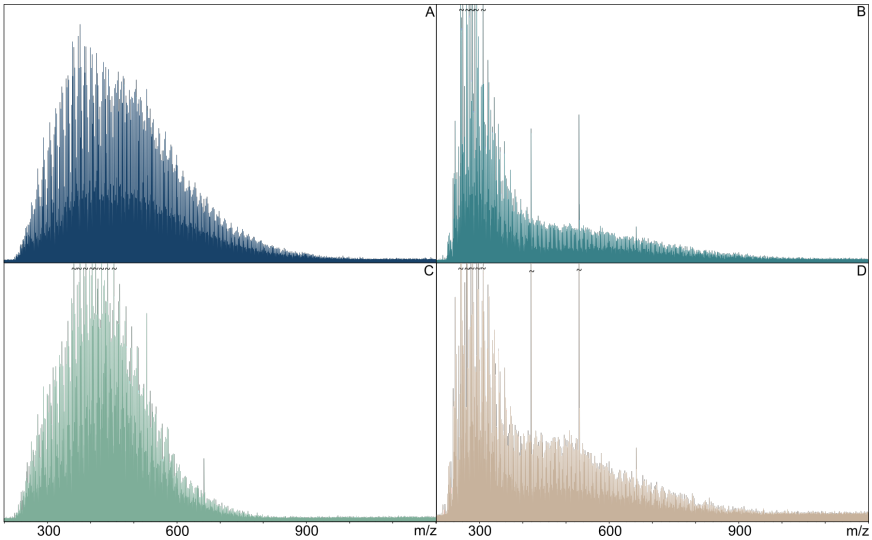

Figure 2.3 (+) APPI spectra of HFOs A-D in 50:50 toluene:propan-2-ol solvent

Figure 2.3 shows that high signal to noise was achieved for HFOs A and C, although a lower signal-to-noise was observed for HFO D. Weaker signals for petroleum samples may be indicative of heavier, more complex sources or fractions (McKenna, 2009). HFOs B and D appear similar with greater spectral intensity in the *m*/*z* 250 – 400 region.

The characteristics of the oil distributions were found to alter following the change in solvent, exemplified in Figure 2.4 for HFO C. Both an increase in peak density and shift in the centre of the distribution to higher *m*/*z* is noticeable.

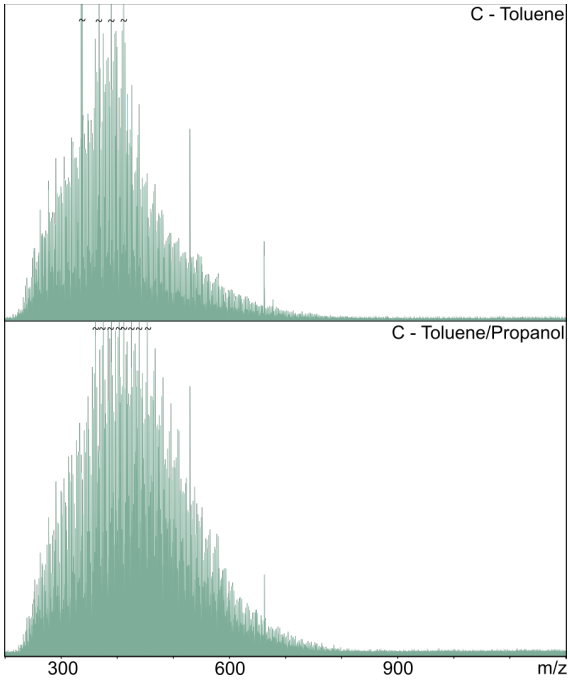

Figure 2.4 Comparison of (+) APPI spectra of HFO C dissolved in toluene solvent and 50:50 toluene:propan-2-ol solvent

The increase in peak intensity seen in Figure 2.4 illustrates an increase from 4993 to 6766 monoisoptic peak assignments made for HFO C. A histogram of the mass accuracy of peak assignments for all HFO samples for shows a normal distribution centred on 0 ppm with the majority of assignments made to an accuracy within 1 ppm (Figure 2.5).

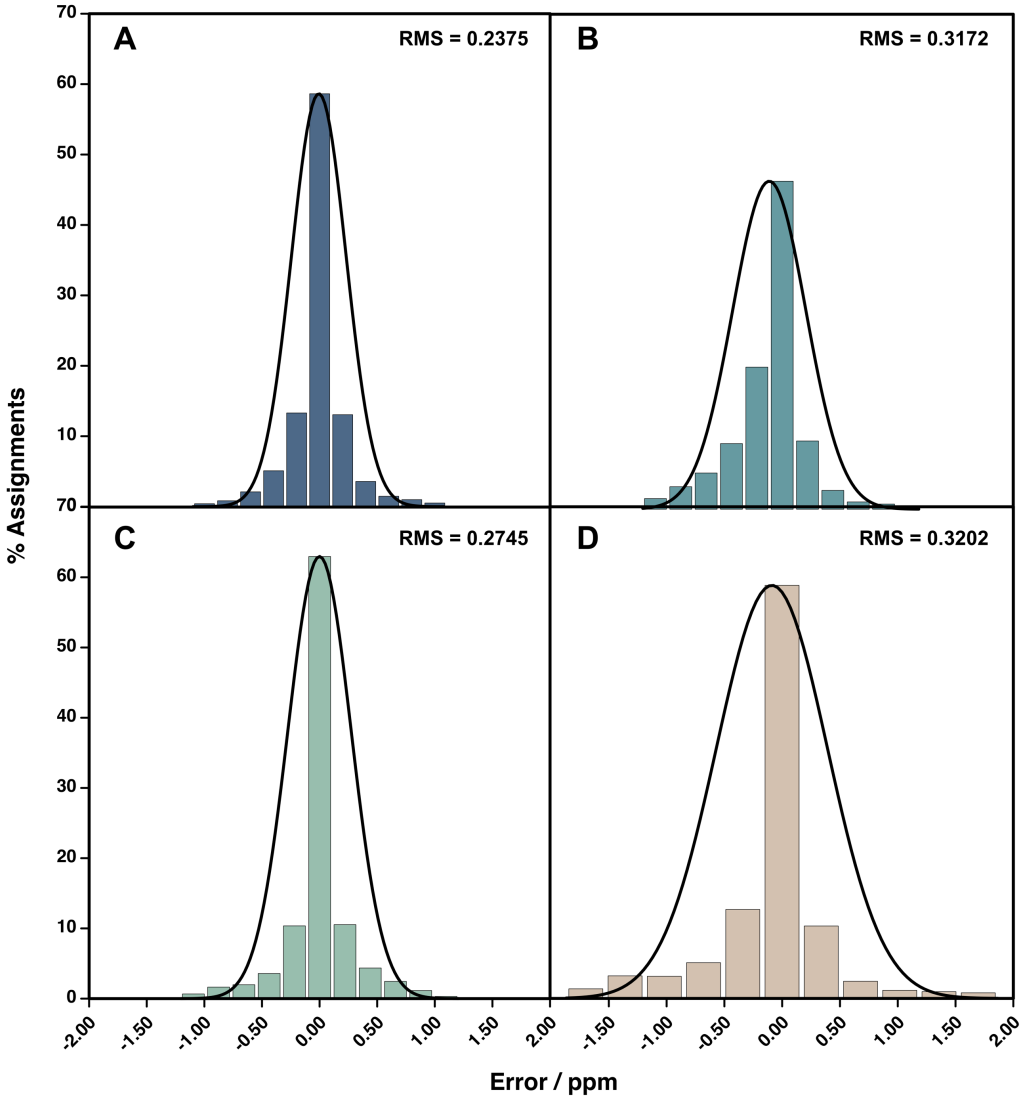

Figure 2.5 Histograms showing spread of mass errors and overall RMS error for assigned peaks in (+) APPI spectra of HFOs A-D

Figure 2.5 demonstrates the sub-ppm mass accuracy of the instrument across the entire assigned peak list and indicates that the calibration has been successful in negating the effects of space-charge in the cell, which can cause a shift to higher ppm errors at higher *m*/*z*.

The compound class distribution obtained for the HFOs dissolved in the more protic 50:50 toluene:propan-2-ol mixture and following adjustment of instrument parameters is shown in Figure 2.6.

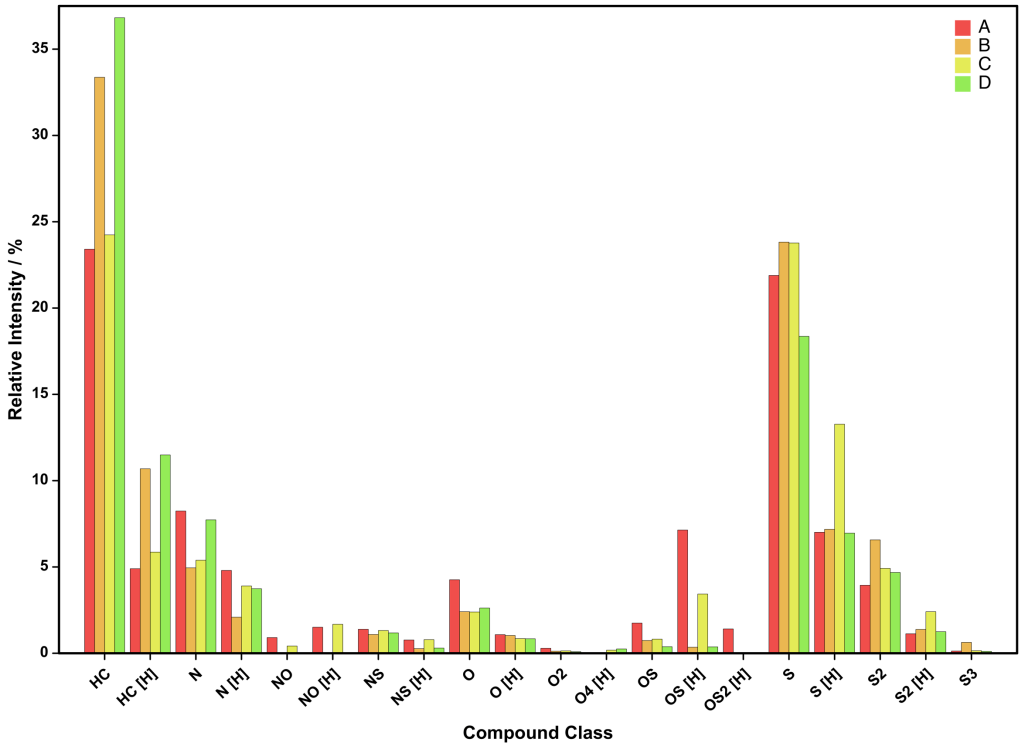

Figure 2.6 Compound class distribution from (+) APPI analysis of HFOs A-D dissolved in 50:50 toluene:propan-2-ol solvent

Figure 2.6 demonstrates that the change in solvent from toluene only to 50:50 toluene:propan-2-ol, as well as adjusting instrument parameters, was successful in accessing a greater range of compound classes, including the N[H] class absent from the preliminary results shown in Figure 2.2. The compositional differences between the HFO samples are also more readily apparent, for instance A maintains a stronger contribution from heteroatom containing classes including O, O_2, OS, OS[H] and OS_2[H] classes. HFOs B and D appear to have similar contributions from major HC and HC[H] classes, although D has a stronger contribution from the N class while B has a stronger contribution from the S_2 class. C had a stronger contribution from the S containing classes, particularly S[H], compared to the other HFOs, suggesting it may have a higher concentration of thiols and sulfides.

2.3.1.2 (-) ESI

(-) ESI data were challenging to obtain but final conditions for the strongest signal were found to be 0.33 mg mL^{-1} of HFOs A-D dissolved in 20:80 toluene:propan-2-ol with 0.05 % NH_4OH added. To prevent the formation of clusters between sample, solvent, and the ammonium hydroxide added to aid deprotonation, low

energy (40 - 60 V) ISD was used. Figure 2.7 shows the (-) ESI mass spectra obtained for HFOs A-D.

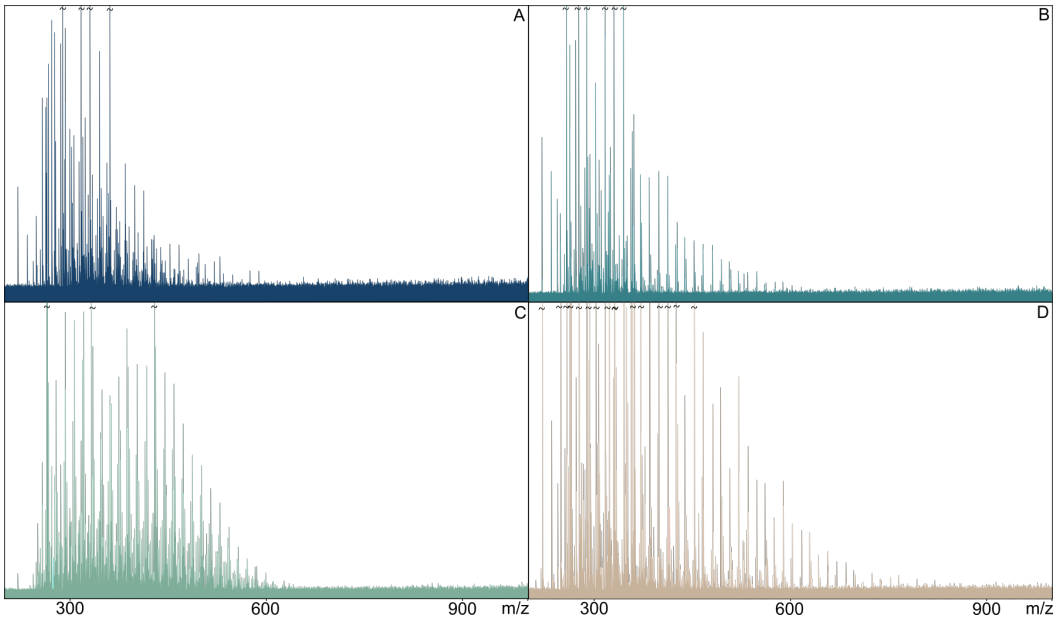

Figure 2.7 (-) ESI spectra of HFO samples A-D

Figure 2.7 demonstrates that despite many adjustments to sample preparation and instrument parameters, the signal was weak for all HFO samples. Poor signal-to-noise has a knock-on effect on data analysis, with many noise peaks being picked alongside low intensity real data peaks. Many peaks in the spectra of HFOs A, B and D were therefore unassigned and the number of successful assignments was low, at 10 – 15 %. However, HFO C responded relatively well to (-) ESI, with 65 % of peaks assigned, suggesting that C has a larger concentration of acidic species compared to the other HFOs, which links to the high TAN observed (Table 2.1).

The compound class distributions obtained for HFOs A-D after analysing the (-) ESI data are shown in Figure 2.8.

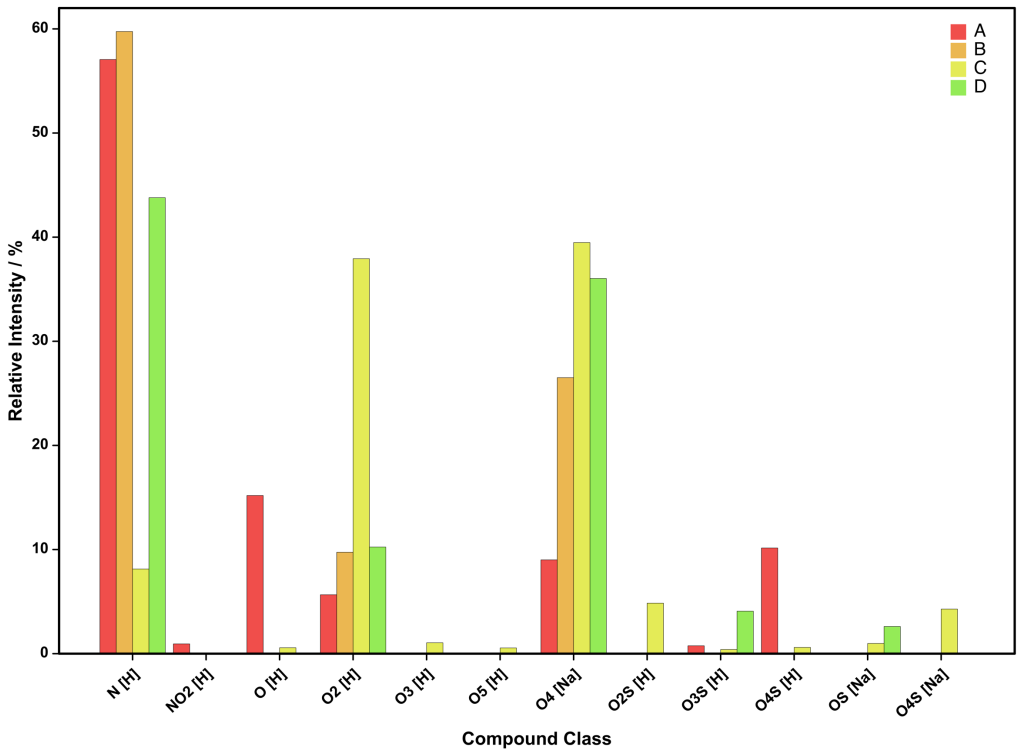

2.8 Compound class distribution from (-) ESI analysis of HFOs A-D

Figure 2.8 shows that HFO C has a predominant contribution from O_2[H] class. Typically, the N[H] class dominates in (+) ESI, and to a lesser extent in (-) ESI, petroleum analyses (Poetz and Wilkes, 2017; Qian et al., 2004), so HFO C may have a high concentration of carboxylic acid species, which may exist as naphthenic acid compounds. A has a relatively strong contribution from the O[H] class, so may have a strong concentration of alcoholic or phenolic compounds. These components of HFOs A and C are likely to give greater ionization response in ESI, while the signal remains weak for HFOs B and D due to a lack of polar components. Further data analysis and visualization was carried out to gain a greater understanding of the molecular properties of species that made a strong contribution from O containing classes to HFOs A and C.

A DBE plot of the O[H] of HFO A is shown in Figure 2.9a. A van Krevelen plot of H/C against O/C ratio for the O_2[H] class of HFO C is shown in Figure 2.9b.

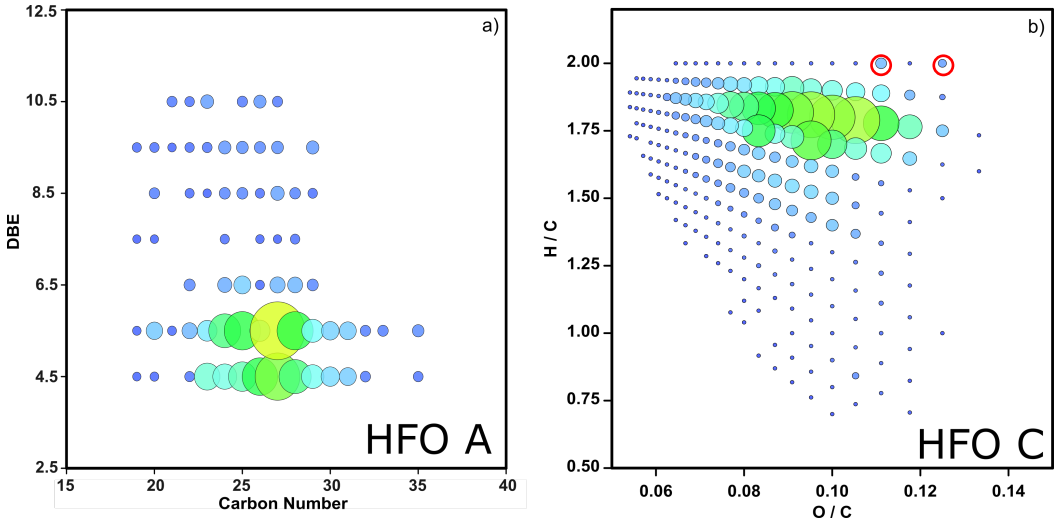

Figure 2.9 Plots showing a) DBE vs. carbon number for the O[H] class of HFO A and b) van Krevelen diagram for the O_2[H] class of HFO C, with coordinates corresponding to common contaminants palmitic and stearic acid circled in red

The plot of DBE against carbon number shown in Figure 2.9a starts at 4.5, and so the relatively strong contribution from the O[H] for HFO A is may be attributed to phenolic compounds as opposed to moieties such as straight chain alkyl alcohols. HFO A differs from the other samples in that it has a lower relative contribution from other oxygen containing compounds, including O_4[Na], which may be representative of naphthenic acid fraction compounds (Barrow et al., 2009), such that a low TAN was recorded for this sample. The coordinates of greatest intensity in the van Krevelen plot shown in Figure 2.9b indicate that the O_2[H] class of HFO C comprises carboxylic acids and that the associated alkyl chain backbone is mostly saturated. This is expected in petroleum fractions derived from crude sources as double bonds present in molecular structure will have undergone hydrogenation reactions over time. The indicated C_{16} and C_{18} acids are expected to be common contaminants stearic and palmitic acid, likely arising from other sources such as biological substances. As these common contaminants comprise a relatively low proportion of the overall compound class intensity this confirms that the relatively strong contribution from the O_2[H] class to the (-) ESI spectrum of HFO C is not due predominantly to these fatty acid species.

2.3.1.3 (+) ESI

(+) ESI data were obtained with 0.33 mg mL^{-1} of HFOs A-D in 20:80 toluene

propanol with the addition of 0.05 % HCOOH, with low energy (40 – 60 V) ISD. The spectra obtained are shown in Figure 2.10.

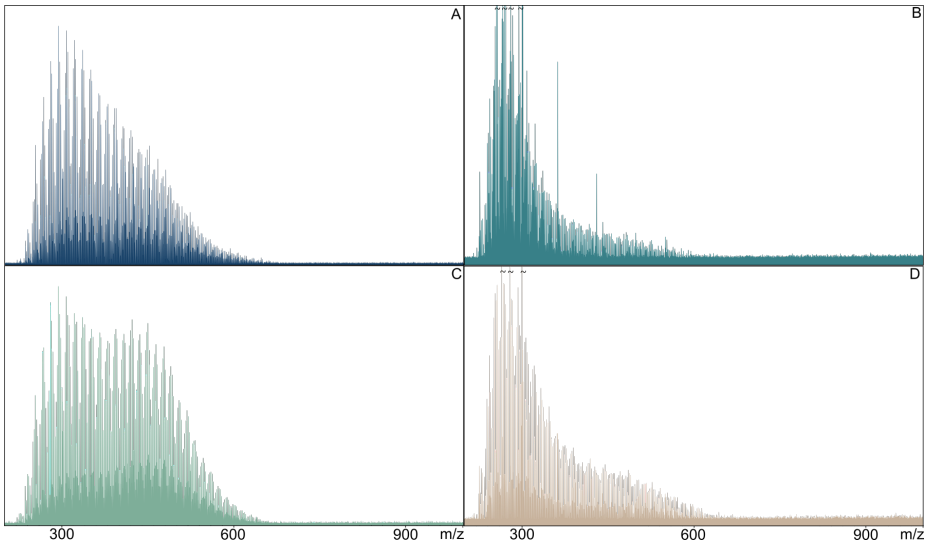

Figure 2.10 (+) ESI spectra of HFOs A-D

Figure 2.10 shows that B and D had lower signal-to-noise than samples A and C, which may indicate that these HFOs contain fewer polar species. The spectral distributions of HFOs B and D appear similar at low *m*/*z*.

The compound class distribution obtained following data analysis is shown in Figure 2.11.

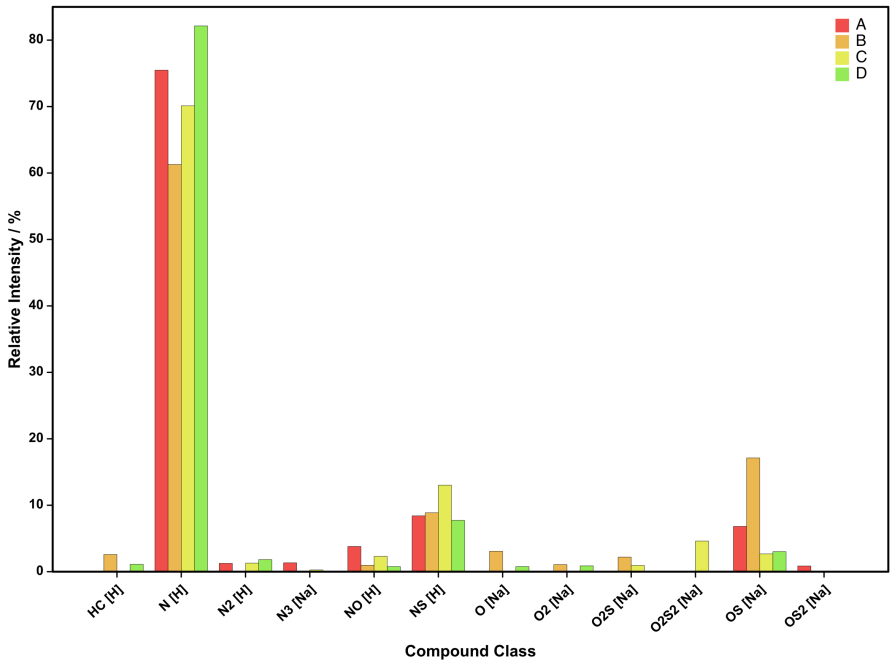

Figure 2.11 Compound class distribution from (+) ESI analysis of HFOs A-D

There are few compositional differences immediately noticeable in Figure 2.11, with the class distribution dominated by the N[H] class as is typical in ESI spectra. HFO C has a slightly greater contribution from the NS[H] class while B has a stronger contribution from the OS[Na] class compared to the other HFOs. B and D also have a small contribution from the HC[H] class, consistent with the (+) APPI data shown in Figures 2.2 and 2.6, as well as small contributions from other O-containing classes.

A plot of DBE against carbon number for the major N[H] class is shown for HFOs A-D in Figure 2.12.

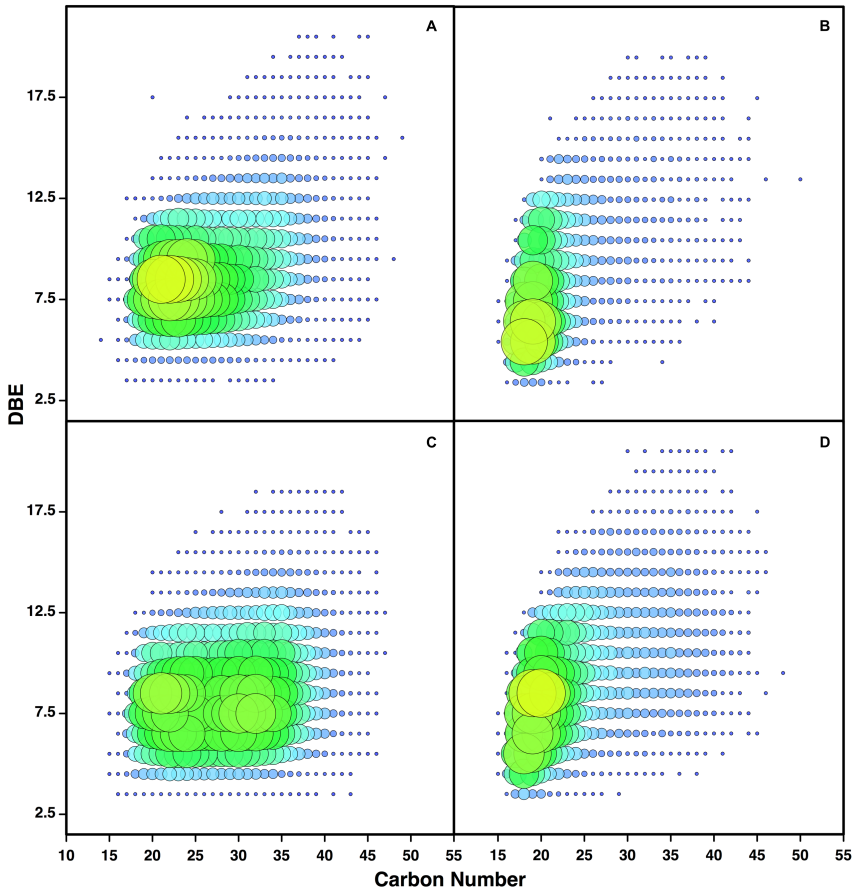

Figure 2.12 DBE vs. carbon number plots for the N[H] class of HFOs A-D

Figure 2.12 shows that HFOs B and D appear to have some similarity with their strongest contributions to the N[H] compound class at low carbon number, suggesting that there may be fewer molecules with extensive alkyl substitution on aromatic cores.

HFO C had a strong response to ESI experiments, so CID was carried out to characterise the aromatic cores of the basic, polar nitrogen containing molecules

present (Zhang et al., 2013). In Figure 2.13a the region of the N[H] DBE plot identified in the isolated window of the whole (+) ESI spectrum is highlighted, while Figure 2.13b highlights the DBE plot following the activation of CID.

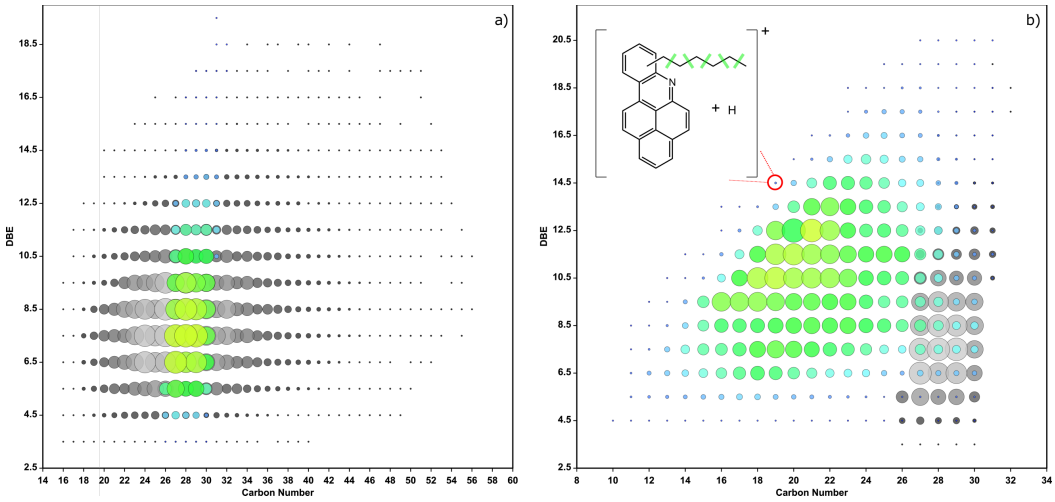

Figure 2.13 DBE vs. carbon number plots for the N[H] class of HFO C with highlighted regions showing the DBE plot following sequential a) quadrupole isolation and b) activation of CID

Figure 2.13b shows the sequential losses of $–CH_2$ along the alkyl chain to the stable N-containing aromatic cores. The slope of the DBE plot at the planar limit approaches the maximum value of 1 (Hsu et al., 2011b), indicating that the addition of hydrocarbon rings may be serial and non-linear, corresponding to peri-condensed cores (Cho et al., 2011), as shown in the example structure illustrated. To provide a more detailed molecular characterization, a narrower isolation window could be used prior to fragmentation (Liu et al., 2019; Wang et al., 2018) or alternative fragmentation techniques such as infra-red multiphoton dissociation (IRMPD) could be used (Mayer and Poon, 2009).

2.3.1.4 Summary of HFO Composition

Studying each HFO sample by (+) APPI and (+/-) ESI allowed several key compositional differences to be identified.

HFO A may have a high concentration of oxygen containing species, with a strong contribution from O, O[H], OS, OS[H], OS_2[H], NO and NO[H] classes in its (+) APPI spectrum, and a strong contribution from the O[H] class in its (-) ESI spectrum. Further investigation of (-) ESI data showed that the high O[H] content of A may be largely phenolic in nature, as the class has a minimum DBE of 4.5.

The high oxygen content, which may be present in compounds such as phenols, of HFO A may lead to polar interactions with detergents and dispersants and may limit the activity of basic additives in particular.

HFO B consistently had its spectra centred on lower *m*/*z*, while DBE plots were typically dominated by low carbon number species. B had strong contributions to spectral intensity from the usually predominant HC and HC[H] classes in its (+) APPI spectrum, and the N[H] class in (+) ESI spectrum, with limited contributions from other heteroatom containing classes. In the (-) ESI data B had a notable, although small, contribution from O and S-containing classes.

HFO D appeared to have some similarities with HFO B, particularly in low *m*/*z* regions of (+) APPI and (+) ESI spectra, as well as having predominant contributions from the expected classes. However, in the (+) APPI data HFO D consistently had a strong contribution from the N class while B did not.

Under study by all three ionisation modes, HFO C had the strongest contributions from heteroatom containing classes. In its (+) APPI spectrum the S[H] class made a particularly strong contribution, suggesting that HFO C may have a high concentration of thiols and sulfides. The OS[H], NO and NO[H] classes also made a strong contribution to spectral intensity. HFO C had a stronger response to (+/-) ESI than the other samples, with a relatively strong contribution from the NS[H] class in (+) mode and a predominant contribution from the O_2[H] class in (-) mode. Further analysis showed that the O_2[H] class largely comprised non-contaminant carboxylic acid species. The high acid content identified by (-) ESI, combined with the high content of sulfur-containing species identified by (+) APPI, may cause this HFO to be particularly problematic under engine conditions or to react atypically with formulated additives.

2.3.2 SAR/A Fractionation

The (+) ESI data provided the least information on the compositional differences between the whole HFOs. Without further investigation, it may be concluded that there is little difference between the polar, basic, components of the four samples studied. In order to gather further information on these components, and to limit the impact of signal suppression, the asphaltene fraction can be isolated by precipitation in n-alkanes (Akbarzadeh et al., 2007). Fractionating whole oil samples into asphaltene and maltene components has been previously shown to afford access to a greater number of individual molecular formulae (Cho et al., 2012).

2.3.2.1 SAR/A – Preliminary Method and (+) ESI Analysis

The compound class distribution for the maltenes and asphaltenes, separated roughly through extraction of the n-pentane soluble fraction, of HFOs A-D is shown in Figure 2.14.

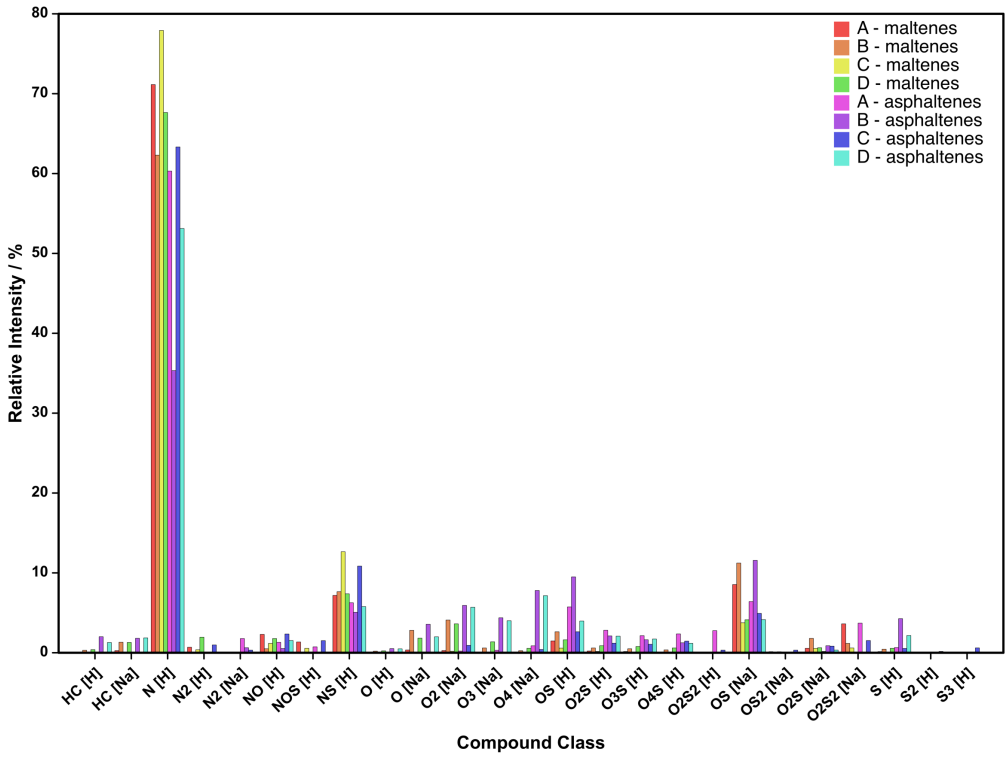

Figure 2.14 Compound class distribution from (+) ESI analysis of maltene and asphaltene fractions obtained from a rough separation method for HFOs A-D

Figure 2.14 shows that there is generally a lower contribution to spectral intensity from the N[H] class for the asphaltene fractions, with a corresponding increase in intensity from other heteroatom classes such as O_x[Na], O_xS_y[H] and S_y[H] classes. HFO C retains a stronger contribution from the NS[H] class compared to the other HFOs, which is internally consistent between the whole oil data and that from both maltene and asphaltene fractions. HFO B also retains a stronger contribution from the OS[Na] class.

While the results shown in Figure 2.14 provide evidence of internal consistency across the range of experimental parameters used, similarities between the maltenes and asphaltene data also suggest that the rough fractionation method may not have provided an efficient separation of pentane derived maltenes and asphaltenes from the whole oil sample.

2.3.2.2 SAR/A – ASTM D3279 Method (+) ESI Analysis

With the aim of obtaining a more efficient separation, the procedure outlined in the standardised ASTM D3279-07 method, routinely used to isolate the asphaltene fraction from whole oils using reflux followed by filtration of the n-heptane insolubles, was followed.

The spectra for the maltene and asphaltene fractions of HFOs A-D are shown in Figure 2.15.

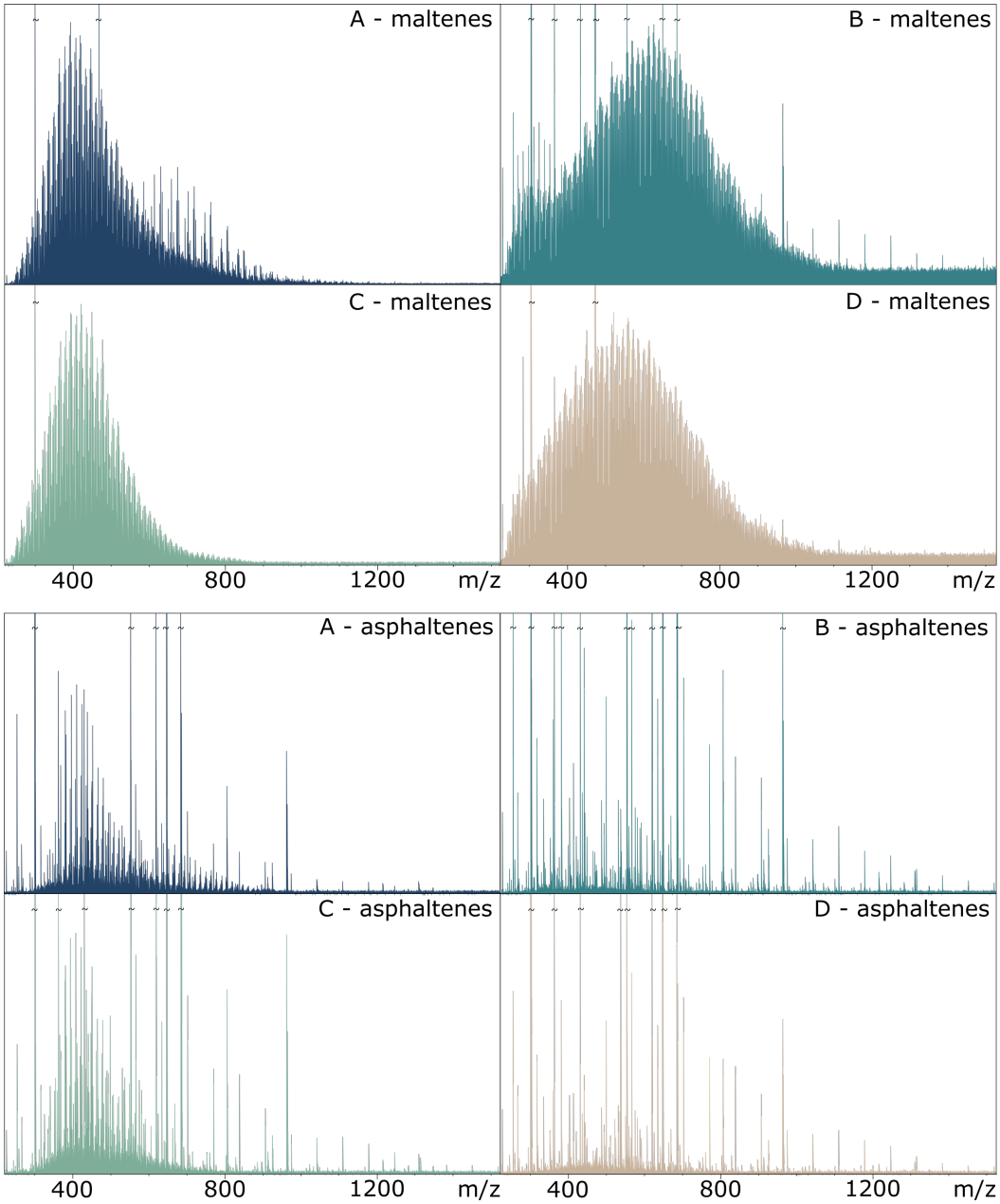

Figure 2.15 (+) ESI spectra of maltene and asphaltene fractions obtained from ASTM D3279-07 for HFOs A-D

Figure 2.15 shows that the asphaltene spectra are generally lower intensity than the maltene spectra. Although the maltene spectra for HFOs B and D have lower signal-to-noise than those shown for the whole oil in Figure 2.10, there is a less intense contribution at *m*/*z* 200-400, suggesting that these species may have been isolated in the n-heptane insoluble fraction.

The compound class distribution for the maltene and asphaltene fractions of HFOs A-D are shown in Figure 2.16.

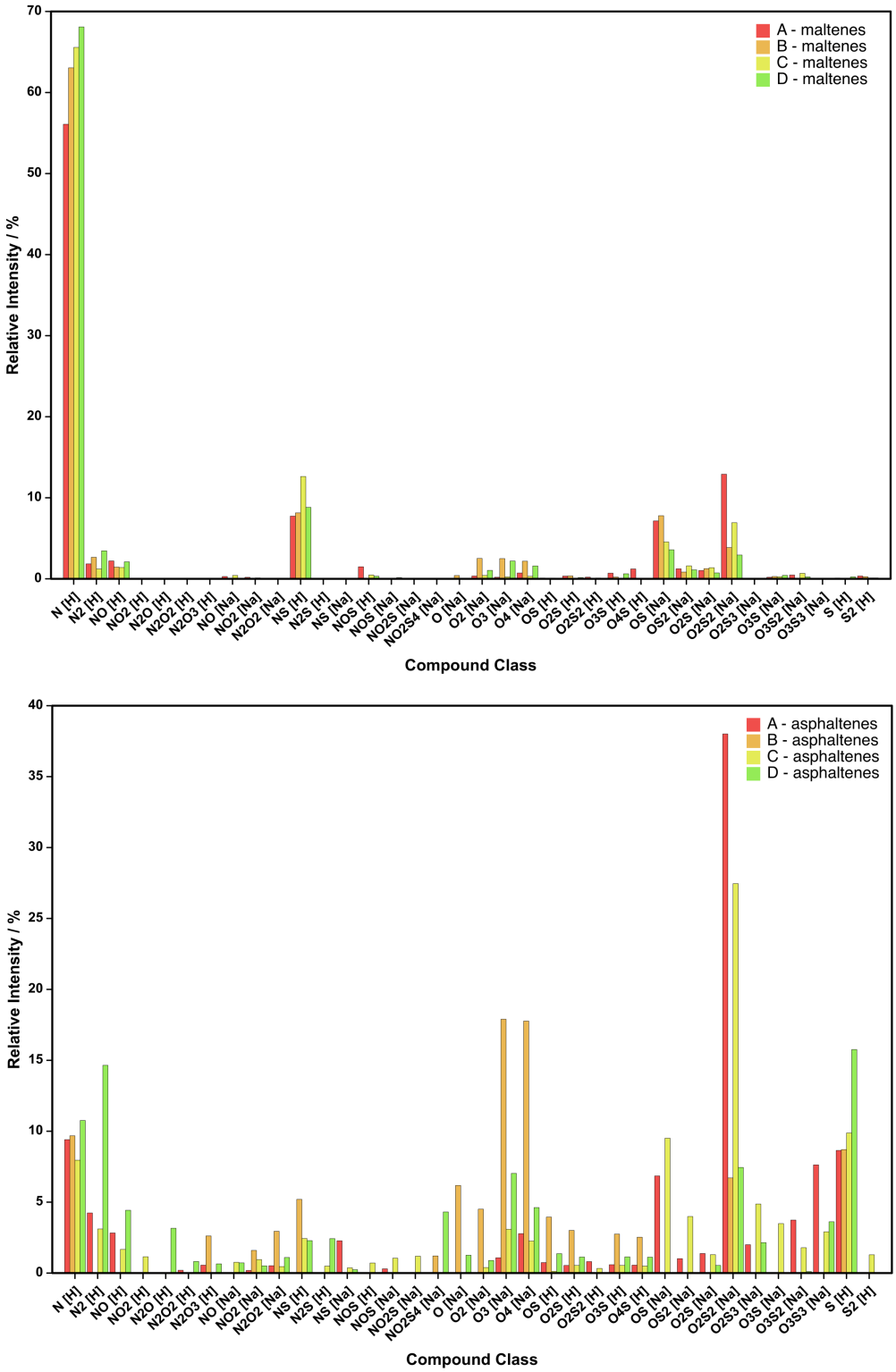

Figure 2.16 Compound class distribution from (+) ESI analysis of maltene and asphaltene fractions obtained from ASTM D3279-07 for HFOs A-D

When analysing the whole oil HFO samples few conclusions could be drawn from the (+) ESI results. However, after isolating the asphaltene fraction from the whole oil and analysing the maltene and asphaltene fractions separately,

differences in composition became clearer. Furthermore, the data shown in Figure 2.16 suggests a far more efficient separation has occurred in the reflux heptane compared to the rough pentane fractionation method, with the maltene class distribution comparable to that of the whole oil while the asphaltene class distribution is more dissimilar.

HFOs B and D continue appear to have some similarities, including strong contributions from the O_x[Na] classes. However, HFO D appears to have a stronger contribution from the nitrogen-containing classes, particularly N_2[H] in the asphaltene fraction. The data in Figure 2.16 suggests that O-containing species in all HFOs may be predominantly in the asphaltene fraction. The S[H] class, which when observed in (+) ESI data most likely corresponds to sulfides, appears to be largely isolated in the asphaltene fraction, with HFO D having the greatest contribution from this class. On the other hand, the strong contribution from the NS[H] class observed for HFO C in both whole oil and rough fractionation data, here appears to be predominantly in the maltene fraction.

To further explore the efficiency of the separation, DBE plots of the usually predominant N[H] class are compared for the maltene and asphaltene fractions of HFOs A-D in Figure 2.17.

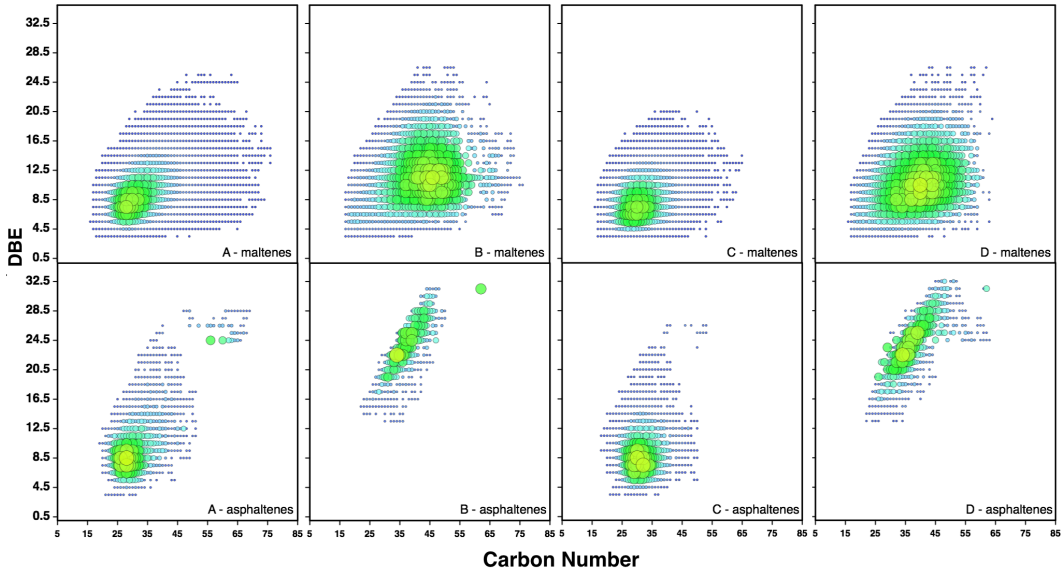

Figure 2.17 DBE vs. carbon number plots of the N[H] class of maltene and asphaltene fractions for HFOs A-D

Figure 2.17 shows that B and D have undergone the most efficient separation, which may be due to a greater initial asphaltene content. Furthermore, Figure 2.17 shows that, while HFOs B and D have a strong contribution from low carbon

number species in the whole oil, removing the n-heptane insoluble species has allowed access to higher carbon number species in the maltene fraction that may not have been identified without SAR/A fractionation. The asphaltene DBE plots of HFOs A and C show a shift to lower carbon number compared to the maltene DBE plots, which may be due to the solubility of extended alkyl chains in n-heptane solvent.

2.3.2.3 Summary of SAR/A Fractionation

The initial SAR/A fractionation performed using a rough method of repeatedly washing the HFOs in n-pentane appeared to provide a poor separation, although some preliminary data was successfully obtained. In particular, the asphaltenes appeared to have a greater contribution to spectral intensity from O- and S-containing classes.

With the more efficient separation afforded following implementation of the ASTM D3279-07 method, further compositional differences between the HFOs became more apparent. The asphaltene fractions of HFOs B and D have a stronger contribution from O_x classes, while those of A and C have a greater contribution from O_xS_y classes. Importantly, the asphaltene fractions of the HFOs were able to be directly characterised and compared, even though previous studies found that the inherently acidic nature of these compounds makes analysis by (+) ESI challenging (Klein et al., 2006).

Overall, the SAR/A experimentation was successful, contributing to the compositional data and allowing comparisons between the samples where few compositional differences could be determined from the (+) ESI analysis of the whole oil sample. Other procedures are used to isolate asphaltenes, including Soxhlet extraction (Giraldo-Davila et al., 2016; Petrova et al., 2013), which could be explored to provide a greater efficiency of asphaltene isolation. In addition, the use of (+) APPI could provide greater ionization coverage of a wider range of compound classes, particularly when analyzing asphaltene molecules.

2.4 Conclusions

The analysis of whole HFO samples by (+) APPI and (+/-) ESI allowed several key compositional differences between the HFO samples to be identified. In particular, HFOs A and C were found to have strong contributions from heteroatom containing classes, including O and S. (-) ESI analysis provided complementary information on the functional properties of these classes, suggesting that HFO A has a high concentration of phenolic species while HFO C has a high carboxylic acid content. HFO C was also found to have a high thiol or sulfide content. From the whole oil data, few notable compositional features were identified for HFOs B and D, although both were observed to have a significant contribution from low *m*/*z* and low carbon number species.

Although it provided molecular-level characterisation of the acidic components of HFO C, obtaining data using (-) ESI for HFOs was found to be more challenging. Overall (+) APPI provided the most extensive coverage of composition, however, including for HFOs A and C that had a greater relative contribution from classes that correspond to more polar species such as NO, NO[H] and O_2. When studying HFOs using FTICR MS, therefore, future research is recommended to be performed utilizing (+) APPI for ionization.

Separation, following a standard reflux and filtration method, prior to (+) ESI analysis provided further compositional information and comparison of the asphaltene fractions of each HFO. Both HFOs B and D, for which few notable compositional features were observed when studying whole HFO, were found to have a strong contribution from O-containing classes in the asphaltene fraction. The asphaltene fraction of HFO D was also found to have a stronger contribution from N-containing classes. The strong contribution from the NS[H] class observed for HFO C in whole oil data was observed only in the maltene fraction. The asphaltene fractions of HFOs A and C were found to have stronger contribution from the O_xS_y classes.

The differences in composition determined between the HFOs and their asphaltene fractions advance understanding of their properties. The high carboxylic acid content indicated for HFO C links to its high TAN and may be associated with greater corrosivity and its lower market value, while although HFO A has a strong contribution from O-containing classes, their phenolic functionality may make this a milder oil with low TAN. HFOs B and D both

contain O-containing asphaltenes, which may be linked to asphaltene handling issues as intermolecular interactions between these species lead to flocculation and deposition. The milder behaviour of HFO D could be linked to a greater proportion of N-containing species that may respond more appropriately to additive chemistries or moderate interactions between O-containing asphaltenes.

Using multiple ionization techniques when studying whole HFOs, and a prior separation step such that their maltene and asphaltene fractions are analysed separately, has afforded an extensive compositional coverage. However, a more efficient separation of n-heptane insoluble fraction, using Soxhlet extraction, followed by an in depth (+) APPI analysis including fragmentation of the species likely to precipitate in engine oils, can be performed with the aim of better understanding asphaltene handling issues.

2.5 References

Akbarzadeh K, Hammami A, Kharrat A, Zhang D, Allenson S, Creek J, et al. Asphaltenes - Problematic but Rich in Potential. Oilfield Review 2007; 19: 22-43.

Barrow M, Headley J, Peru K, Derrick P. Data Visualization for the Characterization of Naphthenic Acids within Petroleum Samples. Energy & Fuels 2009; 23: 2592-2599.

Chen Z, Zhang L, Zhao S, Shi Q, Xu C, Xu C. Molecular Structure and Association Behavior of Petroleum Asphaltene. Structure and Modeling of Complex Petroleum Mixtures 2016; 168: 1-38.

Cho Y, Ahmed A, Islam A, Kim S. Developments in FT-ICR MS Instrumentation, Ionization Techniques, and Data Interpretation Methods for Petroleomics. Mass Spectrometry Reviews 2015; 34: 248-263.

Cho Y, Jin J, Witt M, Birdwell J, Na J, Roh N, et al. Comparing Laser Desorption Ionization and Atmospheric Pressure Photoionization Coupled to Fourier Transform Ion Cyclotron Resonance Mass Spectrometry To Characterize Shale Oils at the Molecular Level. Energy & Fuels 2013; 27: 1830-1837.

Cho Y, Kim Y, Kim S. Planar Limit-Assisted Structural Interpretation of Saturates/Aromatics/Resins/Asphaltenes Fractionated Crude Oil Compounds Observed by Fourier Transform Ion Cyclotron Resonance Mass Spectrometry. Analytical Chemistry 2011; 83: 6068-6073.

Cho Y, Na J, Nho N, Kim S. Application of Saturates, Aromatics, Resins, and Asphaltenes Crude Oil Fractionation for Detailed Chemical

Characterization of Heavy Crude Oils by Fourier Transform Ion Cyclotron Resonance Mass Spectrometry Equipped with Atmospheric Pressure Photoionization. Energy & Fuels 2012; 26: 2558-2565.

Elbaz A, Gani A, Hourani N, Emwas A, Sarathy S, Roberts W. TG/DTG, FT-ICR Mass Spectrometry, and NMR Spectroscopy Study of Heavy Fuel Oil. Energy & Fuels 2015; 29: 7825-7835.

Giraldo-Davila D, Chacon-Patino M, Orrego-Ruiz J, Blanco-Tirado C, Combariza M. Improving compositional space accessibility in (+) APPI FT-ICR mass spectrometric analysis of crude oils by extrography and column chromatography fractionation. Fuel 2016; 185: 45-58.

Goldstein HL, Siegmund CW. Influence of Heavy Fuel Oil Composition and Boiler Combustion Conditions on Particulate-Emissions. Environmental Science & Technology 1976; 10: 1109-1114.

Guillemant J, Albrieux F, Lacoue-Negre M, de Oliveira LP, Joly JF, Duponchel L. Chemometric Exploration of APPI(+)-FT-ICR MS Data Sets for a Comprehensive Study of Aromatic Sulfur Compounds in Gas Oils. Analytical Chemistry 2019; 91: 11785-11793.

Halff A, Younes L, Boersma T. The likely implications of the new IMO standards on the shipping industry. Energy Policy 2019; 126: 277-286.

Hammami A, Phelps CH, Monger-McClure T, Little TM. Asphaltene Precipitation from Live Oils: An Experimental Investigation of Onset Conditions and Reversibility. Energy & Fuels 2000; 14: 14-18.

Headley J, Peru K, Barrow M, Derrick P. Characterization of naphthenic acids from Athabasca oil sands using electrospray ionization: The significant influence of solvents. Analytical Chemistry 2007; 79: 6222-6229.

Hsu C, Hendrickson C, Rodgers R, McKenna A, Marshall A. Petroleomics: advanced molecular probe for petroleum heavy ends. Journal of Mass Spectrometry 2011a; 46: 337-343.

Hsu C, Lobodin V, Rodgers R, McKenna A, Marshall A. Compositional Boundaries for Fossil Hydrocarbons. Energy & Fuels 2011b; 25: 2174-2178.

Huba AK, Huba K, Gardinali PR. Understanding the atmospheric pressure ionization of petroleum components: The effects of size, structure, and presence of heteroatoms. Science of the Total Environment 2016; 568: 1018-1025.

Jameel AGA, Elbaz AM, Emwas AH, Roberts WL, Sarathy SM. Calculation of Average Molecular Parameters, Functional Groups, and a Surrogate Molecule for Heavy Fuel Oils Using H-1 and C-13 Nuclear Magnetic Resonance Spectroscopy. Energy & Fuels 2016; 30: 3894-3905.

Kabel K, Abdelghaffar A, Farag R, Maysour N, Zahran M. Synthesis and evaluation of PAMAM dendrimer and PDPF-b-POP block copolymer as asphaltene inhibitor/dispersant. Research on Chemical Intermediates 2015; 41: 457-474.

Klein G, Angstrom A, Rodgers R, Marshall A. Use of saturates/aromatics/resins/asphaltenes (SARA) fractionation to determine matrix effects in crude oil analysis by electrospray ionization Fourier transform ion cyclotron resonance mass spectrometry. Energy & Fuels 2006; 20: 668-672.

Liu L, Song CX, Tian SB, Zhang QD, Cai XH, Liu YR, et al. Structural characterization of sulfur-containing aromatic compounds in heavy oils by FT-ICR mass spectrometry with a narrow isolation window. Fuel 2019; 240: 40-48.

Marshall A, Rodgers R. Petroleomics: Chemistry of the underworld. Proceedings of the National Academy of Sciences of the United States of America 2008; 105: 18090-18095.

Mayer PM, Poon C. The Mechanisms of Collisional Activation of Ions in Mass Spectrometry. Mass Spectrometry Reviews 2009; 28: 608-639.

McKenna AM. Detailed Characterization of Heavy Crude Oils and Asphaltenes by Ultrahigh

Resolution Fourier Transform Ion Cyclotron

Resonance Mass Spectrometry. Chemistry and Biochemistry. Doctor of Philosophy. Florida State University, 2009, pp. 248.

Petrova L, Abbakumova N, Zaidullin I, Borisov D. Polar-solvent fractionation of asphaltenes from heavy oil and their characterization. Petroleum Chemistry 2013; 53: 81-86.

Poetz S, Wilkes H. Compositional Characterization of Acidic Petroleum Constituents Using Negative Ion Mode Electrospray Ionization Coupled with Fourier Transform-Ion Cyclotron Resonance Mass Spectrometry. In: McGenity TJ, Timmis KN, Nogales B, editors. Hydrocarbon and Lipid Microbiology Protocols: Petroleum, Hydrocarbon and Lipid Analysis. Springer Berlin Heidelberg, Berlin, Heidelberg, 2017, pp. 217-230.

Qian K, Edwards K, Diehl J, Green L. Fundamentals and applications of electrospray ionization mass spectrometry for petroleum characterization. Energy & Fuels 2004; 18: 1784-1791.

Qian K, Rodgers R, Hendrickson C, Emmett M, Marshall A. Reading chemical fine print: Resolution and identification of 3000 nitrogen-containing aromatic compounds from a single electrospray ionization Fourier

transform ion cyclotron resonance mass spectrum of heavy petroleum crude oil. Energy & Fuels 2001; 15: 492-498.

Rodgers R, Klein G, Yen A, Asomaning S, Marshall A. Compositional analysis of petroleum asphaltenes by FT-ICR mass spectrometry. Abstracts of Papers of the American Chemical Society 2006; 231.

Rodgers R, McKenna A. Petroleum Analysis. Analytical Chemistry 2011; 83: 4665-4687.

Shi Q, Hou DJ, Chung KH, Xu CM, Zhao SQ, Zhang YH. Characterization of Heteroatom Compounds in a Crude Oil and Its Saturates, Aromatics, Resins, and Asphaltenes (SARA) and Non-basic Nitrogen Fractions Analyzed by Negative-Ion Electrospray Ionization Fourier Transform Ion Cyclotron Resonance Mass Spectrometry. Energy & Fuels 2010; 24: 2545-2553.

Speight JG. Petroleum Chemistry and Refining: CRC Press, 1997.

Uhler AD, Stout SA, Douglas GS, Healey EM, Emsbo-Mattingly SD. 13 - Chemical character of marine heavy fuel oils and lubricants. In: Stout SA, Wang Z, editors. Standard Handbook Oil Spill Environmental Forensics (Second Edition). Academic Press, Boston, 2016, pp. 641-683.

Vermeire MB. Everything You Need to Know About Marine Fuels. Chevron Global Marine Products, 2012.

Wang W, Dong M, Song CX, Cai XH, Liu YR, Liu ZL, et al. Structural information of asphaltenes derived from petroleum vacuum residue and its hydrotreated product obtained by FT-ICR mass spectrometry with narrow ion isolation windows. Fuel 2018; 227: 111-117.

Wiehe IA, Jermansen TG. Design of synthetic dispersants for asphaltenes. Petroleum Science and Technology 2003; 21: 527-536.

Zhang L, Zhang Y, Zhao S, Xu C, Chung K, Shi Q. Characterization of heavy petroleum fraction by positive-ion electrospray ionization FT-ICR mass spectrometry and collision induced dissociation: Bond dissociation behavior and aromatic ring architecture of basic nitrogen compounds. Science China-Chemistry 2013; 56: 874-882.

3. Industrial HFO Study: Application to Asphaltene Handling Issues

3.1 Introduction

Chapter 2 established that HFOs are an ultra-complex mixtures, for which, in common with many petroleum-related substances, detailed compositional analysis at the molecular level can be successfully attained through the use of ultra-high resolution mass spectrometry techniques (Palacio Lozano et al., 2019; Schmidt et al., 2018). Petroleum may be divided into four fractions based on their polarity and solubility: saturates, aromatics, resins and asphaltenes (SARA) (Akbarzadeh et al., 2007). Asphaltenes are typically defined as the fraction of petroleum insoluble in n-alkanes such as n-heptane, but soluble in toluene (Sheu and Storm, 1995), the classical physical model of petroleum considers asphaltenes as solute, with the remaining SAR fractions acting as non-solvent, solvent, and dispersant respectively (Wiehe, 2008). Asphaltenes are prone to flocculation above a critical concentration, when a component in an incompatible blend, or when self-incompatible (Durand et al., 2010; Wiehe and Kennedy, 2000). The resultant deposition can lead to pipeline blockages, impeding pigging or necessitating it at more regular intervals, and the undesirable black paint formation in marine engines (Jameel et al., 2019; Vermeire, 2012) depicted in Figure 2.1. Additives can be formulated to stabilize against black paint formation (Kabel et al., 2015), although their performance is marine heavy fuel oil (HFO) dependent owing to global variations in composition. Further compounding their handling problems, asphaltenes can also act as inhibitors in desulfurization processes (Le Lannic et al., 2007).

Desulfurization efficiency is of growing importance with restrictions on sulfur content in HFOs tightening in line with regulations set by the International Maritime Organization (IMO) 2020 (Halff et al., 2019; Jameel et al., 2019). Catalyst fouling and inhibition of desulfurization processes is often attributed to basic nitrogen-containing species and aromatic compounds (Guillemant et al., 2019b; Zeuthen et al., 2001). As the large stable aromatic cores of asphaltenes are capable of stabilizing charge through delocalization (Kafer et al., 2019), and terminating free radical reactions through recombination and disproportionation (Bukowski and Milczarska, 1983), they may also present an impediment in some desulfurization processes, particularly where transformation of cooccurring refractory aromatic sulfur compounds is required (Guillemant et al., 2019b).

Although their chemical structure is still not fully understood (Jameel et al., 2019), at the molecular level, asphaltenes are now widely considered to comprise polycyclic aromatic hydrocarbon (PAH) cores (Dickie and Yen, 1967) with average molecular mass around 750 Da, and sometimes containing heteroatoms such as N, O, or S (Mullins, 2011; Mullins et al., 2012), the presence of which may exacerbate asphaltene handling problems, cause catalyst fouling, or alter responsiveness to additives (Guillemant et al., 2019a; Jameel et al., 2019). Evidence for both island or archipelago type asphaltenes, shown in Figure 1.7, has been presented (Chacon-Patino et al., 2017; Nyadong et al., 2018; Tang et al., 2015). Interpretation of asphaltene core structure, and comment on the likely predominance of island or archipelago type asphaltenes using Fourier transform ion cyclotron resonance mass spectrometry (FTICR MS) analyses have previously been limited to inspection of fragment ion spectra, comparison of average molecular weight (Mw), plots of double bond equivalent (DBE) against carbon number, and DBE distributions (Chacon-Patino et al., 2017; Chacon-Patino et al., 2018a; Chacon-Patino et al., 2018b; Tang et al., 2015). Consistent boundaries have been used to define regions of nitrogen-class DBE plots by the possible structure of aromatic cores (Guillemant et al., 2019a). Although a precise definition of the compositional boundaries for island and archipelago type asphaltenes has not yet been attained, consistent estimates may be applied when comparing samples analyzed in a similar manner to account for differences in ionization efficiency between the two moieties (Nyadong et al., 2018), with island-derived fragment ions considered to be those with DBE consistent with parent ions (Chacon-Patino et al., 2018b).

Principal component and hierarchical clustering analyses (PCA and HCA) have previously been used for fingerprinting (Stout et al., 2001), indicating geological origin (Chiaberge et al., 2013; Krajewski et al., 2018), likely sources of oil spills (Islam et al., 2016), discriminating between natural and industry linked oil sand process-affected waters (Barrow et al., 2009), as well as visualization and comparison of multiple petroleomics data sets (Hur et al., 2010; Kafer et al., 2019; Lozano et al., 2017). The location of variables relative to the circle of correlations in a PCA loadings plot may be used to determine those which contribute most significantly to the differences between samples (Abdi and Williams, 2010), and their position used to elucidate the underlying differences in bulk properties or behavior between complex samples. The application of PCA and HCA to multiple (+) APPI-FTICR MS data sets as recently been used to discriminate between gas oils that had undergone different desulfurization processes. The confirmation of

alkylated dibenzothiophene species as refractory species even in deeply hydrotreated samples, was validated, as well the ability to identify the treatment processes of unknown samples (Guillemant et al., 2019b). Such approaches may therefore provide an indication of similarities between multiple HFO samples, as well as identifying key compound types that may be responsible for undesirable bulk properties.

In Chapter 2, refluxing in n-heptane followed by filtration offered improved asphaltene fraction isolation over repeatedly washing HFOs suspended on filter paper with n-pentane. Soxhlet extraction has been used for asphaltene fractionation (Jameel et al., 2019), and is routinely used to obtain hydrophobic components, including petroleum-related substances, from soil (McGill and Rowell, 1980; Thomas et al., 2019). In this Chapter, Soxhlet extraction using n-heptane was performed to further optimize the isolation of the asphaltene fraction of eight HFO samples. In the proof of concept study (Chapter 2) atmospheric pressure photoionization (APPI) was found to provide the broadest compositional coverage for HFO samples. APPI has been used in other studies of heavier oils (Farenc et al., 2016; Santos et al., 2018b; Zhang et al., 2014) and their asphaltene fractions (Pereira et al., 2014; Santos et al., 2018a), as it more efficiently ionizes non-polar and aromatic compounds (Cho et al., 2017; Pereira et al., 2014) due to a lower reliance on ion-molecule chemistry, and is less susceptible to ion suppression than other techniques including electrospray ionization (ESI) and atmospheric pressure chemical ionization (APCI) (Annesley, 2003; Hanold et al., 2004).

Tandem mass spectrometry (MS/MS) methods can be used to elucidate structural information by, for example, utilizing quadrupole isolation to select precursor ions, before producing fragments using a neutral collision gas (McLafferty, 2011). Although collision-induced dissociation (CID) is used widely, proceeding via vibrational energy pathways which makes the method selective towards cleavage of the weakest bonds (Mayer and Poon, 2009), there are several limitations to this technique. For instance, more efficient fragment generation is offered through the use of heavier neutral collision gases, however the costs associated with these often limits the user to lighter nitrogen or argon, where multiple collisions may be required to generate fragment species of interest (Douglas, 1998). Furthermore, the increase in ion kinetic energy required to induce dissociation in CID can limit the observation of low m/z product ions (Little et al., 1994; Payne and Glish, 2001). Following precursor selection, fragment ions generated by CID in the collision

cell must then be transferred to the ICR cell, such that without careful tuning m/z range biases and ion losses can occur, resulting in failure to detect lower abundance species. In infra-red multiple-photon dissociation (IRMPD) the ion energy is increased by photon absorption, while fragmentation occurs inside the ICR cell (Polfer, 2011), overcoming ion transfer issues. As such, the detection of lower molecular weight species and sensitivity to lower abundance species is improved. IRMPD has been used to access core structures of asphaltenes of mass-selected isolation windows (Chacon-Patino et al., 2017). By fragmenting asphaltenes, the stable aromatic cores may be characterized, and an assessment of predominance of island or archipelago structures may be made, as well as determining whether heteroatoms are located predominantly in aromatic cores or in substituent chains.

Based upon the improved understanding of bulk properties attained through the compositional analysis of HFOs A-D (Chapter 2), four further HFOs were provided by Lubrizol with the aim of understanding differences in their asphaltene handling issues and responsiveness to additive chemistries. The results of bulk analyses of HFOs E-H are presented in Table 3.1, data for HFOs A-D is shown in Table 2.1.

Table 3.1 Summary of results of bulk analyses for HFOs E-H

HFO	S / %	Asphaltene / %	kV / $mm^2\ s^{-1}$	Density / $kg\ m^{-3}$	TAN / mg KOH g^{-1}
E	0.46	3.6	162	0.987	5.5
F	3.16	8.2	405	0.990	< 0.2
G	2.58	3.18	398	1.083	0.2
H	1.2738	3.9	380	0.988	0.31

HFO E was provided as it has sulfur content below 0.5 % and so meets IMO 2020, however it is not clear from the bulk data whether desulfurization has occurred, and if so what process it has undergone and what effect this may have had on molecular-level composition. HFO F, despite its high asphaltene content, is responsive to additive chemistries, and is provided such that FTICR MS analysis can improve understanding of these observations. HFO G and H were provided for detailed compositional analysis as, despite apparent similarities in their bulk properties, HFO G presents solubility issues whereas HFO H is milder.

In this study, PCA and HCA are performed on grouped heteroatom class data from (+) APPI-FTICR MS analyses, and the results combined with information from DBE and carbon number distributions presented in a novel manner for multiple IRMPD fragment classes simultaneously. A more comprehensive characterisation of the asphaltene fractions of all 8 HFO samples is therefore afforded, improving understanding of HFO bulk characteristics and performance in the field, as well as their responsiveness to additive chemistries designed to stabilize them against asphaltene handling problems.

3.2 Materials and Methods

3.2.1 Soxhlet Extraction (C_7 Soxhlet asphaltenes)

Soxhlet apparatus containing HFO samples A-H (Lubrizol Ltd, Derby, UK) and ~100 mL of n-heptane (Fisher Scientific, Hemel Hempstead, Hertfordshire, United Kingdom) were heated to 130 °C for 22 h. The solid asphaltene residue remaining on the filter was dissolved in toluene (Honeywell Speciality Chemicals Seelze GmbH, Hanover, Germany) and filtered prior to direct infusion experiments.

3.2.2 FTICR MS

C_7 Soxhlet asphaltene fractions isolated from HFO samples A-H were dissolved in toluene (Honeywell Speciality Chemicals Seelze GmbH, Hanover, Germany). Mass spectra were acquired using a 12 T solariX Fourier transform ion cyclotron resonance (FTICR) mass spectrometer (Bruker Daltonik GmbH, Bremen, Germany), coupled to an APPI II source operated in positive-ion mode. Nitrogen was used as the drying gas at a temperature of 220 °C and at a flow rate of 4 L min^{-1}. The nebulizing gas was nitrogen and was maintained at a pressure of 1.2 bar. A krypton lamp was used to produce photons with energy 10.6 eV. Samples were introduced by direct infusion using a syringe pump at a rate of 1000 μL h^{-1} without the activation of in-source dissociation. Low concentration tuning mix (Agilent Technologies, San Francisco, CA, USA) was used as an external calibrant. 4 M data sets were acquired in the detection range *m*/*z* 147-1800 for 300 scans. The data were zero-filled once and apodized using a Sine-Bell function prior to applying a fast Fourier transform. For apodized data, the measured resolving power at *m*/*z* 400 was typically 450,000 to 850,000 depending on the sample studied. IRMPD experiments were performed on an isolation window of an *m*/*z* width of 50 centered on *m*/*z* 564 using a continuous wave, 25 W, CO_2 LASER (Synrad Inc., Washington, USA) operating at 60 % power output. Photons were

produced at a wavelength of 10.6 μm and pulsed into the ICR cell for 0.8 s prior to detection with the low mass cut-off (LMCO) lowered to *m*/*z* 98.3. The spectra were phased with a Half Hanning apodization setting of 0.18 – 0.6 before baseline correction using FTMS Processing 2.1.0 (Bruker Daltonik GmbH, Bremen, Germany). Phased spectra were internally calibrated using homologous series and analyzed using DataAnalysis 4.2 (Bruker Daltonik GmbH, Bremen, Germany), prior to the data being imported into Composer 1.5.6 (Sierra Analytics, Modesto, CA, USA) for compositional analysis, searching for homologous series within elemental constraints (Table 3.2) with a maximum assignment error of 1 ppm permitted. Mass lists generated from IRMPD spectra were cut to remove peaks above *m*/*z* 537.5. To more effectively perform PCA and HCA analyses and to simplify visualization, compound classes were grouped according to heteroatom content. $N_nO_xS_y$ labels were used to denote groups of heteroatom classes where one class possessed n, x or y in excess of 1. Aabel NG2 v.5.2 (Gigawiz Ltd. Co., Tulsa, Oklahoma, USA), OriginPro 2016, and KairosMS (University of Warwick, Coventry, UK) in-house software was used for data categorization, visualization, and statistical analysis. RStudio program (RStudio Inc., Boston, Massachusetts, USA) was used for PCA analysis using dudi.pca from the ade4 package and visualized using fviz_pca from the factoextra package, and HCA analysis was carried out using agglomerative clustering and the Canberra method.

Table 3.2 Composer 1.5.6 parameters for assignment of molecular formulae

Parameter	**Constraints**
Polarity	Positive
Ion properties	Adducts = H; allow radical and adduct/loss ions; remove isolated assignments
m/*z* range	Asphaltenes 200-1300; Isolation 530-600; IRMPD 100-600
DBE range	-0.5 - 40
Element ranges	C: 0-200; H: 0-1000; N: 0-2; O: 0-6; S: 0-3

3.3 Results and Discussion

3.3.1 C_7 Soxhlet Asphaltene Fractions of HFOs A-H

The asphaltene fractions from eight HFO samples isolated by Soxhlet extraction in n-heptane were compared for an overview of compositional differences. The grouped class distribution for the asphaltene fractions of HFOs A-H is shown in Figure 3.1, with the individual class distribution data shown in Figure 3.2.

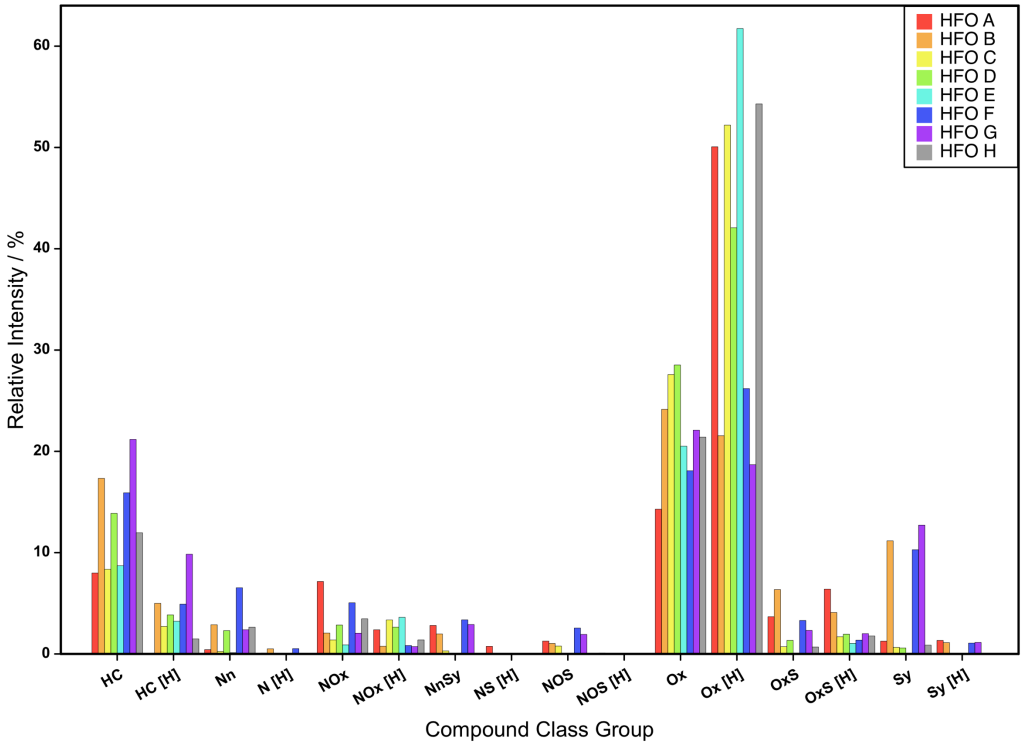

Figure 3.1 – Grouped compound class distribution for C_7 Soxhlet asphaltene fractions of HFOs A-H

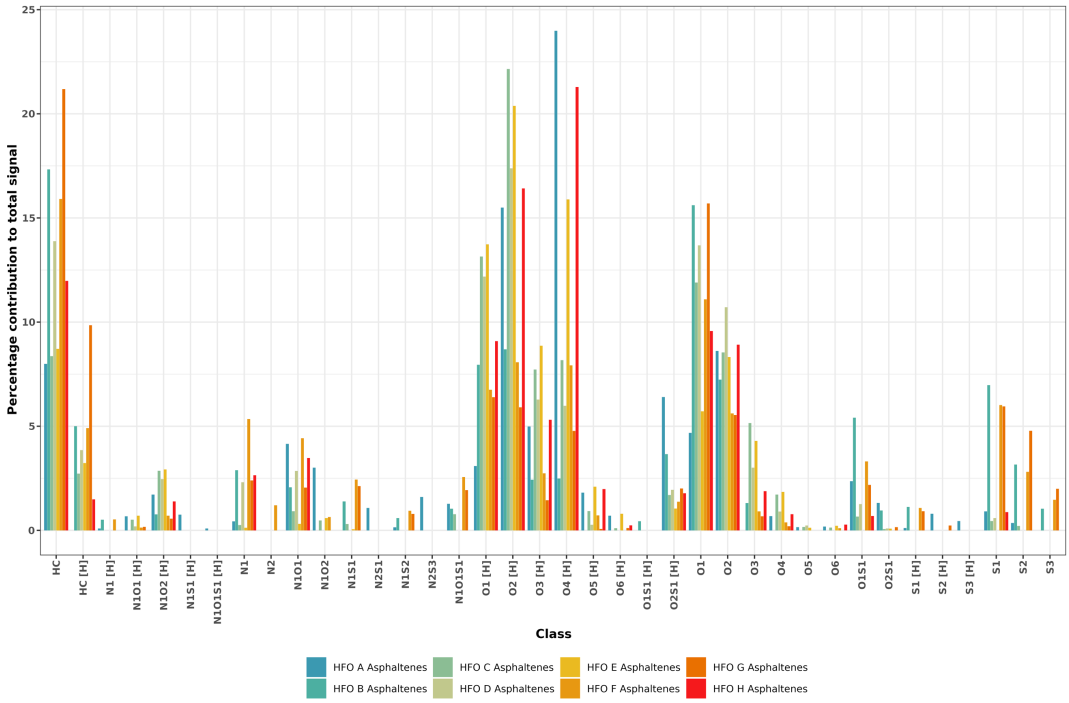

Figure 3.2 – Individual compound class distribution for C_7 Soxhlet asphaltene fractions of HFOs A-H

For HFOs A, C, E, and H a relatively strong contribution was observed for oxygen-containing classes, particularly O_x[H] classes. HFO E appeared to have a correspondingly lower contribution from the HC, HC[H] and N_n classes, while the majority of S-containing classes were not detected for the asphaltene fraction of this sample. These features may be indicative of a desulfurization process involving an oxidation step.

The class distributions of the asphaltene fractions of HFOs B, F, and G appear similar, in particular the strong contributions from S-containing classes. However, several observations that may explain differences in bulk behavior can be made. For example, HFO F appears to have a greater relative contribution from several nitrogen-containing classes, particularly N_n, N[H], and NO, which may be important for responsiveness to additive chemistries designed to stabilize HFOs against asphaltene flocculation, deposition and black paint formation. HFO G appears to have a strong contribution from the HC and HC[H] classes, while HFOs B and G have a strong contribution from the O class. O-containing compounds, which may include some asphaltenes, can affect responsiveness to additive chemistries due to their interactions with the polar, O-containing functionalities on additives such as dispersants (Boukherissa et al., 2009). The HC[H] class makes a less substantial contribution to the other asphaltene

fractions, indicating that the hydrocarbon substances present in HFO G may differ to those present in other samples and cause handling issues.

HFO H has a relatively strong contribution from the NO class, similar to HFOs A and F, and from the O_x[H] classes, similar to HFO E, and in contrast to the high contribution from the O class observed in problematic HFOs B and G. These similarities between HFOs that are known to respond well to additive chemistry, or those with a low sulfur content, may be responsible for the absence of apparent asphaltene handling issues for HFO H.

Demonstrating the efficiency of the C_7 Soxhlet fractionation, the distribution of DBE detected in the S class of the asphaltene fraction of HFO A is compared to that detected in the whole HFO and in the maltene fraction in Figure 3.3, broken down into plots of DBE against carbon number in Figure 3.4.

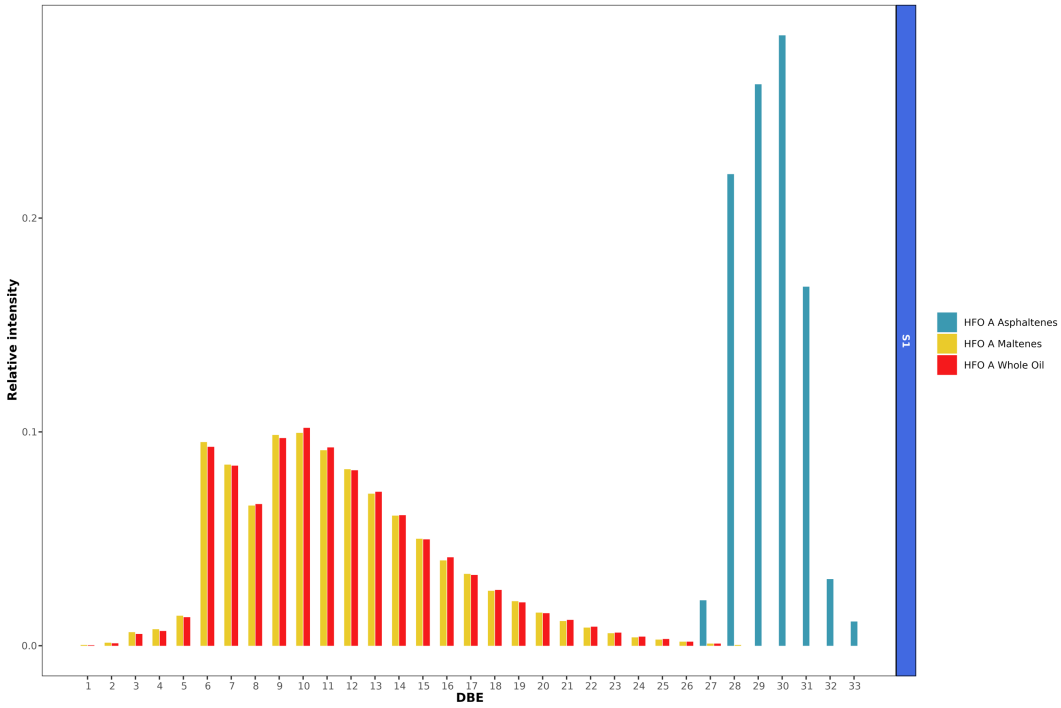

Figure 3.3 – Distribution of DBE values of the S class, compared between whole HFO A, and its maltene and asphaltene fractions, demonstrating the efficient isolation of the asphaltene fraction using Soxhlet extraction, and that in whole HFOs the species detected are similar to those detected in the maltene fraction

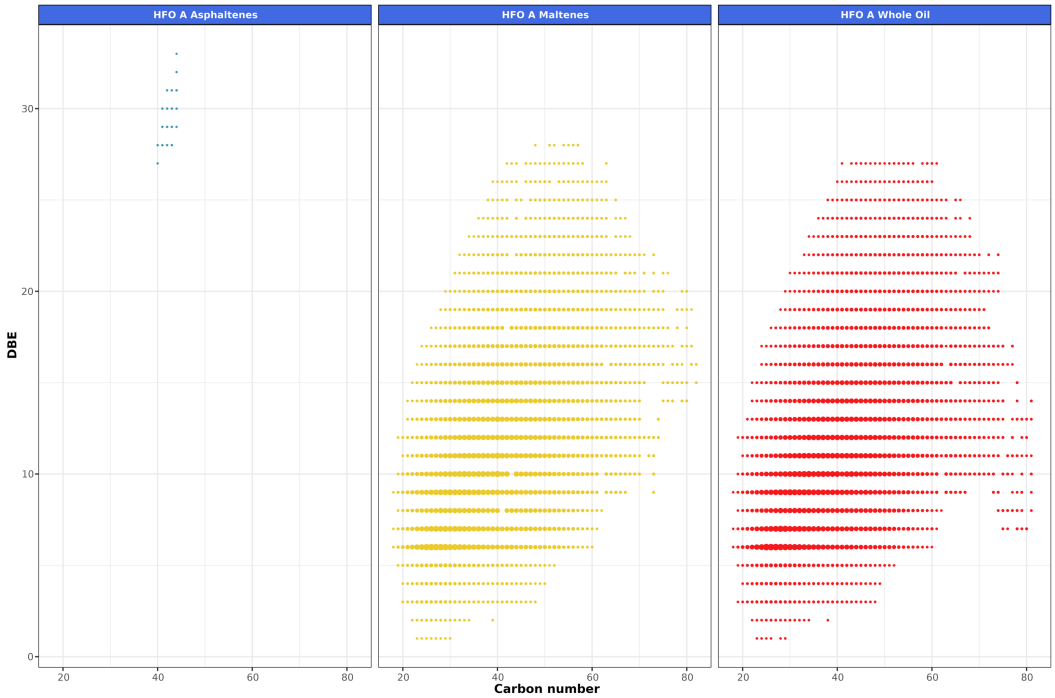

Figure 3.4 – Plots of DBE against carbon number for the S class of HFO A, demonstrating the similarity between the maltene fraction and the whole oil, and the extended compositional access afforded by asphaltene fraction isolation

The S class DBE distribution shown in Figure 3.3 demonstrates the expected similarity between species detected in the whole HFO and the maltene fraction, which may result from a predominant detection of aromatic fraction species when studying whole oils (Cho et al., 2012). There is a large increase in contribution to relative intensity beginning from DBE 6, corresponding to the minimum required to form a benzothiophenic species. Figure 3.3 also shows that higher DBE species were detected in the asphaltene fraction such that the compositional space of the HFO accessible was extended following separation. The similarity between whole HFO A and its C_7 Soxhlet maltene fraction is demonstrated further in the class distribution data presented in Figure 3.5.

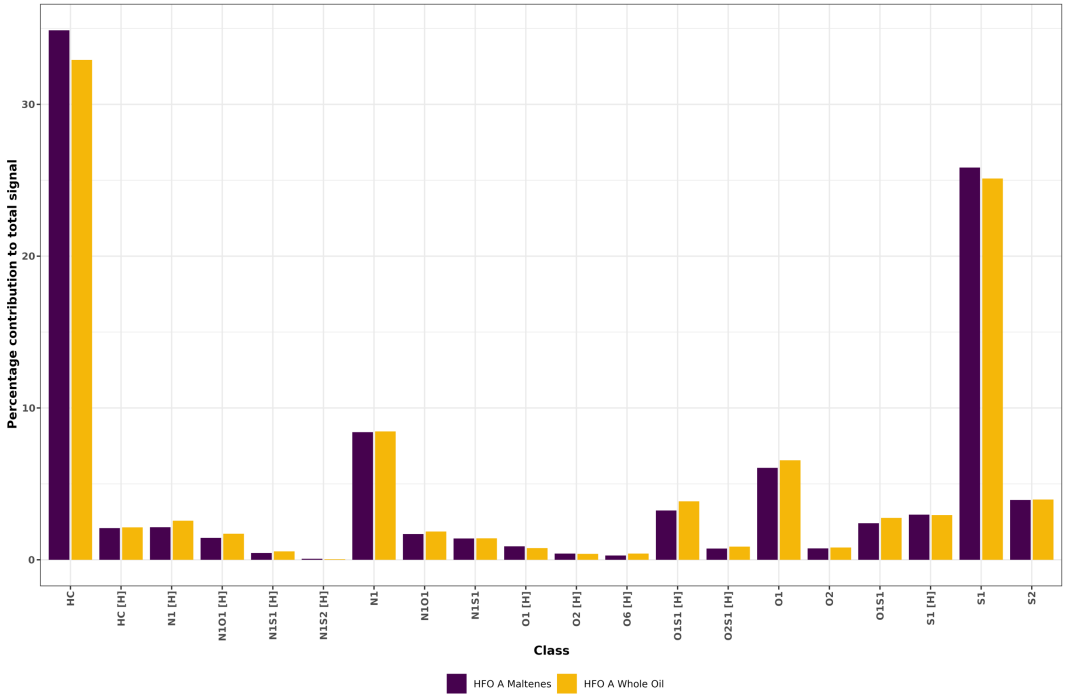

Figure 3.5 - Classes distribution for whole HFO A and its and C_7 Soxhlet maltene fraction, demonstrating similarity between species ionized preferentially in whole HFO and in the maltene fraction

3.3.2 IRMPD Fragmentation of HFO A-H Asphaltene Fractions

To gain an understanding of whether heteroatoms are primarily contained within the stable aromatic cores of asphaltene molecules, smaller aromatic moieties, or on substituent alkyl chains, the asphaltene fractions of HFOs A-H were subjected to tandem mass spectrometry experiments using IRMPD for fragmentation of precursor ions isolated in a window of width *m*/*z* 50 centered on *m*/*z* 564. Lower abundance species are detected more readily and a greater resolving power is afforded in isolation mass spectra compared to broadband mass spectra (Palacio Lozano et al., 2019). This can be demonstrated by the relative abundance of some N_nS_y classes, which are only readily detected in the broadband mass spectra of HFO A, but detected in the isolation spectra of several HFOs (Figures 3.2 and 3.6).

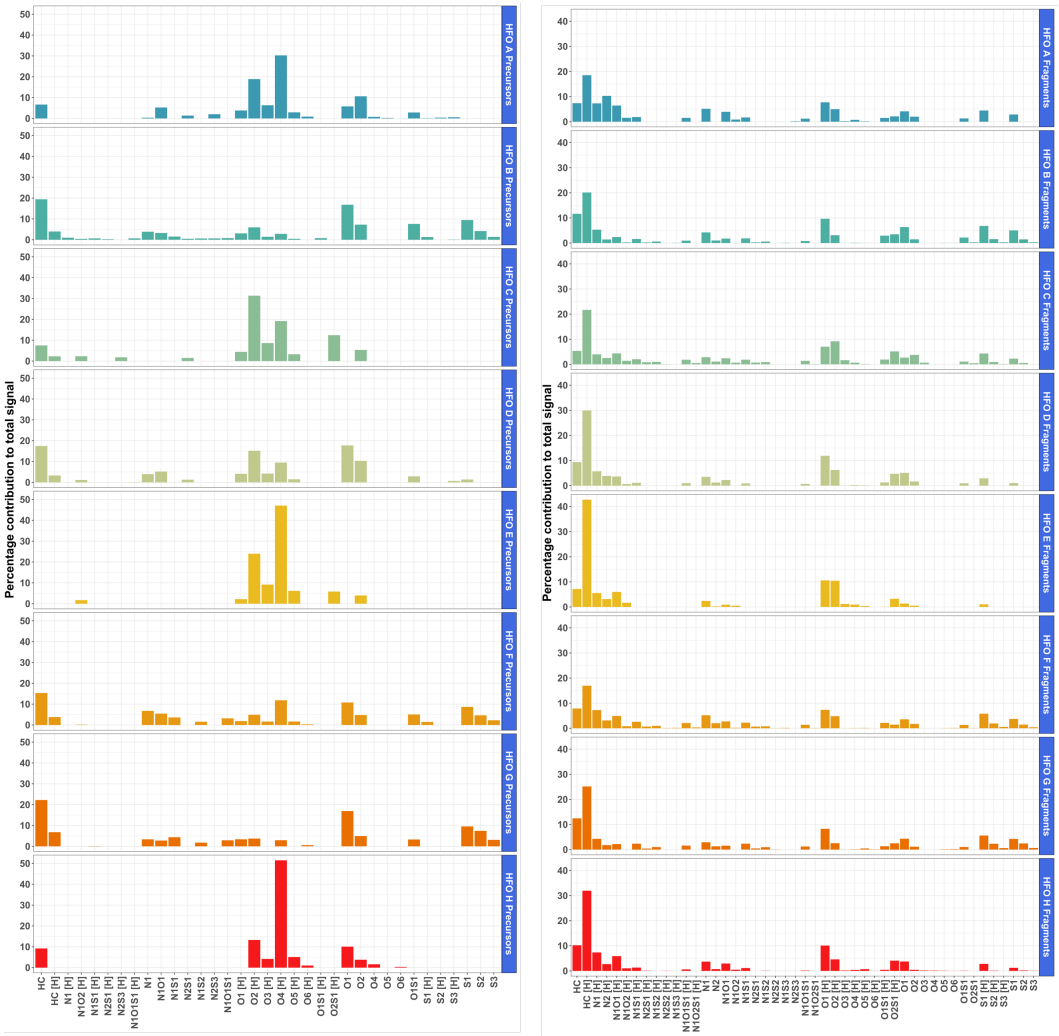

Figure 3.6 – Individual compound class distributions of precursors and fragment ions for each HFO. Fragments generally have a stronger relative intensity from compound classes containing fewer heteroatoms, and there is a shift from radical (odd-electron) precursors to even-electron fragments, with the HC[H] class predominant in fragment spectra. The change in predominance from odd-electron precursors to even-electron fragments occurs due to greater fragmentation efficiency of radical compared to protonated precursors. Additionally, even-electron fragments may be generated from odd-electron precursors during fragmentation

The change in relative intensity of compound class groups comparing fragmentation spectra to the corresponding precursor isolation spectra for each HFO is shown in Figure 3.7. The individual and grouped class distribution data used to generate Figure 3.7 are shown in Figures 3.6, 3.8 and 3.9. A change in heteroatom class assignment occurs when the fragments detected contain fewer heteroatoms relative to the precursor parent ions. A negative change in relative intensity indicates that a compound class group is detected at lower relative

intensity in the fragmentation spectra compared to the precursor ion isolation spectra, indicating that such species fragment more readily.

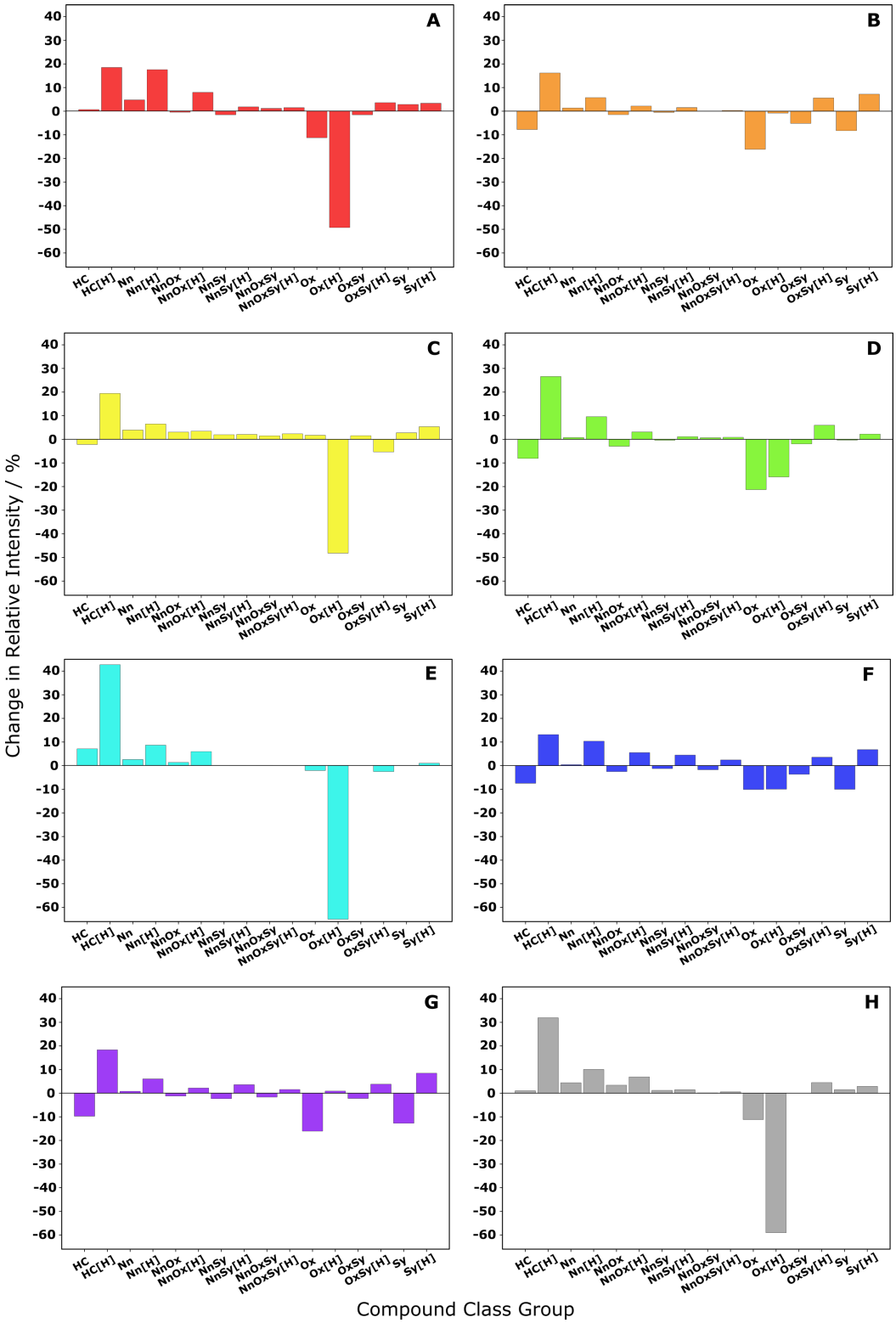

Figure 3.7 – Change in relative intensity of compound class groups comparing IRMPD fragment to the corresponding precursor ion spectra for each HFO sample

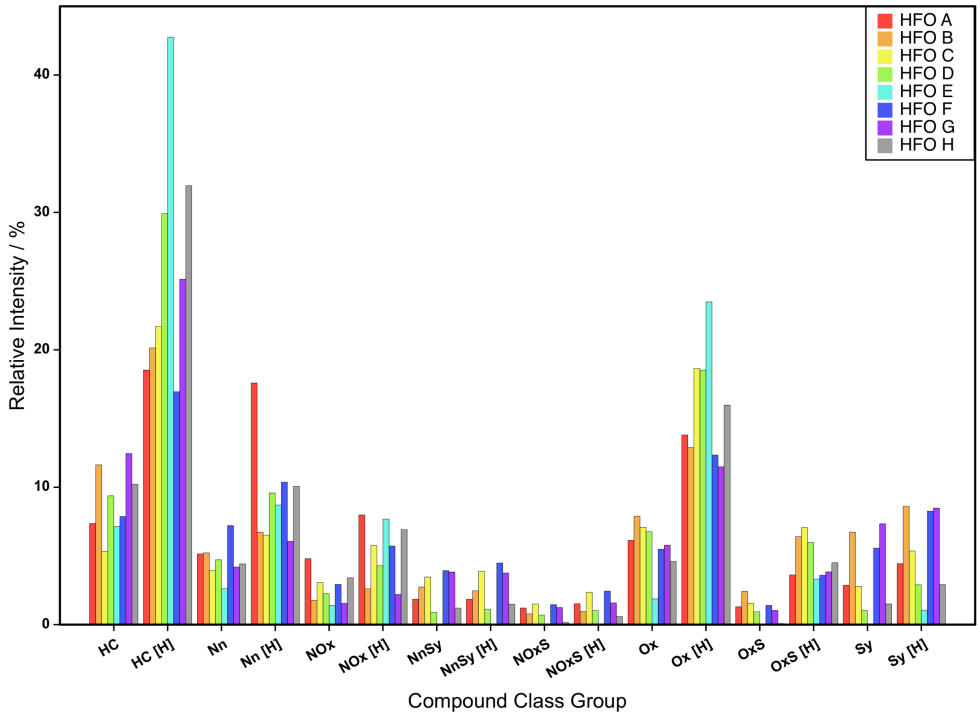

Figure 3.8 – Grouped compound class distribution for IRMPD fragment ion spectra

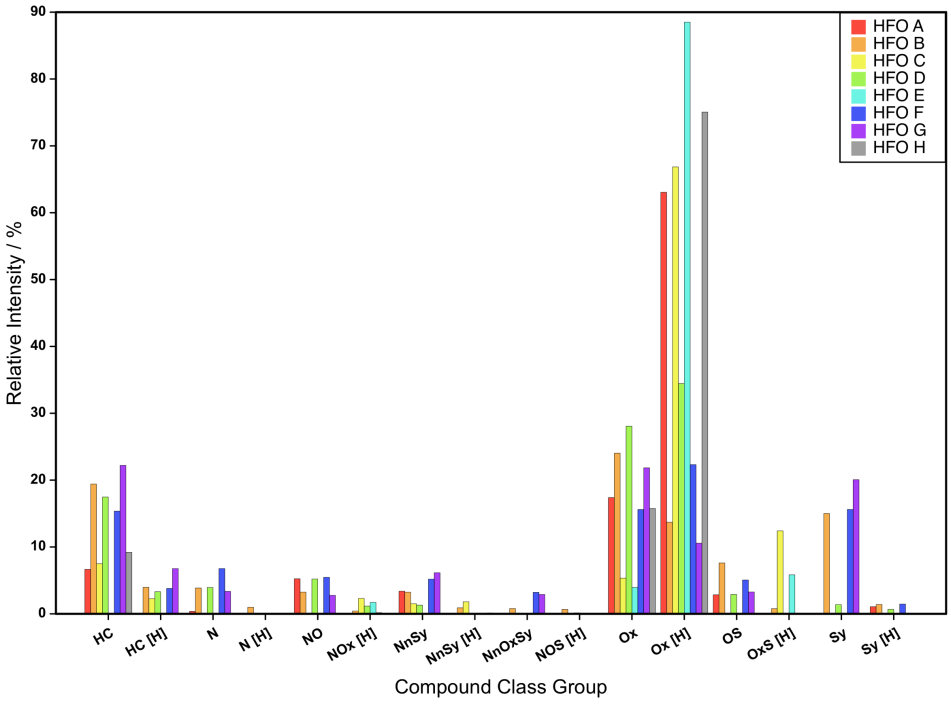

Figure 3.9 – Grouped compound class distribution from precursor ion isolation spectra

Figure 3.7 shows that generally, a shift from radical (odd-electron) to even-electron classes is observed following fragmentation, which is due to the greater reactivity of radical precursor species causing them to fragment more readily. Following IRMPD fragmentation, the largest decrease in the relative intensities was observed for the O_x[H] classes for several HFOs, most notably for HFOs A, C, E, and H. This is likely due to these classes comprising functionalities including carboxylic acids, which are capable of forming good leaving groups such as OH, COOH, CO_2 and H_2O. As a result, a shift from O_x[H] predominance to O_x or HC and HC[H] classes may be observed. HFOs B and G, on the other hand, appear to have had a similar change in the relative intensities of compound class groups, with a more pronounced decrease in the O_x and S_y classes.

Figure 3.1 showed that the broadband asphaltene spectra of HFO E had low relative contribution from the N_n and N[H] classes, however Figure 3.7 indicates that N_n[H] class fragment ions have been generated for HFO E, which may be derived from parent ions containing more than one heteroatom, for instance those assigned to NO_x[H] classes. For HFO F, N-containing classes were detected in both the broadband asphaltene mass spectrum and the IRMPD fragment spectrum. While N-containing precursor ions were detected in relatively high abundance for HFO F, a considerable contribution from N_n and N_n[H] fragment ions was also detected, as demonstrated by the positive change in intensities indicated in Figure 3.7, while the contribution from HC and HC[H] fragments is comparatively low, suggesting that nitrogen-containing stable aromatic cores may predominate in its asphaltene fraction.

HFOs E and H have a sharp increase in HC[H] relative intensity following fragmentation, which suggests that the precursors for these samples, predominantly O_x[H] species, may be more likely to have heteroatoms present in alkyl chains rather than in stable aromatic cores. Although HFO A also had a strong contribution to its precursor ion spectrum from O_x[H] classes, it also had a relatively high contribution from the NO class, similar to HFOs D and F, although these appear to have generated a stronger relative proportion of N_n[H] class fragment ions.

Class distributions provide limited information on whether heteroatoms are contained within stable aromatic cores or on alkyl substituents, as the fragment that carries charge, and is therefore detected, may not necessarily be the asphaltene core. To more robustly characterize and compare fragment ions

between samples, boxplots in Figure 3.10 demonstrate a novel means by which to visualize the spread of fragment DBE and carbon number for multiple heteroatom classes simultaneously. These boxplots are compared against the intensity weighted mean DBE and carbon number, and maximum and minimum DBE and carbon number, of all precursor ions detected. Comparison of fragment properties for asphaltene structural information is typically performed through comparison of multiple plots of DBE against carbon number, which is time consuming and makes cross referencing challenging.

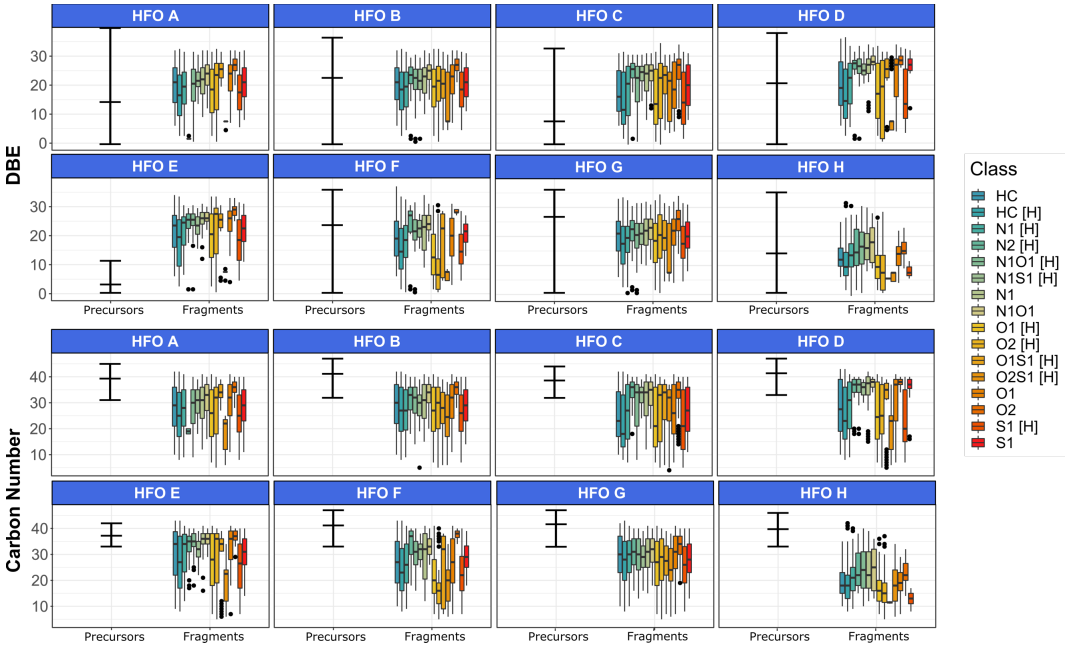

Figure 3.10 – Intensity weighted mean and dispersity of DBE and carbon number of fragment ion classes contributing greater than 2.5 % displayed as boxplots. The intensity weighted mean and range of DBE and carbon number for all precursor ions detected in the isolation spectra is indicated for comparison

Figure 3.10 demonstrates the rapid and relative ease of comparison of multiple fragment DBE and carbon number distributions, as compared to the more traditional process of inspecting each individual heteroatom class and sample. While the mean intensity weighted carbon number for the precursor ions is similar for all samples, HFOs A, C, and E have relatively low intensity weighted mean DBE in their precursors. This could be due to these samples having a lower asphaltene content and higher proportion of oxygenated compounds, such that the heptane-insoluble fraction, and consequently precursor isolation spectra, instead comprises high carbon number, high polarity species. For HFO E such polar species may be particularly predominant if the HFO has undergone a desulfurization process involving oxidation, although generation of higher DBE

fragments from precursors may also be due to rearrangement reactions of these species following photon absorption. Nevertheless, some fragments that may be related to asphaltene core structure can be visualized and compared between all samples. Over 70 % of the relative intensity of the precursor ion NO class (Figure 3.11) is assigned to species with DBE of 25 or above, so, as a rough approximation, fragment ions maintaining DBE over 25 are considered to be derived from island-type asphaltene precursors.

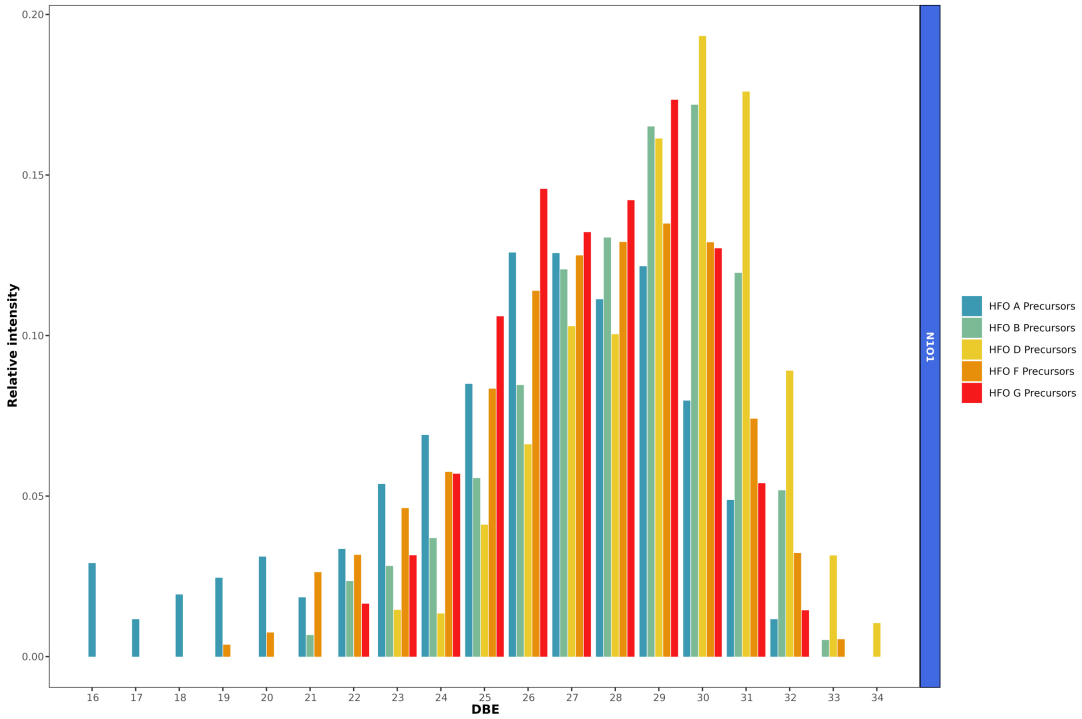

Figure 3.11 – DBE distribution of NO class from precursor ion spectra, demonstrating the predominance of species with DBE between 25 and 32 in the majority of samples

Nitrogen-containing fragments with DBE values over 25 were detected in the majority of samples, although for HFO H a more pronounced spread to lower DBE values is observed. For HFOs D and E these fragments typically also have carbon number in excess of 35, suggesting a greater degree of alkylation which may improve their handling properties, such as easier blending with distillates. While it is possible for high DBE nitrogen-containing class fragments to be derived from archipelago-type asphaltene precursors, the alkyl linkage is likely to be cleaved during IRMPD fragmentation, so they can therefore be considered component moieties of island-type asphaltene precursors. Relatively high DBE N[H] class species were also detected in HFO G, while N_2[H] class species concentrated at higher DBE were detected in HFOs B, C, D, and G, spreading to

lower DBE values in HFOs E, F, and H. Generally, the intensity weighted mean DBE was lower in the HC and HC[H] fragment classes for HFOs C, D, E, and H, compared to those for A, B, and G.

In general, fragments with DBE in excess of 25, more likely to be derived from island-type asphaltene precursors (Figure 3.11), were assigned to the odd-electron nitrogen-containing classes in HFOs that present fewer asphaltene handling issues. Conversely, HFOs that have higher DBE fragments predominantly in even-electron nitrogen-containing classes, which may correspond to more polar, basic compounds which are more prone to inhibiting hydrotreatment processes (Guillemant et al., 2019a), and in the hydrocarbon classes, which may be indicative of more extensive aromatic structures, might be more problematic (Gabrienko et al., 2014; Zeuthen et al., 2001). Furthermore, HFOs that contain a higher proportion of nitrogen-containing archipelago-type asphaltenes, which have lower steric hindrance than island-type, and therefore greater flexibility within the alkyl chains permitting movement and reorientation of individual cores, may lead to more rapid fouling of catalysts and a greater propensity to flocculation and deposition.

3.3.3 PCA and HCA Analyses

Comparing tandem mass spectrometry data between multiple samples is time consuming and makes cross referencing challenging. PCA and HCA analyses have been identified as suitable methods for comparing multiple petroleum data sets rapidly (Grewer et al., 2010; Headley et al., 2011; Hur et al., 2010; Lozano et al., 2017; Stout et al., 2001), and are here applied for the first time to fragmentation data.

For the asphaltene and IRMPD fragmentation data, classes were grouped depending on heteroatom content. The results of the PCA and HCA analyses for IRMPD fragment data are shown in Figures 3.12 and 3.13, with the variables plot corresponding the PCA analysis shown in Figure 3.14. The results of PCA and HCA analyses of the broadband asphaltene spectra are shown in Figures 3.15-3.17. For the fragment data a sufficient proportion of the variance could be explained in the first two principal components (74.2 %), while the cophenetic correlation coefficient in HCA analysis was 0.96, confirming efficient clustering (Saraçli et al., 2013; Sokal and Rohlf, 1962).

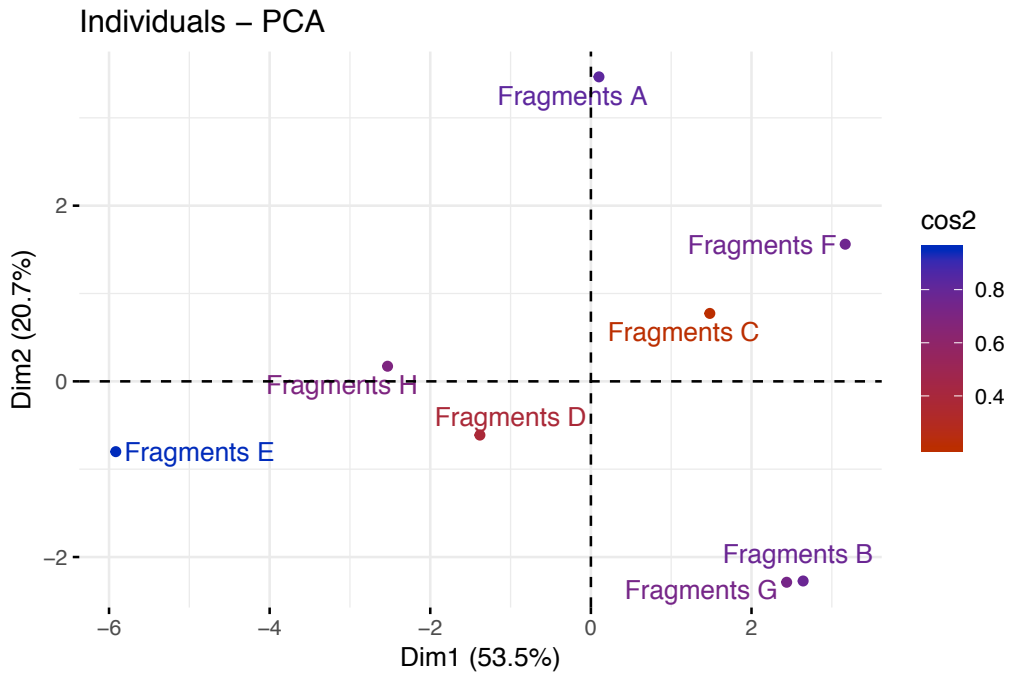

Figure 3.12 – PCA analysis for grouped compound class distributions detected in IRMPD fragmentation spectra

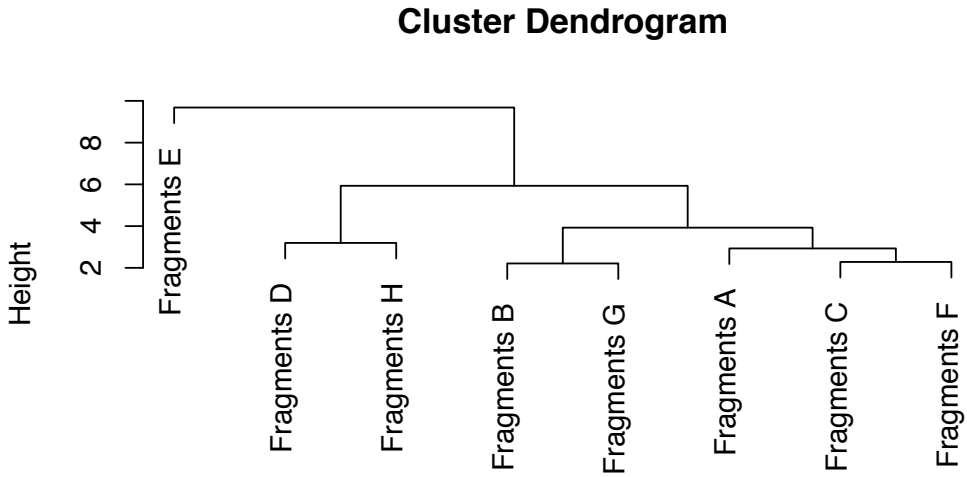

Figure 3.13 - HCA analysis for grouped compound class distributions detected in IRMPD fragmentation spectra

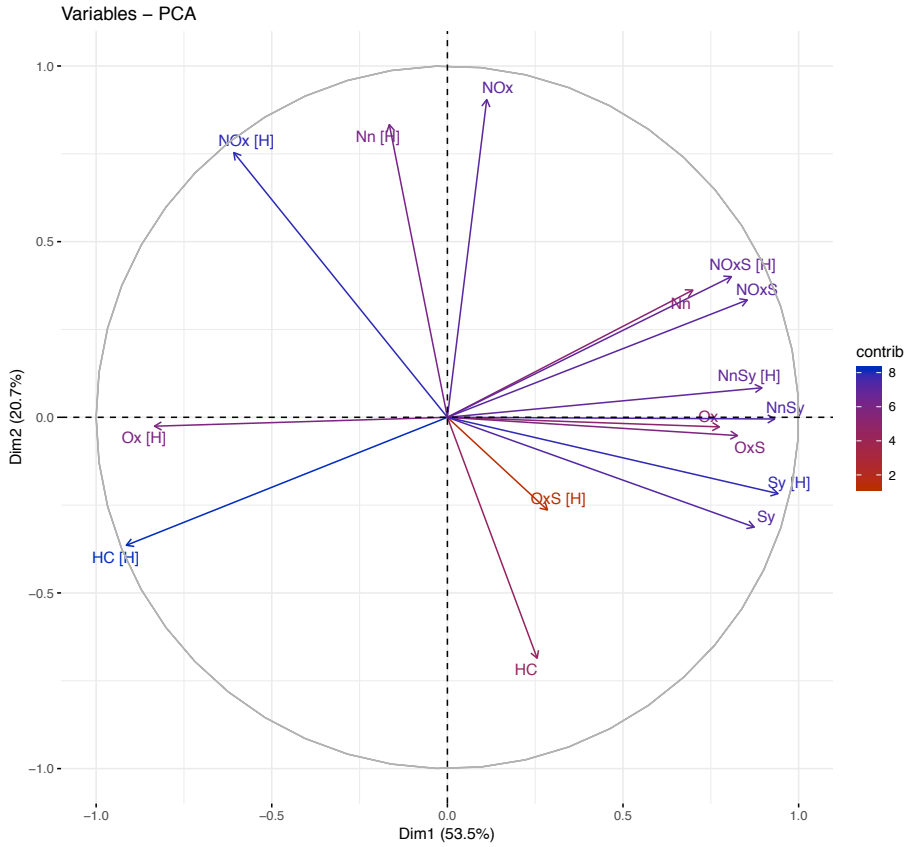

Figure 3.14 – Variables plot for PCA analysis of IRMPD fragmentation data

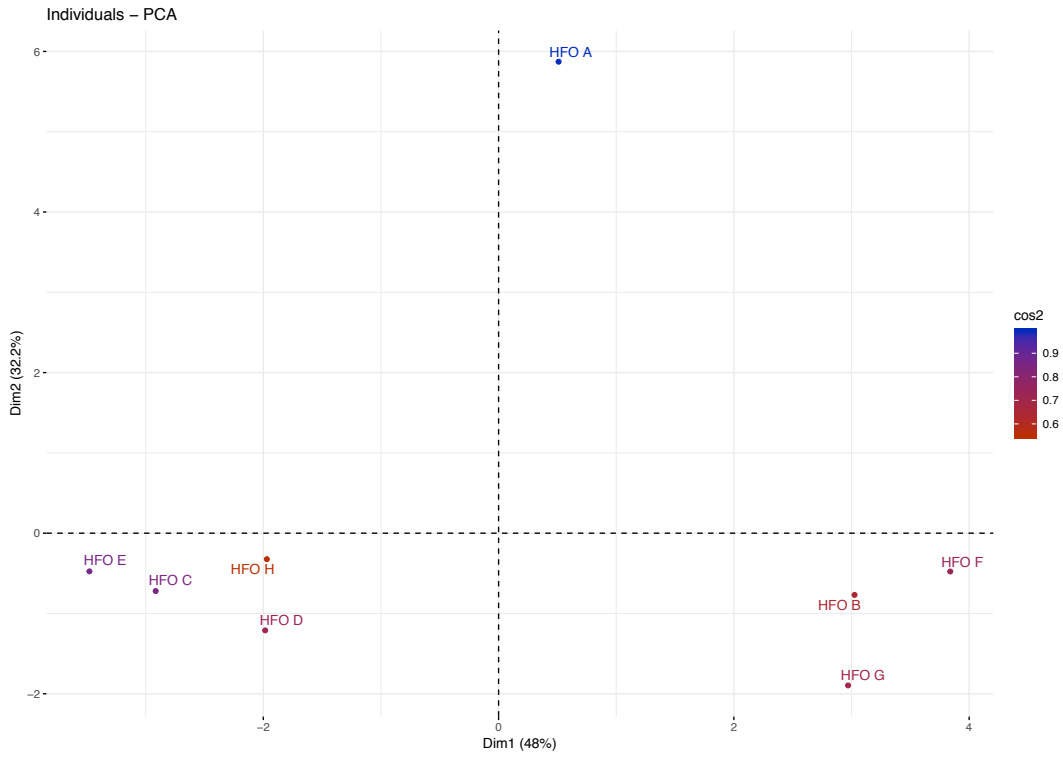

Figure 3.15 – PCA analysis for grouped compound class distributions detected in broadband asphaltene spectra

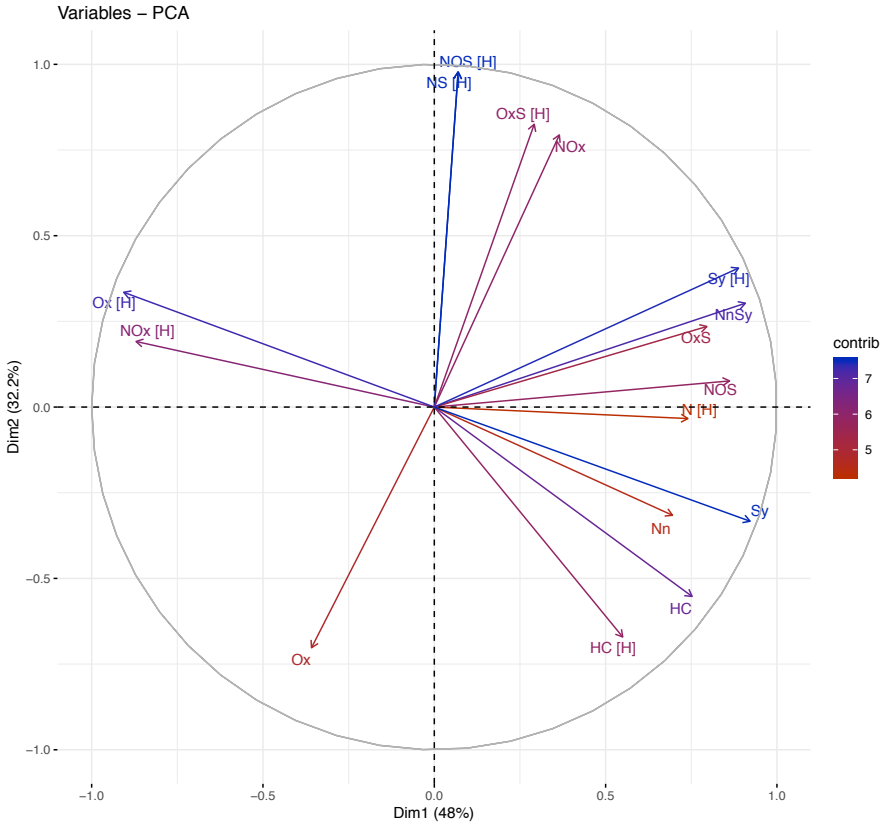

Figure 3.16 – Variables plot for PCA analysis of grouped compound class distributions detected in broadband asphaltene spectra

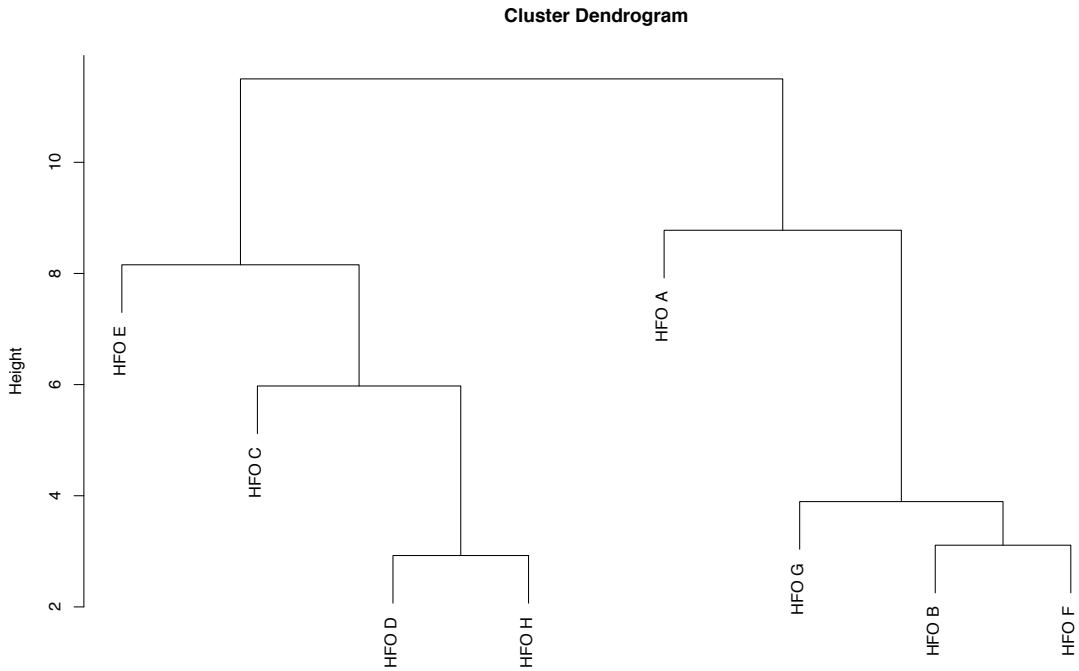

Figure 3.17 – HCA analysis for grouped compound class distributions detected in broadband asphaltene spectra. The cophenetic correlation coefficient was 0.91

The PCA and HCA analyses are consistent but display some complementary information that may be useful in understanding variations in HFO bulk behavior. A summary of the findings of the statistical analyses, presenting groupings of similar HFO samples, and the compound class variables underlying these observations, is provided in Table 3.3.

Table 3.3 Summary of findings from statistical analysis of asphaltene and IRMPD fragment data

	HFO Groupings	**Compound Classes**
Asphaltenes	A B, F, G C, D, E, H	NS[H] and NOS[H] HC, HC[H], S_y O_x, NO_x[H]
Fragments	A, C, F B, G D, E, H	NO_xS and N_nS_y HC, S_y, and S_y[H] O_x[H] and NO_x[H]

Figure 3.12 suggests that the asphaltene fragments of HFOs B and G, and to a lesser extent HFOs A, C, and F, and HFOs D, E, and H, group closely. Figure 3.13 corroborates a greater degree of similarity between HFOs B and G, but suggests that HFO E is less similar to the other samples while HFO A groups less closely to HFOs C and F than they do to one another. Inspection of the variable loading plot shown in Figure 3.14 suggests that the grouping of D, E, and H is due to contributions from O_x[H] and NO_x[H] fragments. The NO_x[H] class group variable is located close to the circle of correlations (Abdi and Williams, 2010) due to its relatively strong contribution to the second principal component, suggesting that the presence of this class at higher relative abundance may be linked to easier handling. HFOs C and F group closely due to contributions from the NO_xS and N_nS_y odd- and even-electron fragments, whereas HFO A appears to differ slightly from these through NO_x class content. The fragments of B and G appear to be similar based on HC, S_y, and S_y[H] class contributions, reflecting the similarity in the change in compound class group relative intensities observed in Figure 3.7 yet extending understanding with complementary insight. As the S_y[H] class group contributes most strongly to the first principal component and is located closest to the circle of correlations, it is likely that a high relative abundance of this class may be linked to a higher likelihood of asphaltene handling issues.

The PCA and HCA analysis of the fragment data provide information complementary to that of broadband asphaltene data and can be combined with DBE and carbon number distributions, such as those shown in Figure 3.10, to improve molecular-level understanding. While HFO A appears to differ greatly from all other HFO samples in the whole asphaltene PCA shown in Figure 3.15, due to contributions from the NS[H] and NOS[H] classes, species assigned to these classes are also detected in the fragment spectra of HFOs C and F. However, fragment PCA analysis indicates that what sets the fragments of HFO A apart is NO_x content. Cross-referencing with the DBE boxplots (Figure 3.10), suggests that these species are found in stable aromatic cores with neutral DBE ranging predominantly between 15 and 27. The asphaltene PCA and HCA groups HFOs B, F, and G closely, although it is known that HFO F presents fewer asphaltene handling problems. The fragment PCA suggests that this may be due to the presence of nitrogen-containing species that form odd-electron fragments in the stable aromatic cores of HFO F, as opposed to the higher proportion of S and high DBE HC cores observed in HFOs B and G. The asphaltene PCA groups HFOs C, D, E and H closely, largely due to the relative proportions of several oxygen-containing class groups, whereas the fragment PCA provides additional insight. The greater variation separating HFO C is due to contributions from nitrogen and sulfur-containing class groups, and that separating HFO E from the other samples is contributions from O_x[H] classes.

3.4 Conclusions

The combined analytical approach, summarized below, provides a comprehensive means by which to simultaneously compare the asphaltene fractions of marine HFOs.

- Soxhlet extraction was used to isolate the n-heptane insoluble fraction of eight HFOs (C_7 Soxhlet Asphaltenes).
- The fractions were dissolved in toluene and studied using (+) APPI-FTICR MS, which provided efficient and preferential compositional access to asphaltenes. Such an approach remains useful for identifying molecular-level differences that may be responsible for varying bulk behavior and responsiveness to additive packages.
- Fragmentation using IRMPD provided greater insight into asphaltene structure.

- Comparison of DBE and carbon number distributions for multiple compound classes is made possible utilizing novel representation modes, yielding improved structural insight.
- Combining grouped IRMPD fragment data with PCA and HCA analyses identified variables that may underly similarities and differences in HFO bulk behavior that may not be immediately obvious. This is pertinent as comparing multiple class distributions and cross-referencing becomes increasingly inefficient and unfeasible for complex data.

The molecular-level profiling of the HFO asphaltene fractions and their fragments further advances understanding of factors that may underly differences in the observed bulk properties and behaviours. HFOs B, D, and F have a relatively high asphaltene content as determined by bulk analysis, but the greater responsiveness to additive chemistries and the lesser degree to which D and F suffer from asphaltene handling issues may be explained the nitrogen-containing functionalities in the stable aromatic cores generated by IRMPD fragmentation. Although bulk data suggests HFOs G and H are similar, the FTICR MS analysis suggests that the solubility issues of G can be explained by the presence of highly condensed PAH fragments, which may precipitate in bulk engine oils. HFOs A has a lower asphaltene content, while C and E have high TAN, and as such it is likely that their n-heptane insoluble fraction is comprised of more polar species, reflected in their greater contributions from oxygen-containing classes. The high oxygen content detected for HFO E suggests that it has undergone an oxidizing desulfurization process such that meets IMO 2020, however due to its high TAN, as with HFO C, this likely corresponds to a high concentration of carboxylic acid species which may cause problems with corrosion and reduce its market value. HFO A is milder and is responsive to additive chemistries, and the analysis carried out in this chapter further indicates that this may be due to a greater concentration of nitrogen-containing compounds in its n-heptane insoluble fraction.

Simultaneous analysis of multiple HFO samples with differing properties, such as responsiveness to additives or propensity to asphaltene handling issues, and the identification of problematic components, may drive improvements in formulations with the eventual development of simpler and more universally applicable chemistries.

The methodology employed in this study may also be applied to the characterisation of crude oil and heavy petroleum, including environmental samples such as oil-sands bitumen, as well as more generally to fragmentation spectra where comparison of molecular-level characteristics is of interest.

3.5 References

Abdi H, Williams LJ. Principal component analysis. Wiley Interdisciplinary Reviews: Computational Statistics 2010; 2: 433-459.

Akbarzadeh K, Hammami A, Kharrat A, Zhang D, Allenson S, Creek J, et al. Asphaltenes - Problematic but Rich in Potential. Oilfield Review 2007; 19: 22-43.

Annesley TM. Ion suppression in mass spectrometry. Clinical Chemistry 2003; 49: 1041-1044.

Barrow M, Headley J, Peru K, Derrick P. Data Visualization for the Characterization of Naphthenic Acids within Petroleum Samples. Energy & Fuels 2009; 23: 2592-2599.

Boukherissa M, Mutelet F, Modarressi A, Dicko A, Dafri D, Rogalski M. Ionic Liquids as Dispersants of Petroleum Asphaltenes. Energy & Fuels 2009; 23: 2557-2564.

Bukowski A, Milczarska T. Asphalts as Inhibitors of Radical Polymerization. Journal of Applied Polymer Science 1983; 28: 1001-1009.

Chacon-Patino M, Rowland S, Rodgers R. Advances in Asphaltene Petroleomics. Part 1: Asphaltenes Are Composed of Abundant Island and Archipelago Structural Motifs. Energy & Fuels 2017; 31: 13509-13518.

Chacon-Patino ML, Rowland SM, Rodgers RP. Advances in Asphaltene Petroleomics. Part 2: Selective Separation Method That Reveals Fractions Enriched in Island and Archipelago Structural Motifs by Mass Spectrometry. Energy & Fuels 2018a; 32: 314-328.

Chacon-Patino ML, Rowland SM, Rodgers RP. Advances in Asphaltene Petroleomics. Part 3. Dominance of Island or Archipelago Structural Motif Is Sample Dependent. Energy & Fuels 2018b; 32: 9106-9120.

Chiaberge S, Fiorani T, Savoini A, Bionda A, Ramello S, Pastori M, et al. Classification of crude oil samples through statistical analysis of APPI FTICR mass spectra. Fuel Processing Technology 2013; 106: 181-185.

Cho Y, Birdwell JE, Hur M, Lee J, Kim B, Kim S. Extension of the Analytical Window for Characterizing Aromatic Compounds in Oils Using a Comprehensive Suite of High-Resolution Mass Spectrometry Techniques

and Double Bond Equivalence versus Carbon Number Plot. Energy & Fuels 2017; 31: 7874-7883.

Cho YJ, Na JG, Nho NS, Kim S. Application of Saturates, Aromatics, Resins, and Asphaltenes Crude Oil Fractionation for Detailed Chemical Characterization of Heavy Crude Oils by Fourier Transform Ion Cyclotron Resonance Mass Spectrometry Equipped with Atmospheric Pressure Photoionization. Energy & Fuels 2012; 26: 2558-2565.

Dickie JP, Yen TF. Macrostructures of the asphaltic fractions by various instrumental methods. Analytical Chemistry 1967; 39: 1847-1852.

Douglas DJ. Applications of Collision Dynamics in Quadrupole Mass Spectrometry. Journal of the American Society for Mass Spectrometry 1998; 9: 101-113.

Durand E, Clemancey M, Lancelin JM, Verstraete J, Espinat D, Quoineaud AA. Effect of Chemical Composition on Asphaltenes Aggregation. Energy & Fuels 2010; 24: 1051-1062.

Farenc M, Corilo YE, Lalli PM, Riches E, Rodgers RP, Afonso C, et al. Comparison of Atmospheric Pressure Ionization for the Analysis of Heavy Petroleum Fractions with Ion Mobility-Mass Spectrometry. Energy & Fuels 2016; 30: 8896-8903.

Gabrienko AA, Subramani V, Martyanov ON, Kazarian SG. Correlation between Asphaltene Stability in n-Heptane and Crude Oil Composition Revealed with In Situ Chemical Imaging. Adsorption Science & Technology 2014; 32: 243-255.

Grewer DM, Young RF, Whittal RM, Fedorak PM. Naphthenic acids and other acid-extractables in water samples from Alberta: What is being measured? Science of the Total Environment 2010; 408: 5997-6010.

Guillemant J, Albrieux F, de Oliveira LP, Lacoue-Negre M, Duponchel L, Joly JF. Insights from Nitrogen Compounds in Gas Oils Highlighted by High-Resolution Fourier Transform Mass Spectrometry. Analytical Chemistry 2019a; 91: 12644-12652.

Guillemant J, Albrieux F, Lacoue-Negre M, de Oliveira LP, Joly JF, Duponchel L. Chemometric Exploration of APPI(+)-FT-ICR MS Data Sets for a Comprehensive Study of Aromatic Sulfur Compounds in Gas Oils. Analytical Chemistry 2019b; 91: 11785-11793.

Halff A, Younes L, Boersma T. The likely implications of the new IMO standards on the shipping industry. Energy Policy 2019; 126: 277-286.

Hanold KA, Fischer SM, Cormia PH, Miller CE, Syage JA. Atmospheric pressure photoionization. 1. General properties for LC/MS. Analytical Chemistry 2004; 76: 2842-2851.

Headley J, Barrow M, Peru K, Fahlman B, Frank R, Bickerton G, et al. Preliminary fingerprinting of Athabasca oil sands polar organics in environmental samples using electrospray ionization Fourier transform ion cyclotron resonance mass spectrometry. Rapid Communications in Mass Spectrometry 2011; 25: 1899-1909.

Hur M, Yeo I, Park E, Kim Y, Yoo J, Kim E, et al. Combination of Statistical Methods and Fourier Transform Ion Cyclotron Resonance Mass Spectrometry for More Comprehensive, Molecular-Level Interpretations of Petroleum Samples. Analytical Chemistry 2010; 82: 211-218.

Islam A, Ahmed A, Hur M, Thorn K, Kim S. Molecular-level evidence provided by ultrahigh resolution mass spectrometry for oil-derived doc in groundwater at Bemidji, Minnesota. Journal of Hazardous Materials 2016; 320: 123-132.

Jameel AGA, Khateeb A, Elbaz AM, Emwas AH, Zhang W, Roberts WL, et al. Characterization of deasphalted heavy fuel oil using APPI (+) FT-ICR mass spectrometry and NMR spectroscopy. Fuel 2019; 253: 950-963.

Kabel K, Abdelghaffar A, Farag R, Maysour N, Zahran M. Synthesis and evaluation of PAMAM dendrimer and PDPF-b-POP block copolymer as asphaltene inhibitor/dispersant. Research on Chemical Intermediates 2015; 41: 457-474.

Kafer U, Groger T, Ruger CP, Czech H, Saraji-Bozorgzad M, Wilharm T, et al. Direct inlet probe - High-resolution time-of-flight mass spectrometry as fast technique for the chemical description of complex high-boiling samples. Talanta 2019; 202: 308-316.

Krajewski LC, Lobodin VV, Johansen C, Bartges TE, Maksimova EV, MacDonald IR, et al. Linking Natural Oil Seeps from the Gulf of Mexico to Their Origin by Use of Fourier Transform Ion Cyclotron Resonance Mass Spectrometry. Environmental Science & Technology 2018; 52: 1365-1374.

Le Lannic K, Guibard I, Merdrignac I. Behavior and role of asphaltenes in a two-stage fixed bed hydrotreating process. Petroleum Science and Technology 2007; 25: 169-186.

Little DP, Speir JP, Senko MW, Oconnor PB, McLafferty FW. Infrared Multiphoton Dissociation of Large Multiply-Charged Ions for Biomolecule Sequencing. Analytical Chemistry 1994; 66: 2809-2815.

Lozano DCP, Orrego-Ruiz JA, Hernandez RC, Guerrero JE, Mejia-Ospino E. APPI(+)-FTICR mass spectrometry coupled to partial least squares with genetic algorithm variable selection for prediction of API gravity and CCR of crude oil and vacuum residues. Fuel 2017; 193: 39-44.

Mayer PM, Poon C. The Mechanisms of Collisional Activation of Ions in Mass Spectrometry. Mass Spectrometry Reviews 2009; 28: 608-639.

McGill WB, Rowell MJ. Determination of Oil Content of Oil Contaminated Soil. Science of the Total Environment 1980; 14: 245-253.

McLafferty FW. A Century of Progress in Molecular Mass Spectrometry. Annual Review of Analytical Chemistry 2011; 4: 1-22.

Mullins OC. The Asphaltenes. In: Cooks RG, Yeung ES, editors. Annual Review of Analytical Chemistry, Vol 4. 4, 2011, pp. 393-418.

Mullins OC, Sabbah H, Eyssautier J, Pomerantz AE, Barre L, Andrews AB, et al. Advances in Asphaltene Science and the Yen-Mullins Model. Energy & Fuels 2012; 26: 3986-4003.

Nyadong L, Lai JF, Thompsen C, LaFrancois CJ, Cai XH, Song CX, et al. High-Field Orbitrap Mass Spectrometry and Tandem Mass Spectrometry for Molecular Characterization of Asphaltenes. Energy & Fuels 2018; 32: 294-305.

Palacio Lozano DC, Gavard R, Arenas-Diaz JP, Thomas MJ, Stranz DD, Mejía-Ospino E, et al. Pushing the analytical limits: new insights into complex mixtures using mass spectra segments of constant ultrahigh resolving power. Chemical Science 2019; 10: 6966-6978.

Payne AH, Glish GL. Thermally assisted infrared multiphoton photodissociation in a quadrupole ion trap. Analytical Chemistry 2001; 73: 3542-3548.

Pereira TMC, Vanini G, Oliveira ECS, Cardoso FMR, Fleming FP, Neto AC, et al. An evaluation of the aromaticity of asphaltenes using atmospheric pressure photoionization Fourier transform ion cyclotron resonance mass spectrometry - APPI(+/-)FT-ICR MS. Fuel 2014; 118: 348-357.

Polfer NC. Infrared multiple photon dissociation spectroscopy of trapped ions. Chemical Society Reviews 2011; 40: 2211-2221.

Santos JM, Vetere A, Wisniewski A, Eberlin MN, Schrader W. Comparing Crude Oils with Different API Gravities on a Molecular Level Using Mass Spectrometric Analysis. Part 2: Resins and Asphaltenes. Energies 2018a; 11.

Santos JM, Wisniewski A, Eberlin MN, Schrader W. Comparing Crude Oils with Different API Gravities on a Molecular Level Using Mass Spectrometric Analysis. Part 1: Whole Crude Oil. Energies 2018b; 11.

Saraçli S, Doğan N, Doğan İ. Comparison of hierarchical cluster analysis methods by cophenetic correlation. Journal of Inequalities and Applications 2013; 2013: 203.

Schmidt EM, Pudenzi MA, Santos JM, Angolini CFF, Pereira RCL, Rocha YS, et al. Petroleomics via Orbitrap mass spectrometry with resolving power above 1 000 000 at m/z 200. Rsc Advances 2018; 8: 6183-6191.

Sheu EY, Storm DA. Colloidal Properties of Asphaltenes in Organic Solvents. In: Sheu EY, Mullins OC, editors. Asphaltenes: Fundamentals and Applications. Springer US, Boston, MA, 1995, pp. 1-52.

Sokal R, Rohlf F. Sokal RR, Rohlf FJ. The comparison of dendrograms by objective methods. Taxon 11: 33-40. Taxon 1962; 11: 33-40.

Stout SA, Uhler AD, McCarthy KJ. A Strategy and Methodology for Defensibly Correlating Spilled Oil to Source Candidates. Environmental Forensics 2001; 2: 87-98.

Tang WJ, Hurt MR, Sheng HM, Riedeman JS, Borton DJ, Slater P, et al. Structural Comparison of Asphaltenes of Different Origins Using Multi-stage Tandem Mass Spectrometry. Energy & Fuels 2015; 29: 1309-1314.

Thomas MJ, Collinge E, Witt M, Lozano DCP, Vane CH, Moss-Hayes V, et al. Petroleomic depth profiling of Staten Island salt marsh soil: 2 omega detection FTICR MS offers a new solution for the analysis of environmental contaminants. Science of the Total Environment 2019; 662: 852-862.

Vermeire MB. Everything You Need to Know About Marine Fuels. Chevron Global Marine Products, 2012.

Wiehe IA. Process Chemistry of Petroleum Macromolecules. FL: CRC Press: Boca Raton, 2008.

Wiehe IA, Kennedy RJ. The oil compatibility model and crude oil incompatibility. Energy & Fuels 2000; 14: 56-59.

Zeuthen P, Knudsen KG, Whitehurst DD. Organic nitrogen compounds in gas oil blends, their hydrotreated products and the importance to hydrotreatment. Catalysis Today 2001; 65: 307-314.

Zhang YH, Zhang LZ, Xu ZM, Zhang N, Chung KH, Zhao SQ, et al. Molecular Characterization of Vacuum Resid and Its Fractions by Fourier Transform Ion Cyclotron Resonance Mass Spectrometry with Various Ionization Techniques. Energy & Fuels 2014; 28: 7448-7456.

4. Industrial Lubricant Base Oil Oxidation Study

4.1 Introduction

Lubricant oils are essential for motor engine operation; their sustained function between drain intervals is essential to ensure fuel efficiency and to extend engine lifetime through prevention of overheating and mechanical wear. Among the processes limiting lubricant performance, necessitating regular oil change intervals, is oxidation, which is inevitable given exposure to air and extreme heat conditions within the engine environment. Oxidation can lead to acid formation, which can cause corrosion of engine parts; oil thickening, which reduces pumpability; and sludge and varnish formation, which can impede oil flow through narrow tubing (Levermore et al., 2001; Maleville et al., 1995; Mortier et al., 2010). The ingress of fuel into the lubricant oil can exacerbate such processes (Levermore et al., 2001; Mortier et al., 2010), which is of rising concern with the drive to replace traditional petroleum-derived diesel with biodiesel, which is less stable towards oxidation (Sazzad et al., 2016; Tang et al., 2008b).

Although extremely complex, petroleum-based diesel fuels typically contain few olefins in their component molecular structures due to the reactivity of double bonds, which leads to their depletion over time. Biofuels, however, possess a far greater degree of unsaturation than traditional fuels, are so are more susceptible to oxidative attack across double bonds (Knothe, 2007; Pullen and Saeed, 2012). Once peroxide radicals are formed, chain reactions both within the biodiesel itself and where fuel ingress into the lubricant oil occurs, can lead to the formation of oxidation products, often incorporating carbonyl functionalities or extended alkyl chains (Bacha et al., 2015; Knothe, 2007; McCormick et al., 2007). Additive packages, which typically comprise detergents, viscosity modifiers, pour point depressants, and antioxidant compounds, may be added to improve performance and extend the lifetime of lubricant base oils (Mortier et al., 2010). Antioxidants are typically designed to act either as radical scavengers, forming ring-stabilized or sterically hindered radicals, or as peroxide decomposers, converting reactive peroxide species to alcohols (Dunn, 2008; Knothe, 2007; Mortier et al., 2010).

FTICR MS is well suited to the study of complex, petroleum-related mixtures, such as lubricant base oils, affording speciation of aromatic hydrocarbon components according to alkyl- and naptheno-substitution, as well as detection of saturated and aromatic sulfur-containing species (Hourani et al., 2015). Recent

advances in two dimensional gas chromatography (GCXGC) and atmospheric pressure chemical ionization (APCI) MS approaches have improved characterisation of the hydrocarbon components of base and motor oils (Hourani and Kuhnert, 2012; Manheim et al., 2019a; Manheim et al., 2019b; Wang and Zhang, 2007). Previous biodiesel oxidation studies have been limited to the analysis of low molecular weight and low carbon number species using GC-MS (Besser et al., 2017; Frauscher et al., 2017); an ultra-high resolution compositional analysis of heavier components and a study of the oxidative transformation of lubricant base oils with respect to biodiesel fuel ingress has not yet been attempted. While some bulk analyses (Knothe, 2007) can be used to monitor oxidative changes, such as viscosity measurements, infrared (IR) spectroscopy, and total acid number (TAN), studies of deposits on steel plates demonstrated that such methods provided limited insight into the chemistries underlying automatic transmission fluid durability (Tipton et al., 1998). As bulk measurements of the fluid phase remain a widely used, low-cost, and rapid means by which to monitor the impact of oxidation on base oils studied under a range of experimental conditions, they are here utilized prior to the analysis of select samples by ultra-high resolution mass spectrometry. Chapter 2 demonstrated that negative mode (-) electrospray (ESI) selectively accesses acidic species in oils. As a primary concern associated with lubricant oil oxidation is acid formation, (-) ESI may be a suitable choice for their molecular-level characterization, but to mitigate the challenges associated with working with this technique encountered in Chapter 2, which may be particularly exacerbated by formulated base oil matrices, (-) nanelectrospray (nESI) was instead selected as the ionization technique to be applied to the largest number of samples in this study. nESI offers greater sensitivity and tolerance to aqueous solutions and salt contamination due to the smaller droplets initially produced, possessing a greater charge density, compared to ESI (Karas et al., 2000) which initially produces larger droplets as indicated in Figure 1.5.

Hyphenating chromatography to ultra-high resolution mass spectrometry provides an additional dimension of separation, improving mass measurement and resolution, sensitivity towards and detection of lower abudance species, and insight into the isomeric complexity of petroleum-related mixtures (Barrow et al., 2014; Luo et al., 2009; Szulejko and Solouki, 2002). GC-APCI-FTICR MS is an approach that has been utilized to compare pyrolysis bio-oils and their esterified products, with individual extracted ion chromatogram (EIC) traces for molecular assignments used to elucidate the transformations occuring as a result of

upgrading (Palacio Lozano et al., 2019). The effectiveness of additives, including antioxidant compounds such as zinc dialklyldithiophosphate (ZDDP), at extending base oil lifetime has been assessed in a similar manner using lower resolution GC-MS methods (Ahmad et al., 2015). While quantification is not possible using direct infusion (DI) FTICR MS, due to the differing response factors and ion suppression within multi-component mixtures (Annesley, 2003; Sterner et al., 2000), integration of EICs and comparison of area-under-curve (AUC) for selected species affords a semi-quantitative analysis in hyphenated approaches (Koulman et al., 2009).

Oxidation testing may be performed in an engine for conditions that most closely reflect those in the real world, however as engine testing (Daniel and Kunz, 2014) is expensive and energetically demanding, assessment of the suitability of utilizing benchtop tests is paramount (Besser et al., 2014). Therefore, the results of an engine test for a fully formulated 5W-30 engine oil with diesel, containing 5 % biodiesel by volume (B5), added are compared against those of the bench top method. Additionally, fully formulated 5W-30 engine oil and unformulated base oil samples, with and without the inclusion of diesel, containing 100 % biodiesel by volume (B100), are all subject to benchtop oxidation.

4.2 Materials and Methods

4.2.1 Base Oil Oxidation

A group II lubricant base oil (Lubrizol Ltd., Derby, U.K.) was subject to a benchtop oxidation test in the presence of an iron catalyst. Fully formulated 5W-30 engine oil, containing antioxidant additive package, viscosity modifier and pour point depressant, and unformulated base oil, with and without the addition of a B100 diesel, were reacted over a period of 168 hr in the presence of an iron catalyst. The fully formulated 5W-30 engine oil containing the antioxidant additive package, viscosity modifier, and pour point depressant, was also subject to the OM 646 LA engine test (Daniel and Kunz, 2014) with the addition of a B5 diesel (Lubrizol Ltd., Derby, U.K.). The fluid phase of each reaction vessel was sampled at 0, 72, 96, 120, 144, and 168 hr. Bench top oxidation, engine testing, and sampling was carried out by Lubrizol Ltd. The samples generated and the analytical techniques by which they were studied are summarized in Table 4.1.

Table 4.1 Oxidation test samples generated and analytical techniques applied in each case: infrared spectroscopy (IR), kinematic viscosity (kυ), (-) nESI and positive mode (+) electrospray (ESI)

Base Oil	**Sampling Interval / hr**					
	0	72	96	120	144	168
Unformulated	IR, kυ (-) nESI (+) ESI	IR, kυ (-) nESI	IR, kυ	IR, kυ	IR, kυ	IR, kυ (-) nESI (+) ESI GC-APCI
Unformulated + B100	IR, kυ (-) nESI (+) ESI	IR, kυ (-) nESI	IR, kυ	IR, kυ	IR, kυ	IR, kυ (-) nESI (+) ESI GC-APCI
Formulated	IR, kυ (-) nESI (+) ESI	IR, kυ (-) nESI	IR, kυ	IR, kυ	IR, kυ	IR, kυ (-) nESI (+) ESI GC-APCI
Formulated + B100	IR, kυ (-) nESI (+) ESI	IR, kυ (-) nESI	IR, kυ	IR, kυ	IR, kυ	IR, kυ (-) nESI (+) ESI GC-APCI
Engine Test Formulated + B5	IR, kυ (-) nESI (+) ESI	IR, kυ (-) nESI	IR, kυ	IR, kυ	IR, kυ	IR, kυ (-) nESI (+) ESI GC-APCI

4.2.2 Bulk Measurements

IR measurements of oxidation were made by Lubrizol Ltd according to standardized method DIN 51453 (DIN, 2004) for all sampling intervals using a Spectrum Two FT-IR spectrometer (PerkinElmer, Seer Green, Buckinghamshire, UK) fitted with an Oil Express 4 autosampler. A background was constructed from 1970 cm^{-1} to 580 cm^{-1} and the peak height at 1710 cm^{-1}, representative of absorption in the carbonyl stretching region, was measured. The value at 0 hr was subtracted from the height at all subsequent sampling time points. Oxidation in units of A cm^{-1} were calculated as shown in Equation 4.1.

$$Oxidation\ (A\ cm^{-1}) = \frac{peak\ height\ at\ 1710\ cm^{-1}}{cell\ path\ length\ in\ mm} \times 10 \qquad (4.1)$$

Kinematic viscosity (kυ) measurements were made by Lubrizol Ltd according to standardized method ASTM D7279 for all sampling intervals using an ISL VH1 HOULLON Viscometer (Integrated Scientific Ltd, Rotherham, South Yorkshire,

UK). The percentage change in kυ compared to that at 0 hr was calculated to give units of % Δkυ.

4.2.3 DI-FTICR MS Experiments

Mass spectra were acquired using a 12 T solariX Fourier transform ion cyclotron resonance (FTICR) mass spectrometer (Bruker Daltonik GmbH, Bremen, Germany). 0 and 168 hr samples we dissolved at 0.05 mg mL^{-1} in a 20:80 mixture of toluene and propan-2-ol (Fisher Scientific, Hemel Hempstead, Hertfordshire, United Kingdom) with formic acid (Sigma-Aldrich Company Ltd., Gillingham, Dorset, United Kingdom) added at 0.5 % to aid protonation. Samples were introduced using a syringe pump at a rate of 260 μL h^{-1} and ionized using an Apollo II electrospray (ESI) source operated in positive (+) ion mode, with activation of in-source dissociation (ISD) at 60 V for 400 scans. 0, 72, and 168 hr samples were dissolved at 0.05 mg mL^{-1} in a 20:80 mixture of toluene and propan-2-ol (Fisher Scientific, Hemel Hempstead, Hertfordshire, United Kingdom) and ionized using a custom built nano-electrospray (nESI) source operated in negative (-) ion mode without the activation of in-source dissociation for 250 scans. Nitrogen was used as the drying gas at a temperature of 220 °C and a flow rate of 4 L min^{-1} in (+) ESI experiments, and at 250 °C and a flow rate of 2.5 L min^{-1} in (-) nESI experiments. The nebulizing gas was nitrogen and was maintained at a pressure of 2 bar in (+) ESI experiments. After acquiring spectra in the detection range *m*/*z* 221-3000 in (+) ESI experiments and *m*/*z* 92-1500 in (-) nESI experiments, the data were zero-filled once and apodized using a Sine-Bell function prior to applying a fast Fourier transform. For apodized data, the resolving power at *m*/*z* 400 ranged from 300,000 to 700,000, varying with sample and experimental procedure. The mass spectra were internally calibrated using homologous series and analyzed using DataAnalysis 4.2 (Bruker Daltonik GmbH, Bremen, Germany), prior to the data being imported into Composer 1.5.6 (Sierra Analytics, Modesto, CA, USA) for compositional analysis.

4.2.4 GC-FTICR MS Experiments

168 hr samples were dissolved at 3 mg mL^{-1} in dichloromethane (Sigma Aldrich Chemie GmbH, Munich, Bavaria, Germany). Mass spectra were acquired using a 7 T solariX 2XR FTICR mass spectrometer (Bruker Daltonik GmbH, Bremen, Germany), coupled to a GC 450 (Bruker Daltonik GmbH, Bremen, Germany) and GC-APCI II source. 1 μL injection volume onto a 30 m BR-5 ms column was used

with He as the carrier gas, with the temperature program as follows: 60 °C held for 1 min, ramping 6 °C min^{-1} up to 300 °C and held for 9 min. The instrument was operated in positive-ion mode. Nitrogen was used as the drying gas at a temperature of 240 °C at a flow rate of 4 L min^{-1}. The nebulizing gas was nitrogen and was maintained at a pressure of 2 bar. 2 MW data sets were acquired using magnitude mode, with a detection range of *m*/*z* 107–3000 and 95 % data profile reduction. 2ω (quadrupolar) detection was used, affording high resolution at the rapid scan rate required for hyphenation to GC. The data were zero-filled once and apodized using a Sine-Bell function prior to applying a fast Fourier transform. A lock mass of *m*/*z* 223.06345 (a polysiloxane) was used for online calibration. For the apodized data, the measured resolving power at m/z 200 was 330,000. Data were analyzed using DataAnalysis 4.2 (Bruker Daltonik GmbH, Bremen, Germany) in 10 min time retention intervals with the first 10 min used for background subtraction. Assignments were made using Composer 1.5.7 (Sierra Analytics, Modesto, CA, USA).

4.2.5 Data Analysis and Visualization

Inkscape, Origin Pro 2016 (OriginLab Corporation, Northampton, Massachusetts, USA), Aabel NG2 v.5.2 (Gigawiz Ltd. Co., Tulsa, Oklahoma, USA), and KairosMS in-house software were used for data analysis, visualization, and to generate figures.

4.3 Results and Discussion

4.3.1 Bulk Measurements

Figure 4.1 indicates that oxidation is most severe in the unformulated base oil, and in the unformulated base oil with B100 included, with the measured oxidation greater at 72 hr in these samples than at 168 hr in the fully formulated engine oil. The addition of the additive package to the lubricant oil may therefore be considered to limit oxidation substantially. Where B5 diesel is included in the engine test oxidation only begins to rise more rapidly in the 168 hr sample, behaving similarly to the formulated base oil without biodiesel included which had been subjected to the harsher conditions of the benchtop test.

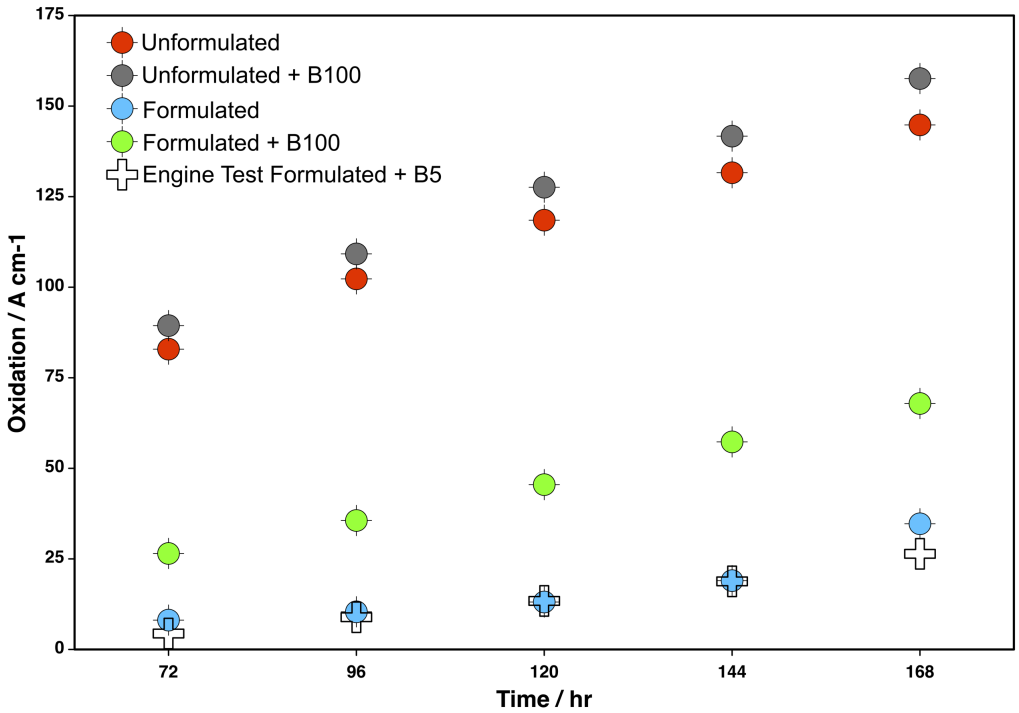

Figure 4.1 – Oxidation measured according to DIN 51453 by IR spectroscopy, compared between each sampling point throughout the benchtop and OM 646 LA engine tests

The results shown in Figure 4.2 demonstrate that the components of the additive package and the viscosity modifier may be effective in preventing increases in kυ for the fully formulated engine oil, and for that with B5 diesel included in the engine test. When fully formulated engine oil is combined with B100 diesel in the benchtop test the kυ rises sharply between 120 and 144 hr, such that it exceeds the kυ of unformulated base oil at 144 and 168 hr. In the early stages of the oxidation test the extreme conditions may cause cracking of the hydrocarbon backbone and removal of peroxide species. This may lead to an initial decrease in kυ, as demonstrated for the fully formulated engine oil, as well as that with B5 biodiesel included in the engine test. However, once viscosity begins to increase the lubricant oil typically thickens rapidly. Interactions between the components in the fully formulated engine oil and species present at higher concentration in the B100 diesel than in the B5 diesel, for example reactive double bonds, may have lead to runaway processes such as alkyl chain lengthening reactions, causing a greater increase in kυ. This may have been exacerbated further by the presence of the iron catalyst and difference in operating conditions of the benchtop test compared to the engine test, leading to the breakdown of unstable additive compounds. Furthermore, the reaction products formed may be less prone to

forming solid deposition on the reactor walls, such that they remain in the fluid phase and increase its observed viscosity. Comparing samples taken from the fluid phase without combined analysis of solid deposits (Tipton et al., 1998) may limit understanding of oxidative processes and the effectiveness of additive packages. Furthermore, additive package performance has been demonstrated to be biodiesel dependent (Knothe, 2007) with effects that may not be long lasting in storage (Tang et al., 2008a); diminishing performance may also be accelerated under harsher conditions.

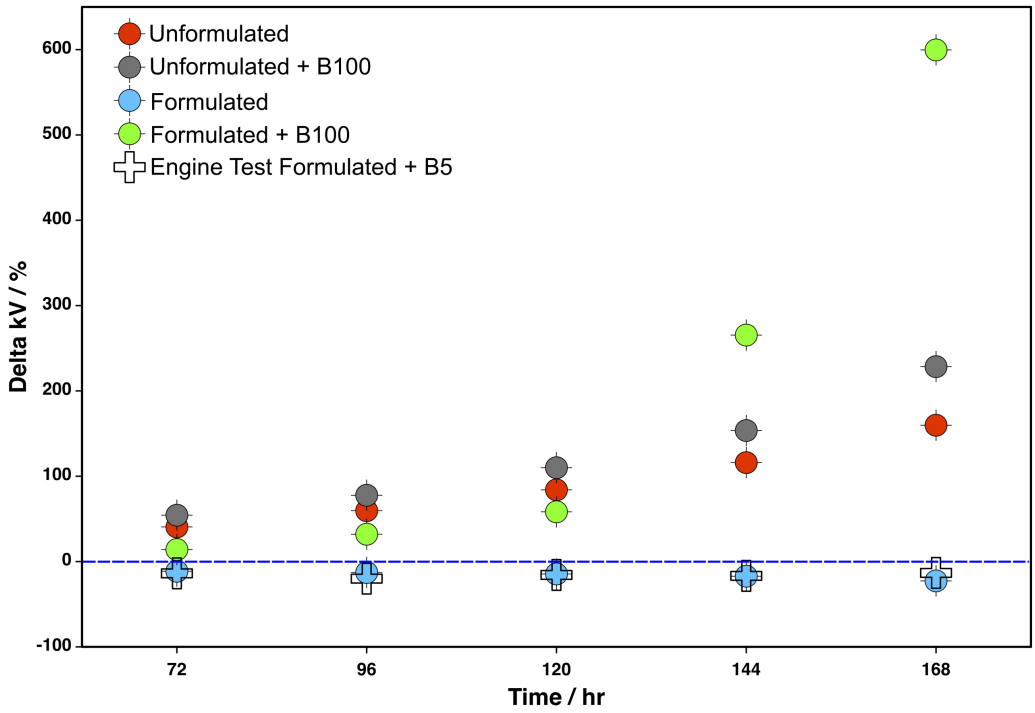

Figure 4.2 – Percentage change in kυ from that at 0 hr for each sampling point during the benchtop and OM 646 LA engine test

Bulk measurements such as IR and kυ provide limited information on lubricant base oil oxidation. For instance, the oxidation measured by IR spectroscopy depends upon the height of the carbonyl peak at 1710 cm^{-1}, however oxygen containing species that do not contain a carbonyl bond, such as ethers and alcohols, are not detected in this way. Although alkyl chain lengthening and a greater degree of alkyl branching may be implied by increasing kυ, the range of molecular transformations that may lead to increased viscosity cannot be distinguished by this technique.

4.3.2 DI-FTICR MS Experiments

The deprotonated compound class distribution for 0 hr and 168 hr sampling points, obtained using (-) nESI, is shown in Figure 4.3. In general, a shift in contribution from O_x[H] classes with low values of x at 0 hr, to O_x[H] classes with high values of x at 168 hr, is observed. The predominant contribution from O_3S[H] class to fully formulated engine oil samples at 0 hr is reduced somewhat at 168 hr, implying that the species detectable may have been diminished through their role in antioxidation processes. van Krevelen (van Krevelen, 1950) plots are widely used to visualize simultaneously the oxygen content and degree of unsaturation in the hydrocarbon backbone of selected components. These plots have been utilized further with structural relationships between species indicated by characteristic connecting lines (Kim et al., 2003), and prevalence of compound types, such as lipids, lignin, and condensed hydrocarbons, identified through relative populations at coordinate regions (Echavarri-Bravo et al., 2019; Rivas-Ubach et al., 2018). Multiple molecular assignments may possess the same H/C and O/C ratio, so each data point may represent a sum of intensities. Figure 4.4 extends the van Krevelen visualization for the O_x[H] classes detected by (-) nESI, comparing the fully formulated engine oil and unformulated base oil, both with B100 diesel added.

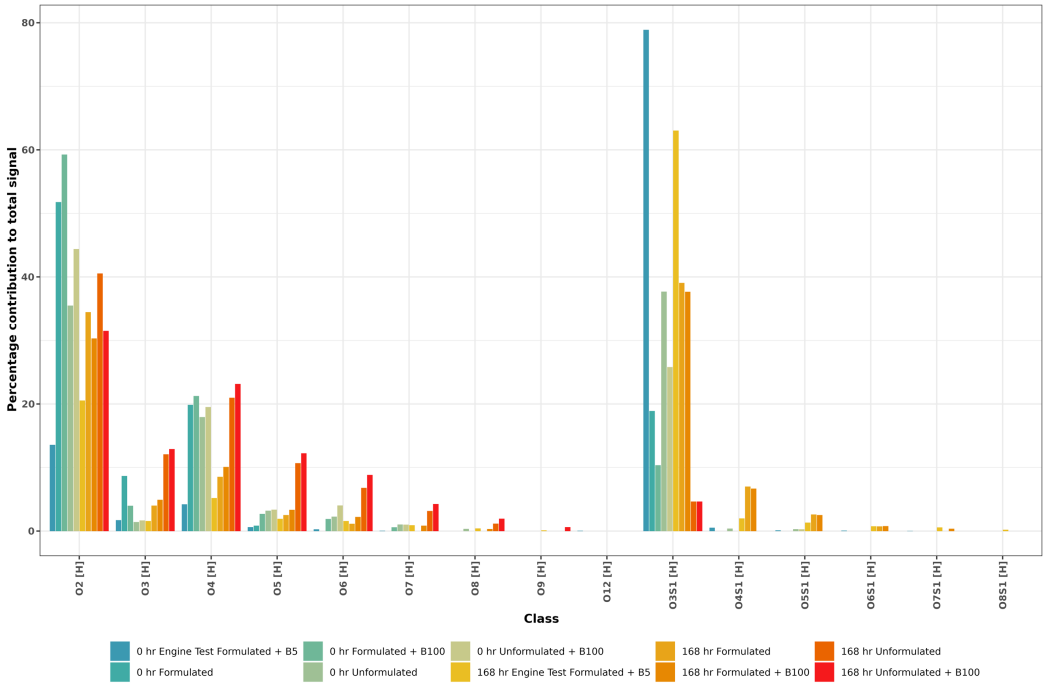

Figure 4.3 – (-) nESI deprotonated compound class distribution for 0 hr and 168 hr sampling points, demonstrating sharp increase in high x O_x[H] class assignments after oxidation testing

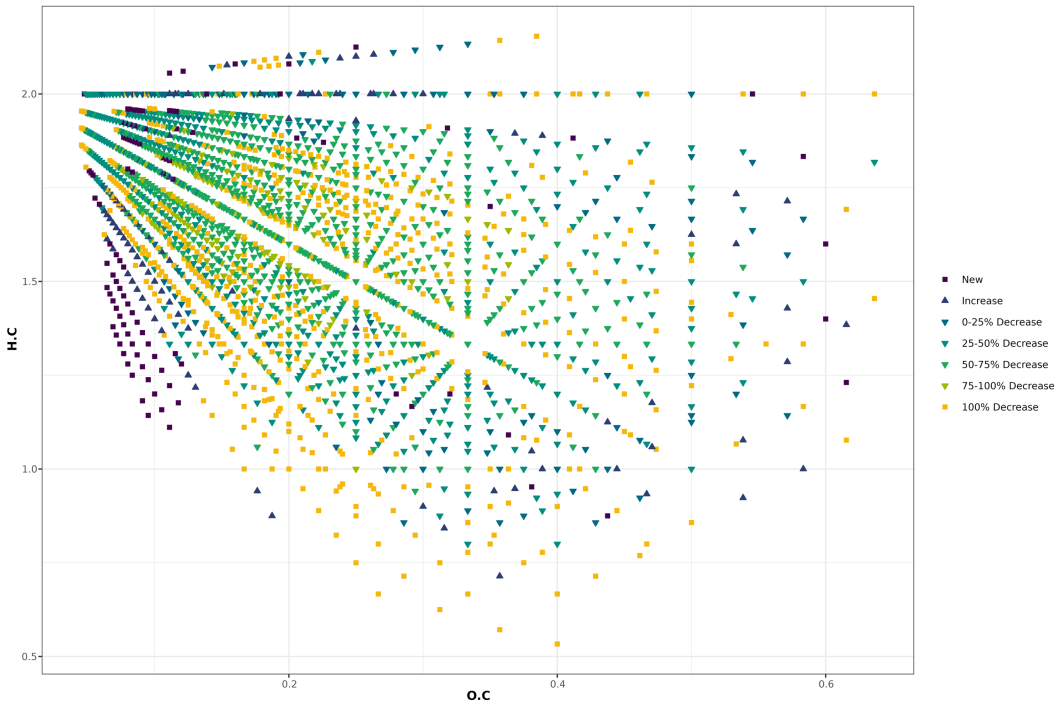

Figure 4.4 – van Krevelen diagram showing percentage change in total intensity of O_x[H] class assignments in (-) nESI at each coordinate point between unformulated base oil and fully formulated engine oil with B100 diesel included at 168 hr

Each marker in Figure 4.4 indicates the percentage change in summed intensity at each coordinate following the addition of the additive package, viscosity modifier, and pour point depressant to the lubricant oil. Figure 4.4 demonstrates that a large proportion of species, particularly those with high O/C ratio, detected in the unformulated base oil are not observed in fully formulated engine oil, demonstrating the effectiveness of the additive package in preventing extensive oxygenation. Figure 4.4 demonstrates that the additive package may be particularly effective against the formation of highly oxygenated species, as the intensity at a high proportion of assignments with O/C greater than 0.2 have disappeared or decreased by over 50 % compared to the unformulated base oil sample. In addition to establishing the effectiveness of additive packages by comparing formulated engine oil and unformulated base oil samples, the visualization method demonstrated in Figure 4.4 could be used to track changes in intensity of van Krevelen coordinates at time points across the oxidation test.

As each coordinate may be representative of multiple molecular compositions, the number of unique and common peaks between these two samples was calculated, such that the number of O_x[H] assignments no longer detected in the

fully formulated engine oil could be established. While there were 2561 O_x[H] class assignments in common, 1264 O_x[H] class peaks detected in the unformulated base oil sample were no longer detected in the fully formulated engine oil sample. These findings reinforce those shown in Figure 4.4, and further demonstrate the effectiveness of the additive package in limiting the amount polar, acidic, oxygen containing species formed in base oils under oxidative conditions.

The change in the number of peaks assigned to O_x[H] classes in (-) nESI data was compared between 72 hr and 0 hr, and 168 hr and 0 hr (Figure 4.5), to establish how severely oxidation had progressed within the first testing interval, and to compare the number of assignments detected at the end of the test. The rate of oxidation relative to the sampling time points could then be determined, and the antioxidant effectiveness of the additive package could be further investigated. The results shown in Figure 4.5 indicate that the rate of oxidation is reduced in the fully formulated engine oil, and that the additive is particularly effective against oxidation exacerbated by biodiesel ingress into lubricant oils. However, Figure 4.5 also indicates a large proportion of oxygen-containing products are formed in the first 72 hr, particularly in unformulated base oil, suggesting that earlier oxidation test sampling points are required to better understand the molecular transformations occurring during oxidation.

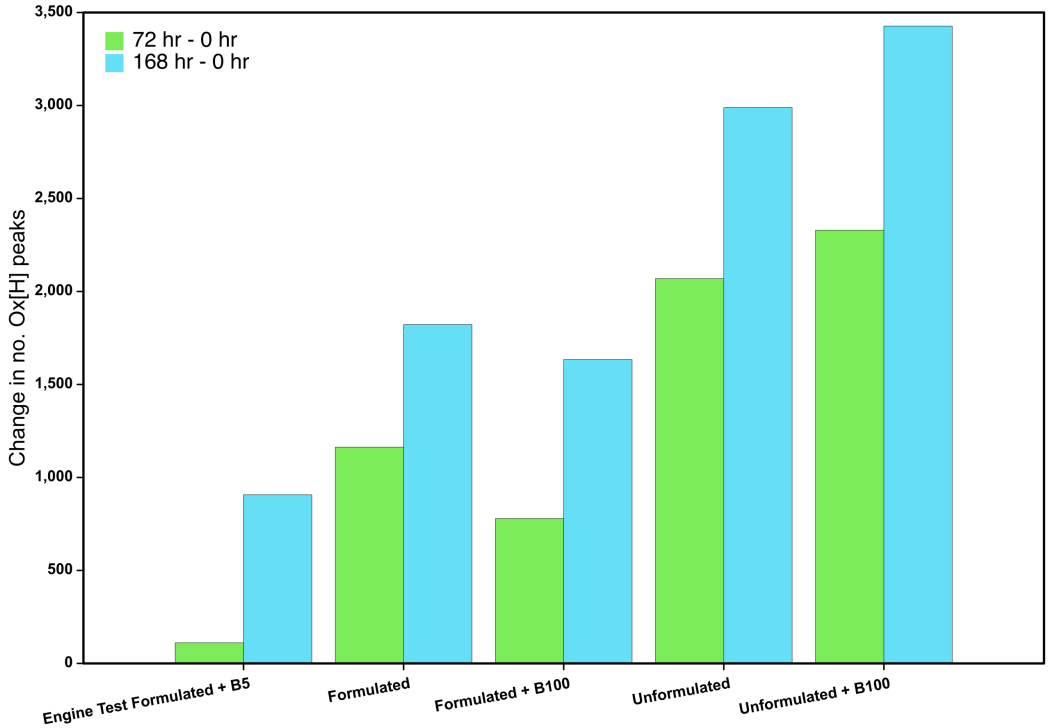

Figure 4.5 – Change in number of peaks assigned to O_x[H] classes in (-) nESI spectra comparing the 72 hr and 168 hr to the 0 hr samples

Monitoring the change in relative intensity and number of assignments to the O_x[H] class by (-) nESI provides information predominantly on species that deprotonate readily, such as carboxylic acids. Other oxygen-containing species may be formed, such as alcohols, aldehydes, and ketones (Levermore et al., 2001), and so the samples were also studied by (+) ESI. The protonated compound class distribution at 0 hr and 168 hr obtained from (+) ESI mass spectra are shown in Figure 4.6. The sharp increase in contributions from O_x[H] classes demonstrates that oxygenation has been extensive. Given that these species are detected in positive-ion mode they may be representative of non-carboxylic acid oxidation products.

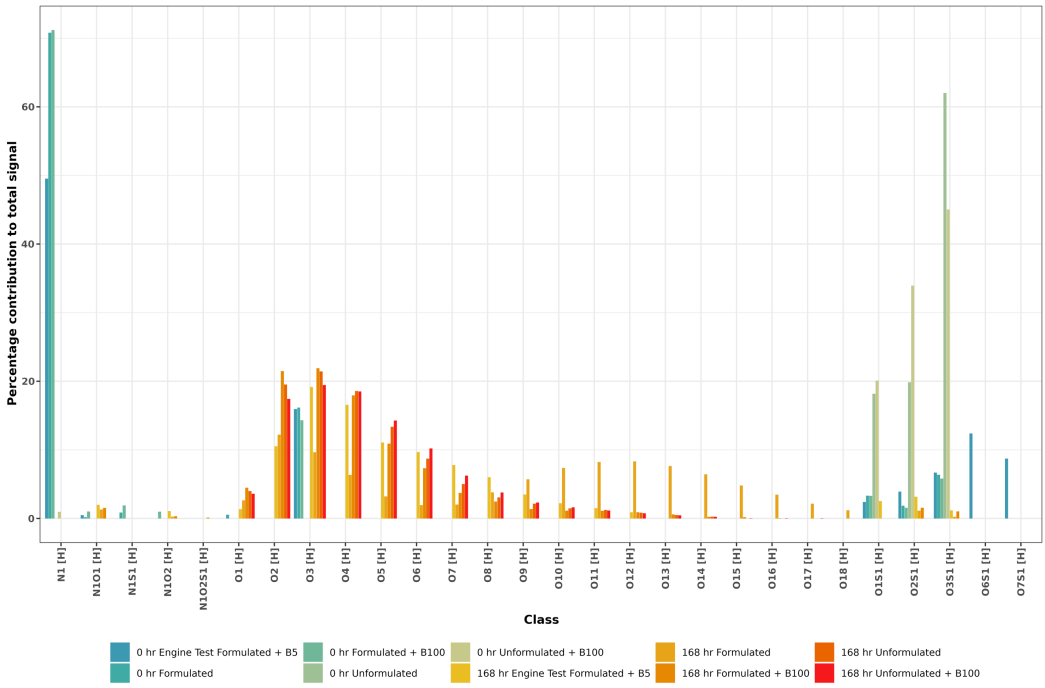

Figure 4.6 – (+) ESI protonated compound class distribution for 0 hr and 168 hr sampling points, demonstrating sharp increase O_x[H] class assignments after oxidation testing

Plots of number of double bond equivalents (DBE) against carbon number for the O_2[H] classes detected using (+) ESI and (-) nESI for the 168 hr samples are shown in Figure 4.7. The neutral DBE of a species will decrease by 0.5 when protonated, as occurs in (+) ESI, and increase by 0.5 when deprotonated, as occurs in (-) nESI. Inspection of DBE plots affords molecular speciation, differentiating between long chain carboxylic acids and other oxygen-containing species, for example. The 168 hr O_2[H] class DBE plots obtained using (+) ESI in Figure 4.7a shows that the more intense homologous series start at DBE 4.5 (neutral DBE 5). This is in contrast to starting at DBE 1.5 (neutral DBE 1), with assignments that may

correspond to palmitic and stearic acid predominant, in the O_2[H] class DBE plots obtained using (-) nESI (Figure 4.7b). This further suggests that, while (-) nESI preferentially ionizes carboxylic acid containing species, (+) ESI accesses a wider range of compound types generated in the oxidation process, such as ketones and esters.

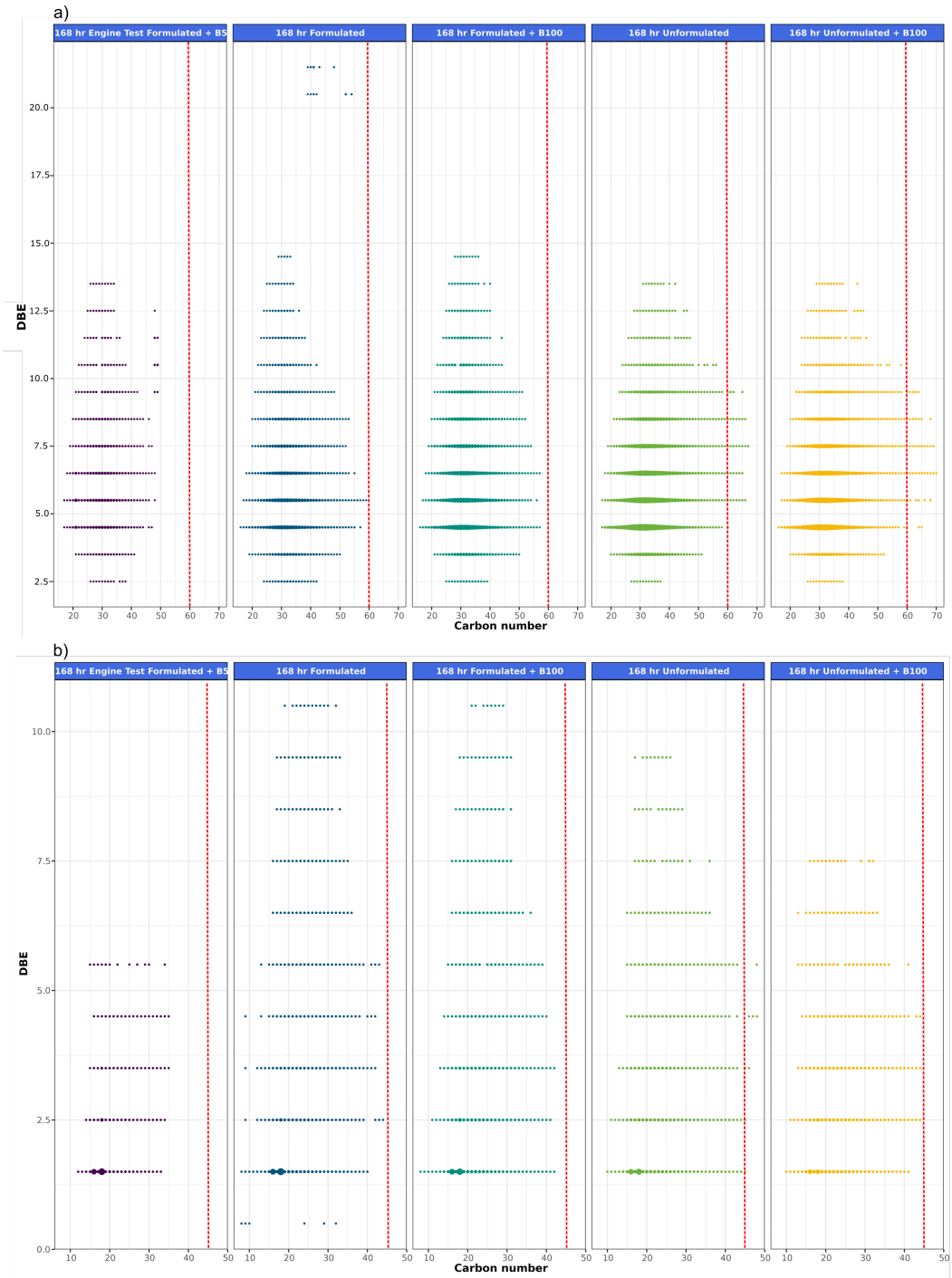

Figure 4.7 – Plots of DBE against carbon number for the O_2[H] classes detected 168 hr samples using a) (+) ESI and b) (-) nESI. The complementarity between the differing ionization polarities is demonstrated by the contrast in DBE and carbon number ranges detected

The red vertical dashed lines in the O_2[H] class DBE plots shown in Figure 4.7 are used to indicate that a carbon number of 60 in (+) ESI and 45 in (-) nESI was only exceeded in unformulated base oils, which suggests that the additive package is effective against alkyl chain lengthening reactions that can occur as a result of oxidative processes (Levermore et al., 2001; Naldu et al., 1984). Furthermore, while GC-MS can be used to characterize low molecular weight oxidation products such as ethanol, acetic acid and propanoic acid, up to a maximum of approximately 320 g mol^{-1} and carbon number of 18 (Besser et al., 2017), Figure 4.7 demonstrates the capability of FTICR MS to extend analysis to higher carbon number species.

4.3.3 GC-FTICR MS Experiments

Hyphenated FTICR MS experiments can provide an extra dimension of separation, improving detection of low abundance species (Barrow et al., 2014). Therefore, to better elucidate sample composition and establish the effectiveness of formulations against oxidation, the 168 hr samples were analyzed using GC-APCI-FTICR MS on an instrument equipped with 2ω detection (Boldin and Nikolaev, 2011; Cho et al., 2017; Schweikhard, 1991). In its application to oxidized lubricant base oils, prior separation may reduce competition for ionize between matrix and analyte species, improving detection of compounds of interest, as well as provide information of isomeric complexity of selected molecules.

Traditional comparison of GC-FTICR MS data sets by averaging mass spectra over time slices (Kim et al., 2019; Thomas et al., 2019) and generating a compound class distribution based on relative spectral intensity appeared to yield little information on compositional differences between samples, as shown in Figure 4.8. Without further investigation, it could be concluded that few differences ca. be observed between the profiles obtainable for the end of test samples as the relative proportions, which do not necessarily reflect absolute concentration, of their component compound classes are largely similar.

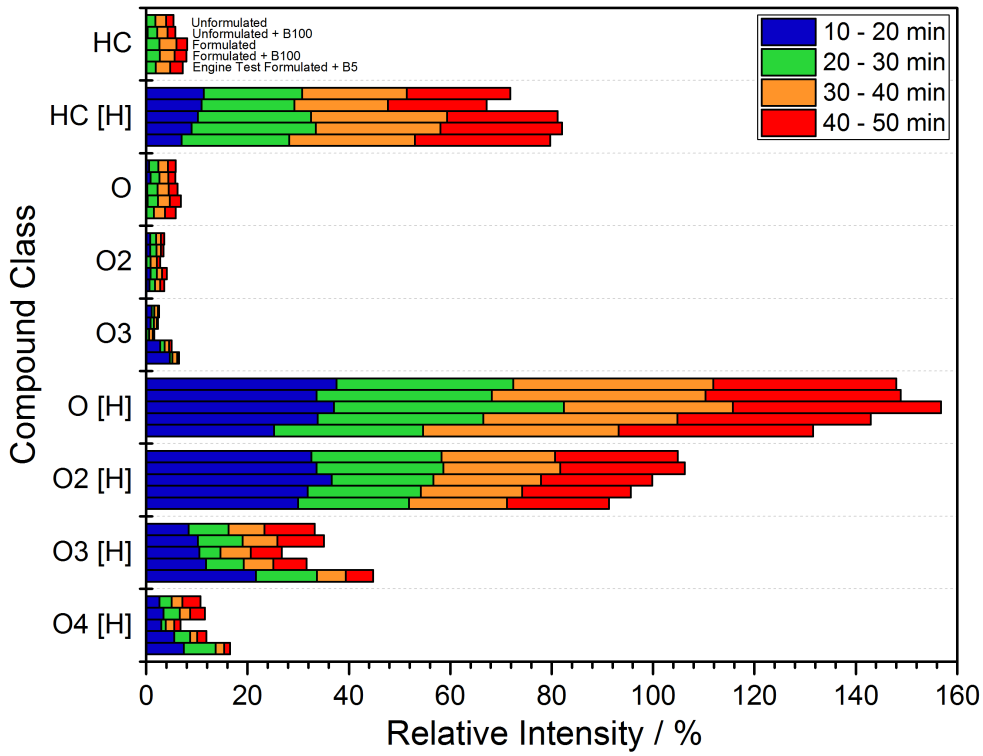

Figure 4.8 – Stacked compound class distribution obtained by averaging mass spectra over 10 min intervals of the total ion chromatogram from GC-APCI-FTICR MS analysis of 168 hr samples

KairosMS, a software tool capable of processing hyphenated data sets without manually dividing the total ion chromatogram (TIC) into retention time intervals, has been recently been developed in-house, but outside of this project. Using KairosMS, the AUC of each compound class EIC could be measured and compared for a semi-quantitative analysis. The normalized AUC class distribution is compared between the samples at 168 hr in Figure 4.9a, with a focus on samples containing biodiesel shown in Figure 4.9b. Figure 4.9 demonstrates that compositional information complementary to DI-FTICR MS data is indeed obtainable through hyphenated analysis, and made feasible using recently developed software tools. Furthermore, the relative contributions presented in Figure 4.9 are semi-quantitative as they compare the AUC of class chromatographic traces, rather than relative mass spectral intensities as compared in Figure 4.8.

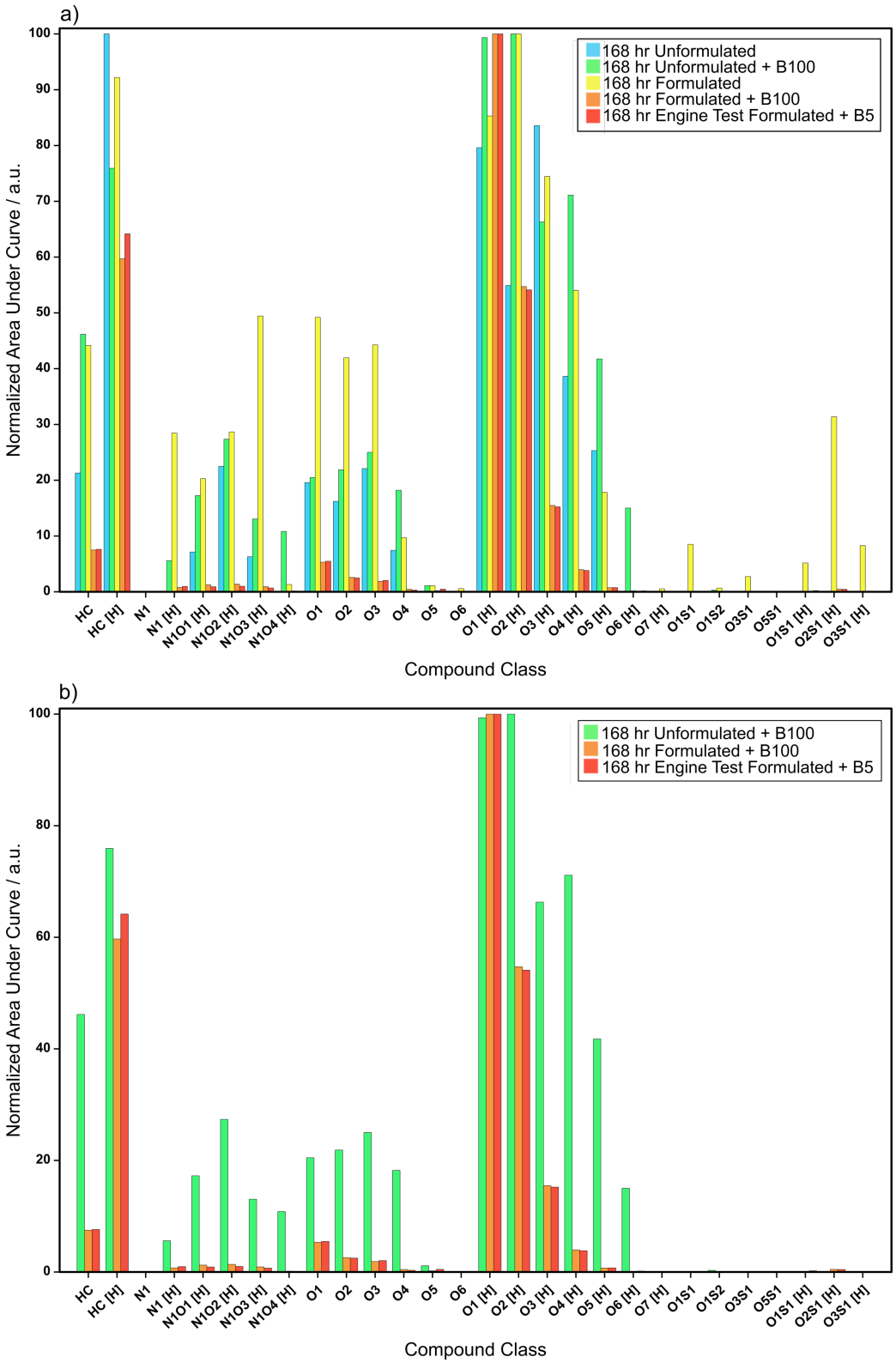

Figure 4.9 – Compound class distributions obtained through measure of AUC for the whole class EIC from positive-mode GC-APCI-FTICR MS data at 168 hr for a) all samples and b) all samples containing biodiesel

The fully formulated engine oil without any biodiesel added may retain a large proportion of unreacted additive chemicals until the end of the oxidation test, which may explain its relatively high proportion of heteroatom containing classes such as O_xS_y and O_xS_y[H]. In addition to organosulfur compounds designed to act as peroxide decomposers (Soleimani et al., 2018), such classes are likely to contain detergent type molecules or their component moities, for example structures containing sulfonate head groups. These compounds are included in additive formulations to both neutralize acidic oxidation products, limiting corrosion, and to form a film on the metal surfaces of engines, preventing deposit formation (Nassar et al., 2017). The formulated base oil without any biodiesel added also has a relatively high proportion of O_x classes, which may correspond to alkylphenols used as radical scavenging antioxidants to stop chain propagation (Soleimani et al., 2018).

Figure 4.9b demonstrates the similarity between the benchtop oxidation test and the more expensive engine test, despite the lower proportion of biodiesel in the included fuel, suggesting that results obtained through this method while additive packages undergo development may be a viable indicator of formulation effectiveness. Although all samples contain a relatively high proportion of O_x[H] compounds, the addition of the additive package appeared to substantially reduce the proportion of O_x[H] compounds with high x values detected, as well as O_x and NO_x[H] classes. In addition to O_xS_y, and O_xS[H] classes, however, the fully formulated engine oil without any biodiesel included appeared to also contain a relatively high proportion of O_x and NO_x[H] class compounds, which may be due to the breakdown of unstable additive compounds under the extreme conditions of the benchtop test.

The semi-quantitative findings shown in Figure 4.9 correlate with those shown in Figure 4.1, with the greatest contributions from O_x[H] classes with high values of x observed in the unformulated base oil with biodiesel included. This reflects the high value of oxidation calculated from IR measurements. However, the GC-APCI-FTICR MS analysis allows a greater depth of compositional information to be inferred. The contributions from different oxygen-containing classes that may underly the absorbance in the C=O region, such as aldehydes and ketones, compounds more likely be accessed by (+) APCI, are compared semi-quantitatively in Figure 4.9, while some molecular speciation is made possible by inspection of their associated DBE plots (Figure 4.7).

EICs for molecular composition $[C_{28}H_{54}O + H]^+$, selected within a narrow window of 0.0005 Da, a width only possible when using an instrument of ultra-high resolution, are shown in Figure 4.10. The poor resolution of the EICs and the foldover in intensity may be due to column degradation in the presence of highly acidic oxidation products, leading to polysiloxanes being leached and dominating the TIC and mass spectra. This may also underly the high sample concentration found to be required for analyte species to be detected in this work. In further studies, a prior sample derivatization step or a stationary phase more stable towards polar compounds could be used (Berthod et al., 2018) for improved GC-APCI-FTICR MS analysis of oxidized base oils, such that isomers of interest can be accurately resolved, counted, and compared between samples. EICs may also be obtained for specific molecular assignments of interest, and the abundance of particular isomers may be compared between samples. If combined with isotopic labelling approaches (Frauscher et al., 2017), elucidation of oxidative degradation mechanisms and identification of the least stable biodiesel, base oil, and additive components may then become possible.

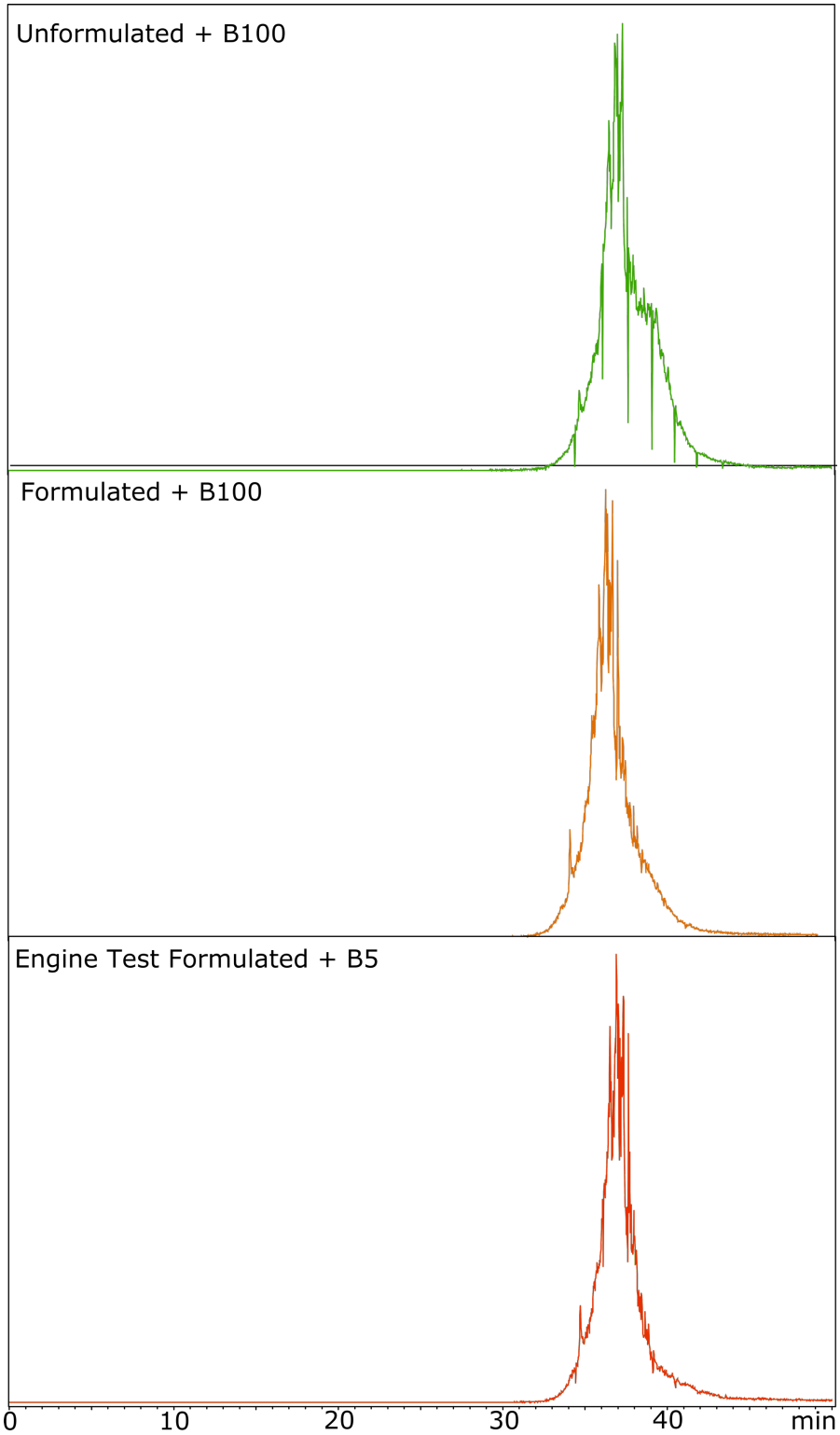

Figure 4.10 EICs for molecular composition $[C_{28}H_{54}O + H]^+$ for fully formulated engine oils and unformulated base oils with biodiesel added at 168 hr, demonstrating isomeric complexity and similarity between the benchtop and engine test samples

While the EICs shown in Figure 4.10 do not permit sufficient resolution to determine the number of isomers present in each sample, the traces for the benchtop and engine test samples appear similar, suggesting that the oxidation products formed through these two procedures are comparable. In combination with the AUC data shown in Figure 4.9, it may be concluded that benchtop tests are capable of providing a cost-effective first pass, or possibly full alternative, to engine tests, when additive packages undergo development. To verify this finding more robustly, a lubricant oil with the same biodiesels added would need to undergo both benchtop and engine testing, and the results obtained compared using the complementary bulk IR and kυ, and ultra-high resolution DI and GC-FTICR MS techniques.

4.4 Conclusions

Bulk measurements indicated that oxidation progressed between 72 hr and 168 hr, however comparing 0 hr, 72 hr, and 168 hr sampling points using (-) nESI-FTICR MS showed that the majority of acidic oxidation products assigned to the O_x[H] classes had been formed within the first 72 hr. The count of additional O_x[H] molecular assignments increased only slightly to the final sampling point of 168 hr, which suggests that the increased oxidation observable by bulk measurements is due to increasing concentrations of species formed early in the test. In further studies, earlier and more regular time points need to be sampled, such that the onset of oxidation can be better identified and compared between samples.

Using (+) ESI in addition to (-) nESI afforded molecular speciation of non-acidic oxidation products, indicating that species such as alcohols, ketones, and esters had also been formed. FTICR MS analyses accessed higher molecular weight and carbon number species than were previously observable using previous GC analyses. The higher carbon number species, formed more extensively in unformulated samples, may be linked to increased viscosity, while increased numbers of oxygen-containing compounds may contribute to increased oxidation observable using IR measurements. Additive products that target more extensively aklyated compounds, or those containing non-carbonyl oxygen-containing functionalities, could be among those developed for lubricant oil formulations.

Hyphenated GC-FTICR MS allowed the isomeric complexity between end of test samples to be roughly compared, and afforded a semi-quantitative assessment of additive package performance. In further investigations, hyphenated analyses could be applied to samples taken at earlier and more regular oxidation intervals, such that the disappearance and appearance of individual isomers could be tracked to better understand which required targeting to alleviate the bulk changes observed. These species could be among those targeted when developing additive packages.

FTICR MS provides a qualititave analysis when using DI, or semi-quantitative analysis when hyphentated with GC, and as such the relative changes in O_x[H] contributions do not reflect the significant changes in oxidation and viscosity indicated by bulk measurements. Due to competition for ionization between analyte and matrix species, including additive compounds, a comparison between formulated and unformulated base oils, and those with biodiesel added, is challenging. Despite these limitations, FTICR MS has been demonstrated as a viable tool to extend industry understanding of oxidation processes at the molecular level, furthering development of lubricant oil formulations.

4.5 References

Ahmad I, Ullah J, Ishaq M, Khan H, Khan R, Ahmad W, et al. Oxidative Stability of the Plain and Additized Mineral Base Oil Samples Monitored through Gas Chromatography-Mass Spectrometry. Energy & Fuels 2015; 29: 6522-6528.

Annesley TM. Ion suppression in mass spectrometry. Clinical Chemistry 2003; 49: 1041-1044.

Bacha K, Ben-Amara A, Vannier A, Alves-Fortunato M, Nardin M. Oxidation Stability of Diesel/Biodiesel Fuels Measured by a PetroOxy Device and Characterization of Oxidation Products. Energy & Fuels 2015; 29: 4345-4355.

Barrow MP, Peru KM, Headley JV. An Added Dimension: GC Atmospheric Pressure Chemical Ionization FTICR MS and the Athabasca Oil Sands. Analytical Chemistry 2014; 86: 8281-8288.

Berthod A, Ruiz-Angel MJ, Carda-Broch S. Recent advances on ionic liquid uses in separation techniques. Journal of Chromatography A 2018; 1559: 2-16.

Besser C, Pisarova L, Frauscher M, Hunger H, Litzow U, Orfaniotis A, et al. Oxidation products of biodiesel in diesel fuel generated by artificial alteration and identified by mass spectrometry. Fuel 2017; 206: 524-533.

Besser C, Steinschutz K, Dorr N, Novotny-Farkas F, Allmaier G. Impact of engine oil degradation on wear and corrosion caused by acetic acid evaluated by chassis dynamometer bench tests. Wear 2014; 317: 64-76.

Boldin IA, Nikolaev EN. Fourier transform ion cyclotron resonance cell with dynamic harmonization of the electric field in the whole volume by shaping of the excitation and detection electrode assembly. Rapid Communications in Mass Spectrometry 2011; 25: 122-126.

Cho E, Witt M, Hur M, Jung MJ, Kim S. Application of FT-ICR MS Equipped with Quadrupole Detection for Analysis of Crude Oil. Analytical Chemistry 2017; 89: 12101-12107.

Daniel K, Kunz P. CEC-L-99-08, Evaluation of Engine Crankcase Lubricants. In: Mang T, editor. Encyclopedia of Lubricants and Lubrication. Springer Berlin Heidelberg, Berlin, Heidelberg, 2014, pp. 221-225.

DIN. Testing Of Lubricants - Determination Of Oxidation And Nitration Of Used Motor Oils - Infrared Spectrometric Method 51453. German Institute for Standardisation (Deutsches Institut für Normung), 2004.

Dunn RO. Antioxidants for improving storage stability of biodiesel. Biofuels Bioproducts & Biorefining-Biofpr 2008; 2: 304-318.

Echavarri-Bravo V, Tinzl M, Kew W, Cruickshank F, Mackay CL, Clarke DJ, et al. High resolution fourier transform ion cyclotron resonance mass spectrometry (FT-ICR MS) for the characterisation of enzymatic processing of commercial lignin. New Biotechnology 2019; 52: 1-8.

Frauscher M, Besser C, Allmaier G, Dorr N. Elucidation of oxidation and degradation products of oxygen containing fuel components by combined use of a stable isotopic tracer and mass spectrometry. Analytica Chimica Acta 2017; 993: 47-54.

Hourani N, Kuhnert N. High molecular weight non-polar hydrocarbons as pure model substances and in motor oil samples can be ionized without fragmentation by atmospheric pressure chemical ionization mass spectrometry. Rapid Communications in Mass Spectrometry 2012; 26: 2365-2371.

Hourani N, Muller H, Adam FM, Panda SK, Witt M, Al-Hajji AA, et al. Structural Level Characterization of Base Oils Using Advanced Analytical Techniques. Energy & Fuels 2015; 29: 2962-2970.

Karas M, Bahr U, Dulcks T. Nano-electrospray ionization mass spectrometry: addressing analytical problems beyond routine. Fresenius Journal of Analytical Chemistry 2000; 366: 669-676.

Kim D, Kim S, Son S, Jung M-J, Kim S. Application of Online Liquid Chromatography 7 T FT-ICR Mass Spectrometer Equipped with Quadrupolar Detection for Analysis of Natural Organic Matter. Analytical Chemistry 2019; 91: 7690-7697.

Kim S, Kramer RW, Hatcher PG. Graphical method for analysis of ultrahigh-resolution broadband mass spectra of natural organic matter, the van Krevelen diagram. Analytical Chemistry 2003; 75: 5336-5344.

Knothe G. Some aspects of biodiesel oxidative stability. Fuel Processing Technology 2007; 88: 669-677.

Koulman A, Woffendin G, Narayana VK, Welchman H, Crone C, Volmer DA. High-resolution extracted ion chromatography, a new tool for metabolomics and lipidomics using a second-generation orbitrap mass spectrometer. Rapid Communications in Mass Spectrometry 2009; 23: 1411-1418.

Levermore DM, Josowicz M, Rees WS, Janata J. Headspace analysis of engine oil by gas chromatography/mass spectrometry. Analytical Chemistry 2001; 73: 1361-1365.

Luo ZH, Heffner C, Solouki T. Multidimensional GC-Fourier Transform Ion Cyclotron Resonance MS Analyses: Utilizing Gas-Phase Basicities to Characterize Multicomponent Gasoline Samples. Journal of Chromatographic Science 2009; 47: 75-82.

Maleville X, Faure D, Legros A, Hipeaux JC. Oxidation of Mineral Base Stocks of Petroleum Origin - Relationship Between Chemical-Composition, Thickening and Oxidized Degradation Products. Revue De L Institut Francais Du Petrole 1995; 50: 405-443.

Manheim J, Wehde K, Zhang WTJ, Vozka P, Romanczyk M, Kilaz G, et al. Identification and Quantitation of Linear Alkanes in Lubricant Base Oils by Using GCxGC/EI TOF Mass Spectrometry. Journal of the American Society for Mass Spectrometry 2019a.

Manheim J, Zhang YY, Viidanoja J, Kenttamaa HI. An Automated Method for Chemical Composition Analysis of Lubricant Base Oils by Using Atmospheric Pressure Chemical Ionization Mass Spectrometry. Journal of the American Society for Mass Spectrometry 2019b; 30: 2014-2021.

McCormick RL, Ratcliff M, Moens L, Lawrence R. Several factors affecting the stability of biodiesel in standard accelerated tests. Fuel Processing Technology 2007; 88: 651-657.

Mortier RM, Fox MF, Orszulik S. Chemistry and technology of lubricants: Third edition, 2010.

Naldu SK, Klaus EE, Duda JL. Evaluation of Liquid-Phase Oxidation-Products of Ester and Mineral-Oil Lubricants. Industrial & Engineering Chemistry Product Research and Development 1984; 23: 613-619.

Nassar AM, Ahmed NS, El-shazly RI, el Menem YKA. Preparation and evaluation of the mixtures of sulfonate and phenate as lube oil additives. International Journal of Industrial Chemistry 2017; 8: 383-395.

Palacio Lozano DC, Gavard R, Jones HE, Thomas MJ, Ramírez CX, Mejia-Ospino E, et al. Revealing Greater Complexity by Coupling of Gas Chromatography to Ultrahigh Resolution Mass Spectrometry for the Analysis of Bio-Oils. Advances in Hyphenated Mass Spectrometry, London, U. K., 2019.

Pullen J, Saeed K. An overview of biodiesel oxidation stability. Renewable & Sustainable Energy Reviews 2012; 16: 5924-5950.

Rivas-Ubach A, Liu YN, Bianchi TS, Tolic N, Jansson C, Pasa-Tolic L. Moving beyond the van Krevelen Diagram: A New Stoichiometric Approach for Compound Classification in Organisms. Analytical Chemistry 2018; 90: 6152-6160.

Sazzad BS, Fazal MA, Haseeb A, Masjuki HH. Retardation of oxidation and material degradation in biodiesel: a review. Rsc Advances 2016; 6: 60244-60263.

Schweikhard L. Theory of Quadrupole Detection Fourier Transformion Cyclotron-Resonance. International Journal of Mass Spectrometry and Ion Processes 1991; 107: 281-292.

Soleimani M, Dehabadi L, Wilson L, Tabil L. Antioxidants Classification and Applications in Lubricants, 2018.

Sterner JL, Johnston MV, Nicol GR, Ridge DP. Signal suppression in electrospray ionization Fourier transform mass spectrometry of multi-component samples. Journal of Mass Spectrometry 2000; 35: 385-391.

Szulejko JE, Solouki T. Potential analytical applications of interfacing a GC to an FT-ICR MS: Fingerprinting complex sample matrixes. Analytical Chemistry 2002; 74: 3434-3442.

Tang H, De Guzman RC, Salley SO, Ng SKY. The oxidative stability of biodiesel: Effects of FAME composition and antioxidant. Lipid Technology 2008a; 20: 249-252.

Tang HY, Abunasser N, Wang A, Clark BR, Wadumesthrige K, Zeng SD, et al. Quality survey of biodiesel blends sold at retail stations. Fuel 2008b; 87: 2951-2955.

Thomas MJ, Collinge E, Witt M, Lozano DCP, Vane CH, Moss-Hayes V, et al. Petroleomic depth profiling of Staten Island salt marsh soil: 2 omega detection FTICR MS offers a new solution for the analysis of environmental contaminants. Science of the Total Environment 2019; 662: 852-862.

Tipton CD, Huston ME, Wetsel WR. Fundamental Studies on ATF Friction, Part II. SAE International, 1998.

van Krevelen DW. Graphical-statistical method for the study of structure and reaction processes of coal. Fuel 1950; 29: 269-284.

Wang FCY, Zhang L. Chemical composition of group II lubricant oil studied by high-resolution gas chromatography and comprehensive two-dimensional gas chromatography. Energy & Fuels 2007; 21: 3477-3483.

5. Effect of Solvent and Flow Rate on Observed Crude Oil Profiles and Ion-Type Ratios

5.1 Introduction

Ultra-high resolution mass spectrometry (MS) techniques, such as Fourier transform ion cyclotron resonance (FTICR) and Orbitrap MS, offer unrivalled performance for the analysis of complex mixtures including petroleum (Palacio Lozano et al., 2019; Schmidt et al., 2018). Atmospheric pressure photoionization (APPI) is an ionization technique regularly used for petroleum analysis, providing the broadest overview of oil composition as demonstrated in Chapter 2, accessing both polar and non-polar compounds (Sama et al., 2018). Sample preparation procedures and instrument operating conditions have been shown to greatly affect the species and compositional profile observed in studies employing a range of ionization techniques, including electrospray ionization (ESI), atmospheric pressure laser ionization (APLI), atmospheric pressure chemical ionization (APCI), laser desorption ionization (LDI), laser induced acoustic desorption (LIAD), and direct analysis in real time (DART) (Barrow et al., 2016; Benigni et al., 2016; Cho et al., 2012; Gao et al., 2011; Headley et al., 2007; Herrera et al., 2008; Lozano et al., 2016; Peru et al., 2019; Romao et al., 2016). Furthermore, while some petroleomics researchers have observed and predicted differing results in APPI experiments (Ahmed et al., 2015; Ahmed et al., 2017; Cho et al., 2013) by varying factors well known to affecting the relative intensities of molecular species and ion-types ratios (Robb et al., 2000), often these are not carefully considered prior to the analysis of complex samples using this ionization technique.

Toluene is one of the most widely used solvents in APPI MS studies (Ahmed et al., 2013) owing to the dopant effect toluene affords during gas-phase ionization (Purcell et al., 2006). Toluene can be used in combination with other solvents such as propan-2-ol (Griffiths et al., 2014), as was demonstrated in Chapter 2. Several reaction pathways are known influence the relative ratio of radical ions and protonated species observed in APPI experiments, such as the reaction of dopant ions with solvent molecules, which in turn may react by proton transfer with analytes possessing a high proton affinity (Robb et al., 2000). PAHs dissolved in toluene have been shown to preferentially form protonated ions at high vaporizer temperatures (Ahmed et al., 2012), with protonation likely proceeding via a two-step electron transfer and hydrogen transfer mechanism (Syage, 2004). The

mechanisms for dopant-assisted APPI are shown in Equation scheme 1.5 (Hanold et al., 2004).

In Chapter 2 it was found that species which prefer to ionize via protonation pathways may not always be detected when toluene is used as the sole solvent system for complex mixture analysis using (+) APPI-FTICR MS. For example, the N[H] class is well-known to comprise a large proportion of observed petroleum profiles by electrospray ionization (ESI). The N[H] class may also be observed using APPI and is typically representative of pyridinic compounds, in contrast to the N class which typically corresponds to pyrrolic compounds (Purcell et al., 2007b), and the use of a more protic solvent, such as propan-2-ol, in combination with toluene improves access to this class and to a wider range of molecular classes overall (Griffiths et al., 2014). The presence of protic solvents has also been demonstrated to significantly increase the $[M+H]^+$ yield of PAHs in headspace APPI analyses (Syage, 2004).

Other analyses of petroleum-related mixtures have employed solvent systems comprising dichloromethane (DCM) (Thomas et al., 2019) or acetonitrile (ACN) (Barrow et al., 2015). With conventional resources diminishing, oil production is shifting to heavier reserves, such as the oil sands bitumen mined in the Athabasca region of Alberta, Canada. Approximately 3 barrels of water are required to produce one barrel of synthetic crude oil (Barrow et al., 2016), generating large volumes of oil sands process-affected water (OSPW). OSPW is a complex mixture that cannot be discharged into the environment, and so is stored in expansive tailings ponds (Martin, 2015). It was recently suggested that extraction of petroleum-related organic components can be maximized utilizing solutions predominantly comprising ethyl acetate (EA), rather than the more routinely used DCM (Peru et al., 2019). Improved access to the compositional space may be afforded (Han et al., 2016; Nyakas et al., 2013), and the resulting profiles have been considered useful for statistical comparison to environmental samples (Yi et al., 2017). To the best of our knowledge, the effect of this solvent on the observed profile has not yet been investigated with respect to the analysis of crude oil.

APPI offers a large dynamic range and superior sensitivity at low flow rates, particularly when compared to APCI, a related ionization method (Hanold et al., 2004). However, higher flow rates have been found to cause a decrease in signal intensity in APPI experiments, possibly due to larger ionization volumes limiting the distance travelled by light emitted from a krypton lamp, as a result of photon

absorption by solvent vapor. A loss of dopant radical cations was suspected, leading to a decrease in response from analytes forming ions through charge exchange, and while analytes proceeding via proton transfer pathways were not as seriously affected, some saturation of their signal was observed at higher flow rates (Kauppila et al., 2005). Other studies have also suggested that light penetration through the sample volume is limited at higher flow rates, reducing the efficiency of ionization, and that chemical ionization or photoionization followed by hydrogen abstraction can lead to increased formation of $[M+H]^+$ ions under a variety of APPI conditions (Short et al., 2007).

Flow rates ranging from 180 μL h^{-1} to 3000 μL h^{-1} are typically used in petroleomics studies (Bae et al., 2010; Chacon-Patino et al., 2017; Chacon-Patino et al., 2018a; Chacon-Patino et al., 2018b; Chiaberge et al., 2013; Griffiths et al., 2014; Krajewski et al., 2017; Lozano et al., 2017; Pereira et al., 2014; Santos et al., 2018a; Santos et al., 2018b; Thomas et al., 2019; Zhang et al., 2014), and differences in the preferential formation of protonated species (Krajewski et al., 2017) or radical ions (Bae et al., 2010; Lozano et al., 2017) has been observed. A systematic assessment of the effect of flow rate when applying (+) APPI-FTICR to the study of petroleum-related samples has not been carried out, and so the impact of varying this parameter upon the results obtained is not known. Although the radical and protonated classes can be used to differentiate pyrrolic and pyridinic nitrogen-containing classes (Purcell et al., 2007b) and thiophenic and sulfidic sulfur-containing classes (Purcell et al., 2007a), respectively, the work presented here demonstrates that a loss of speciation may occur when higher flow rates are used. Increased deuterated ion formation has been observed at higher flow rates of both analyte and deuterated methanol solutions (Cho et al., 2013), with deuterated pyrrolic species also formed preferentially, in hydrogen-deuterium exchange studies. Such loss of speciation may lead to amalgamation of protonated and radical classes, and in turn cause researchers to report only the double bond equivalents (DBE) value and summed relative intensities for the neutral molecular formulae.

Design of experiments (DoE) has previously been used to optimize experimental parameters for ESI (Guillemant et al., 2019a) and APPI-FTICR MS (Guillemant et al., 2019b) analysis of petroleum samples, with a flow rate of 3000 μL h^{-1} suggested to be optimal for positive-mode (+) APPI analysis of crude oils (Santos et al., 2019). However, the responses considered were factors such as maximum intensity, total number of ions, or molecular classes generated; the relative

proportions of radical and protonated classes were not reported. In this work DoE was carried out with the radical and protonated species ion-type ratio as the response factor to improve understanding of the impact of solvent system, sample concentration, and flow rate on the observed (+) APPI profile. The investigation into solvent effects and flow rate, and the DoE study, were carried out in parallel, with injection flow rates ranging between 400 and 4000 μL h^{-1} investigated.

5.2 Materials and Methods

5.2.1 Sample Preparation

An Iraqi crude oil (ONTA, Toronto, Ontario, Canada) was dissolved at 0.05 mg mL^{-1} in toluene (Honeywell Speciality Chemicals Seelze GmbH, Hanover, Germany) and mixtures comprising toluene and propan-2-ol (Honeywell Speciality Chemicals Seelze GmbH, Hanover, Germany), chloroform (Merck KGaA, Darmstadt, Hesse, Germany), acetonitrile, dichloromethane, ethyl acetate, n-hexane, chloroform, acetone, ethanol (Fisher Scientific, Hemel Hempstead, Hertfordshire, U.K.), and acetic acid (Fluka Analytical, Munich, Bavaria, Germany) for the solvent and flow rate studies.

A 1 mg mL^{-1} solution of 1,2-benzodiphenylene sulfide (Sigma-Aldrich Company Ltd., Gillingham, Dorset, United Kingdom) in toluene stock solution was spiked at 1 % into 0.05 mg mL^{-1} solutions of the Iraqi crude oil for experiments involving a model compound.

A South American crude oil was dissolved at concentrations of 0.05, 0.175, and 0.300 mg mL^{-1} in mixtures of toluene and propan-2-ol for the DoE study.

Polarity indices, solvent groups (Snyder, 1974), pKa values, vapor pressures, boiling points, proton affinities and ionization efficiencies (Lias et al., 2010; Sato et al., 2016; Silwal et al., 2010) of the solvents used in this study are shown in Table 5.1.

Table 5.1 – Properties of solvents used (Lias et al., 2010; Sato et al., 2016; Silwal et al., 2010), with cosolvents used in the first and second stages of the study ordered by polarity index

Solvent	Polarity Index	pKa	Ionization Efficiency / eV	Vapor Pressure / kJ mol^{-1}	Boiling Point / K	Proton Affinity / kJ mol^{-1}
Toluene	2.3	41	8.828 ± 0.001	37 ± 3	383.8 ± 0.2	784.0
n-hexane	0.0	N/A	10.13 ± 0.10	31 ± 1	341.9 ± 0.3	672.5
DCM	3.4	N/A	11.33 ± 0.04	29.03 ± 0.08	313 ± 1	628.0
Propan-2-ol	4.3	17.1	10.17 ± 0.02	45 ± 3	355.5 ± 0.4	793.0
Ethyl acetate	4.3	25	10.01 ± 0.05	35 ± 2	350.2 ± 0.2	835.7
Chloroform	4.4	15.5	11.37 ± 0.02	31.32 ± 0.08	334.3 ± 0.2	157.8‡
Acetonitrile	6.2	25	12.20 ± 0.01	33.45 ± 0.21	354.8 ± 0.4	779.2
Acetone	5.1	19.6	9.703 ± 0.006	31.27	329.3 ± 0.3	812
Ethanol	5.2	16	10.48 ± 0.07	42.3 ± 0.4	351.5 ± 0.2	776.4
Acetic Acid	6.2	4.75	10.65 ± 0.02	51.6 ± 1.5	391.2 ± 0.6	783.7

‡Calculated value from Silwal et al. (Silwal et al., 2010)

5.2.2 APPI-FTICR MS

Mass spectra were acquired using a 12 T solariX Fourier transform ion cyclotron resonance (FTICR) mass spectrometer (Bruker Daltonik GmbH, Bremen, Germany), coupled to an APPI II source operated in positive-ion (+) mode. Nitrogen was used as the drying gas at a temperature of 220 °C and at a flow rate

of 4 L min^{-1}. The nebulizing gas was nitrogen and was maintained at a pressure of 1.2 bar. A krypton lamp was used to produce photons with energy 10.0 and 10.6 eV. Samples were introduced by direct infusion using a syringe pump at a rate of 800 μL h^{-1} for the solvent study, ranging from 400-3600 μL h^{-1} for the flow rate study, and at rates of 600 μL h^{-1} , 2300 μL h^{-1}, and 4000 μL h^{-1} for the DoE study, without the activation of in-source dissociation.

4 M data sets were acquired in the detection range *m*/*z* 147-1800 for 400 scans for the solvent study or 100 scans for the flow rate study; for the DoE study, the detection range *m*/*z* 221-1500 was used and 50 scans were acquired. The DoE was a 2^3 full factorial design with 5 centerpoints. Further details of the DoE variables can be found in Table 5.2.

Table 5.2. Design of Experiment Parameters. 3 factors (sample concentration, toluene fraction, and flow rate) were studied using a full factorial 2^3 design, using a single replicate of 13 runs including 5 centerpoints. All terms were free from aliasing.

Standard Order	**Run Order**	**Centerpoint?**	**Blocks**	**Crude Oil Concentration / mg mL^{-1}**	**Toluene Fraction / %**	**Flow Rate / μL h^{-1}**
2	1	No	1	0.300	20	600
4	2	No	1	0.300	100	600
10	3	Yes	1	0.175	60	2300
6	4	No	1	0.300	20	4000
3	5	No	1	0.050	100	600
11	6	Yes	1	0.175	60	2300
9	7	Yes	1	0.175	60	2300
8	8	No	1	0.300	100	4000
13	9	Yes	1	0.175	60	2300
7	10	No	1	0.050	100	4000
12	11	Yes	1	0.175	60	2300
1	12	No	1	0.050	20	600
5	13	No	1	0.050	20	4000

5.2.3 Data Processing

The data were zero-filled once and apodized using a Sine-Bell function prior to applying a fast Fourier transform. The solvent study and DoE spectra were phased with a Half Hanning apodization (Kilgour) setting of 0.2 – 0.6 before baseline correction using ftmsProcessing 2.1.0 (Bruker Scientific LLC, Billerica, MA, USA). Spectra were internally calibrated using homologous series and analysed using DataAnalysis 4.2 (Bruker Daltonik GmbH, Bremen, Germany), prior to the data being imported into Composer 1.5.7 (Sierra Analytics, Modesto,

CA, USA) for compositional analysis, with elemental constraints C = 0-200; H = 0-1000 ; N= 0-4; O = 0-4; S = 0-6 (Table 5.3). Aabel NG2 v.5.2 (Gigawiz Ltd. Co., Tulsa, Oklahoma, USA), and Origin 2016 (OriginLab Corporation, Northampton, MA, USA), was used for data visualization. Minitab Express 1.1.0 (Minitab LLC, State College, PA, USA) was used for DoE analysis.

Table 5.3. Composer 1.5.7 parameters for the assignment of molecular formulae

Parameter	**Constraints**
Polarity	Positive
Ion properties	Adducts = H; allow radical and adduct/loss ions; remove isolated assignments
m/*z* range	*m*/*z* 200-1300
DBE range	-0.5 - 40
Element ranges	C = 0-200; H = 0-1000 ; N= 0-4; O = 0-4; S = 0-6

5.3 Results and Discussion

5.3.1 Effect of Solvent on Observed Profile and Ion-Type Ratio

Figure 5.1 shows the absorption mode (+) APPI mass spectra of the Iraqi crude oil in 7 initial solvent systems, all investigated on the same day under the same instrument conditions: 100 % toluene, and 80:20 mixtures of toluene with: n-hexane, DCM, propan-2-ol, ethyl acetate, chloroform, and ACN. Although most mass envelopes appear similar, that of 80:20 toluene:ethyl acetate spectrum clearly differs from the rest with a lower overall signal intensity for the crude oil distribution (representing a decrease by an approximate factor of 10) and a shift to higher *m*/*z* represented by an increase in M_w by 14.6 compared to the average M_w of the other solvent systems studied.

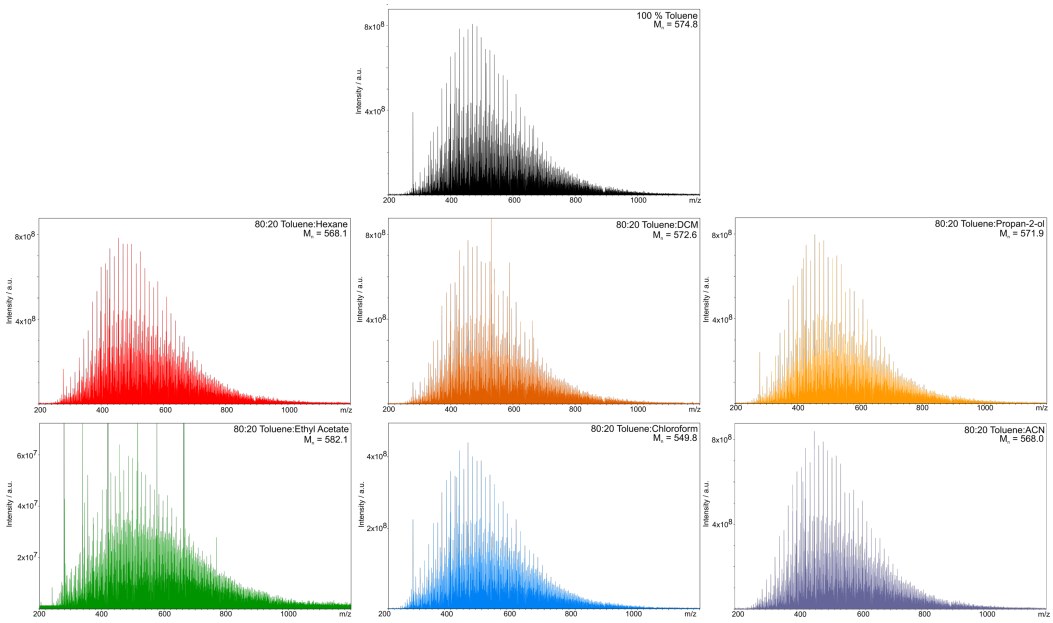

Figure 5.1 – Enlarged (+) APPI mass spectra, showing Iraqi crude oil distribution and M_w in the seven solvent systems initially studied

Figure 5.2 compares the full compound class distribution for the Iraqi crude oil across the seven solvent systems initially studied, demonstrating that in most cases the radical classes dominated while the protonated classes made relatively low contributions to spectral intensity. The inverse was observed for the 80:20 toluene:ethyl acetate solvent system. For instance, the average ratio of radical to protonated class intensity is 7.26 over the other the solvent systems, in contrast to a ratio of 0.06 in 80:20 toluene:ethyl acetate (Figure 5.3). The effect of the ethyl acetate cosolvent is particularly notable when comparing the ratio of the relative intensity of radical/protonated species containing one or more sulfur atoms (Figure 5.4). The ratio of radical to protonated S class species has previously been used as an indicator of the most suitable experimental parameters in (+) APPI-FTICR MS analysis (Guillemant et al., 2019b).

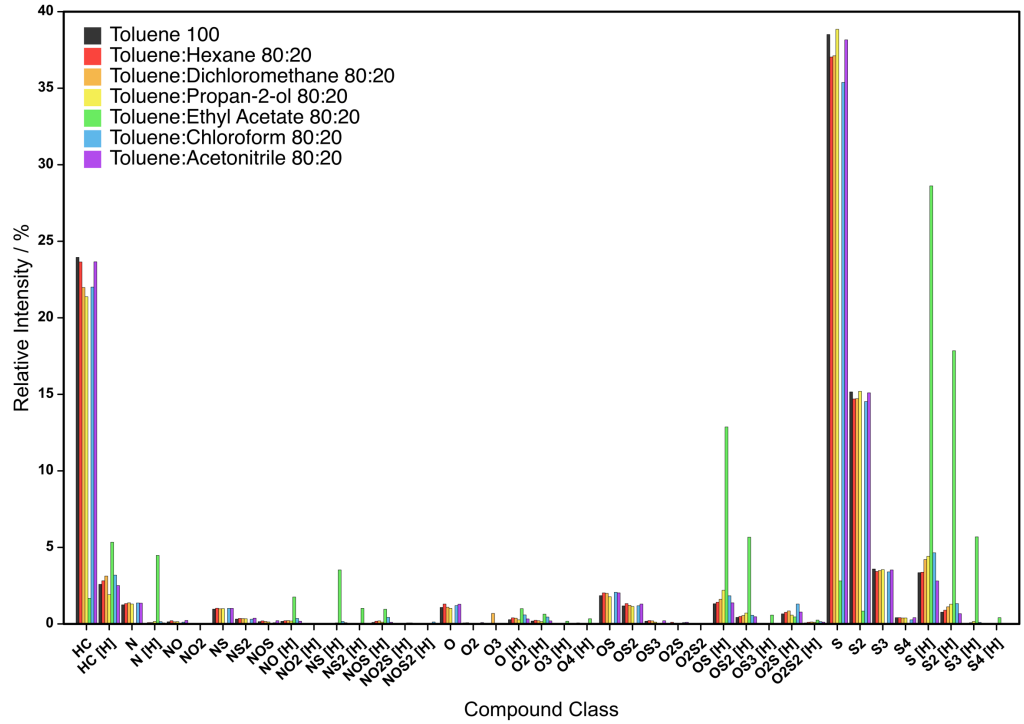

Figure 5.2 – Compound class distribution observed for the Iraqi crude oil in different solvent systems

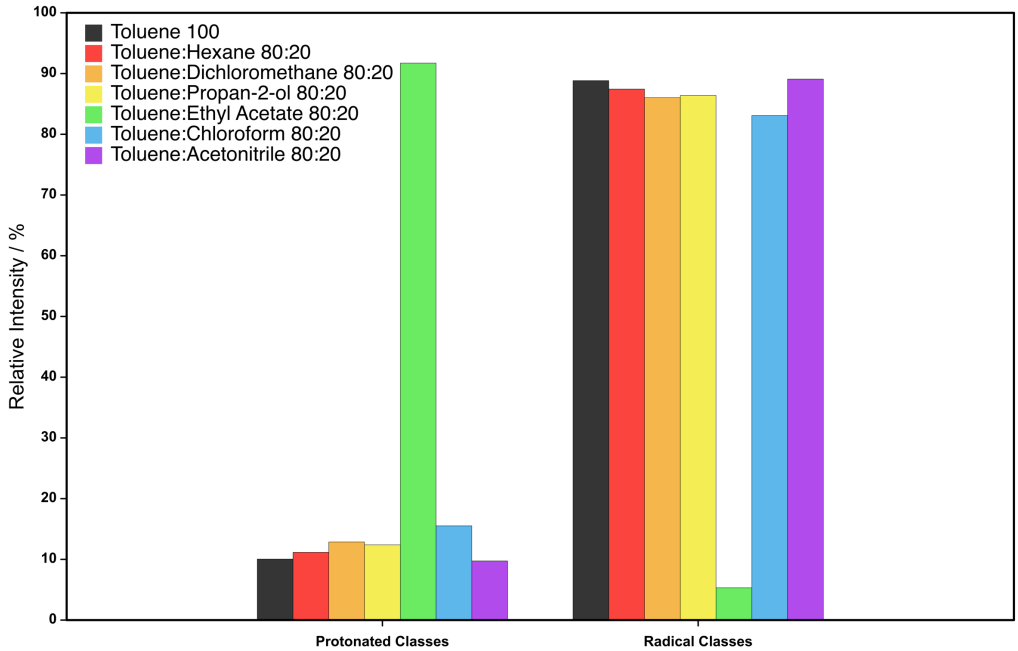

Figure 5.3 – Summed relative intensity of protonated and radical ion classes assigned in solvent systems initially studied

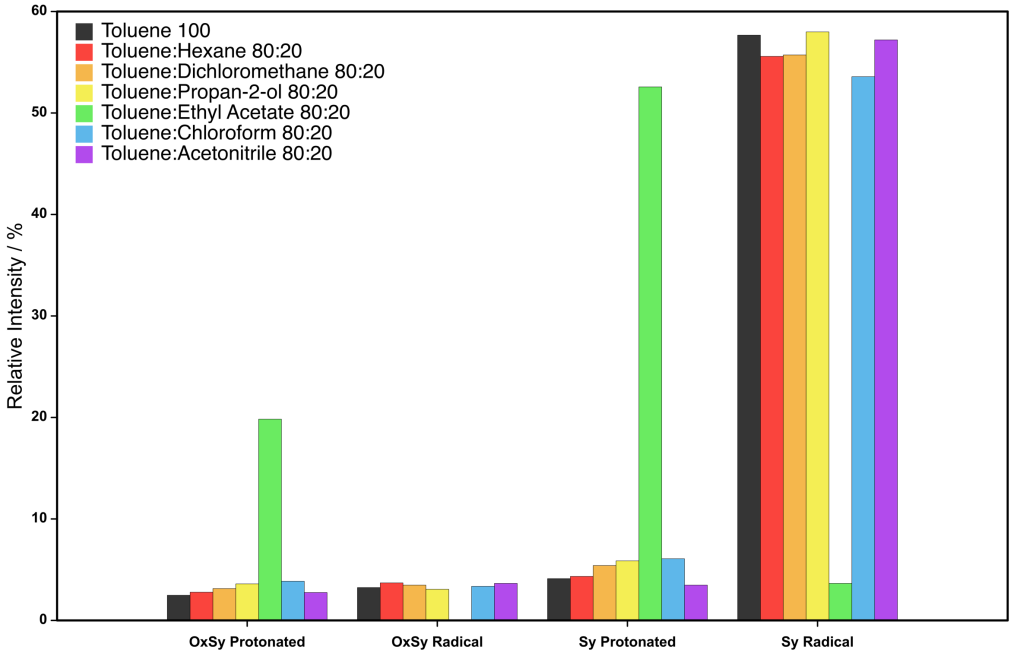

Figure 5.4 – Summed relative intensity of protonated and radical ion classes containing at least one sulfur atom assigned in solvent systems initially studied

There are several possible explanations for the preferential formation of protonated species in the solvent system containing ethyl acetate. Although aprotic and incapable of forming hydrogen bonds, the protonated form of ethyl acetate can be stabilized across three resonance structures, and the proton may then be transferred to analyte molecules. A study of APCI, a technique similar to APPI, suggested that the formation of $[M+H]^+$ species via proton transfer from a protonated solvent molecule is more energetically favorable than through charge transfer from a radical solvent molecule (Herrera et al., 2008). As ethyl acetate is capable of resonance stabilizing a proton, such pathways may be predominant when it is component in a solvent system. In addition, the conditions of ionization, including high temperature and the presence of water in the local environment, sample, solvent, or source, may facilitate the hydrolysis of ethyl acetate to produce acetic acid and ethanol. A scheme illustrating the hypothetical process is shown in Figure 5.5. Acetic acid, if generated in this manner, may provide a source of labile protons, acting as a stronger acid in the gas-phase than $HO_2\bullet$ (Kauppila et al., 2002). It is also possible that interactions between ethyl acetate molecules increase the ionization volume, limiting analyte photoabsorption, and causing a loss of signal intensity and predominance of $[M+H]^+$ ions (Kauppila et al., 2005; Short et al., 2007). Irrefutably identifying the cause underlying the observed effect is beyond the scope of this work, however.

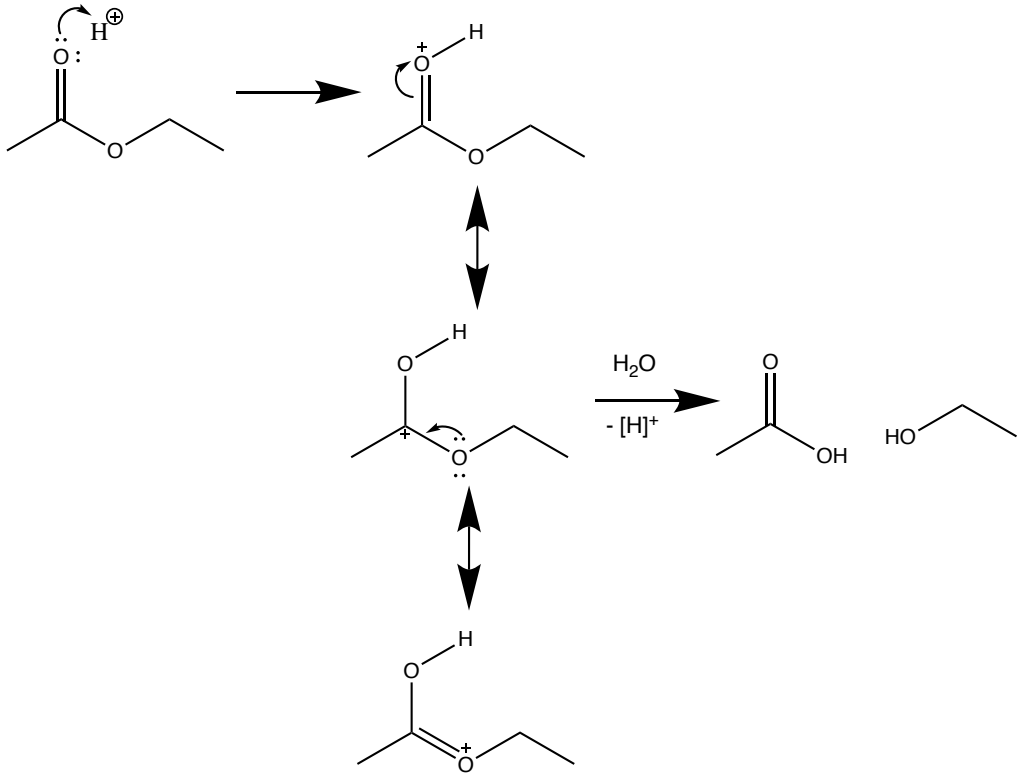

Figure 5.5 – Hypothetical scheme illustrating ethyl acetate generating sources of labile protons; its resonance stabilized protonated form, and its hydrolysis product acetic acid. $[H]^+$ may be generated in the source as indicated in Equation scheme 5.1

The range of species detected in the N[H] and S[H] classes in the toluene:ethyl acetate solvent system appear similar to those of the N and S classes in other solvent systems, suggesting a loss of molecular speciation by ion-type. This similarity is exemplified in Figure 5.6, where DBE distributions of the protonated classes in toluene:ethyl acetate closely reflect those of the radical classes in toluene:propan-2-ol. The DBE plots in Figures 5.7 and 5.8 further demonstrate the greater peak densities in the protonated classes in toluene:ethyl acetate, which reflect the radical classes in toluene:propan-2-ol. Combined DBE distributions of the N and N[H] classes, and S and S[H] classes, in toluene:propan-2-ol, also reflect those of the protonated classes in toluene:ethyl acetate (Figures 5.9 and 5.10 respectively).

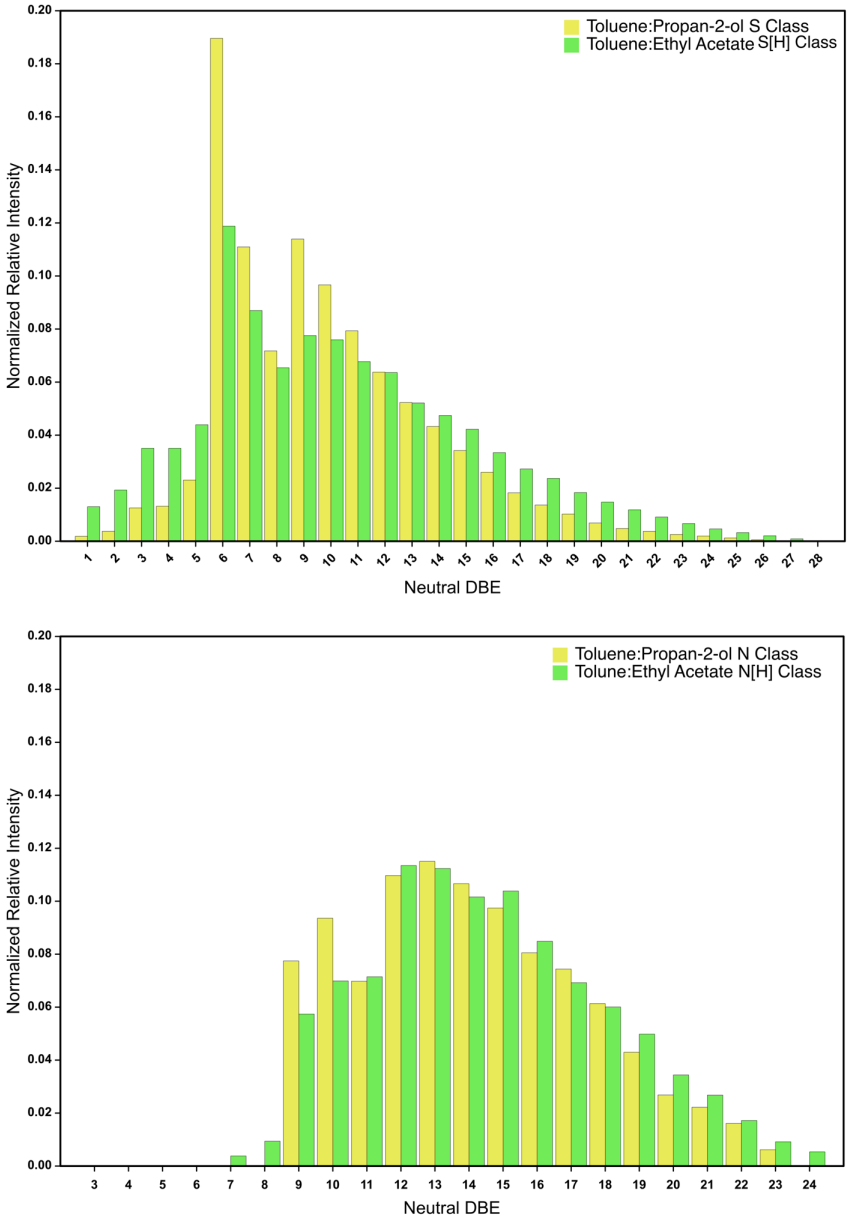

Figure 5.6 – DBE distributions demonstrating the similarity between the radical S and N and protonated S[H] and N[H] classes in toluene:propan-2-ol and toluene:ethyl acetate solvent systems

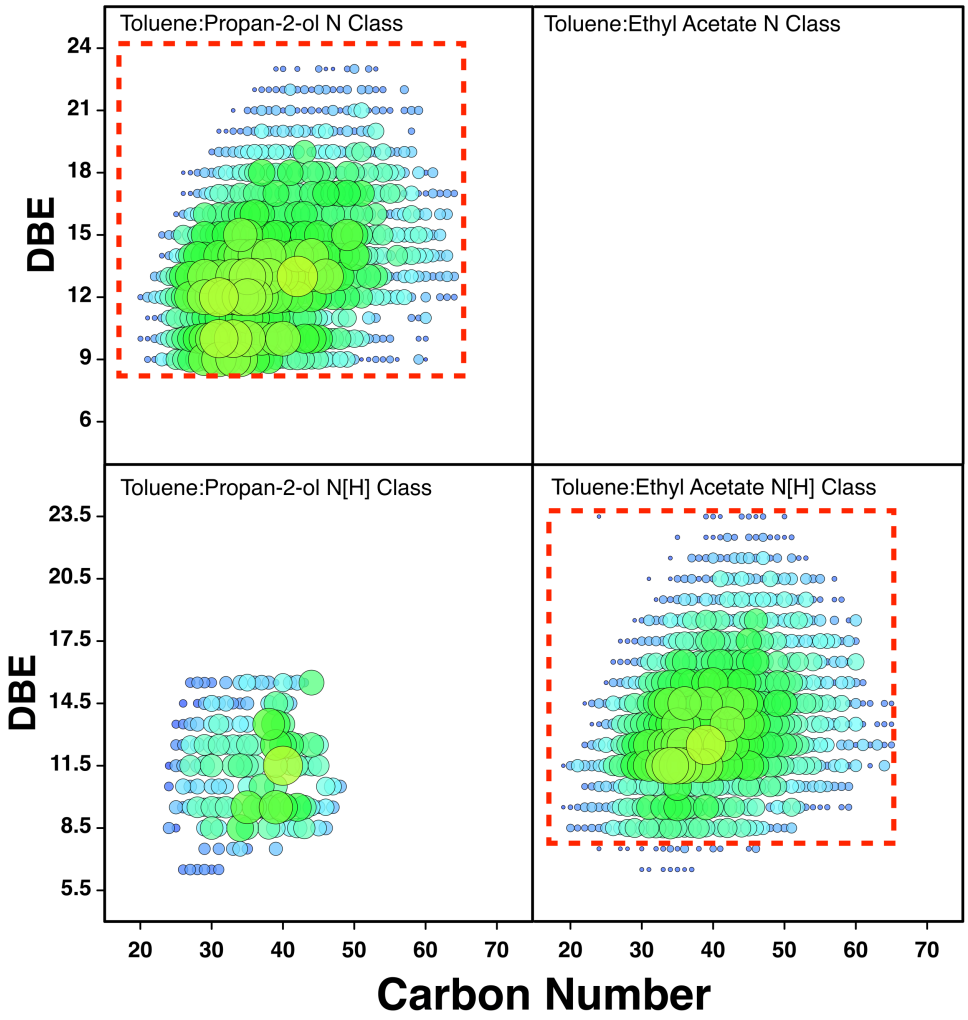

Figure 5.7 – DBE vs. carbon number plots for N and N[H] classes in toluene:propan-2-ol and toluene:ethyl acetate solvent systems, with squares surrounding corresponding DBE and carbon number values demonstrating the similarity between the species apparent in the N class and N[H] class of each, respectively. The N[H] class was observed at low relative intensity in the toluene:propan-2-ol solvent system, while the N class was not detected in the toluene:ethyl acetate solvent system

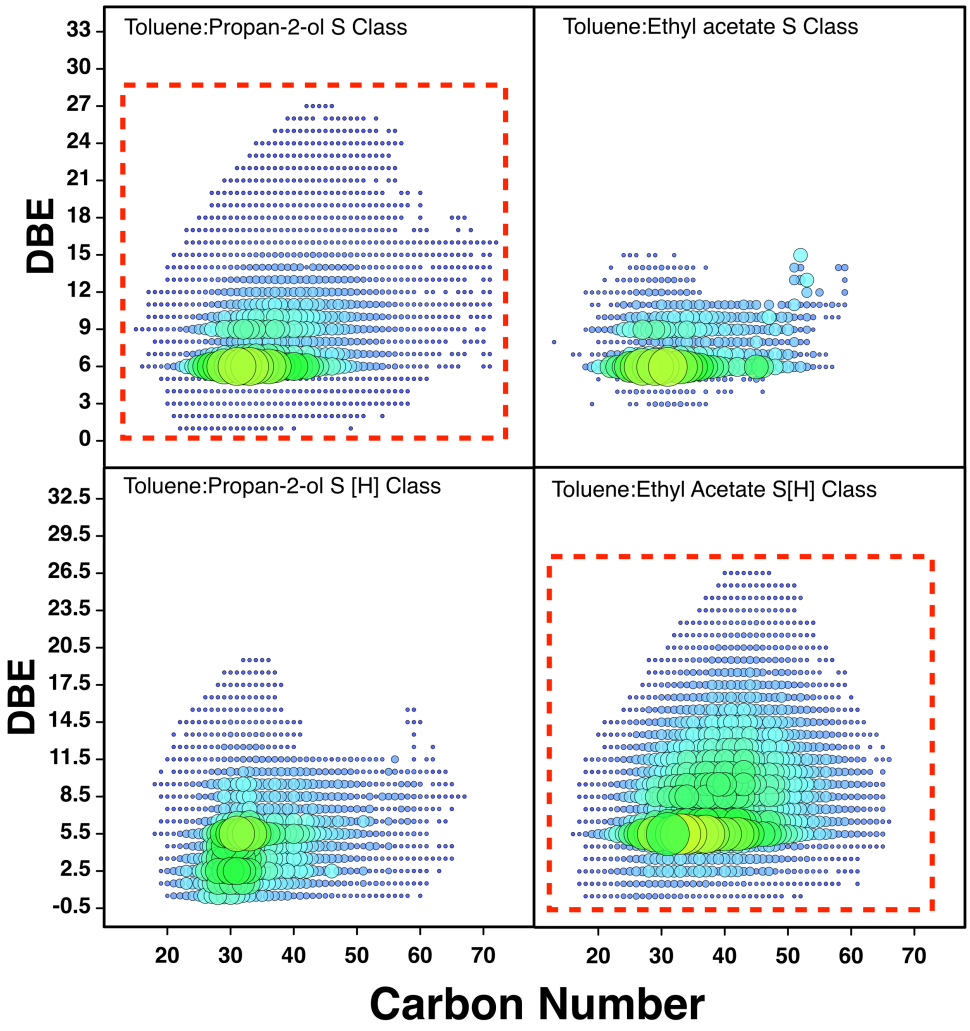

Figure 5.8 – DBE vs. carbon number plots for S and S[H] classes in toluene:propan-2-ol and toluene:ethyl acetate solvent systems, demonstrating similarity between the species apparent in the S class and S[H] class of each, respectively. The S[H] class and S class were observed at low relative intensity in the toluene:propan-2-ol and toluene:ethyl acetate solvent systems respectively

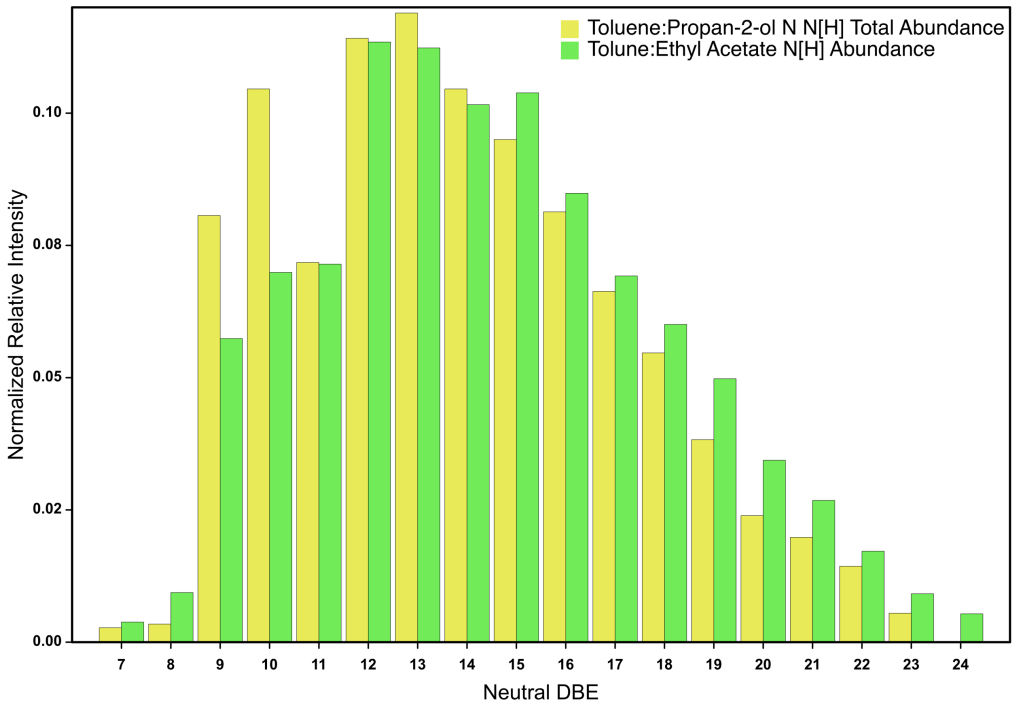

Figure 5.9 – Summed N and N[H] class DBE distribution for the toluene:propan-2-ol solvent system compared the N[H] class DBE distribution for the toluene:ethyl acetate solvent system

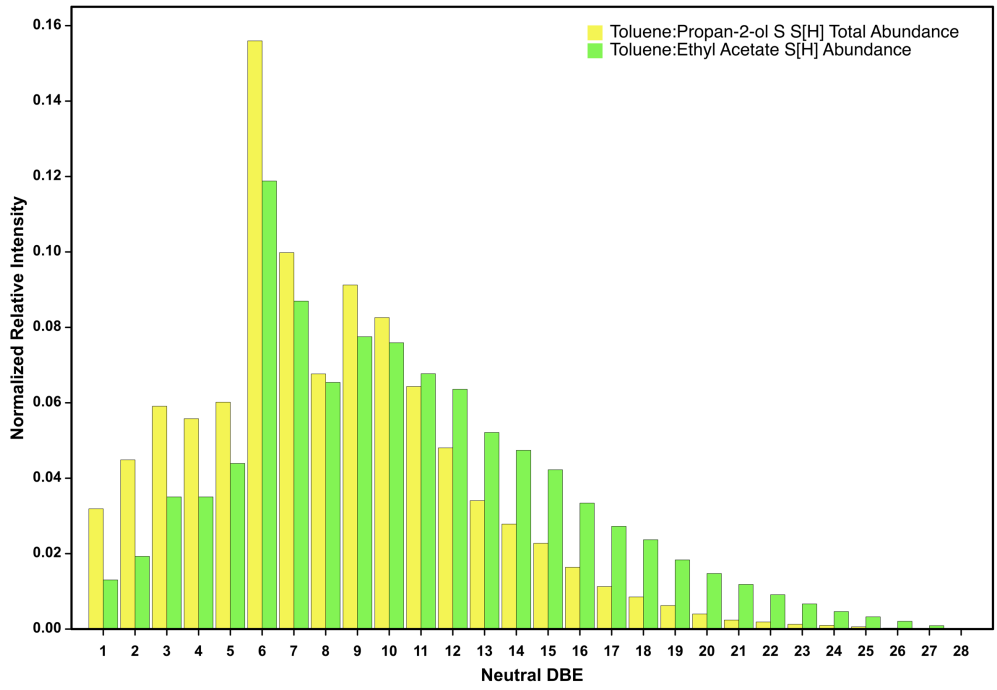

Figure 5.10 - Summed S and S[H] class DBE distribution for the toluene:propan-2-ol solvent system compared the S[H] class DBE distribution for the toluene:ethyl acetate solvent system

The findings shown in Figures 5.6 and 5.7 suggest that nitrogen-containing compounds, both pyridines and carbazoles, ionize via protonation pathways in the toluene:ethyl acetate solvent system, causing a loss of speciation between N and N[H] classes. As such, the DBE distribution of the N[H] class in the toluene:ethyl acetate solvent system closely reflects that of the combined N and N[H] classes in the toluene:propan-2-ol solvent system (Figure 5.9). Although the number of assignments made to the N[H] class is low for the toluene:propan-2-ol solvent system, the most intense homologous series begins at DBE 8.5, and there is also a relatively intense homologous series of DBE 11.5 (Figure 5.7 and 5.11), a separation of 3 DBE and characteristic of pyridinic species (Purcell et al., 2007b). In the toluene:ethyl acetate solvent system, however, the N[H] class is densely populated, with DBE plots and distributions that appear similar to those for the N class (Figure 5.6) and combined N and N[H] class (Figure 5.9) of the toluene:propan-2-ol solvent system, losing such speciation for pyrdinic compounds. Hydrogen-deuterium exchange studies (Acter et al., 2017; Cho et al., 2013), or hyphenated chromatography FTICR MS experiments (Thomas et al., 2019) in which the EIC traces of both ion-type molecular assignments were compared, could be used to confirm whether radical molecules in a given solvent system were instead proceeding via protonation pathways in another.

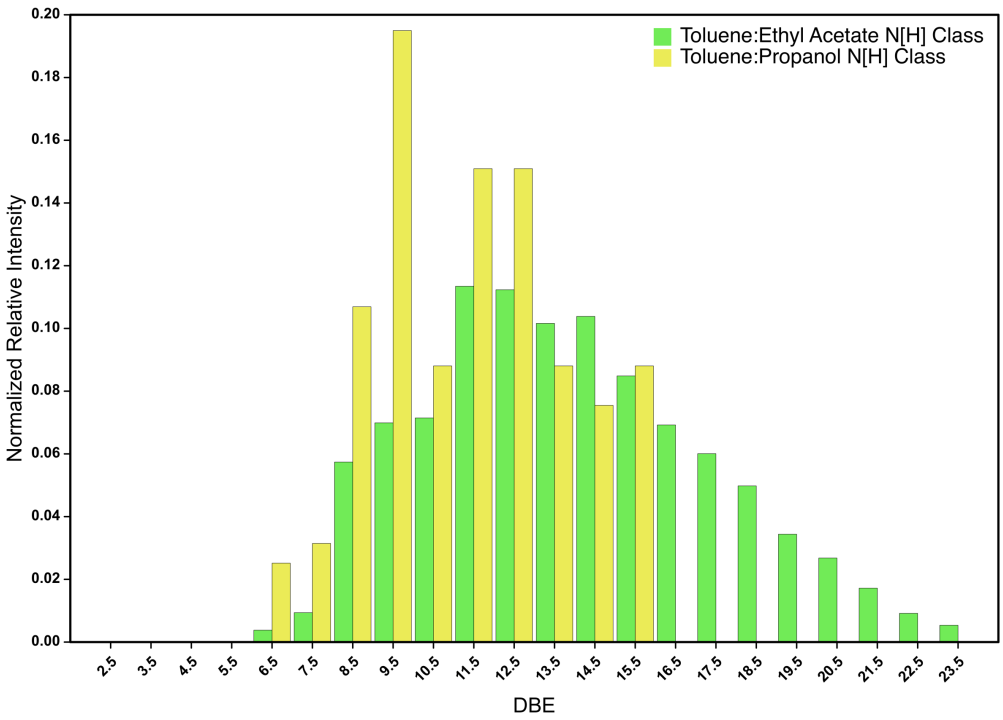

Figure 5.11 – DBE distribution of the N[H] class compared between the toluene:ethyl acetate and toluene:propan-2-ol solvent systems

5.3.2 Effect of Further Solvent Systems on Ion-Type Ratio

To investigate the possible factors underlying the observations made initially for the toluene:ethyl acetate solvent system, the Iraqi crude oil profile was analysed in four additional solvent systems:

- 80:20 toluene:acetone, as acetone also has a low ionization efficiency and high proton affinity,
- 99:1 toluene:ethyl acetate, to assess the effect of a lower ethyl acetate volume fraction,
- 79.75:19.75 toluene:ethanol, with acetic acid added at 0.5 %, to determine whether the effect is due to hydrolysis of ethyl acetate, and the products generated by this process, as hypothesized in Figure 5.5,
- 79.75:19.75 toluene:propan-2-ol, with acetic acid added at 0.5 %, to assess whether the addition of acetic acid altered the previously observed ratio for the 80:20 toluene:propan-2-ol system.

As shown in Figures 5.2 and 5.6, the S[H] and S class contributed the greatest spectral intensity in the toluene:ethyl acetate and other initial solvent systems respectively, and has previously been used to investigate the effects of experimental parameters (Guillemant et al., 2019b). The ratio of relative intensities of these compound classes was therefore monitored as an indicator of protonated species formation, particularly as benzothiophenic species are usually detected in the radical S class (Purcell et al., 2007a) starting at a DBE of 6. The normalized relative intensities of the S and S[H] classes in these further solvent systems are compared against those in the solvent systems data originally investigated in Figure 5.12.

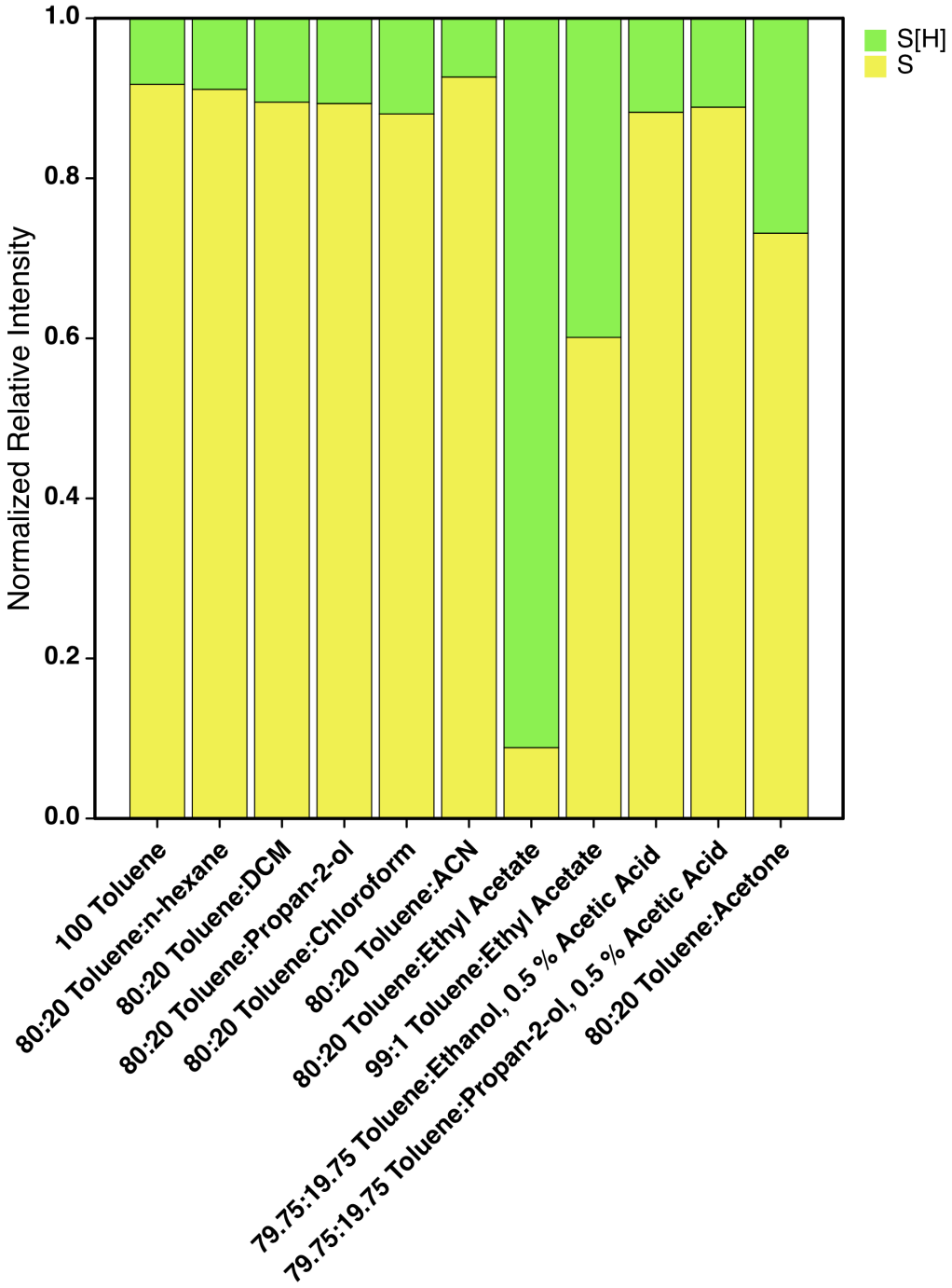

Figure 5.12 – Normalized relative intensities of S and S[H] classes for all solvent systems studied

The hypothetical scheme shown in Figure 5.5 indicates that hydrolysis of ethyl acetate produces acetic acid. Should the hypothesized reaction under (+) APPI conditions indeed be occurring, the inclusion of 0.5 % acetic acid in the toluene:ethanol solvent system should produce a similar ion-type ratio to the 99:1 toluene:ethyl acetate solvent system. The findings shown in Figure 5.12 therefore suggest that hydrolysis of ethyl acetate can be ruled out as the mechanism

underlying the preferential formation of protonated species, as the relative proportions of S and S[H] class relative intensities in the 79.75:19.75 toluene:ethanol with 0.5 % acetic acid solvent system more closely reflect that of 80:20 toluene:propan-2-ol solvent system. Lowering the volume fraction of ethyl acetate to 1 % in the solvent system effects a reduction in the ion-type ratio, and while significant, it is less profound than when ethyl acetate is at 20 %. The 80:20 toluene:acetone solvent system also has a substantially lower radical:protonated ratio that may be linked to the low ionization efficiency or high proton affinity of the acetone cosolvent.

5.3.3 Correlating Solvent Properties with Observed Ion-Type Ratios

The factors leading to increased formation of protonated species may include solvent volatility. Figures 5.13 and 5.14 show no correlation, however, between the ratio of radical and protonated species with total vapor pressure of the solvent system, calculated using Raoult's Law, or the volatility of the 20 % v/v solvent. There also appears to be no consistent trend between ionization efficiency of the 20 % v/v solvent and the S/S[H] ratio (Figure 5.15). In APPI, charge exchange is widely considered to be favored by lower proton affinity solvents, while proton transfer is favored by higher proton affinity solvents (de Hoffman and Stroobant, 2007), however Figure 5.16 suggests that the S/S[H] ratio increases with proton affinity up to ca. 800 kJ mol^{-1}, above which the ratio decreases.

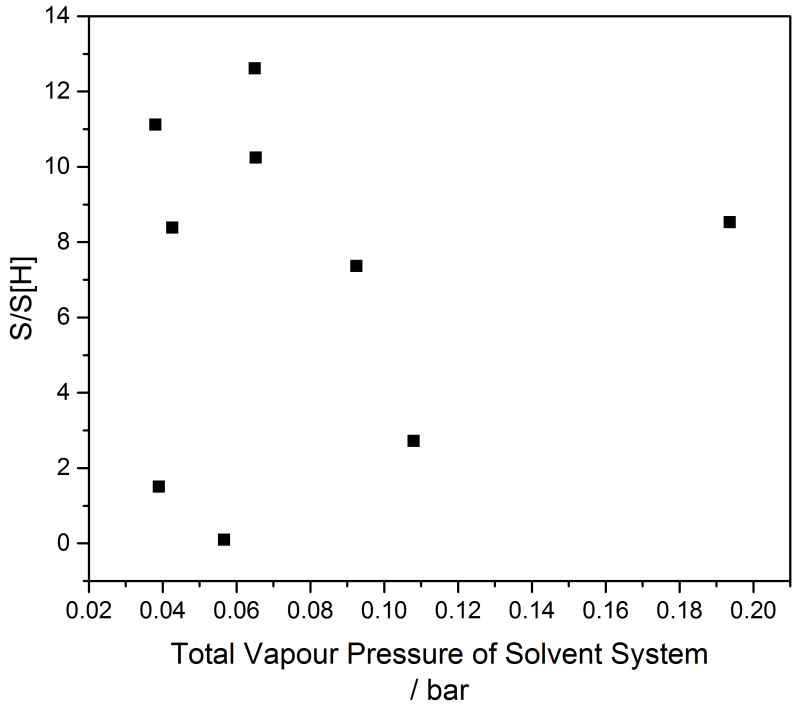

Figure 5.13 - Change in S/S[H] with total vapour pressure of solvent system

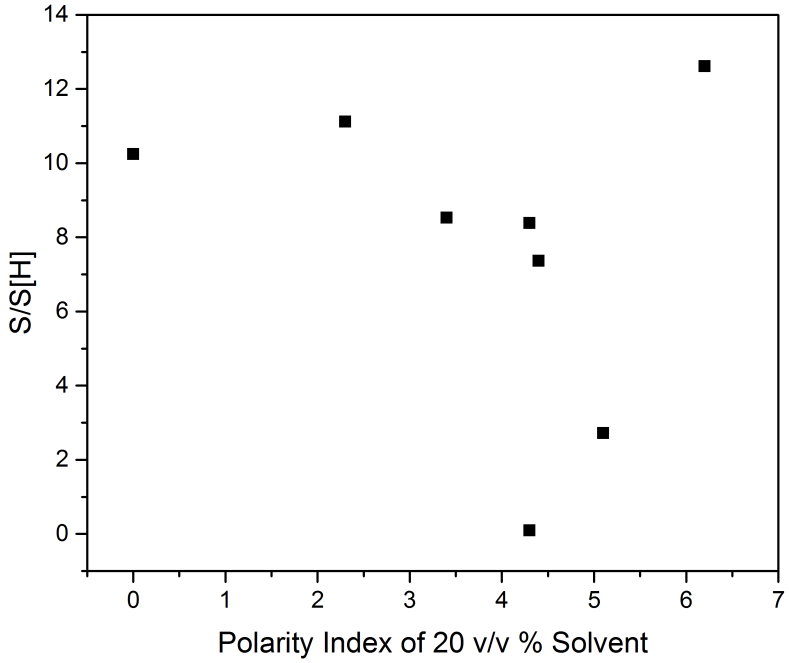

Figure 5.14 - Change in S/S[H] with polarity index of solvent added at 20 v/v % to solvent system

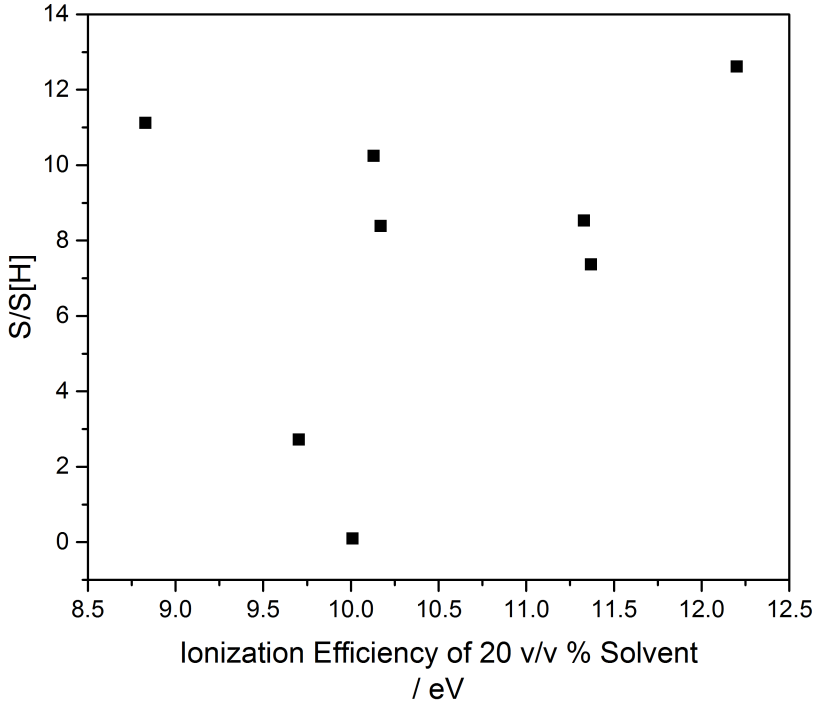

Figure 5.15 – Change in S/S[H] with ionization efficiency of solvent added at 20 v/v % to solvent system

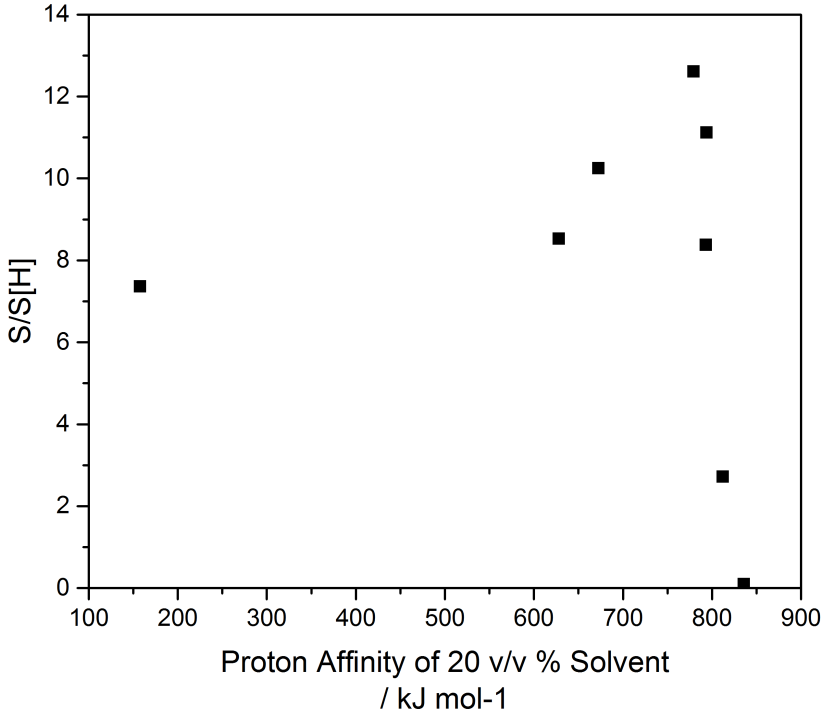

Figure 5.16 – Change in S/S[H] ratio with proton affinity of the 20 v/v % solvent. A tipping point in the observed ratio appears to occur where the proton affinity of the added solvent exceeds ca. 777 kJ mol^{-1}

While no correlation between the ion-type ratio and total vapor pressure, or cosolvent polarity index or ionization efficiency, was found, Figure 5.16 suggests that the proton affinity of the solvent system impacts the results obtained. Solvent proton affinity must therefore be considered as capable of influencing the relative proportions of radical and protonated species observed in APPI-FTICR MS.

The findings on this section show that the proton affinity of solvents must be taken into particular consideration when comparing results between studies where different sample preparation steps or hyphenation steps are employed, for example in liquid chromatography (LC), or extraction of analyte compounds of interest. Other ionization methods, particularly electrospray ionization, are known to suffer ionization suppression (Annesley, 2003; Huba et al., 2016), particularly when analytes are in the presence of large, more highly charged molecules, salts, or other non-volatile solute, or when the pH of the solvent system is varied (King et al., 2000; Peru et al., 2019). Therefore the impact of solvent choice on ionization has implications beyond petroleomics and APPI experiments, particularly in emerging fields such as quantitative proteomics, where LC is widely used with a range of solvent mobile phases (Elliott et al., 2009; Li et al., 2017).

5.3.4 Design of Experiment (DoE) Study with Ion-Type Ratio as Response Factor

A DoE study was carried out to establish whether concentration, toluene solvent fraction, and flow rate had significant effect on the ion-type ratio of radical to protonated species (R/P) observed (magnitude and direction shown in Figure 5.17, with standardized effects shown in Figure 5.18). Flow rate was among the factors targeted, as this experimental parameter is varied widely in the field, although the impact upon the results obtained remains poorly understood. All factors, and the majority of their interactions, were found to be significant, while a non-linear effect is suggested given that the R/P at the centerpoint does not sit on a straight line between the minimum and maximum values of any factor. While the volume fraction of toluene in the solvent system has the greatest impact on R/P, with higher toluene content most strongly favoring the formation of radical species, flow rate was also shown to be a significant factor, with higher flow rates increasing the relative proportion of protonated species detected. Thus, the total volume fraction of toluene in the solvent system and the flow rate were found to be the main factors influencing R/P, with a less significant effect demonstrated for the sample concentration and its interactions with the other factors. Samples prepared with 100 % toluene volume fraction effected the highest R/P response, while a high flow rate gave a lower response.

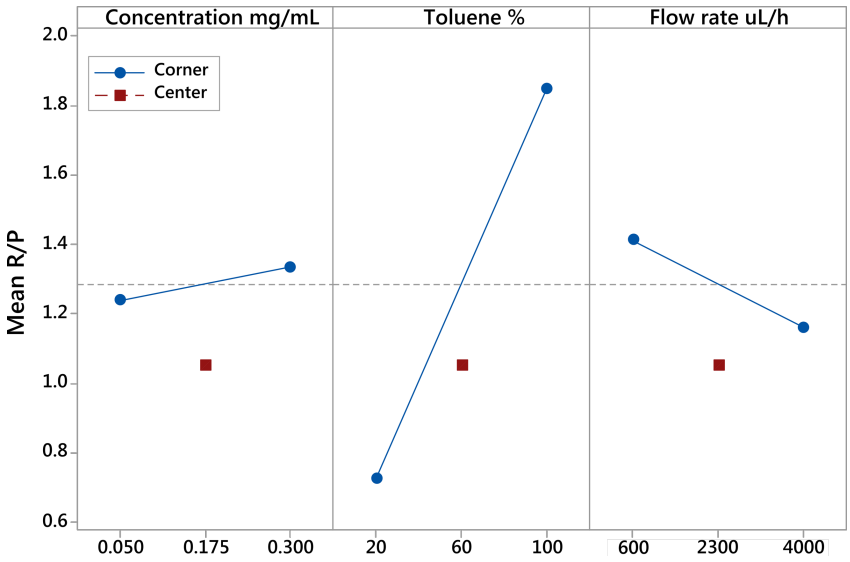

Figure 5.17 – Summary of DoE study where response factor is the mean ratio of radical to protonated species (R/P). While higher sample concentration and larger toluene solvent fraction increase radical ion formation, a high flow rate decreases the relative proportion of radical species detected. Red squares are indicative of the effect at the centerpoint

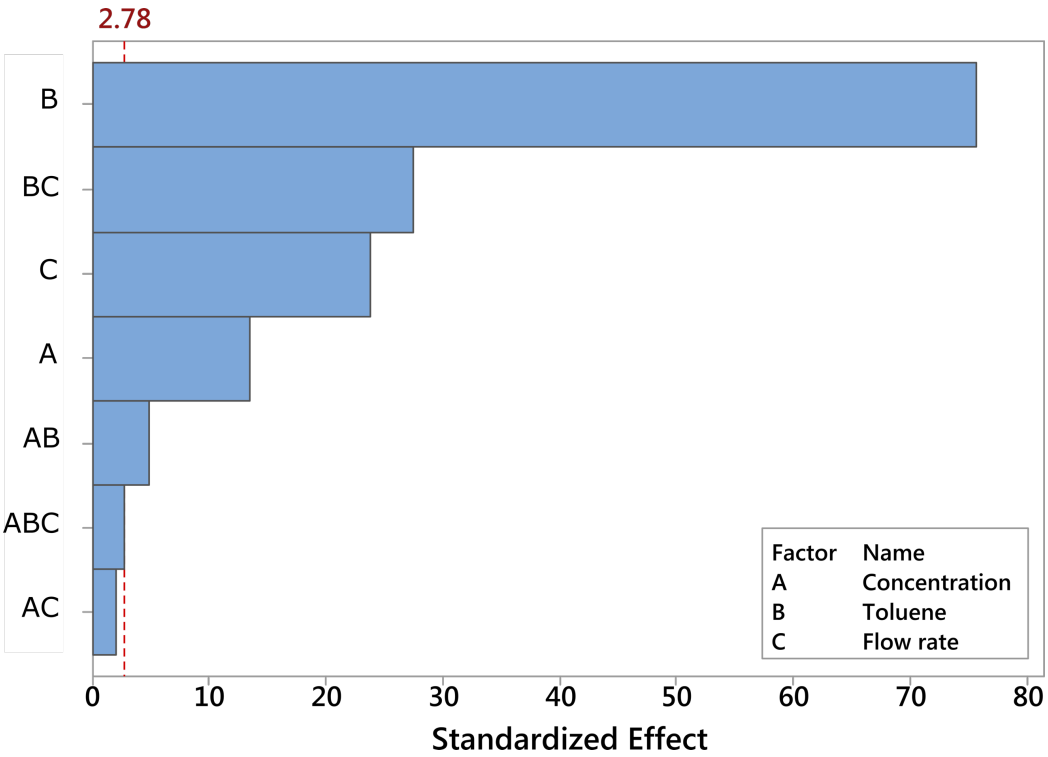

Figure 5.18 – Pareto chart of standardized effects for DoE experiments. The response is the mean ratio of radical and protonated species detected (R/P). Factors that exceed the dashed reference line are statistically significant at the $\alpha = 0.05$ level

To illustrate the effect observed when only the flow rate is altered, and concentration and toluene volume fraction are kept constant, enlarged regions of DoE mass spectra of the South American crude oil at 600 and 4000 μL h^{-1} are shown in Figure 5.19. These demonstrate the decrease in mass spectral intensity with increasing flow rate, and the more severe effect on radical ions assigned to the HC and S classes. A peak assigned to the N[H] class has an increased intensity, however, and dominates the spectrum at 4000 μL h^{-1}. Predominant N[H] peaks in the same spectral window have been observed in an APPI study of asphaltene fractions, however the flow rate used was not reported (McKenna et al., 2019).

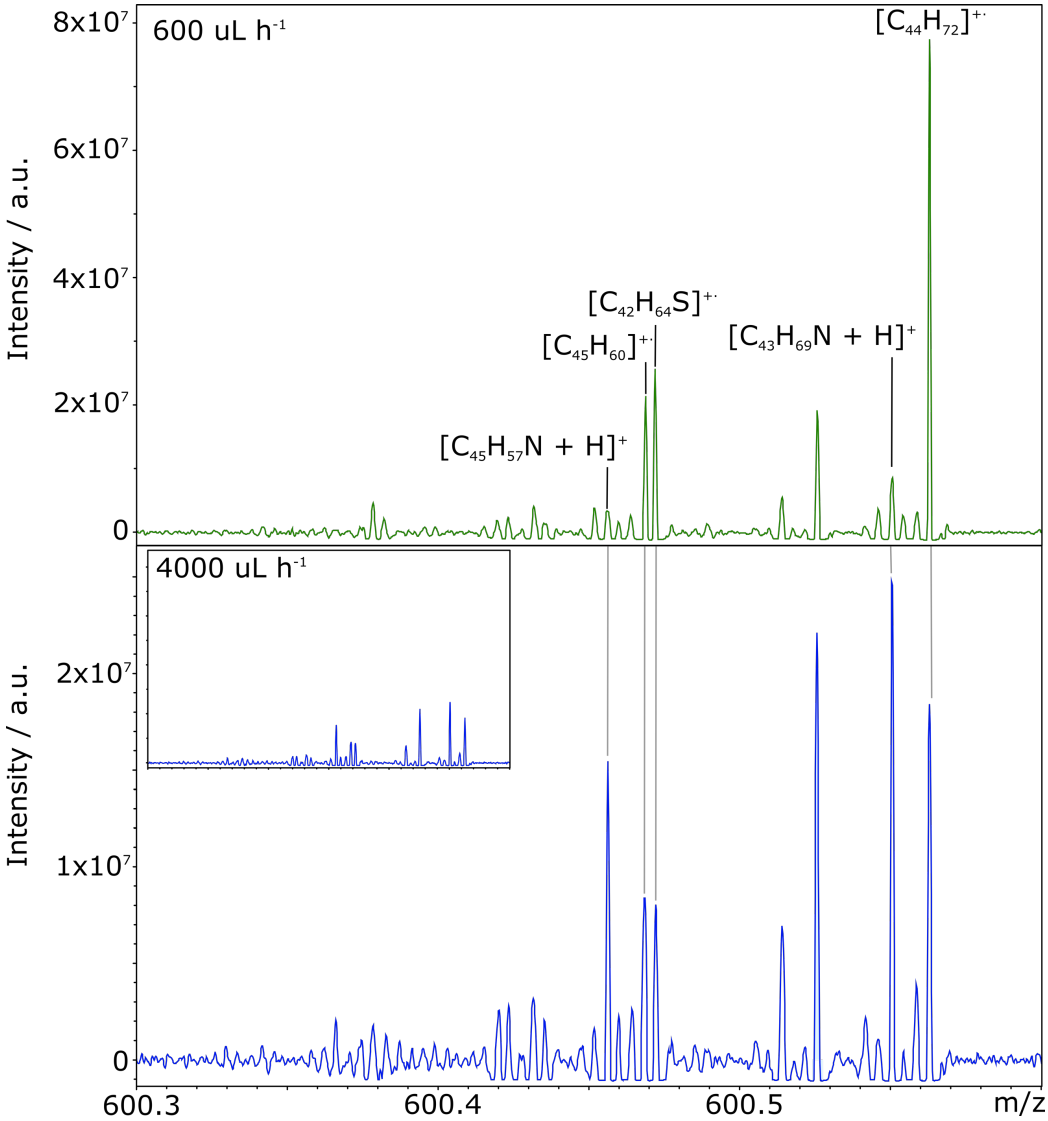

Figure 5.19 – Enlarged regions of phase corrected MS from DoE experiments on the South American crude oil at 0.05 mg mL^{-1} in 20:80 toluene:propan-2-ol, comparing the profiles at an injection flow rate of 600 µL h^{-1} and 4000 µL h^{-1}. A decrease in overall intensity (inset within lower panel on intensity scale equivalent to upper panel), a shift in ion-type predominance, and higher response for species assigned to the N[H] class, is observed at the higher flow rate

5.3.5 Effect of Flow Rate on Ion-Type Ratio

Flow rate was varied in selected solvent systems to determine whether the decrease in signal intensity and preferential formation of protonated species in the toluene:ethyl acetate solvent system would be reflected in other solvent systems at higher flow rates.

The crude oil in toluene:propan-2-ol solvent system was initially studied at flow rates ranging from 400-3200 μL h^{-1}. In parallel, the same system was spiked with thiophenic compound 1,2-benzodiphenylene sulfide, a sulfur-containing species with a neutral DBE of 12, and studied at the same range of flow rates. Consistent with other studies of model compounds by APPI (Acter et al., 2017), the protonated species was not observed, possibly due to a lack of alkylation about its core structure, however the radical ion was detected. The monoisotopic absolute intensity of the 1,2-benzodiphenylene sulfide model compound radical ion in the spiked system is compared against the S/S[H] class and DBE 6/5.5 ratios detected in the Iraqi crude oil in Figure 5.20.

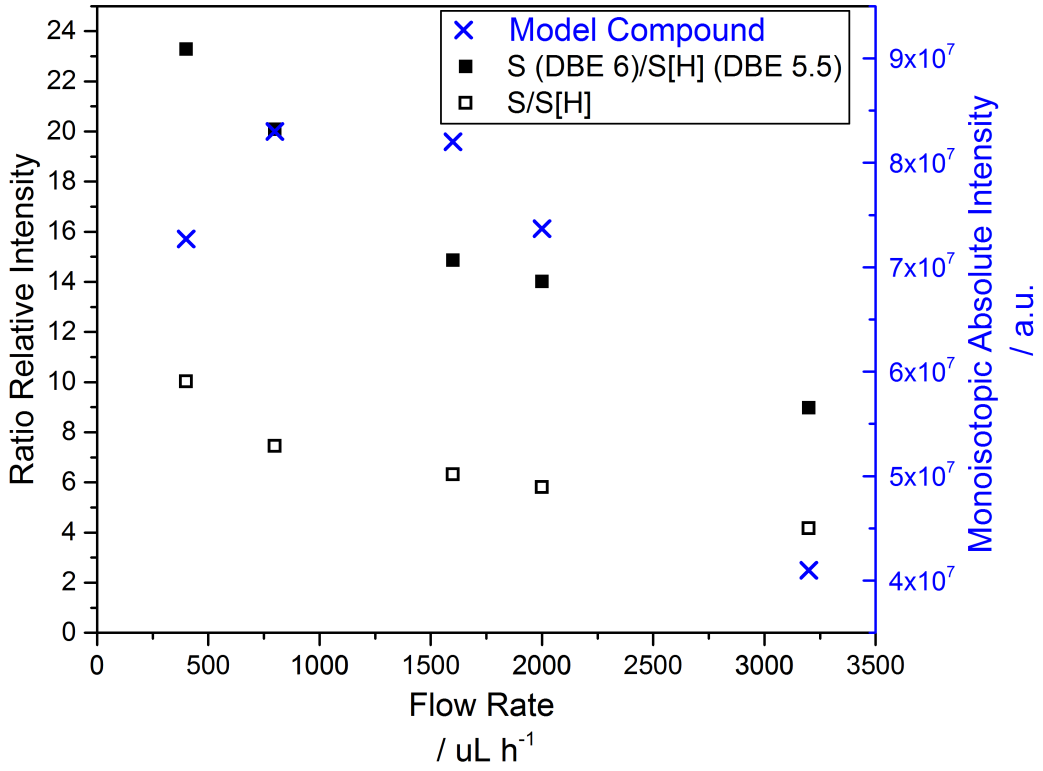

Figure 5.20 – Change in ratio S/S[H], and homologous series DBE 6/5.5 therein, in the Iraqi crude oil in toluene:propan-2-ol solvent system, and the monoisotopic absolute intensity of spiked model compound, with increasing flow rate

Figure 5.20 shows that, although the monoisotopic absolute intensity of the model compound does increase slightly between 400 and 800 μL h^{-1} and remains relatively stable up to 1600 μL h^{-1}, the model compound intensity decreases with increasing flow rate thereafter. A similar general decrease in model compound intensity with increasing flow rate is observed in the toluene and 80:20 toluene:acetone solvent systems (Figure 5.21). In the 99:1 toluene:ethyl acetate solvent system, however, the model compound intensity is low at 1000 μL h^{-1} and

at all other flow rates studied, with no change greater than 0.1 % relative to the intensity at 1000 μL h^{-1}.

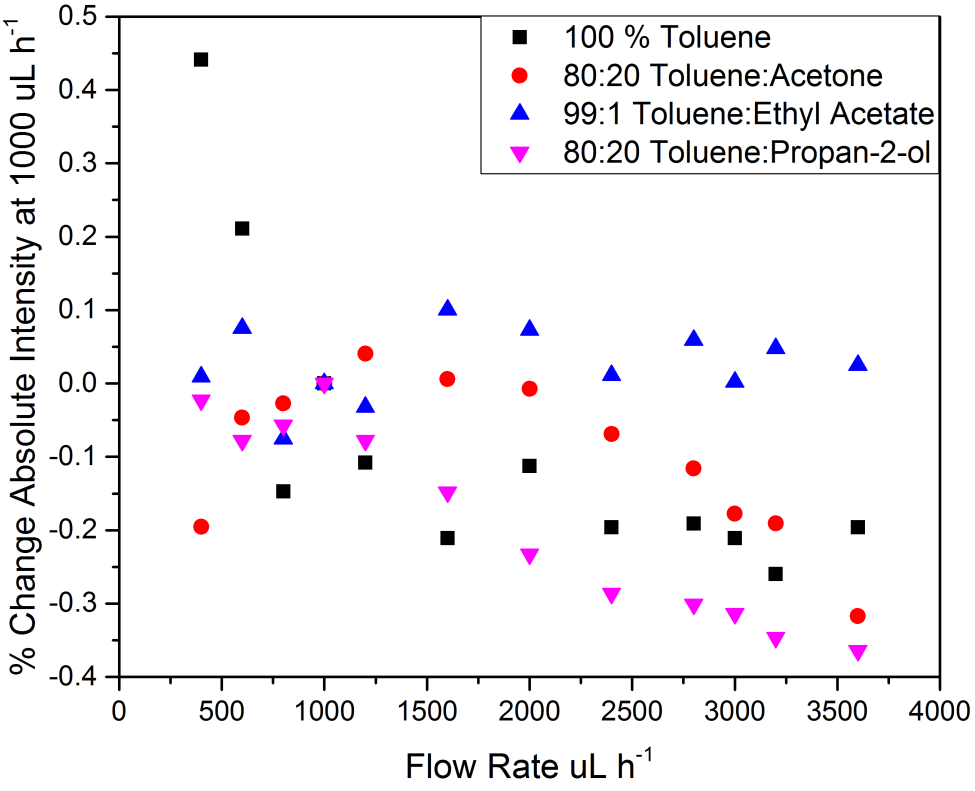

Figure 5.21 – Percent change in monoisotopic absolute intensity of model compound spiked into Iraqi crude oil dissolved in different solvent systems with flow rate relative to observed intensity at 1000 μL h^{-1}

A non-linear decrease in the ratio of relative intensity between radical ions and protonated species, a result predicted by the DoE data, is also demonstrated in Figure 5.20. The change in relative abundance of the S[H] class and the change in S/S[H] ratio of the Iraqi crude oil in different solvent systems with varying flow rate is explored further, with results shown in Figure 5.22. The relative intensity of the S[H] class shows a general increase with flow rate, except in toluene only; and in 99:1 toluene:ethyl acetate, where it appears to plateau above 1600 μL h^{-1}. Similarly, the S/S[H] ratio decreases with increasing flow rate, particularly in 80:20 toluene:propan-2-ol and 80:20 toluene:acetone, the latter of which sees the ratio drop below 1, indicating the onset of the preferential formation and predominance of protonated species above 2800 μL h^{-1}. Similar shifts in ion-type predominance from radical to protonated have been predicted in theoretical

studies where the temperature of sample desolvation is increased (Ahmed et al., 2017).

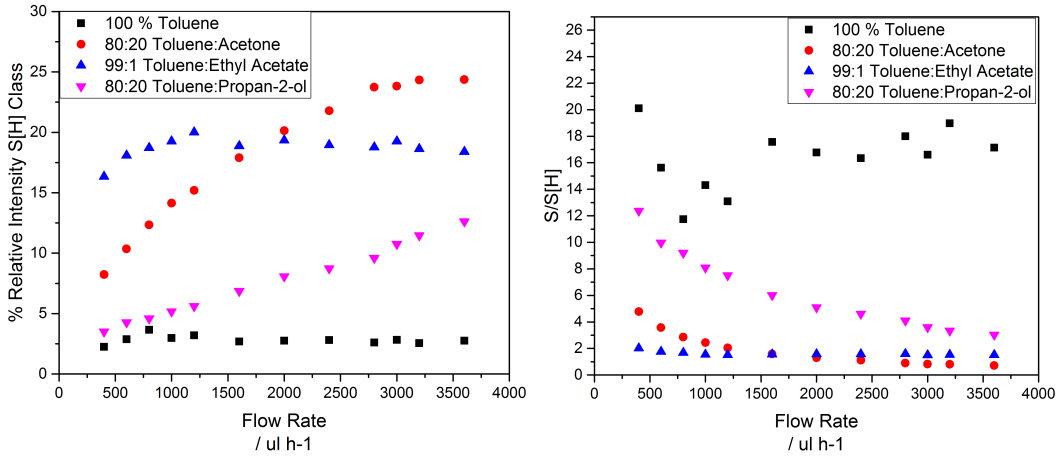

Figure 5.22 – Change in relative intensity of S[H] compound class and change in S/S[H] ratio with increasing flow rate in different solvent systems

The results shown in Figures 5.20 and 5.22 highlight the need for caution where higher flow rates are used in APPI, particularly for the study of complex mixtures. While a loss of signal intensity may reduce sensitivity, such that lower abundance species may not be detected, the preferential formation of protonated species makes speciation of compound types less feasible, effecting a reduction in compositional access and loss of sample information. Furthermore, should a species be protonated at higher flow rate that may have formed a radical ion at lower flow rate, any subsequent fragmentation efficiency may be reduced given its greater stability, therefore limiting the elucidation of structural information.

The factors underlying the decrease in radical ion intensity at higher flow rates have been discussed elsewhere, with early APPI studies suggesting that dopant toluene ions must not be entirely consumed in dopant-solvent reactions in order for radical species to be generated efficiently. However, higher flow rates are known to drive dopant-solvent reactions to completion (Robb and Blades, 2006). Other studies have shown that higher flow rates produce larger solvent clusters, which drive recombination reactions, effectively lowering the sensitivity of APPI overall, with protonated species formation less severely affected (Ahmed et al., 2015; Kauppila et al., 2005; Robb and Blades, 2005).

The impact of the solvent system and flow rate on the observed profile and relative proportions of radical and protonated species has implications for studies of real-world complex samples. Indeed, researchers working in the field of

petroleomics have identified that flow rates exceeding 1500 uL h^{-1} have been observed to have a negative impact on signal intensity (Acter et al., 2018), with formation of solvent clusters and their subsequent reaction with toluene dopant ions identified as a possible cause that more significantly impacts radical ion signal (Ahmed et al., 2015). Nevertheless, analyte solution flow rate is an often-overlooked factor in petroleomics research and contrasting findings on observed ion-type ratios are therefore common. For example, in a recent study reporting a flow rate of 50 μL min^{-1} (i.e. 3000 μL h^{-1}) many thousands of unique molecular formulae were identified, the majority of which were protonated species, and it was subsequently inferred that APPI favors protonation of analyte components (Krajewski et al., 2017). In another study, reporting a record 244,779 assignments, APPI appeared to favor radical ions, and reports the use of a flow rate of 500 μL h^{-1} (Palacio Lozano et al., 2019). The differences in ion-type ratio and preferential compound class detection reported across the literature are in line with the findings of this study.

5.4 Conclusions

Several factors were found to have a significant impact on the signal intensity, observed profile, and ion-type ratio in two crude oils analyzed by (+) APPI-FTICR MS. The solvent system employed, particularly the use of high proton affinity solvents in combination with toluene, and to a lesser extent the use of toluene at low volume fraction, had the greatest impact. The use of higher flow rates, widely utilized by petroleomics researchers without the impact being previously well understood, also inverts the ion-type ratio in several solvent systems.

The use aprotic solvents with high proton affinities, such as ethyl acetate and acetone, increased the number of protonated species detected, with species that would ordinarily ionize via radical pathways, such as thiophenes and pyrroles, appearing to ionize instead via protonation pathways. This affects a loss in molecular speciation, previously made possible through observing characteristic patterns in DBE plots and distributions. Although not as severe as the effect observed when ethyl acetate is used as cosolvent, a trend of increasing protonated species formation and decreasing radical ion formation was observed in other solvent systems with increasing flow rate. While signal intensity could be increased by raising flow rate to an optimum around 1000 μL h^{-1}, higher flow rates affected a loss in signal intensity.

Experimental parameters, including solvent system and flow rate, have a critical influence on the characterisation of complex samples such as petroleum, and are an important consideration when comparing compositional profiles. The widely reported observations of predominantly protonated species may be an ionization phenomenon and care should be taken to determine whether experimental factors have influenced the results obtained. The findings of this study are important beyond compositional analysis of petroleum samples. In particular, the consideration of solvent properties, such as proton affinity, may be particularly important in hyphenated mass spectrometry methods and in applications such as quantitative proteomics.

5.5 References

Acter T, Kim D, Ahmed A, Ha JH, Kim S. Application of Atmospheric Pressure Photoionization H/D-exchange Mass Spectrometry for Speciation of Sulfur-containing Compounds. Journal of the American Society for Mass Spectrometry 2017; 28: 1687-1695.

Acter T, Lee S, Cho E, Jung M-J, Kim S. Design and Validation of In-Source Atmospheric Pressure Photoionization Hydrogen/Deuterium Exchange Mass Spectrometry with Continuous Feeding of D2O. Journal of The American Society for Mass Spectrometry 2018; 29: 85-94.

Ahmed A, Choi CH, Choi MC, Kim S. Mechanisms Behind the Generation of Protonated Ions for Polyaromatic Hydrocarbons by Atmospheric Pressure Photoionization. Analytical Chemistry 2012; 84: 1146-1151.

Ahmed A, Choi CH, Kim S. Mechanistic study on lowering the sensitivity of positive atmospheric pressure photoionization mass spectrometric analyses: size-dependent reactivity of solvent clusters. Rapid Communications in Mass Spectrometry 2015; 29: 2095-2101.

Ahmed A, Ghosh MK, Choi MC, Choi CH, Kim S. Which Hydrogen Atom of Toluene Protonates PAH molecules in (+)-Mode APPI MS Analysis? Journal of the American Society for Mass Spectrometry 2013; 24: 316-319.

Ahmed A, Lim D, Choi CH, Kim S. Correlation between experimental data of protonation of aromatic compounds at (+) atmospheric pressure photoionization and theoretically calculated enthalpies. Rapid Communications in Mass Spectrometry 2017; 31: 1023-1030.

Annesley TM. Ion suppression in mass spectrometry. Clinical Chemistry 2003; 49: 1041-1044.

Bae E, Na JG, Chung SH, Kim HS, Kim S. Identification of about 30 000 Chemical Components in Shale Oils by Electrospray Ionization (ESI) and Atmospheric Pressure Photoionization (APPI) Coupled with 15 T Fourier Transform Ion Cyclotron Resonance Mass Spectrometry (FT-ICR MS) and a Comparison to Conventional Oil. Energy & Fuels 2010; 24: 2563-2569.

Barrow M, Peru K, Fahlman B, Hewitt L, Frank R, Headley J. Beyond Naphthenic Acids: Environmental Screening of Water from Natural Sources and the Athabasca Oil Sands Industry Using Atmospheric Pressure Photoionization Fourier Transform Ion Cyclotron Resonance Mass Spectrometry. Journal of the American Society For Mass Spectrometry 2015; 26: 1508-1521.

Barrow MP, Peru KM, McMartin DW, Headley JV. Effects of Extraction pH on the Fourier Transform Ion Cyclotron Resonance Mass Spectrometry Profiles of Athabasca Oil Sands Process Water. Energy & Fuels 2016; 30: 3615-3621.

Benigni P, DeBord J, Thompson C, Gardinali P, Fernandez-Lima F. Increasing Polyaromatic Hydrocarbon (PAH) Molecular Coverage during Fossil Oil Analysis by Combining Gas Chromatography and Atmospheric-Pressure Laser Ionization Fourier Transform Ion Cyclotron Resonance Mass Spectrometry (FT-ICR MS). Energy & Fuels 2016; 30: 196-203.

Chacon-Patino M, Rowland S, Rodgers R. Advances in Asphaltene Petroleomics. Part 1: Asphaltenes Are Composed of Abundant Island and Archipelago Structural Motifs. Energy & Fuels 2017; 31: 13509-13518.

Chacon-Patino ML, Rowland SM, Rodgers RP. Advances in Asphaltene Petroleomics. Part 2: Selective Separation Method That Reveals Fractions Enriched in Island and Archipelago Structural Motifs by Mass Spectrometry. Energy & Fuels 2018a; 32: 314-328.

Chacon-Patino ML, Rowland SM, Rodgers RP. Advances in Asphaltene Petroleomics. Part 3. Dominance of Island or Archipelago Structural Motif Is Sample Dependent. Energy & Fuels 2018b; 32: 9106-9120.

Chiaberge S, Fiorani T, Savoini A, Bionda A, Ramello S, Pastori M, et al. Classification of crude oil samples through statistical analysis of APPI FTICR mass spectra. Fuel Processing Technology 2013; 106: 181-185.

Cho Y, Ahmed A, Kim S. Application of Atmospheric Pressure Photo Ionization Hydrogen/Deuterium Exchange High-Resolution Mass Spectrometry for the Molecular Level Speciation of Nitrogen Compounds in Heavy Crude Oils. Analytical Chemistry 2013; 85: 9758-9763.

Cho YJ, Na JG, Nho NS, Kim S. Application of Saturates, Aromatics, Resins, and Asphaltenes Crude Oil Fractionation for Detailed Chemical

Characterization of Heavy Crude Oils by Fourier Transform Ion Cyclotron Resonance Mass Spectrometry Equipped with Atmospheric Pressure Photoionization. Energy & Fuels 2012; 26: 2558-2565.

de Hoffman E, Stroobant V. Mass Spectrometry: Principles and Applications, 2007.

Elliott MH, Smith DS, Parker CE, Borchers C. Current trends in quantitative proteomics. Journal of Mass Spectrometry 2009; 44: 1637-1660.

Gao JS, Borton DJ, Owen BC, Jin ZC, Hurt M, Amundson LM, et al. Laser-Induced Acoustic Desorption/Atmospheric Pressure Chemical Ionization Mass Spectrometry. Journal of the American Society for Mass Spectrometry 2011; 22: 531-538.

Griffiths M, Da Campo R, O'Connor P, Barrow M. Throwing Light on Petroleum: Simulated Exposure of Crude Oil to Sunlight and Characterization Using Atmospheric Pressure Photoionization Fourier Transform Ion Cyclotron Resonance Mass Spectrometry. Analytical Chemistry 2014; 86: 527-534.

Guillemant J, Albrieux F, de Oliveira LP, Lacoue-Negre M, Duponchel L, Joly JF. Insights from Nitrogen Compounds in Gas Oils Highlighted by High-Resolution Fourier Transform Mass Spectrometry. Analytical Chemistry 2019a; 91: 12644-12652.

Guillemant J, Albrieux F, Lacoue-Negre M, de Oliveira LP, Joly JF, Duponchel L. Chemometric Exploration of APPI(+)-FT-ICR MS Data Sets for a Comprehensive Study of Aromatic Sulfur Compounds in Gas Oils. Analytical Chemistry 2019b; 91: 11785-11793.

Han J, Yi Y, Lin KR, Birks SJ, Gibson JJ, Borchers CH. Molecular profiling of naphthenic acids in technical mixtures and oil sands process-affected water using polar reversed-phase liquid chromatography-mass spectrometry. Electrophoresis 2016; 37: 3089-3100.

Hanold KA, Fischer SM, Cormia PH, Miller CE, Syage JA. Atmospheric pressure photoionization. 1. General properties for LC/MS. Analytical Chemistry 2004; 76: 2842-2851.

Headley J, Peru K, Barrow M, Derrick P. Characterization of naphthenic acids from Athabasca oil sands using electrospray ionization: The significant influence of solvents. Analytical Chemistry 2007; 79: 6222-6229.

Herrera LC, Grossert JS, Ramaley L. Quantitative Aspects of and Ionization Mechanisms in Positive-Ion Atmospheric Pressure Chemical Ionization Mass Spectrometry. Journal of the American Society for Mass Spectrometry 2008; 19: 1926-1941.

Huba AK, Huba K, Gardinali PR. Understanding the atmospheric pressure ionization of petroleum components: The effects of size, structure, and presence of heteroatoms. Science of the Total Environment 2016; 568: 1018-1025.

Kauppila TJ, Bruins AP, Kostiainen R. Effect of the solvent flow rate on the ionization efficiency in atmospheric pressure photoionization-mass spectrometry. Journal of the American Society for Mass Spectrometry 2005; 16: 1399-1407.

Kauppila TJ, Kuuranne T, Meurer EC, Eberlin MN, Kotiaho T, Kostiainen R. Atmospheric pressure photoionization mass spectrometry. Ionization mechanism and the effect of solvent on the ionization of naphthalenes. Analytical Chemistry 2002; 74: 5470-5479.

King R, Bonfiglio R, Fernandez-Metzler C, Miller-Stein C, Olah T. Mechanistic investigation of ionization suppression in electrospray ionization. Journal of the American Society for Mass Spectrometry 2000; 11: 942-950.

Krajewski LC, Rodgers RP, Marshall AG. 126 264 Assigned Chemical Formulas from an Atmospheric Pressure Photoionization 9.4 T Fourier Transform Positive Ion Cyclotron Resonance Mass Spectrum. Analytical Chemistry 2017; 89: 11318-11324.

Li H, Han J, Pan J, Liu T, Parker CE, Borchers CH. Current trends in quantitative proteomics - an update. Journal of Mass Spectrometry 2017; 52: 319-341.

Lias SG, Bartmess J, Liebman JF, Holmes J, Levin RD, Mallard G. NIST chemistry webbook standard reference database number 69. National Institute of Standards Technology 2010.

Lozano DCP, Orrego-Ruiz JA, Barrow MP, Hernandez RC, Mejia-Ospino E. Analysis of the molecular weight distribution of vacuum residues and their molecular distillation fractions by laser desorption ionization mass spectrometry. Fuel 2016; 171: 247-252.

Lozano DCP, Orrego-Ruiz JA, Hernandez RC, Guerrero JE, Mejia-Ospino E. APPI(+)-FTICR mass spectrometry coupled to partial least squares with genetic algorithm variable selection for prediction of API gravity and CCR of crude oil and vacuum residues. Fuel 2017; 193: 39-44.

Martin JW. The Challenge: Safe release and reintegration of oil sands process-affected water. Environmental Toxicology and Chemistry 2015; 34: 2682-2682.

McKenna AM, Chacon-Patino ML, Weisbrod CR, Blakney GT, Rodgers RP. Molecular-Level Characterization of Asphaltenes Isolated from Distillation Cuts. Energy & Fuels 2019; 33: 2018-2029.

Nyakas A, Han J, Peru KM, Headley JV, Borchers CH. Comprehensive Analysis of Oil Sands Processed Water by Direct-Infusion Fourier-Transform Ion Cyclotron Resonance Mass Spectrometry with and without Offline UHPLC Sample Prefractionation. Environmental Science & Technology 2013; 47: 4471-4479.

Palacio Lozano DC, Gavard R, Arenas-Diaz JP, Thomas MJ, Stranz DD, Mejía-Ospino E, et al. Pushing the analytical limits: new insights into complex mixtures using mass spectra segments of constant ultrahigh resolving power. Chemical Science 2019; 10: 6966-6978.

Pereira TMC, Vanini G, Oliveira ECS, Cardoso FMR, Fleming FP, Neto AC, et al. An evaluation of the aromaticity of asphaltenes using atmospheric pressure photoionization Fourier transform ion cyclotron resonance mass spectrometry - APPI(+/-)FT-ICR MS. Fuel 2014; 118: 348-357.

Peru KM, Thomas MJ, Lozano DCP, McMartin DW, Headley JV, Barrow MP. Characterization of oil sands naphthenic acids by negative-ion electrospray ionization mass spectrometry: Influence of acidic versus basic transfer solvent. Chemosphere 2019; 222: 1017-1024.

Purcell JM, Hendrickson CL, Rodgers RP, Marshall AG. Atmospheric pressure photoionization Fourier transform ion cyclotron resonance mass spectrometry for complex mixture analysis. Analytical Chemistry 2006; 78: 5906-5912.

Purcell JM, Juyal P, Kim DG, Rodgers RP, Hendrickson CL, Marshall AG. Sulfur speciation in petroleum: Atmospheric pressure photoionization or chemical derivatization and electrospray ionization fourier transform ion cyclotron resonance mass spectrometry. Energy & Fuels 2007a; 21: 2869-2874.

Purcell JM, Rodgers RP, Hendrickson CL, Marshall AG. Speciation of nitrogen containing aromatics by atmospheric pressure photoionization or electrospray ionization Fourier transform ion cyclotron resonance mass spectrometry. Journal of the American Society for Mass Spectrometry 2007b; 18: 1265-1273.

Robb DB, Blades MW. Effects of solvent flow, dopant flow, and lamp current on dopant-assisted atmospheric pressure photoionization (DA-APPI) for LC-MS. Ionization via proton transfer. Journal of the American Society for Mass Spectrometry 2005; 16: 1275-1290.

Robb DB, Blades MW. Atmospheric pressure photoionization for ionization of both polar and nonpolar compounds in reversed-phase LC/MS. Analytical Chemistry 2006; 78: 8162-8164.

Robb DB, Covey TR, Bruins AP. Atmospheric pressure photoionisation: An ionization method for liquid chromatography-mass spectrometry. Analytical Chemistry 2000; 72: 3653-3659.

Romao W, Tose LV, Vaz BG, Sama SG, Lobinski R, Giusti P, et al. Petroleomics by Direct Analysis in Real Time-Mass Spectrometry. Journal of the American Society for Mass Spectrometry 2016; 27: 182-185.

Sama SG, Farenc M, Barrere-Mangote C, Lobinski R, Afonso C, Bouyssiere B, et al. Molecular Fingerprints and Speciation of Crude Oils and Heavy Fractions Revealed by Molecular and Elemental Mass Spectrometry: Keystone between Petroleomics, Metallopetroleomics, and Petrointeractomics. Energy & Fuels 2018; 32: 4593-4605.

Santos JM, Pudenzi MA, Wisniewski A, Breitkreitz MC, Eberlin MN. Optimization of Atmospheric Pressure Photoionization for the Crude Oil Analysis Using Ultra-High Resolution Mass Spectrometry. Journal of the Brazilian Chemical Society 2019; 30: 819-829.

Santos JM, Vetere A, Wisniewski A, Eberlin MN, Schrader W. Comparing Crude Oils with Different API Gravities on a Molecular Level Using Mass Spectrometric Analysis. Part 2: Resins and Asphaltenes. Energies 2018a; 11.

Santos JM, Wisniewski A, Eberlin MN, Schrader W. Comparing Crude Oils with Different API Gravities on a Molecular Level Using Mass Spectrometric Analysis. Part 1: Whole Crude Oil. Energies 2018b; 11.

Sato N, Sekimoto K, Takayama M. Ionization Capabilities of Hydronium Ions and High Electric Fields Produced by Atmospheric Pressure Corona Discharge. Mass spectrometry (Tokyo, Japan) 2016; 5: S0067-S0067.

Schmidt EM, Pudenzi MA, Santos JM, Angolini CFF, Pereira RCL, Rocha YS, et al. Petroleomics via Orbitrap mass spectrometry with resolving power above 1 000 000 at m/z 200. Rsc Advances 2018; 8: 6183-6191.

Short LC, Cai SS, Syage JA. APPI-MS: Effects of mobile phases and VUV lamps on the detection of PAH compounds. Journal of the American Society for Mass Spectrometry 2007; 18: 589-599.

Silwal IKC, Rasaiah JC, Szulejko JE, Solouki T. Proton transfer reactions of halogenated compounds: Using gas chromatography/Fourier transform ion cyclotron resonance mass spectrometry (GC/FT-ICR MS) and ab initio calculations. International Journal of Mass Spectrometry 2010; 293: 1-11.

Snyder LR. Classification of the solvent properties of common liquids. Journal of Chromatography A 1974; 92: 223-230.

Syage JA. Mechanism of M+H (+) formation in photoionization mass spectrometry. Journal of the American Society for Mass Spectrometry 2004; 15: 1521-1533.

Thomas MJ, Collinge E, Witt M, Lozano DCP, Vane CH, Moss-Hayes V, et al. Petroleomic depth profiling of Staten Island salt marsh soil: 2 omega detection FTICR MS offers a new solution for the analysis of environmental contaminants. Science of the Total Environment 2019; 662: 852-862.

Yi Y, Han J, Birks SJ, Borchers CH, Gibson JJ. Profiling of dissolved organic compounds in the oil sands region using complimentary liquid-liquid extraction and ultrahigh resolution Fourier transform mass spectrometry. Environmental Earth Sciences 2017; 76.

Zhang YH, Zhang LZ, Xu ZM, Zhang N, Chung KH, Zhao SQ, et al. Molecular Characterization of Vacuum Resid and Its Fractions by Fourier Transform Ion Cyclotron Resonance Mass Spectrometry with Various Ionization Techniques. Energy & Fuels 2014; 28: 7448-7456.

6. pH Effect on Observed Profiles of Oil Sands Process-Affected Waters

6.1 Introduction

The Athabasca oil sands deposits, located in the province of Alberta, Canada, are estimated to contain 1.7–2.5 trillion barrels of oil (Burrowes et al., 2009; Clemente et al., 2003). These non-conventional oil reserves require approximately 2–4 barrels of water to produce 1 barrel of crude oil (Barrow et al., 2016), generating a large volume of oil sands process-affected water (OSPW), which is expected to reach 10^9 m^3 by 2025. (Johnson et al., 2011). OSPW must be stored in tailing ponds as per the zero discharge policy that the industry is required to follow (Government of Canada, 2012; Martin, 2015). Storage of OSPW in close proximity to natural water sources (rivers, ponds, marshes) is of concern due to the possibility of tailings pond leakage and possible seepage into groundwater. Analysis of groundwaters and adjacent natural waters is required in order to monitor for possible leakage, seepage or accidental discharge, as it has been reported that OSPW is toxic to aquatic organisms (Allen, 2008; Marentette et al., 2015; Swigert et al., 2015). The caustic hot water extraction process used to extract the bitumen from the oil sands is known to concentrate the acidic species, namely naphthenic acids (NAs), and related components which are collectively known as naphthenic acid fraction compounds (NAFCs) (Allen, 2008; Headley and McMartin, 2004; Shell Canada Ltd., 2016). NAFC samples are complex mixtures that contain traditionally defined NAs, comprising compounds with a single carboxylic acid group, which follow the generic formula of $C_nH_{2n+Z}O_2$ where Z is the negative, even integer that represents the "hydrogen deficiency" and n is the number of carbon atoms. Alternatively, it is possible to use double bond equivalents (DBE) as a measure of the number of rings and double bonds involving carbon atoms within the molecule. It is now known that the organic contributions to OSPW comprise a wide distribution of other components, including aromatic structures instead of alicyclic, higher oxygen contents (O_x) where molecules may contain hydroxyl or multiple carboxylic acid groups, and nitrogen- and/or sulfur-containing components (Barrow et al., 2015; Barrow et al., 2009; Grewer et al., 2010; Headley et al., 2011a; Headley et al., 2009).

Over the past decade considerable attention has been given to the development of ultrahigh resolution mass spectrometry to both characterize and quantify NAFC in oil sands related samples (Barrow et al., 2016; Barrow et al., 2004; Bowman et al., 2014; Brunswick et al., 2015; Chen et al., 2015; Headley et al., 2016;

Headley et al., 2015; Headley et al., 2014; Headley et al., 2013; Headley et al., 2011b; Huang et al., 2016; Jie et al., 2015; Nyakas et al., 2013; Pereira and Martin, 2015; Pereira et al., 2013; Wilde et al., 2015). Due to the complexity of NAFC mixtures, the results are dependent upon numerous variables associated with the analytical procedure. Chapters 2 and 4 demonstrated that electrospray ionization (ESI) is the most appropriate choice for selective characterisation polar organic compounds, compounds of concern present in OSPW. The findings of Chapter 5, however, showed that the experimental parameters, including solvent system, have a significant effect on the atmospheric pressure photoionization (APPI) response. An awareness of ion suppression, matrix effects, and the need to use additives to create a reasonably stable ionization state (e.g. adding pH modifiers) or using derivatization to enhance ESI response of certain species should be evaluated as these factors can all play a role in the response factor and relative response factors of species as a consequence of the ESI mechanism. To minimize such phenomena in routine environmental research, chromatography or the use of appropriate clean-up methods, such as solid phase extraction, may be used to reduce ion suppression and matrix effects. Other variables such as the extraction pH and solvent used to prepare samples, along with the organic mobile phase chosen, can lead to significant variation in the levels and profiles of NAFCs detected (Barrow et al., 2016; Headley et al., 2013; Headley et al., 2007; Huang et al., 2015). Furthermore, the experimental parameters of the instrumentation, such as choice of ionization method (e.g. ESI, atmospheric pressure chemical ionization (APCI), APPI, electron ionization (EI)) and ionization polarity (+/-) have been shown to have a profound effect on what is detected (Barrow et al., 2015; Barrow et al., 2014; Barrow et al., 2010). The effect of varying these parameters on the results obtained is summarised in Table 6.1. The majority of the numerous analytical protocols associated with OSPW reported utilize negative-ion (-) ESI coupled to mid to ultrahigh resolution mass spectrometers. Sample introductions by flow injection without chromatography and with full chromatographic separations are currently used, both with success (Headley et al., 2016; Headley et al., 2013). The latter bears the advantage of decreased ionization suppression without prior sample cleanup (i.e. solid phase extraction) but also the disadvantage of extended analytical run times. Flow injection analyses typically use a transfer solvent containing 0.1% ammonium hydroxide (NH_4OH) as a pH modifier to aid in the ionization process while chromatographic methods use 0.1% formic acid (HCOOH) to adjust the transfer solvent (mobile phase) to a pH value below the pKa of NAs (~ 4.5) to allow analyte interaction with the liquid chromatography (LC) column phase in order to achieve sufficient separation.

Table 6.1 Summary of experimental parameters varied and effect on OSPW profiles and NAFCs detected as reported in literature

Publication	**Parameter**	**Effect on Profile Obtained**
Barrow et al., 2016	Extraction pH	Higher x O_x class components detected preferentially following acidic extraction compared to basic extraction.
Huang et al., 2016	Extraction solvent system and pH	Basic extraction efficiency of NAs is lower; ethyl acetate preferentially extracts more polar species. Acidic extraction in alkanes and ethyl ether causes a shift to higher carbon number.
Headley et al., 2013	Extraction solvent	Extraction in hexane selective towards O_2-containing species, ethyl acetate more selective towards O_4-containing species.
Headley et al., 2007	Transfer solvent	1-octanol/acetonitrile solvent system accessed a wider range of NAFCs and shifted OSPW distribution to higher *m*/*z*, with O_2-containing species at greater relative intensity.

A variable that has been overlooked with respect to its effects on NAFC analysis is the transfer solvent pH. This study reports the effects of the apparent pH of the transfer solvent upon the response of different organic species (namely the O_x compound classes) present within an Athabasca oil sands derived OSPW extract. Measurement of pH in solvents and aqueous solvent systems is difficult with respect to achieving accurate pH measurements, hence the accepted term for solvent system pH measurements is "apparent pH" and is used throughout this work. To demonstrate that the effects are not instrument-specific, (-) ESI experiments were performed using two different mass spectrometers: a Fourier transform ion cyclotron resonance mass spectrometer (FTICR MS) located at the University of Warwick, UK, and an Orbitrap mass spectrometer, located at the National Hydrology Research Centre, Saskatoon, Canada. Furthermore, two commonly used methods of sample introduction were utilized, namely direct infusion with a syringe pump for FTICR MS and injection into the eluent of a

liquid chromatograph for Orbitrap MS experiments. The results indicate that the transfer solvent apparent pH plays an important role, influencing the relative responses of the compound classes detected and trends observed are independent of the instrument used. Furthermore, transfer solvent apparent pH has a critical impact upon data sets that were acquired using different analytical protocols and used for comparative environmental and monitoring studies along with toxicological investigations (Hughes et al., 2017; Morandi et al., 2015).

6.2 Materials and Methods

6.2.1 OSPW Extract

A large volume extract of Athabasca oil sands-derived OSPW was obtained following the procedures previously described (Janfada et al., 2006; Rogers et al., 2002). Briefly, OSPW (2000 L) and acidified to pH 2 with HCl (Fisher Scientific Company, Ottawa, Ontario, Canada) and serially extracted (3 times) in 2 L batches with dichloromethane (DCM) (Fisher Scientific Company, Ottawa, Ontario, Canada). The combined DCM fractions was evaporated to dryness and the residue was reconstituted in 0.1 M NaOH (VWR International, Edmonton, Alberta, Canada) followed by ultra-filtration using a Millpore®1000 MW cutoff membrane (Sigma-Aldrich Canada Co., Oakville, Ontario, Canada).

6.2.2 Orbitrap MS

Sample characterization was performed using two instruments, the first of which was an LTQ Orbitrap Elite (Thermo Fisher Scientific, San Jose, CA) operating in full scan and negative-ion (-) mode. Mass resolution was set to 240,000 (at *m*/*z* 200) with an *m*/*z* scan range of 100-600; the measured resolving power at *m*/*z* 200 was 268,000. The ESI source was operated as follows: sheath gas flow rate 25 (arbitrary units), spray voltage 2.90 kV, auxiliary gas flow rate 5 (arbitrary units), S lens RF level 67%, heater temperature 50 ^{o}C, and capillary temperature 275 ^{o}C. As per Composer data analysis, the mass error was < 2 ppm for all mass assignments. For the high pH experiment, the transfer solvent used was 50:50 acetonitrile:water containing 0.1% NH_4OH, while the low pH transfer solvent experiment used 50:50 acetonitrile:water containing 0.1% HCOOH. A flow rate of 200 μL min^{-1} was used for both eluent pH conditions (apparent pH 9.1 and 3.2) delivered by an Accela 1250 solvent pump (Thermo Fisher Scientific, San Jose, CA). All apparent pH measurements of the eluent solutions were completed using an Accumet AB15 pH meter (Fisher Scientific Company, Ottawa, Ontario, Canada) calibrated using a three point pH calibration method. Under gentle

magnetic stirring, sufficient time (~ 3 min) was permitted for a stable pH reading to be established. The OSPW extract was diluted 100-fold in non-pH adjusted 50:50 acetonitrile:water. 5 μL of the diluted extract was injected into the transfer solvent stream using a Thermo PAL-HTC Accela autosampler (Thermo Fisher Scientific, San Jose, CA). The software used for instrument control/data acquisition and molecular analysis was Xcalibur version 2.1 (Thermo Fisher Scientific, San Jose, CA) and Composer version 1.5.2 (Sierra Analytics, Inc., Modesto, CA) respectively.

6.2.3 FTICR MS

The OSPW extract was diluted 900-fold in 50:50 acetonitrile:water. Individual aliquots of this stock solution were used and NH_4OH or HCOOH (Sigma-Aldrich Company Ltd., Gillingham, Dorset, United Kingdom) were added at concentrations ranging from 0.025% - 1% to produce solutions over a range of apparent pH values. The apparent pH of each solution was recorded using a Hanna pH 20 meter (Hanna Instruments Ltd., Leighton Buzzard, Bedfordshire, United Kingdom), calibrated with external standards (Thermo Scientific Orion, Thermo Fisher Scientific, Hemel Hempstead, Hertfordshire, United Kingdom). The apparent pHs are reported in Table 6.2.

Table 6.2. Apparent pHs of the nine sample solutions analyzed by infusion (-) ESI-FTICR MS and two transfer solvents by flow injection (-) ESI Orbitrap MS.[a]

Additive	**FTICR MS**					**Orbitrap**
NH_4OH / %	1	0.15	0.10	0.05	0	0.1
Apparent pH	11.2	9.9	9.4	9.3	8.1	9.1
HCOOH / %	0.025	0.05	0.10	0.15		0.1
Apparent pH	3.6	3.3	3.2	3.1		3.2

[a]High purity NH_4OH and HCOOH were added to the samples. The sample with 0% corresponds to the original stock solution without the use of any additives.

Additionally, three organic compounds of varying oxygen content, each containing at least one carboxylic acid group (Figure 6.1), were studied using FTICR MS. Biphenyl-4-carboxylic acid, anthraquinone-2-carboxylic, and trimesic acid (Sigma-Aldrich Company Ltd., Gillingham, Dorset, United Kingdom) represented the O_2, O_4, and O_6 compound classes, respectively, and were dissolved as 0.02 mg mL^{-1} in 50:50 MeCN:H_2O, with the addition of either 0.1% NH_4OH or 0.1% HCOOH.

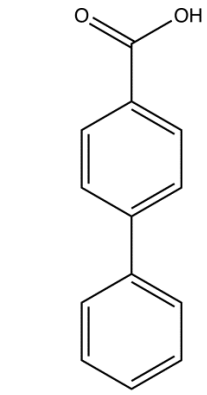

Biphenyl-4-carboxylic acid

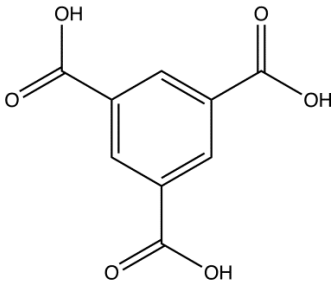

Trimesic acid

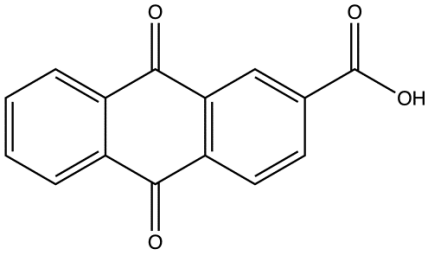

Anthraquinone-2-carboxylic acid

Figure 6.1 Structures of the three compounds used to study signal intensity as a function of the additives used

Mass spectra were acquired using a 12 T solariX Fourier transform ion cyclotron resonance (FTICR) mass spectrometer (Bruker Daltonik GmbH, Bremen, Germany), coupled with an Apollo II ESI source. The instrument was operated in negative-ion (-) mode. Nitrogen was used as the drying gas at a temperature of 220 °C at a flow rate of 4 L min^{-1}. The nebulizing gas was nitrogen and was maintained at a pressure of 1.2 bar. Samples were infused using a syringe pump at a rate of 200 μL h^{-1} without the activation of in-source dissociation. 4 MW data sets were acquired using magnitude mode, with a detection range of *m*/*z* 128-1500. After acquiring 200 scans, the data were zero-filled once and apodized using a Sine-Bell function prior to applying a fast Fourier transform. For the apodized data, the measured resolving power at *m*/*z* 200 was 830,000. Data were internally calibrated using homologous series and analyzed using DataAnalysis 4.2 (Bruker Daltonik GmbH, Bremen, Germany), prior to the data being imported into Composer 1.5.4 (Sierra Analytics, Modesto, CA, USA) for compositional analysis, with assignment parameters presented in Table 6.3; Aabel NG2 v.5.2 (Gigawiz Ltd. Co., Tulsa, Oklahoma, USA) was used for data visualization.

Table 6.3. Composer 1.5.4 parameters for the assignment of molecular formulae

Parameter	**Constraints**
Polarity	Negative
Ion properties	Adducts = H; remove isolated assignments
m/*z* range	*m*/*z* 200-650
DBE range	-0.5 - 40
Element ranges	C = 0-200; H = 0-1000 ; N= 0-2; O = 0-6; S = 0-4

Tuning parameters can play an important role, biasing the detection of either high or low mass analytes. In order to eliminate/reduce effects of the tuning variables and allow only changes caused by adjustments to transfer solvent pH to be studied, initial tuning of the two instruments was not changed during the course of these experiments.

6.3 Results and Discussion

6.3.1 Mass Spectra and Class Distribution

When analysed using the same instrument parameters but different transfer solvent apparent pH values, the OSPW mass spectra obtained showed differences in both intensity and mass distribution. This trend was observed in the data obtained from both Orbitrap and FTICR mass spectrometers. For example, Figure 6.2 illustrates mass spectra obtained using (-) ESI-Orbitrap and FTICR MS under basic and acidic transfer solvent conditions. For the Orbitrap data using acidic transfer solvent, the *m*/*z* distribution was centered in the range of *m*/*z* 240-285, compared to *m*/*z* 195-240 using basic transfer solvent. Similarly, a significant shift to higher *m*/*z* species is observed in the FTICR MS spectra when using acidified conditions. These trends and acquired mass spectra were reproducible for both the Orbitrap and the FTICR throughout the study (rsd = 0.7% and 1.4% respectively) and at a minimum, included duplicate analysis.

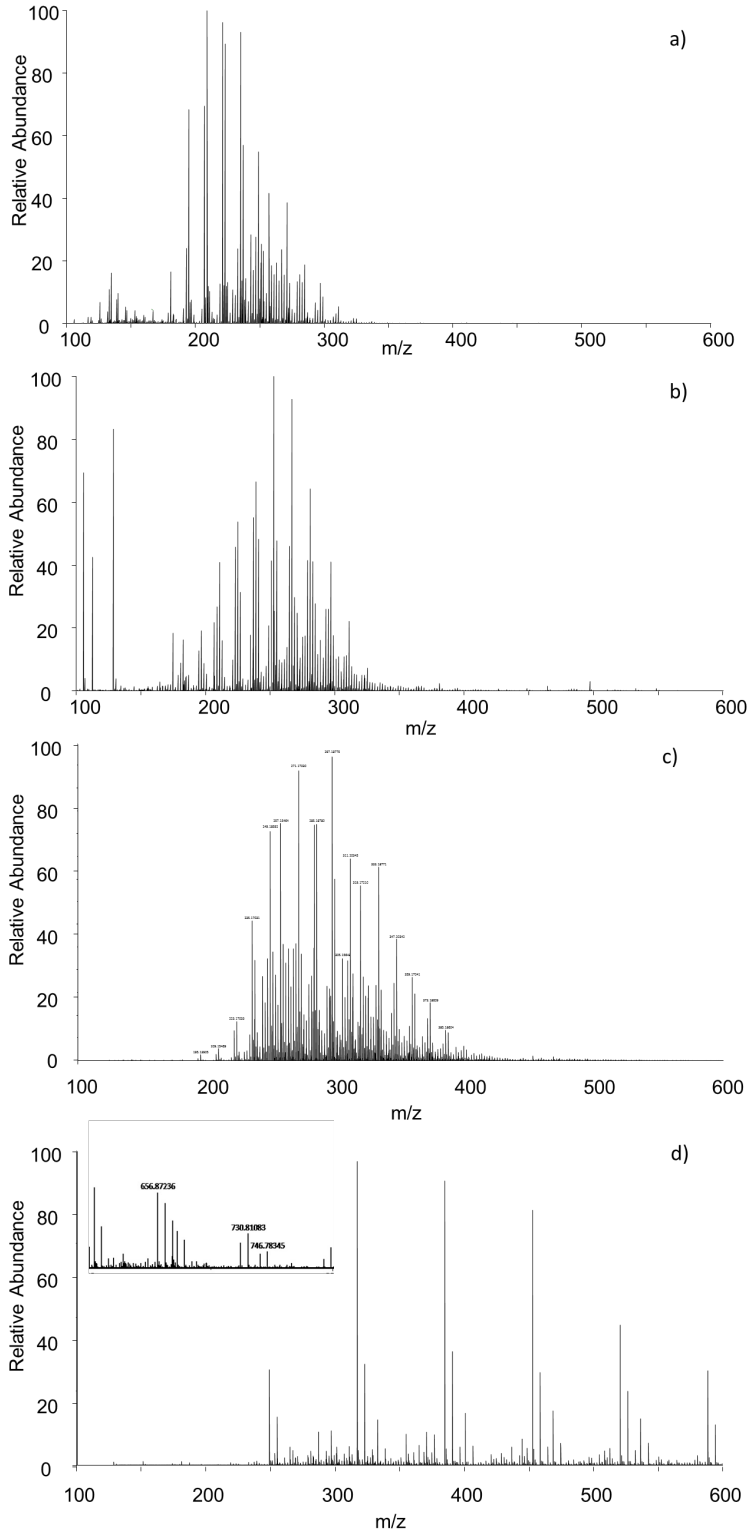

Figure 6.2 Differences in the mass spectra observed under the different conditions: (-) ESI-Orbitrap MS for a) basic eluent (0.1% NH_4OH, pH 9.1) and b) acidic eluent (0.1% HCOOH, pH 3.2), and (-) ESI-FTICR MS for c) basic solvent (0.1% NH_4OH, pH 9.4) and d) acidic solvent (0.1% HCOOH, pH 3.2) with an inset showing *m/z* range 600 - 800

Data processing provided insight into the compositional differences observed in the mass spectra. For example, class distribution plots (Figure 6.3) show that basic transfer solvent conditions favour the lower oxygen-containing species, such as the O_2 class, while acidic transfer solvent conditions favour the higher-containing O_x classes, with the O_4 class being predominant.

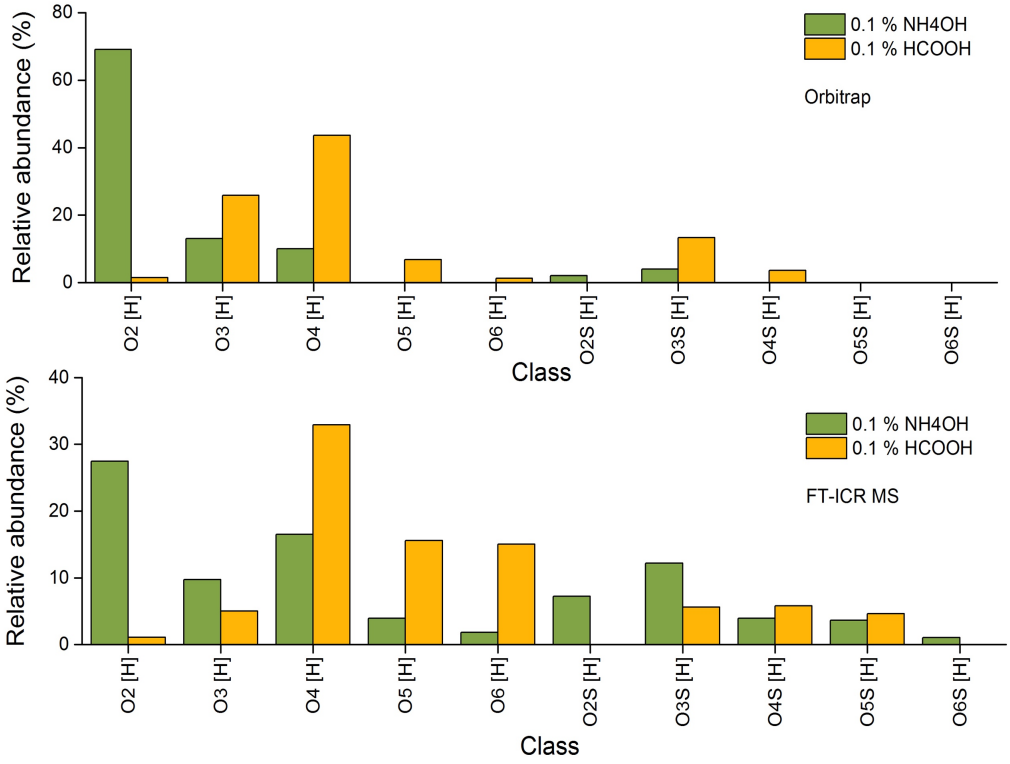

Figure 6.3 Top: class distribution obtained by (-) ESI-Orbitrap MS using basic (0.1% NH_4OH, pH 9.1) and acidic (0.1% HCOOH, pH 3.2) transfer solvents Bottom: class distribution obtained by (-) ESI-FTICR MS using basic (0.1% NH_4OH, pH 9.4) and acidic (0.1% HCOOH, pH 3.2) conditions

As shown in Figures 6.2 and 6.3, similar trends for (-) ESI-MS results were observed by two independent laboratories, each using a different mass spectrometer and different sample introduction method. Due to differences in instrument tuning (influencing operational *m*/*z* ranges) and in resolving power, the number and relative contributions for compound classes observed using the two instruments are not identical. Despite this, both laboratories observed the same trends with respect to the effects of apparent pH of the transfer solvent upon sample profiles. In particular, very similar results were obtained when examining the relative contributions of the O_2 and O_4 classes, in turn affecting the O_2/O_4 ratio that has been proposed as having potential for environmental forensics. Frank et al. reported use of O_2/O_4 ratios as a diagnostic tool during

forensic studies for sample source determination (Frank et al., 2014). It was found that use of a basic transfer solvent favoured the detection of the O_2 species within the NAFC mixture, while an acidic transfer solvent tended to favour increased relative response of the higher oxygen containing species, such as O_3 to O_6 (Figure 6.3). For oil sands-related samples, (-) ESI experiments are traditionally used to study compounds expected to incorporate one or more carboxylic acid groups. The carboxylic acid site must deprotonate for the molecule to form a negatively-charged ion and the addition of acid, lowering the apparent pH, increases the probability of any given carboxylic acid site retaining its proton. At least one, overall negative charge is required, however, for the species to be observed using (-) ESI. Additional carboxylic acid groups increase the probability of deprotonation, while other oxygen-containing functional groups potentially help to stabilize the presence of negative charge (Hindle et al., 2013). As one example regarding the number of carboxylic acid groups, the first acid dissociation constant (pKa1) of propanoic acid is 4.87, while its dicarboxylic counterpart, propanedioic acid, has a pKa1 of 2.83. As a result, it would be expected that lower apparent pHs will suppress overall detection of oil sands components especially those of lower oxygen contents when using (-) ESI experiments. Figure 6.4 represents one of the central findings, where an O_2/O_4 ratio of 1.67 to 6.89 was observed using basic conditions, a ratio of only 0.03 was observed when using acidic conditions. It is therefore clear that the pH of the solution significantly influences the O_2/O_4 ratio and has consequences for environmental forensics. For example, point source determination based on naphthenic acid composition would lead to inaccurate conclusions if the same eluent pH was not used by the same or multiple laboratories for the mass spectrometric analysis. This forensic tool may still be valid if results are compared using the same instrumental conditions and transfer solvent pH, but the validity would no longer hold if data from different laboratories, using different transfer solvent pH, were compared. It is therefore essential that this is taken into account when comparing data between laboratories. In addition, recent toxicity techniques (Hughes et al., 2017; Morandi et al., 2015) rely heavily upon mass spectrometric data, both quantitatively and qualitatively, for the identification of principal toxic components that attribute to end-point responses being measured. Depending upon the apparent pH (basic/acidic) of the eluent being used, the interpretation of the mass spectrometric data would have a significant impact upon the assignment of which components are contributing towards the toxicity of the sample. Quantification of NAs entails the detailed analysis of a complex mixture; biasing the response of low O_x or high O_x components (due to the influence of the

eluent apparent pH) would impact the final quantitative result for identical samples. This, in turn, may lead to incorrect or inconsistent conclusions with respect to toxicity assignment, with adverse consequences for remediation strategies.

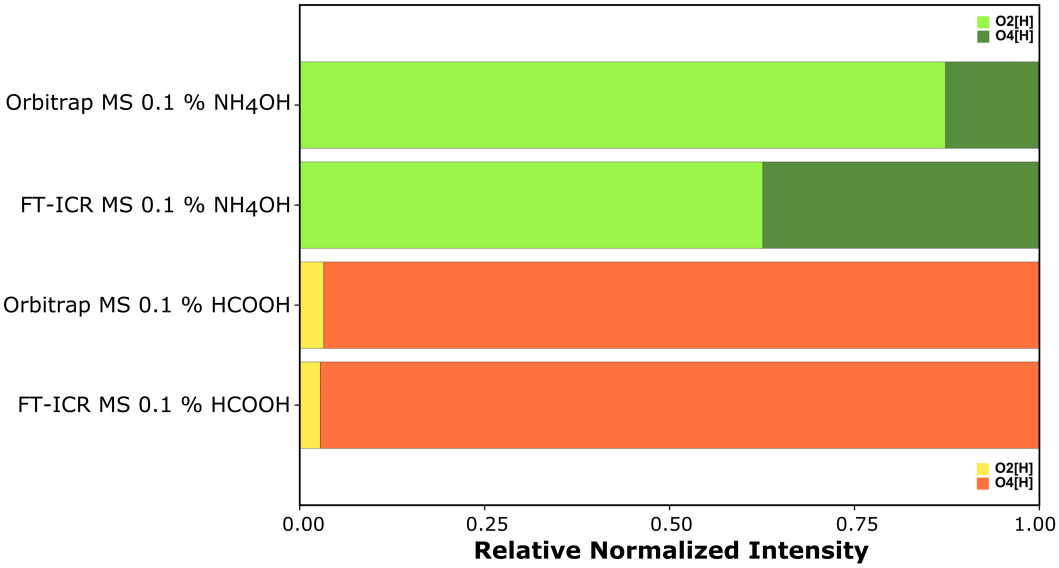

Figure 6.4 Normalized bar chart showing the change in O_2/O_4 ratio with transfer solvent additive

FTICR MS experiments were completed using nine sample solutions, with HCOOH or NH_4OH added to the diluted OSPW extract in quantities ranging from 0.025% to 1%. The O_2/O_4 ratio was relatively consistent when NH_4OH was added and when no additive was used (Figure 6.5), but inverted, with the O_4 class being more prominent, once HCOOH was added. The results demonstrate both the consistency of the observations and the significant change in ratio when changing sample preparation from use of no additives to using just 0.025% HCOOH (apparent pH of 3.6).

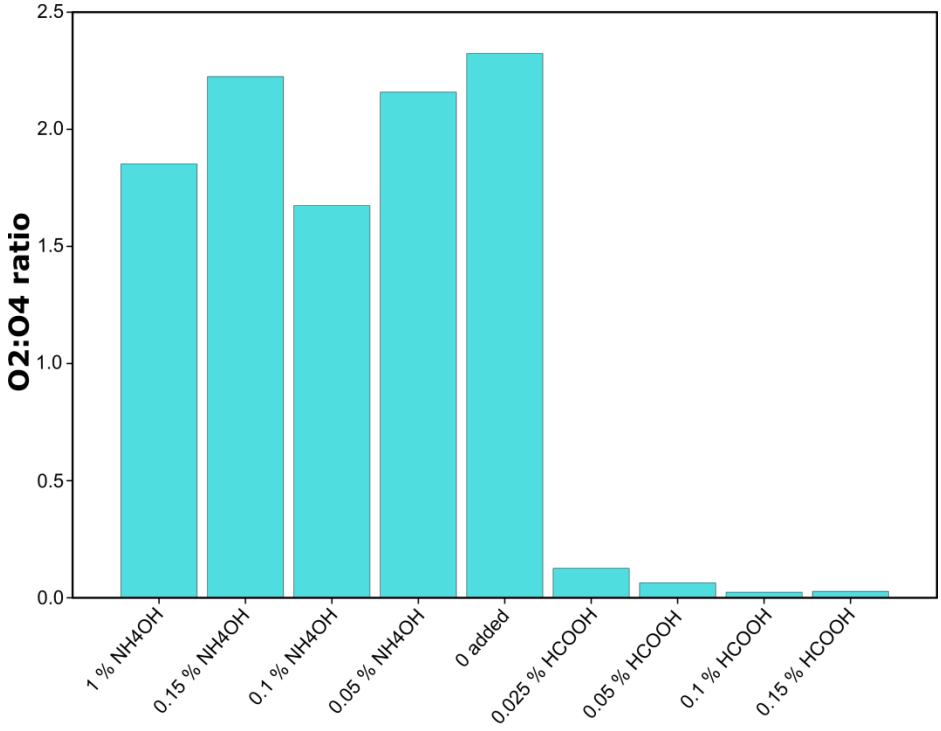

Figure 6.5 Bar chart showing O_2/O_4 ratio for FTICR MS data, as a function of base or acid added to OSPW

As an illustrative example of how oxygen content and structure play important roles in influencing the observed signal, commercially available compounds were examined (Figure 6.1 and Table 6.4), in addition to the characterization of the OSPW, which represents a complex mixture of potentially unknown components.

Table 6.4 O_2, O_4, and O_6 compounds run using FTICR MS to monitor signal response as a function of additives used

Compound	Additive	Intensity / a.u.	Apparent pH
Biphenyl-4-carboxylic acid ($C_{13}H_{10}O_2$)	0.1 % NH_4OH	5.34E+10	8.91
	0.1 % HCOOH	4.79E+08	3.52
Anthraquinone-2-carboxylic acid ($C_{15}H_8O_4$)	0.1 % NH_4OH	5.46E+10	9.19
	0.1 % HCOOH	3.31E+09	3.68
Trimesic acid ($C_9H_6O_6$)	0.1 % NH_4OH	2.81E+10	8.75
	0.1 % HCOOH	1.86E+10	3.59

The three compounds shown in Figure 6.1 (absolute intensities recorded in Table 6.4) are species representative of the O_2, O_4, and O_6 compound classes, where one molecule included a single carboxylic acid group, the second molecule included

one carboxylic acid group and two carbonyl groups, and the third molecule incorporated three carboxylic acid groups. The use of these compounds is illustrative but does not represent a comprehensive investigation of the effects of functional groups and other structural features, which is not within the scope of the current study. Oxygen may be incorporated as hydroxyl, aldehyde, ketone, ether, ester, or carboxylic acid groups, for example, and such structures will differ in ionization response (Hindle et al., 2013). Furthermore, for functionalized aromatic compounds, resonance stabilization and position of substitution (ortho, meta, and para) will also play important roles in determining stability of the anions relative to the neutral molecules. Finally, solubility of different structures (Headley et al., 2007) will also influence the probability of observation during characterization using mass spectrometry. The signals of the singly-charged O_2, O_4, and O_6 species were measured after addition of 0.1% HCOOH or 0.1% NH_4OH to the solutions. Figures 6.6, 6.7, and 6.8 show that the compounds of higher oxygen content have a proportionally higher response, compared to species of lower oxygen content, following addition of acid (lower apparent pH). The O_2:O_4 and O_2:O_4:O_6 ratios therefore inverted when switching from the addition of base to the addition of acid and were at their lowest when using acidic conditions. These results are consistent with the observations for the OSPW sample.

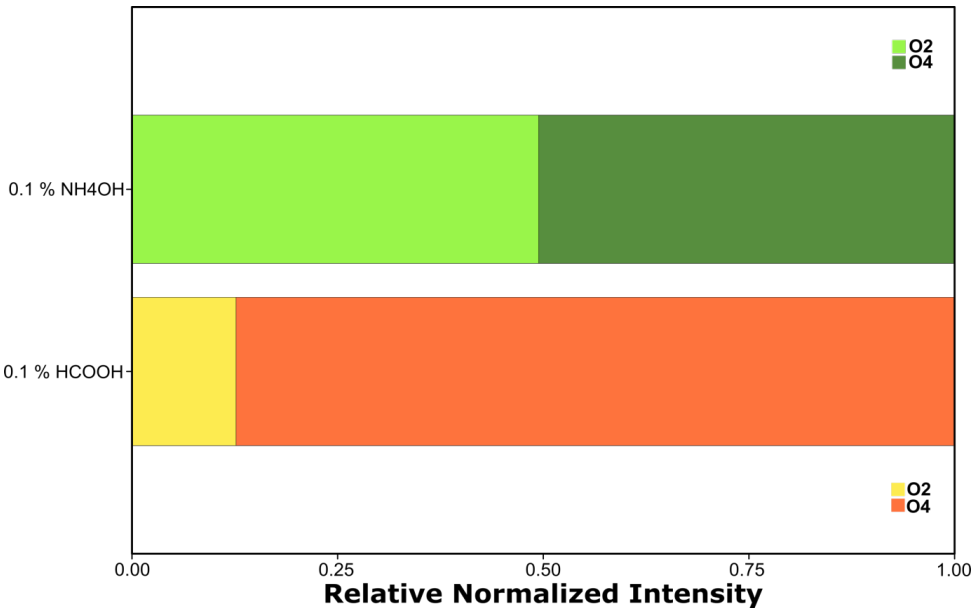

Figure 6.6 Normalized bar chart showing signal ratios acquired by FTICR MS of only the individual O_2 and O_4 compounds, for comparison with the results using the OSPW sample

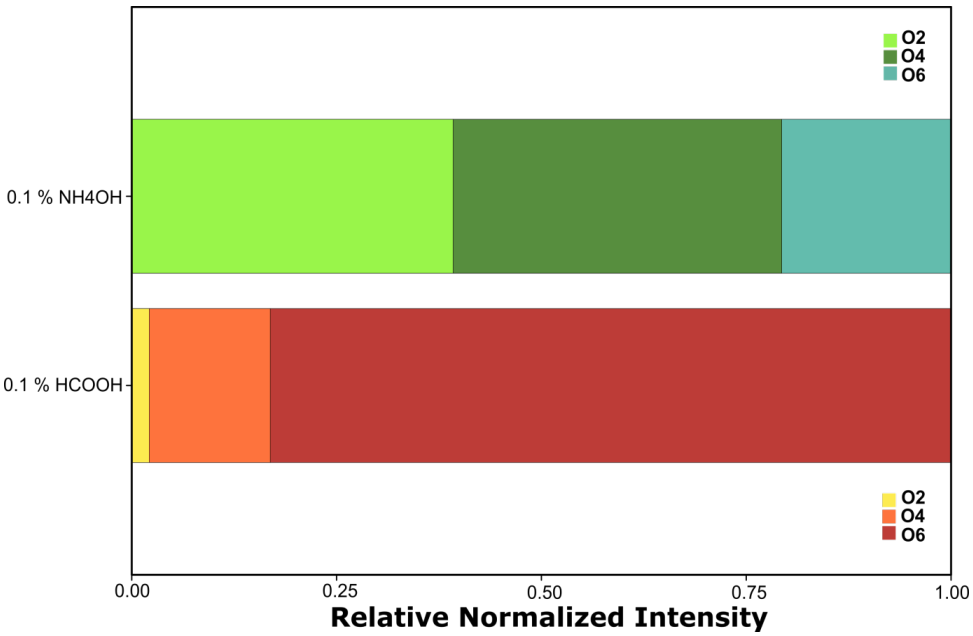

Figure 6.7 Normalized bar chart showing signal ratios acquired by FTICR MS of individual O_2, O_4, and O_6 compounds

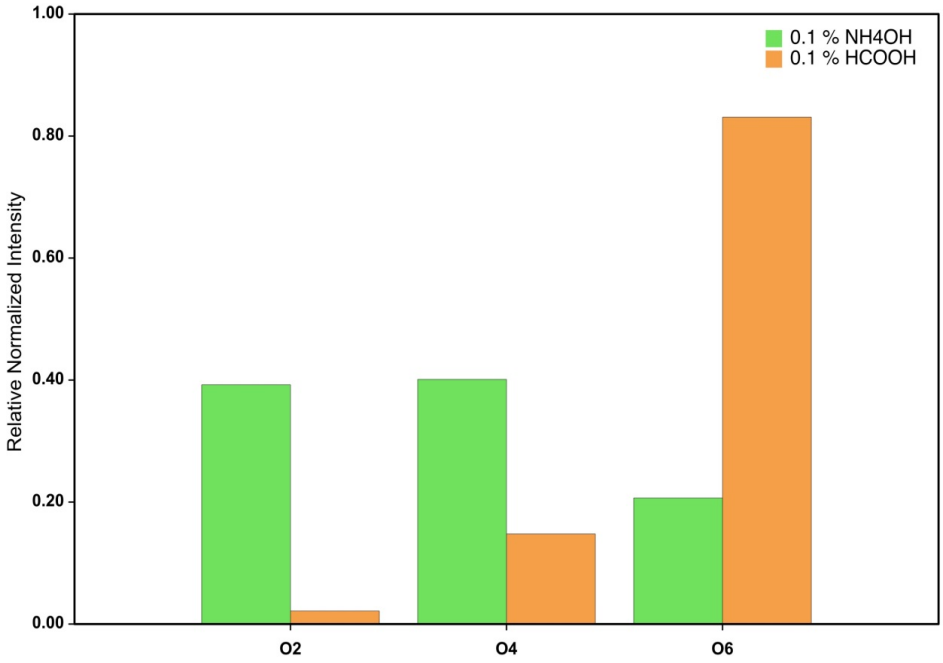

Figure 6.8 Relative normalized signals acquired by FTICR MS of the individual O_2, O_4, and O_6 compounds; alternative representation of data shown in Figure 6.7

O_2-containing species have been reported as the primary components of concern within the NAFC fraction with regards to toxicity towards aquatic ecosystems (Hughes et al., 2017; Morandi et al., 2015; Yue et al., 2015). Monitoring water systems in and around mining activities for NAFC is required to regulate and ensure leakage or accidental spillage of OSPW is not occurring. Development of

analytical methods for monitoring is still ongoing but methods have been recently published that show improved sensitivity and robustness. For example, Brunswick et al. report the use of LC coupled time-of-flight (TOF) MS (LC-TOF-MS) for routine analysis of water samples (Brunswick et al., 2015). This method sums the areas of peaks that match the O_x components detected and reports the total NA concentration from this summation. The method uses an acidic eluent for the LC separation which may, according to the findings of this study, enhance the detection of high O_x species but attenuate the detection of O_2 species. Since it is almost impossible and impractical to calculate the response factor of each component contained with the O_x families, due to a lack of standards for all compositions and isomers, caution is warranted for comparison of results with other methodologies that employ different pH eluent conditions.

6.3.2 DBE of O_2 Class Compounds

As the O_2 class is implicated as the most toxic class of components in OSPW, further data analysis was completed to reveal the effects of transfer solvent apparent pH with respect to O_2 DBE and carbon number distributions. Figure 6.9 illustrates the significant effect of transfer solvent apparent pH on the DBE distributions of the O_2 class of compounds from OSPW extract; an alternative arrangement of the same data is shown in Figure 6.10. At pH 3.2, there are differences between the Orbitrap and FTICR MS data sets at first glance, but closer inspection reveals the contributions for entire homologous series are below 1%. As a result, low intensity summed contributions (e.g. ~ 0.1% - ~ 0.8%) for a given DBE are being compared and caution is warranted when attempting to draw conclusions. Under basic conditions, the percentage contributions become much greater and comparisons of the data become more robust. The percentage contributions for the FTICR MS data are lower due to detection of a greater number of classes than for the Orbitrap MS data, thus each class must represent a smaller fraction. The predominant DBE ranges differed between the Orbitrap MS and FTICR MS data, where higher DBE components were more pronounced in the FTICR MS data. As with O_2/O_4 ratios, DBE plots can be used as forensic tool for NAFC source identification. For comparative studies, it is thus imperative to compare data from similar instruments and to keep the transfer solvent apparent pH consistent.

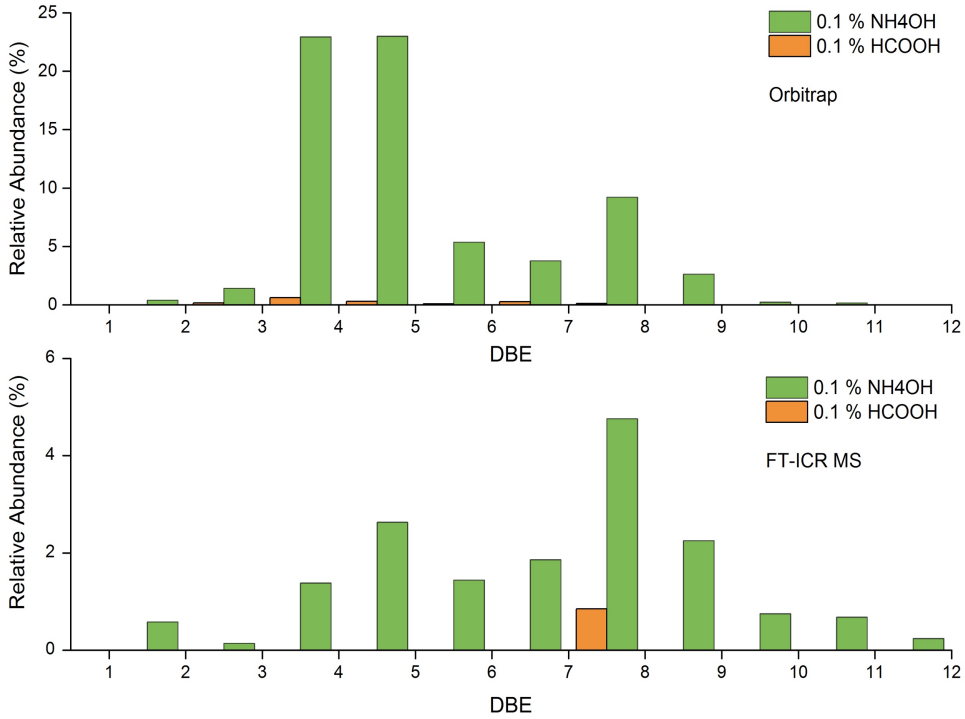

Figure 6.9 O_2 class DBE plots obtained from (-) ESI-Orbitrap (top) and FTICR MS (bottom) data, using acidic and basic conditions

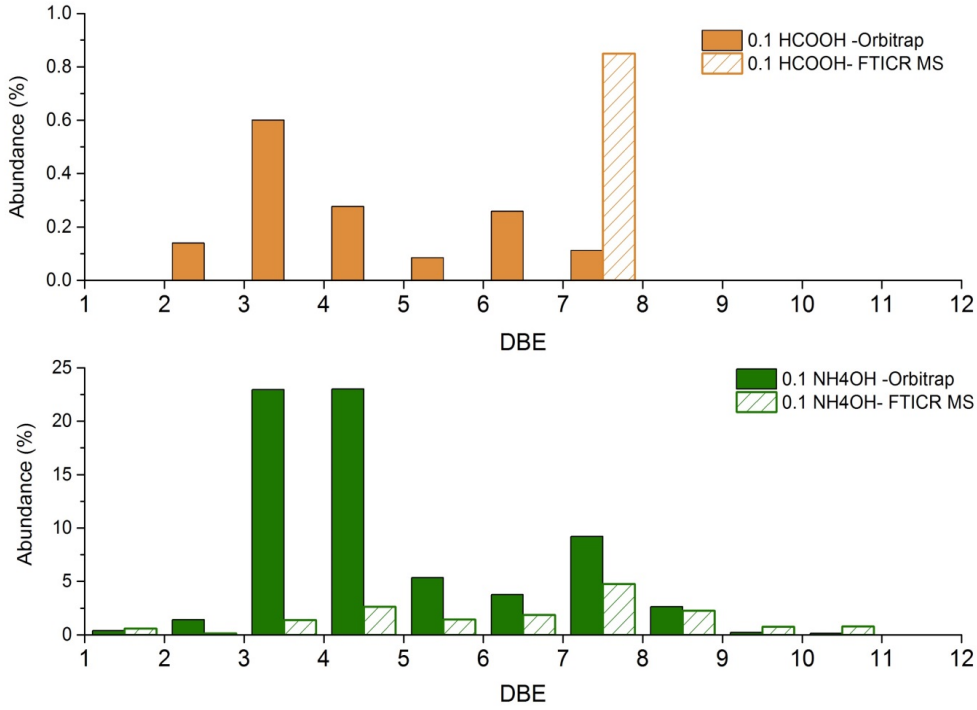

Figure 6.10 O_2 DBE distributions obtained from (-) ESI-Orbitrap and FTICR MS data using acid pH mobile phase (top) and basic pH mobile phase (bottom) with OSPW extract

For further insight, the FTICR MS data in this study was examined in terms of double bond equivalents (DBE) and carbon number for the O_2 class, as a function of pH (Figure 6.11). A steady decrease in the intensity and number of peaks associated with the O_2 class was observed with increasing HCOOH concentration (decreasing pH). Under acidic transfer solvent pH conditions, carbon numbers 15 and higher with DBE 3.5 and 4.5 have decreased or disappeared altogether, once below the detection threshold, as previously highlighted in Figures 6.9 and 6.10. In addition, overall intensities are approximately 400 times lower for the O_2 class when using acidic transfer solvent containing 0.1% HCOOH. Similar trends were observed for the overall NAFC response with the acidic transfer solvent displaying a response of 20 times less than that of the basic pH transfer solvent.

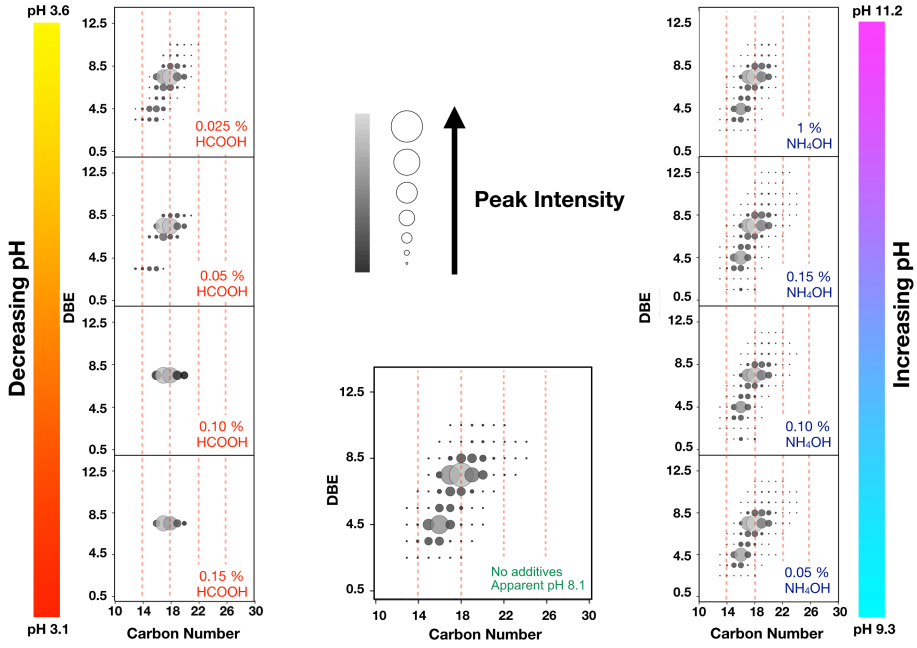

Figure 6.11 DBE vs. carbon number plots using FTICR MS data, showing the decrease in intensity and reduction of number of peaks associated with the O_2 compound class

6.3.3 Van Krevelen plots for O_x Classes

While DBE vs. carbon number plots are useful for examining a single compound class at a time, van Krevelen plots can be used to compare contributions from multiple O_x classes at once. Combined van Krevelen plots of H/C against O/C ratios for the O_x classes (Figure 6.12) show that samples analyzed under basic conditions exhibit a larger number of data points at low O/C coordinate values.

The higher data point density (number of data points within the same H/C vs. O/C space) in the low O/C and low H/C coordinates observed under basic conditions, as compared to data acquired using acidic conditions or using the Orbitrap, can be attributed to the minimum relative abundance filter setting used during data processing; the total number of compositional assignments, however, is indeed higher for the FTICR MS data.

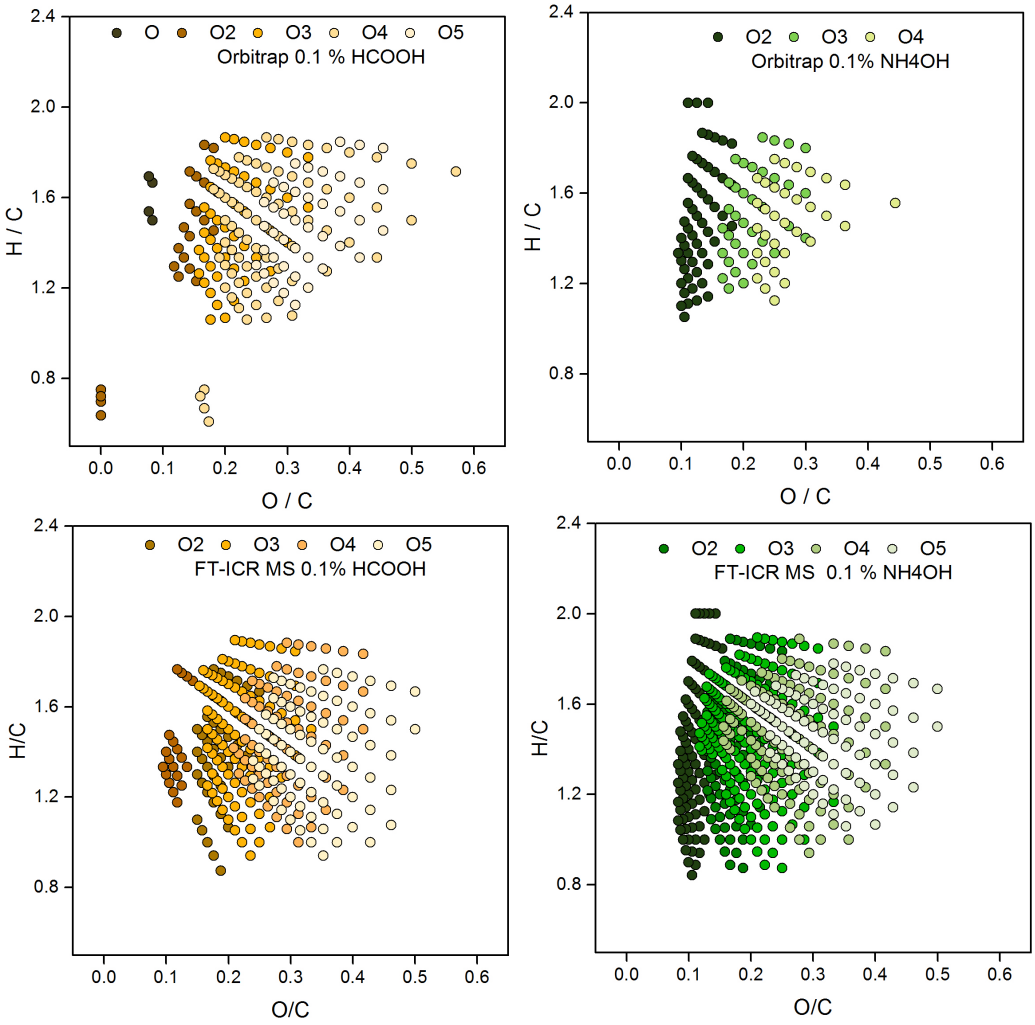

Figure 6.12 H/C against O/C van Krevelen plots for the 0.1 % HCOOH and 0.1 % NH_4OH solutions. Note that the number of relevant molecular compositions used will be higher than the number of data points within the plots; multiple molecular compositions may have the same H/C and O/C ratios, thus resulting in overlapping data points

6.4 Conclusions

Transfer solvent apparent pH has a significant impact on the overall class distribution of NAFCs detected by (-) ESI-MS, regardless of instrument type or method of sample introduction. It is clear that the observed O_2/O_4 ratio is significantly influenced by pH, with consequences for environmental forensics. When attempting to make a comparison of data sets from different laboratories, differences in the apparent pH of the transfer solvent should be accounted for to prevent erroneous interpretation.

The effects of pH presented in this Chapter, as well as those of solvent system in Chapter 5, may also be observed for other multi-component analyses where individual standards are not available. It is therefore essential to develop standardised methods that can be selected from to best suit the intended end use of the data. For example, if O_2 species are of most interest in OSPW samples, the best overall response (both qualitative and quantitative) is achieved using a high pH transfer solvent when analysis is completed by (-) ESI-MS. In terms of relative response, acidic eluent either favors the detection of O_x classes of higher oxygen content or conversely suppresses the lower oxygen contents (e.g. O_2); the latter is more likely, as overall response is reduced by a factor of ~ 20 when using acidic eluent during (-) ESI-MS analysis. The findings from two laboratories, using two varieties of mass spectrometer and different methods of sample introduction, illustrate that very similar trends are observed when monitoring O_2/O_4 ratios. Caution should thus be exercised for oil sands environmental monitoring of the O_2 class and when measuring ratios of NAFCs classes for inter-laboratory comparisons.

A detailed characterization of what is being measured and how is important for improved assessment of the toxicity, fate and transport of environmental contaminants, and to make comparisons between data obtained for petroleum-related samples more robust. A particular solvent system suitable for the analyte of interest, for example toluene:propan-2-ol for the analysis of crude and heavy oils or acetonitrile:water for OSPW, could be routinely used, and apparent pH adjusted to a set value and recorded to facilitate comparison with the results from subsequent studies.

6.5 References

Allen, E. W., 2008. Process water treatment in Canada's oil sands industry: I. Target pollutants and treatment objectives. J. Environ. Eng. Sci. 7:123-128.

Barrow, M. P., Headley, J. V., Peru, K. M., Derrick, P. J., 2009. Data Visualization for the Characterization of Naphthenic Acids within Petroleum Samples. Energy Fuels 23:2592-2599.

Barrow, M. P., Headley, J. V., Peru, K. M., Derrick, P. J., 2004. Fourier transform ion cyclotron resonance mass spectrometry of principal components in oil sands naphthenic acids. J. Chromatgr. A 1058:51-59.

Barrow, M. P., Peru, K. M., Fahlman, B., Hewitt, L. M., Frank, R. A., Headley, J. V., 2015. Beyond Naphthenic Acids: Environmental Screening of Water from Natural Sources and the Athabasca Oil Sands Industry Using Atmospheric Pressure Photoionization Fourier Transform Ion Cyclotron Resonance Mass Spectrometry. J. Am. Soc. Mass Spectrom. 26:1508-1521.

Barrow, M. P., Peru, K. M., Headley, J. V., 2014. An Added Dimension: GC Atmospheric Pressure Chemical Ionization FTICR MS and the Athabasca Oil Sands. Anal. Chem. 86:8281−8288.

Barrow, M. P., Peru, K. M., McMartin, D. W.,Headley, J. V., 2016. Effects of Extraction pH on the Fourier Transform Ion Cyclotron Resonance Mass Spectrometry Profiles of Athabasca Oil Sands Process. Energy Fuels 30:3615-3621.

Barrow, M. P., Witt, M., Headley, J. V., Peru, K. M., 2010. Athabasca oil sands process water: characterization by atmospheric pressure photoionization and electrospray ionization fourier transform ion cyclotron resonance mass spectrometry. Anal. Chem. 82:3727−3735.

Bowman, D. T., Slater, G. F., Warren, L. A., McCarry, B. E., 2014. Identification of individual thiophene-, indane-, tetralin-, cyclohexane-, and adamantane-type carboxylic acids in composite tailings pore water from Alberta oil sands. Rapid Commun. Mass Spectrom. 28:2075-2083.

Brunswick, P., Shang, D., van Aggelen, G., Hindle, R., Hewitt, L. M., Frank, R. A., Haberl, M., Kim, M., 2015. Trace analysis of total naphthenic acids in aqueous environmental matrices by liquid chromatography/mass spectrometry-quadrupole time of flight mass spectrometry direct injection. J. Chromatogr. A, 1405:49-71.

Burrowes, A., Marsh, R., Evans, C., Teare, M., Ramos, S., Rahnama, F., Kirsch, M. -A., Philp, L., Stenson, J., Yemane, M., Horne, J. V., Fong, J., Sankey, G., Harrison, P., 2009. Alberta's Energy Reserves 2008 and Supply/Demand

Outlook 2009–2018; Energy Resources Conservation Board, Government of Alberta: Calgary, Alberta, Canada., pp 220.

Chen, Y., McPhedran, K. N., Perez-Estrada, L., El-Din, M. G., 2015. An omic approach for the identification of oil sands process-affected water compounds using multivariate statistical analysis of ultrahigh resolution mass spectrometry datasets. Sci. Total Environ. 511:230-237.

Clemente, J. S., Prasad, N. G. N., MacKinnon, M. D., Fedorak, P. M., 2003. A Statistical Comparison of Naphthenic Acids Characterized by Gas Chromatography-Mass Spectrometry. Chemosphere 50:1265-1274.

Frank, R. A., Roy, J. W., Bickerton, G., Rowland, S. J., Headley, J. V., Scarlett, A. G., West, C. E., Peru, K. M., Parrott, J. L., Conly, F. M., Hewitt, L. M., 2014. Profiling oil sands mixtures from industrial developments and natural groundwaters for source identification. Environ. Sci. Technol. 48:2660–2670.

Government of Canada. Wastewater System Effluent Regulations. SOR/2012-139. Minister of Justice, Ottawa, ON, Canada. [www Document]. URL: http://lawslois. justice.gc.ca/eng/regulations/SOR-2012-139/FullText.html

Grewer, D. M., Young, R. F., Whittal, R. M., Fedorak, P. M., 2010. Naphthenic acids and other acid-extractables in water samples from Alberta: What is being measured? Sci. Total Environ. 408:5997-6010.

Headley, J. V., Barrow, M. P., Peru, K. M., Fahlman, B., Frank, R. A., Bickerton, G., McMaster, M. E., Parrott, J., Hewitt, L. M., 2011a. Preliminary fingerprinting of Athabasca oil sands polar organics in environmental samples using electrospray ionization Fourier transform ion cyclotron resonance mass spectrometry. Rapid Commun. Mass Spectrom. 25:1899–1909.

Headley, J. V., Kumar, P., Dalai, A., Peru, K. M., Bailey, J., McMartin, D. W., Rowland, S. M., Rodgers, R. P., Marshall, A. G., 2015. Fourier Transform Ion Cyclotron Resonance Mass Spectrometry Characterization of Treated Athabasca Oil Sands Processed Waters. Energy Fuels 29:2768-2773.

Headley, J. V., McMartin, D. W., 2004. A review of the occurrence and fate of naphthenic acids in aquatic environments. J. Environ. Sci. Health, Part A: Toxic/Hazard. Subst. Environ. Eng. 39:1989–2010.

Headley, J. V., Peru, K. M., Armstrong, S. A., Han, X., Martin, J. W., Mapolelo, M. M., Smith, D. F., Rogers, R. P., Marshall, A. G., 2009. Aquatic plant-derived changes in oil sands naphthenic acid signatures determined by low-, high-

and ultrahigh-resolution mass spectrometry. Rapid Commun. Mass Spectrom. 23:515-522.

Headley, J. V., Peru, K. M., Barrow, M. P., 2016. Advances in mass spectrometric characterization of naphthenic acids fraction compounds in oil sands environmental samples and crude oil - A review. Mass Spectrom. Rev. 35:311-328.

Headley, J. V., Peru, K. M., Barrow, M. P., Derrick, P. J., 2007. Characterization of Naphthenic Acids from Athabasca Oil Sands Using Electrospray Ionization: The Significant Influence of Solvents. Anal.Chem. 79:6222−6229.

Headley, J. V., Peru, K. M., Fahlman, B., Colodey, A., McMartin, D. W., 2013. Selective solvent extraction and characterization of the acid extractable fraction of Athabasca oils sands process waters by Orbitrap mass spectrometry. Int. J. Mass Spectrom. 345-347:104-108.

Headley, J. V., Peru, K. M., Janfada, A., Fahlma, B., Gu, C., Hassan, S., 2011b. Characterization of oil sands acids in plant tissue using Orbitrap ultra-high resolution mass spectrometry with electrospray ionization. Rapid Commun. Mass Spectrom. 25:459-462.

Headley, J. V., Peru, K. M., Mohamed, M. H., Wilson, L., McMartin, D. W., Mapolelo, M. M., Lobodin, V. V., Rodgers, R. P., Marshall, A. G., 2014. Atmospheric Pressure Photoionization Fourier Transform Ion Cyclotron Resonance Mass Spectrometry Characterization of Tunable Carbohydrate-Based Materials for Sorption of Oil Sands Naphthenic Acids. Energy Fuels 28:1611-1616.

Hindle, R. Noesthedena, M., Peru, K. M., Headley, J. V., 2013. Quantitative analysis of naphthenic acids in water by liquid chromatography–accurate mass time-of-flight mass spectrometry. J. Chromatogr A. 1286:166-74.

Hughes, S. A., Mahaffey, A., Shore, B., Baker, J., Kilgour, B., Brown, C., Peru, K. M., Headley, J. V., Bailey, H. C., 2017. Using ultrahigh-resolution mass spectrometry and toxicity identification techniques to characterize the toxicity of oil sands process-affected water: The case for classical naphthenic acids. Environ. Toxicol. Chem. 36:3148-3157.

Huang, R., McPhedran, K. N., Sun, N., Chelme-Ayala, P., El-Din, M. G., 2016. Investigation of the impact of organic solvent type and solution pH on the extraction efficiency of naphthenic acids from oil sands process affected water. Chemosphere 146:472-477.

Huang, R., Sun, N., Chelme-Ayala, P., McPhedran, K. N., Changalov, M., Gamal El-Din, M., 2015. Fractionation of oil sands-process affected water using

pH-dependent extractions: A study of dissociation constants for naphthenic acids species. Chemosphere 127:291– 296.

Janfada, A., Headley, J. V., Peru, K. M., Barbour, S. L., 2006. A laboratory evaluation of the sorption of oil sands naphthenic acids on organic rich soils. J. Environ. Sci. Health A Tox. Hazard Subst. Environ. Eng. 41:985-97.

Jie, W., Cao, X., Chai, L., Liao, J., Huang, Y., Tang, X., 2015. Quantification and characterization of naphthenic acids in soils from oil exploration areas in China by GC/MS. Anal. Methods, 7:2149-2154.

Johnson, R. J., Smith, B. E., Sutton, P. A., McGenity, T. J., Rowland, S. J., Whitby, C., 2011. Microbial biodegradation of aromatic alkanoic naphthenic acids is affected by the degree of alkyl side chain branching. ISME. J. 5:486-496.

Marentette, J. R., Frank, R. A., Bartlett, A. J., Gillis, P. L., Hewitt, L. M., Peru, K. M., Headley, J. V., Brunswick, P., Shang, D., Parrott, J. L., 2015. Toxicity of naphthenic acid fraction components extracted from fresh and aged oil sands process-affected waters, and commercial naphthenic acid mixtures, to fathead minnow (Pimephales promelas) embryos. Aquat. Toxicol. 164:108-117.

Martin, J., 2015. The Challenge: Safe release and reintegration of oil sands process affected water. Environ. Toxicol. Chem. 34:2682-2686.

Morandi, G. D., Wiseman, S. B., Pereira, A., Mankidy, R., Gault, I. G. M., Martin, J. W., Giesy, J. P., 2015. Effects-Directed Analysis of Dissolved Organic Compounds in Oil Sands Process-Affected Water. Environ. Sci. Technol. 49:12395-12404.

Nyakas, A., Han, J., Peru, K. M., Headley, J. V., Borchers, C., 2013. The comprehensive analysis of oil sands processed water by direct infusion fourier-transform ion cyclotron resonance mass spectrometry with and without offline UHPLC sample prefractionation. Environ. Sci. Technol. 47:4471−4479.

Pereira, A. S., Bhattacharjee, S., Martin, J. W., 2013. Characterization of Oil Sands Process-Affected Waters by Liquid Chromatography Orbitrap Mass Spectrometry. Environ. Sci. Technol. 47:5504-5513.

Pereira, A. S., Martin, J. W., 2015. Exploring the complexity of oil sands process-affected water by high efficiency supercritical fluid chromatography/orbitrap mass spectrometry. Rapid Commun. Mass Spectrom. 29:735-744.

Rogers, V. V., Liber, K., MacKinnon, M. D., 2002. Isolation and characterization of naphthenic acids from Athabasca oil sands tailings pond water. Chemosphere 48:519-27.

Shell Canada Ltd. 2016. Oil sands performance report 2015. Calgary, AB, Canada: Shell Canada Ltd. [www Document]. URL: https://s01.static-shell.com/content/dam/royaldutchshell/documents/corporate/she-2055-oil-sands-performance-report-2015-final1.pdf

Swigert, J. P., Lee, C., Wong, D. C. L., White, R., Scarlett, A. G., West, C. E., Rowland, S. J., 2015. Aquatic hazard assessment of a commercial sample of naphthenic acids. Chemosphere 124:1-9.

Wilde, M. J., West, C. E., Scarlett, A. G., Jones, D., Frank, R. A., Hewitt, L. M., Rowland, S. J., 2015. Bicyclic naphthenic acids in oil sands process water: Identification by comprehensive multidimensional gas chromatography-mass spectrometry. J. Chromatogr. A, 1378:74-87.

Yue, S., Ramsay, B. A., Wang, J., Ramsay, J., 2015. Toxicity and composition profiles of solid phase extracts of oil sands process-affected water. Sci. Total Environ. 538:573-582.

7. Petroleomics in the Environment: Staten Island Contaminated Soil

7.1 Introduction

The New York/New Jersey (NY/NJ) Estuary supports one the highest population densities in the United States, consequently the shores of one of its main shipping channels, the Arthur Kill, hosts numerous waste generating industries. The NY/NJ Estuary was ranked among the most chemically contaminated waterways in the United States based on surface sediment concentrations and frequency of accidental chemical discharge events (Gunster, 1993; Packer, 1991). Elevated body burdens of toxic substances including heavy metals, petroleum hydrocarbons, and aromatic hydrocarbons have been detected in a wide range of aquatic wildlife (Packer 1991). Analysis of the spatial and down-core extent of contamination from anthropogenic sources including petroleum, industrial, and agricultural chemicals, in estuarine and coastal regions is of rising importance due to increased demand on below ground space, which may contain historic pollution, as well as greater understanding of the long term impact on eco-system health (da Silva and Bicego, 2010; Langston et al., 2012; Oros and Ross, 2004; Vane et al., 2008; Vane et al., 2009; Vane et al., 2011; Vane et al., 2018).

Environmental samples, particularly those contaminated with petroleum-related substances, are highly complex, containing many thousands of components (Alimi et al., 2003; Richardson and Ternes, 2018; Vane et al., 2018; White et al., 2013). Petroleomics (Barrow, 2010; Hsu et al., 2011) research typically utilizes state-of-the-art, high field FTICR instrumentation (Cho et al., 2015; Marshall et al., 2010) which offers ultrahigh resolution and sub-ppm mass accuracy. However, these instruments are typically expensive to obtain and maintain, as well as requiring expert operation. solariX 2xR FTICR MS instruments can operate in a mode where ion detection occurs using 4 cell plates, compared to the usual 2, and as such are able to detect at twice the usual frequency (Cho et al., 2017; Schweikhard et al., 1990). 2ω detection allows for significant improvements in performance compared to other FTICR instrumentation operating at the same field (Pan, 1988), specifically doubling resolution for a set acquisition time or else offering equivalent resolution in half the time (Schweikhard, 1991). The latter makes the technique well suited to hyphenated techniques, including gas chromatography (GC), where a fast scan rate is required to maintain pace with rapidly eluting components (Beens and Brinkman, 2000; Tessarolo et al., 2014; Wang et al., 1997).

7 T FTICR instrumentation equipped with the option of 2ω detection has already demonstrated ultrahigh resolution analytical capabilities in the analysis of petroleum samples (Cho et al., 2017), offering equivalent performance at a lower magnetic field than previously required. This, in turn, reduces the entry cost of FTICR MS for petroleomics and environmental analyses; a 7 T instrument equipped with 2ω detection possesses performance capabilities comparable to a 15 T instrument operating under the traditional conditions of detection at ω. 2ω detection affords the ability to operate an FTICR mass spectrometer at twice the speed for the same resolving power, which is useful for coupling with chromatography, or to operate at the same speed but double the resolving power. Orbitrap MS instrumentation has also been used for environmental analyses when coupled to prior chromatographic separation (Pereira and Martin, 2015), however FTICR MS remains most capable when handling ultra-complex samples. One of the advantages of the ParaCell (Boldin and Nikolaev, 2011; Jertz et al., 2015) in solariX xR and 2xR instruments is the ability to excite ions to a larger orbit radius than the Infinity Cell design, which in turn yields greater signal-to-noise and reduction in space-charge effects (Cho et al., 2017). Here, the application is extended to environmental samples, where coupling GC can increase the scope of analysis to include the observation of multiple isomers for a single molecular formula (Blomberg et al., 2002; Lalli et al., 2017; Schwemer et al., 2015), and to provide an additional dimension of separation, aiding in the detection of low abundance species (Schwemer et al., 2015).

Analyses of environmental samples by direct infusion (DI) into FTICR MS instrumentation have been successful, for example oil sands process-affected water (Barrow et al., 2010; Headley et al., 2011) as demonstrated in Chapter 6, and soil from coastal regions affected by the Deepwater Horizon spill (Chen et al., 2016). Coupling of chromatographic methods with FTICR MS has also been successfully applied to the characterization of petroleum-contaminated soil (Zubair et al., 2015) and weathered crude oils (Rowland et al., 2014). A range of ionization methods are available, including electrospray ionization (ESI), laser desorption ionization (LDI), atmospheric pressure photoionization (APPI), and atmospheric pressure chemical ionization (APCI), the choice of which influences the observed profile (Barrow et al., 2010; Cho et al., 2013; Huba et al., 2016). As demonstrated in Chapter 2, APPI preferentially accesses non-polar, conjugated systems, and produces both protonated and radical ion species, adding to spectral complexity (Cho et al., 2015) while atmospheric pressure chemical ionization APCI accesses both non-polar and polar compounds (Andrade et al., 2008). The

differences in APPI and APCI ionization mechanism are expanded upon in Figure 1.5 and Equation schemes 1.5 and 1.6.

In this study, the shallow salt marsh sediment core from Staten Island, New York, was sampled at 47 intervals to correlate the compositional fingerprints of the petroleum extracts with the history of oil spills this area. Rock-Eval(6) pyrolysis, a geochemical screening technique widely applied to the hydrocarbon bearing source rocks, was used as bulk geochemical reconnaissance method (Könitzer et al., 2016; Slowakiewicz et al., 2015). Rock-Eval generates parameters for total organic carbon (TOC), free hydrocarbons (S1), and bound (polymeric) hydrocarbons (S2). S1 describes the quantity and proportion of volatile hydrocarbons (free oil) S2 the bound hydrocarbons (biopolymers and kerogen). The production index is used as a benchmark for thermal maturity and calculated by dividing the amount of volatile hydrocarbons by total volatile and bound hydrocarbon (S1/S1+S2). In petroleum geochemistry resource assessment studies, immature rocks have a ratio of 0.1 or less, mature samples yield values of 0.1-0.4, and when expulsion occurs the S1 no longer rises (Pharaoh et al., 2018; Slowakiewicz et al., 2015).

In parallel to Rock–Eval pyrolysis screening geochemistry, solvent extracts were profiled using two instruments in different laboratories: DI-APPI FTICR MS using a solariX and GC-APCI FTICR MS using a solariX 2xR. The GC-APCI experiments were performed to access additional species, particularly more volatile components, and provide insight on the isomeric complexity of the extracts (Benigni et al., 2016) as performed in Chapter 4. An ultrahigh resolution mass spectrometer coupled with GC affords the ability to accurately monitor signal intensities within very narrow *m*/*z* windows, including co-eluting components. By following the extracted ion chromatograms (EICs) in a manner not possible with lower resolution instrumentation including time-of-flight and quadrupole mass spectrometers, it is possible to obtain information about the range of isomers present for a single molecular formula (Barrow et al., 2014).

The detailed molecular characterization obtained by DI-APPI FTICR MS (solariX) and GC-APCI FTICR MS (solariX 2xR), along with the bulk information determined by Rock-Eval pyrolysis, allows a fingerprint of the anthropogenic contaminants of soil to be developed. Petroleomic profiles of soil as a function of depth can be used for correlating contamination with the site history, and may be

developed as a tool for understanding the impact of oil and chemical spills in areas with a high concentration of industrial and shipping activity, for example.

7.2 Materials and Methods

7.2.1 Sediment Sampling

A sediment core was collected using an Eijkelkamp peat sampler fitted with a stainless steel gauge (50 cm × 5.2 cm i.d.) at 40 36 27.87912 N, 74 11 27.50687 W (± 5 m) from intertidal zone of Saw Marsh Creek, Staten Island, New York, USA on June 10th 2013 (Figure 7.1). Recovered core sections were stored in pre-cut clean UPVC pipe and transported in a cool box at approximately 4 °C and then frozen at -18 °C. Each core was sectioned continuously at 2 cm intervals up to and including 46 cm depth and at 1 cm up to 51.5 cm depth and then at 2 cm intervals to core base at 90 cm. All sediment intervals were then freeze-dried for 72 h, sieved through a mesh aperture of 2 mm and the < 2 mm fraction ground to a fine powder (Beriro et al., 2014; Vane et al., 2007).

Figure 7.1 Sampling location of core.

7.2.2 Rock-Eval(6) Pyrolysis

Forty seven depth increments from the Saw Marsh Creek core were analyzed using a Rock-Eval(6) pyrolyser. Powdered samples (60 mg dry wt.) were heated from 300 °C to 650 °C at 25 °C min^{-1} in an inert atmosphere of N_2 and the residual carbon then oxidised by the addition of a constant flow of clean compressed oxygen-containing air at 300 °C to 850 °C at 20 °C min^{-1} (hold 5 min) . Hydrocarbons released during the two-stage pyrolysis were measured using a flame ionization detector and CO and CO_2 measured using an IR cell. The performance of the instrument was checked every 10 samples against the accepted values of the Institut Français du Pétrole (IFP) standard (IFP 160 000, S/N1 5-081840). Rock-Eval parameters were calculated by integration of the amounts of HC (thermally-vaporized free hydrocarbons) expressed in mg HC^{-1} g^{-}

[1] rock (S1) and hydrocarbons released from cracking of bound organic matter (OM) expressed in mg HC^{-1} g^{-1} rock (S2). The production index (PI) is given by Equation 7.1.

$$PI = \frac{S1}{S1+S2} \quad (7.1)$$

7.2.3 Soxhlet Extraction

Environmental Protection Agency method 3540c was followed for 5 depth samples. 190 mL dichloromethane (DCM) (Fisher Scientific, Hemel Hempstead, Hertfordshire, UK) was added to each sample and heated at ~40 °C for 22 h to maximise the extraction of hydrophobic components including petroleum-related compounds. The extracts were then cooled before being evaporated under reduced pressure to 10 mL.

7.2.4 Direct Infusion (DI) APPI FTICR MS

Extracts for 5 depths were diluted in dichloromethane (DCM) (Fisher Scientific, Hemel Hempstead, Hertfordshire, UK) before mass spectra were acquired using a 12 T solariX FTICR mass spectrometer (Bruker Daltonik GmbH, Bremen, Germany), coupled to an APPI II source. The instrument was operated in positive-ion mode. Nitrogen was used as the drying gas at a temperature of 200 °C at a flow rate of 4 L min^{-1}. The nebulizing gas was nitrogen and was maintained at a pressure of 1.0 bar. Samples were infused using a syringe pump at a rate of 750 μL h^{-1} without the activation of in-source dissociation. 4 MW data sets were acquired using magnitude mode, with a detection range of *m*/*z* 98-3000. After acquiring 300 scans, the data were zero-filled once and apodized using a Sine-Bell function prior to applying a fast Fourier transform. For the apodized data, the measured resolving power at *m*/*z* 200 was 650,000. Data were internally calibrated using homologous series (Table 7.1) and analyzed using DataAnalysis 4.2 (Bruker Daltonik GmbH, Bremen, Germany). Assignments were made using Composer 1.5.7 (Sierra Analytics, Modesto, CA, USA), searching for homologous series within the elemental constraints C=0-200; H=0-1000; N=0-2; O=0-9; S=0-2; P=0-1 (Table 7.2). Aabel NG2 v.5.2 (Gigawiz Ltd. Co., Tulsa, Oklahoma, USA) was used for data visualization.

Table 7.1 List of multiple homologous series of HC[H] class used for calibrating DI-APPI FTICR MS data

Formula	**Charge**	***m/z***	**Ion DBE**
$C_{15}H_{23}$	1+	203.17943	4.5
$C_{16}H_{25}$	1+	217.19508	4.5
$C_{17}H_{17}$	1+	221.13248	9.5
$C_{18}H_{15}$	1+	231.11683	11.5
$C_{17}H_{27}$	1+	231.21073	4.5
$C_{19}H_{17}$	1+	245.13248	11.5
$C_{18}H_{29}$	1+	245.22638	4.5
$C_{20}H_{19}$	1+	259.14813	11.5
$C_{19}H_{31}$	1+	259.24203	4.5
$C_{20}H_{33}$	1+	273.25768	4.5
$C_{22}H_{21}$	1+	285.16378	12.5
$C_{21}H_{35}$	1+	287.27333	4.5
$C_{22}H_{37}$	1+	301.28898	4.5
$C_{24}H_{21}$	1+	309.16378	14.5
$C_{23}H_{39}$	1+	315.30463	4.5
$C_{25}H_{25}$	1+	325.19508	13.5
$C_{24}H_{41}$	1+	329.32028	4.5
$C_{27}H_{35}$	1+	359.27333	10.5
$C_{29}H_{39}$	1+	387.30463	10.5
$C_{30}H_{43}$	1+	403.33593	9.5
$C_{32}H_{47}$	1+	431.36723	9.5
$C_{34}H_{51}$	1+	459.39853	9.5
$C_{36}H_{55}$	1+	487.42983	9.5
$C_{38}H_{55}$	1+	511.42983	11.5
$C_{40}H_{63}$	1+	543.49243	9.5
$C_{43}H_{67}$	1+	583.52373	10.5
$C_{45}H_{69}$	1+	609.53938	11.5
$C_{47}H_{71}$	1+	635.55503	12.5
$C_{48}H_{77}$	1+	653.60196	10.5
$C_{50}H_{79}$	1+	679.61763	11.5
$C_{52}H_{79}$	1+	703.61763	13.5
$C_{54}H_{81}$	1+	729.63328	14.5
$C_{57}H_{85}$	1+	769.66458	15.5
$C_{59}H_{95}$	1+	803.74283	12.5

$C_{61}H_{101}$	1+	833.78978	11.5
$C_{63}H_{105}$	1+	861.82108	11.5
$C_{65}H_{111}$	1+	891.86803	10.5
$C_{69}H_{117}$	1+	945.91498	11.5
$C_{73}H_{105}$	1+	981.82108	21.5

Table 7.2 Composer 1.5.7 parameters for the assignment of molecular formulae

Parameter	**Constraints**
Polarity	Positive
Ion properties	Adducts = H; allow radical and adduct/loss ions; remove isolated assignments
m/z range	m/z 150-1300
DBE range	-0.5 - 40
Element ranges	C: 0-200; H: 0-1000; N: 0-2; O: 0-9; S: 0-2; P: 0-1

7.2.5 GC-APCI FTICR MS

Extracts for 4 depths were diluted in DCM (Sigma Aldrich Chemie GmbH, Munich, Bavaria, Germany). Mass spectra were acquired using a 7 T solariX 2xR FTICR mass spectrometer (Bruker Daltonik GmbH, Bremen, Germany), coupled to a GC 450 (Bruker Daltonik GmbH, Bremen, Germany) and GC-APCI II source. 1 μL injection volume onto a 30 m BR-5ms column was used with He as the carrier gas, with the temperature program as follows: 60 °C held for 1 min, ramping 6 °C min^{-1} up to 300 °C and held for 9 min. The instrument was operated in positive-ion mode. Nitrogen was used as the drying gas at a temperature of 240 °C at a flow rate of 4 L min^{-1}. The nebulizing gas was nitrogen and was maintained at a pressure of 2.0 bar. 2 MW data sets were acquired using magnitude mode, with a detection range of *m*/*z* 107-3000 and 95 % data profile reduction. 2ω (quadrupolar) detection was used, affording high resolution at the rapid scan rate required for GC-APCI infusion. The data were zero-filled once and apodized using a Sine-Bell function prior to applying a fast Fourier transform. A lock mass of *m*/*z* 223.06345 (a polysiloxane) was used for online calibration. For the apodized data, the measured resolving power at *m*/*z* 200 was 300,000. Data were analyzed using DataAnalysis 4.2 (Bruker Daltonik GmbH, Bremen, Germany) in 10 minute time retention intervals with the first 10 minutes used for background subtraction. Assignments were made using Composer 1.5.7 (Sierra Analytics, Modesto, CA, USA), searching for homologous series within the elemental constraints C=0-200; H=0-1000; N=0-2; O=0-9; S=0-2; P=0-1 (Table 7.2). Aabel NG2 v.5.2 (Gigawiz Ltd. Co., Tulsa, Oklahoma, USA) was used for data visualization.

7.3 Results and Discussion

7.3.1 Rock-Eval(6)Pyrolysis

Inspection of the TOC content and its two major components, S1 and S2, at each sampling interval (Figure 7.2) shows a rapid decrease from surface to 25 cm, which may be due to the presence of natural extractable free hydrocarbon compounds and structural biopolymers in the rooting zone of living marsh plants (Newell et al., 2016). Below 25 cm depth the hydrocarbon content (TOC, S1, S2) was low and invariant with exception of a broad concentration peak at 47 - 49 cm and another at 79 - 81 cm (Figure 7.2). These were taken to indicate anthropogenic oil spills, possibly including the 1990 Exxon pipeline spill. Similarly, corresponding changes were also confirmed by the concentrations of residual carbon (RC %) (non-pyrolyzable) and PI (Figure 7.2). The latter parameter is a widely utilized by hydrocarbon explorationists to assess the amount of generated as compared to potential hydrocarbons. In this current work increasing PI values also appear to have considerable utility for the identification of possible hydrocarbon pollution events.

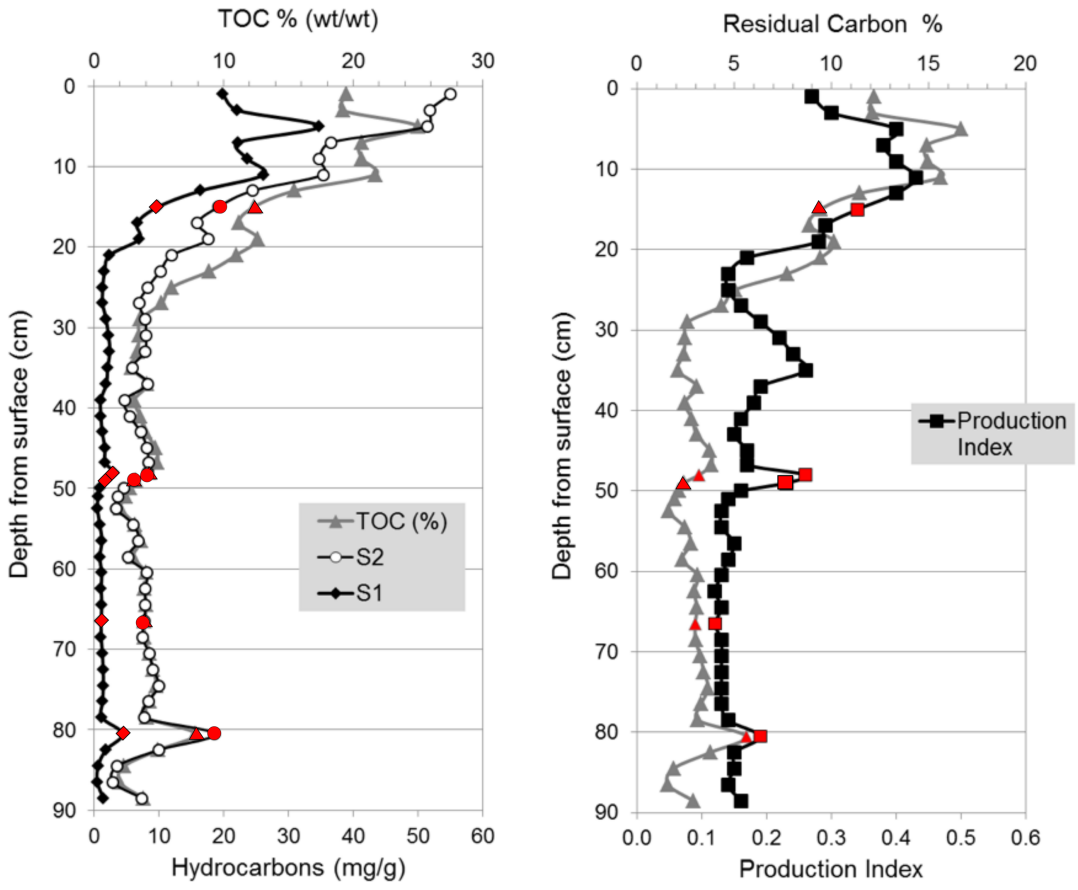

Figure 7.2 TOC and RC analysis by Rock-Eval(6) Pyrolysis

The key sampling depths carried forward for further analysis by FTICR MS methods are indicated by red markers in Figure 7.2, with 67.5 – 69.5 cm included as a sample with low PI for comparison.

7.3.2 DI-APPI FTICR MS

Broadband mass spectra were obtained for soil extracts, produced using soil samples originating from 5 depths, with the spectra shown in Figure 7.3. The mass distribution shifts between extract sampling depths, with 14 - 16 to 67.5 - 69.5 cm centred approximately on *m/z* 350, while 79.5 - 81.5 cm is centred on a higher *m/z* of 500 and has greater spectral intensity over the entire distribution.

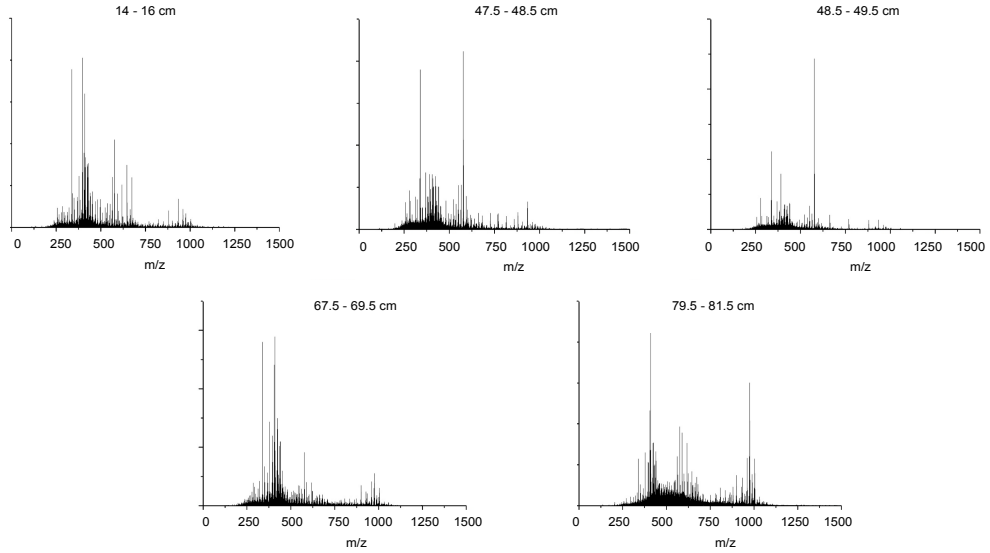

Figure 7.3 DI-APPI FTICR mass spectra for 5 sampling depths

MS data were analyzed by searching for homologous series of peaks separated by the CH_2 (14.01565 Da) repeat unit (Table 7.1). Homologous series of molecular formulae possess the same heteroatom content (compound class) and number of double bond equivalents (DBE) (McLafferty and Turecek, 1993) and increase incrementally with each CH_2 repeat unit by one carbon number (Marshall and Rodgers, 2008). A compound class distribution, showing the total relative intensity of peaks assigned to each compound class, is shown for all sampling depths in Figure 7.4.

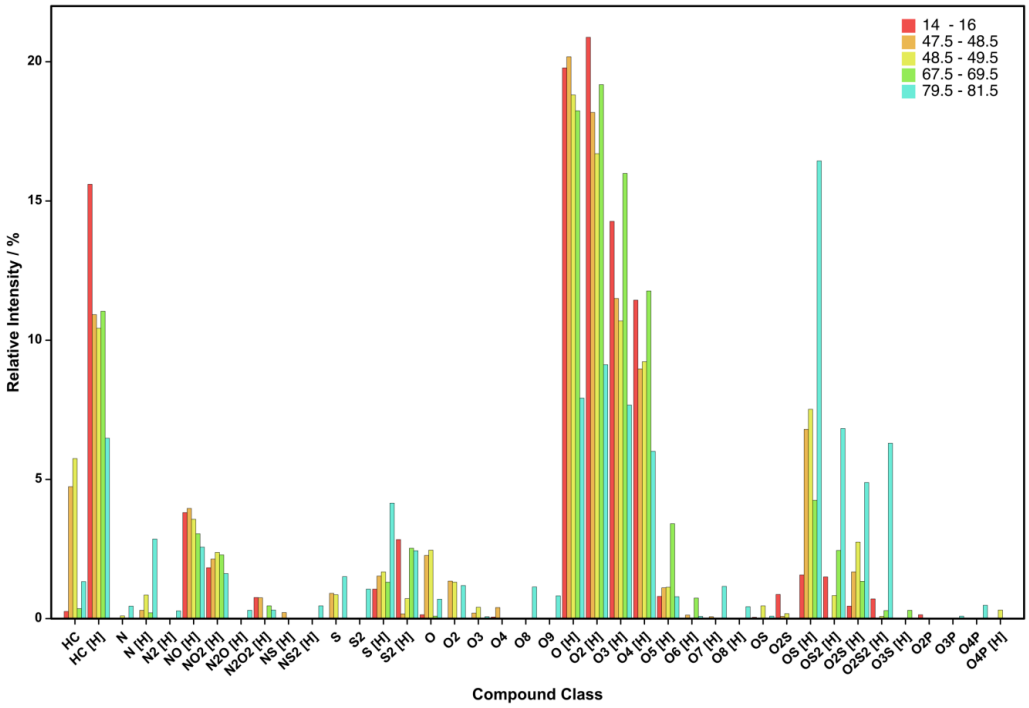

Figure 7.4 Compound class distribution for 5 sampling depths

Several key compositional differences between sampling depths are seen in Figure 7.4, particularly a sharp increase in the relative contribution from high oxygen containing O_x and O_xS_y[H] compounds, when moving from the shallower samples to the deepest sample at 79.5 - 81.5 cm. At the depths of 47.5 - 48.5 and 48.5 - 49.5 cm, there is a relatively strong contribution from the HC radical class, correlating well with the higher concentrations of free and bound hydrocarbons measured by Rock-Eval pyrolysis. The HC radical class most likely comprises polycyclic aromatic hydrocarbons (PAHs), as extensively condensed hydrocarbons can stabilise free radicals readily due to delocalisation throughout the aromatic framework (Creary et al., 1989). The depths of 47.5 - 48.5, 48.5 - 49.5 and 79.5 - 81.5 cm also have contributions from the N containing classes, commonly detected in petroleum-related mixtures, where the N[H] class typically corresponds to pyridinic species that protonate readily, while the N class often represents pyrrolic species that ionize by forming radical species (Table 7.3).

Table 7.3 Example DBE Calculations for selected compositions

Compound Class	**Example Composition**	**DBE Calculation**
HC	$[C_{16}H_{10}]^{+\bullet}$	$16 - (10/2) + 0 + 1 = 12$
HC[H]	$[C_{13}H_{16} + H]^{+}$	$13 - (17/2) + 0 + 1 = 5.5$
N	$[C_{17}H_{13}N]^{+\bullet}$	$17 - (13/2) + (1/2) + 1 = 12$
N[H]	$[C_{17}H_{13}N + H]^{+}$	$17 - (14/2) + (1/2) + 1 = 11.5$
O	$[C_{15}H_{12}O]^{+\bullet}$	$15 - (12/2) + 0 + 1 = 10$
O[H]	$[C_{13}H_{16}O + H]^{+}$	$13 - (17/2) + 0 + 1 = 5.5$
O_2S	$[C_{18}H_{14}O_2S]^{+\bullet}$	$18 - (14/2) + 0 + 1 = 12$
O_2S[H]	$[C_{13}H_{16}O_2S + H]^{+}$	$13 - (17/2) + 0 + 1 = 5.5$

The relative contribution from oxygenated and sulfur-containing radical classes was found to be greater at the sampling depths associated with a spike in PI. Inspection of the plots of number of rings and double bonds, or double bond equivalents (DBE), against carbon number (Figures 7.5-7.7) for individual compound classes can provide information on the likely molecular structures of these compounds (Purcell et al., 2007a; Purcell et al., 2007b, Purcell et al., 2007c). Figure 7.5 shows that the S radical class of 47.5 - 48.5, 48.5 - 49.5 and 79.5 – 81.5 cm starts at 6 DBE and has higher intensities at DBEs of 9, 12, and 15, a pattern characteristic of thiophenic compounds (Hegazi et al., 2012; Hourani et al., 2013; Panda et al., 2007) that, due to their aromatic structure, form radical species during ionization. This is in contrast to the S_y[H] classes that comprise sulfur-containing groups that are more readily protonated during ionization, such as sulfides, which were detected at all depths and in the 79.5 – 81.5 cm sample at a relatively higher intensity. The differentiation between ion types for compositions with the same heteroatoms can be useful indications of differences in structure; the S[H] class begins at a lower DBE than the S radical class and does not have the characteristic pattern of higher intensities at DBE of 6, 9, 12, and 15 (Figure 7.6).

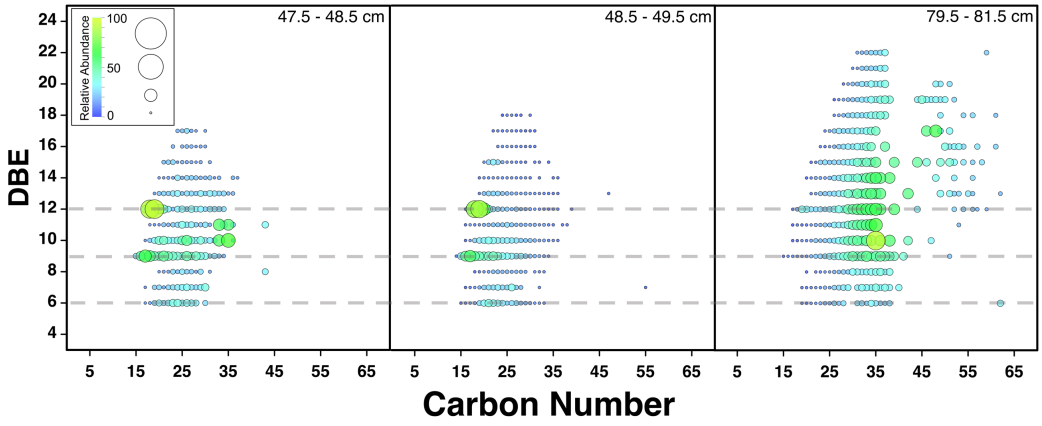

Figure 7.5 Plots of DBE against carbon number for the S class from DI-APPI data, with guidelines for DBE of 6, 9, and 12 corresponding to possible core structures of benzothiophene, dibenzothiophene and tribenzothiophene, respectively

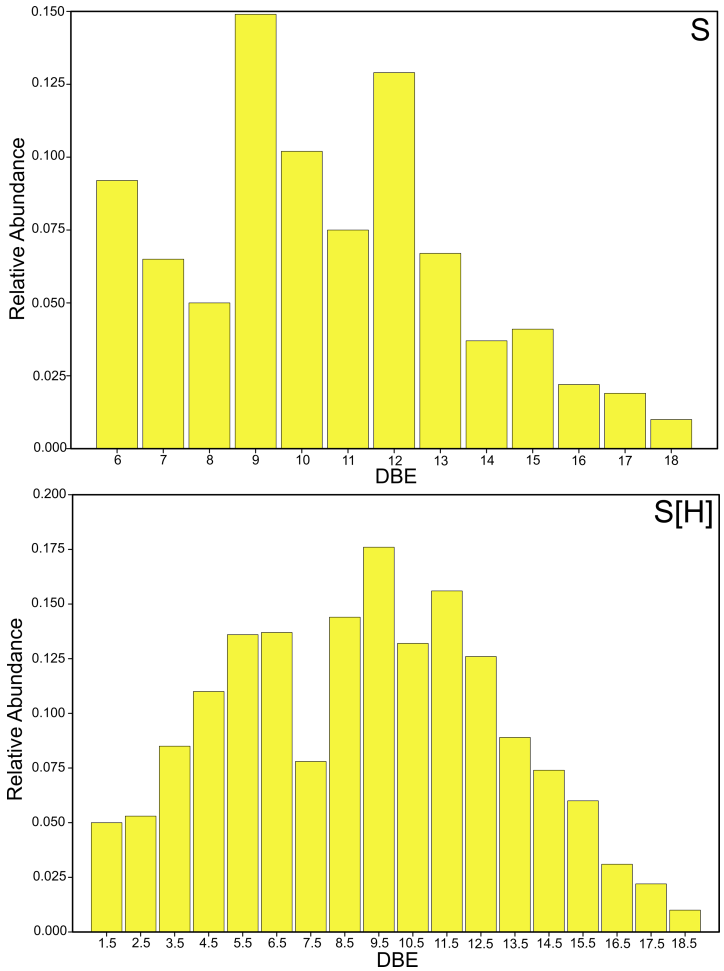

Figure 7.6 Comparison of DBE distributions for the S and S[H] classes from DI-APPI data for the 48.5 – 49.5 cm sampling depth. The prominent spacing of 3 DBE for the S class (e.g. predominant contributions at DBE 6, 9, 12, and 15) is characteristic of thiophenic contributions in petroleum, for example

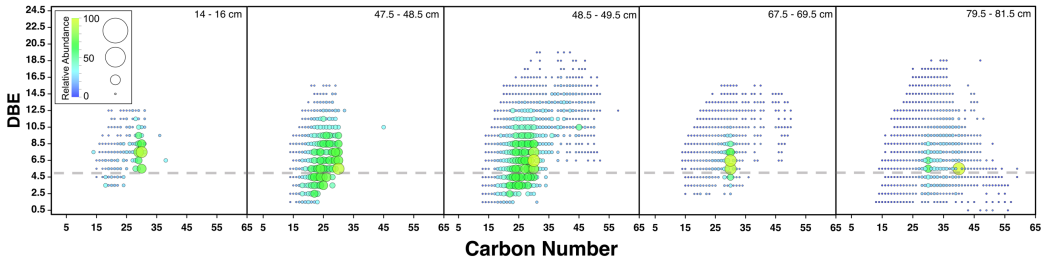

Figure 7.7 Plots of DBE against carbon number for the O_2S[H] class from DI-APPI data, with guideline to show the greater relative intensity contribution from DBE of 5.5 and above

The increase in contribution from highly oxygenated O_x and O_xS_y classes may be linked to ageing of petroleum compounds (Atlas, 1981; Chen et al., 2016; Wang et al., 1998), and may be used to provide information of the timing of contamination due to particular spills (Douglas et al., 1996). Although geochemical tools can be used to more accurately date samples collected in areas with minimal sediment mixing, the samples used in this were collected at a site close to an active creek channel which in turn connects to the main tidal Arthur Kill waterway (a view supported by the changing sedimentology), and are therefore unlikely to provide an interpretable classical chronology (Vane et al., 2010; Vane et al., 2011). The DBE plots of the O_2S[H] class (Figure 7.7) show a higher DBE and carbon number range at two of the depths associated with a spike in PI, and greater relative intensities above DBE 5.5, which may be partly due to oxygenation of benzothiopenic species, that, due to the incorporation of a polar oxygen functionality, are more readily ionized by protonation (Fathalla, 2011; Griffiths et al., 2014). O_xS_y[H] classes may represent sulfoxides, whereas the corresponding radical class (O_xS_y) may have oxygen incorporated as aldehyde or ketone moieties in the hydrocarbon backbone (Bobinger, 2009).

7.3.3 GC-APCI FTICR MS

The total ion chromatogram (TIC) is shown in Figure 7.8 for the 67.5 - 69.5 cm depth sample. The average spectra taken over 10 minute time intervals of the TIC, show a shift in petroleum distribution to higher *m*/*z* with increasing retention time. While 10 minute intervals represent a relatively long period with respect to chromatography, they have been used here simply for the purposes of data visualization to illustrate clear differences between the data corresponding to the time ranges. Furthermore, coupling of GC to FTICR generates large data sets, necessitating a trade-off between time resolved information and the amount of time required for data analysis. It should be noted that the original, time-resolved

information, such as extracted ion chromatograms of individual ions, is retained with an example provided.

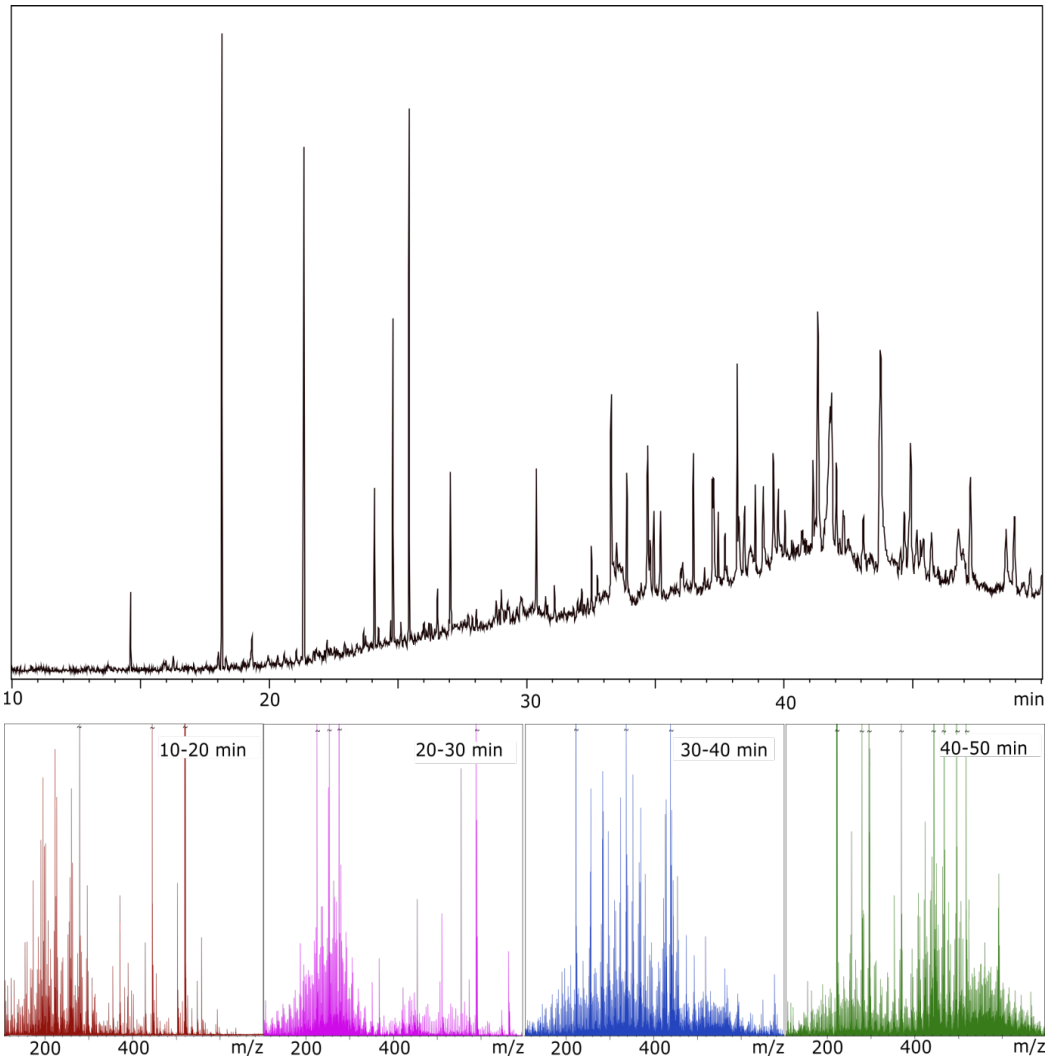

Figure 7.8 Total ion chromatogram for sampling depth 67.5 – 69.5 cm, which was found to have the lowest PI by Rock-Eval pyrolysis, and the mass spectra resulting from averaging the acquired scans over 10 minute intervals

The compound class distribution shown in Figure 7.9 demonstrates that several heteroatom containing compound classes were observed at greater relative intensity when using GC-APCI FTICR MS compared to DI-APPI FTICR MS. The summed class distribution can be disseminated to the distributions observed over 10 minute intervals (Figure 7.10 – 7.13), further demonstrating that several classes were more readily observed by GC-APCI FTICR MS compared to DI-APPI FTICR MS measurements, including low intensity O_x and O_xP classes. Although the N[H] class, typically comprising pyridinic species, is seen at a low relative intensity in all samples, in contrast to DI-APPI the N class, typically comprising

pyrrolic species (Purcell et al., 2007a; Purcell et al., 2007c), is not seen as readily, including in the 79.5 – 81.5 cm sample (Figure 7.13). The two techniques offer complimentary access to sample composition, due both to the differences in the volatility of compounds accessed by DI and GC and the differences in preferential ionization. While the differences in preferential ionization were not extensive when compared to methods such as ESI (Huba et al., 2016), APPI and APCI do offer some complementarity. 0.30 Da regions of mass spectra are shown in Figure 7.14, comparing a spectrum acquired using DI-APPI FTICR MS on a 12 T solariX instrument and a spectrum acquired using GC-APCI FTICR MS on a 7 T solariX 2xR instrument at the 40 - 50 min retention interval. Figure 7.14 shows not only the ultrahigh resolution capabilities of the 12 T and 7 T 2xR instruments, but also heteroatom class assignments common to both DI-APPI and GC-APCI methods, as well as unique molecular compositions in each case. DI-APPI provided a greater ionization response for polycyclic aromatic hydrocarbons and sulfur-containing species, while GC-APCI afforded greater access to more highly oxygenated compounds.

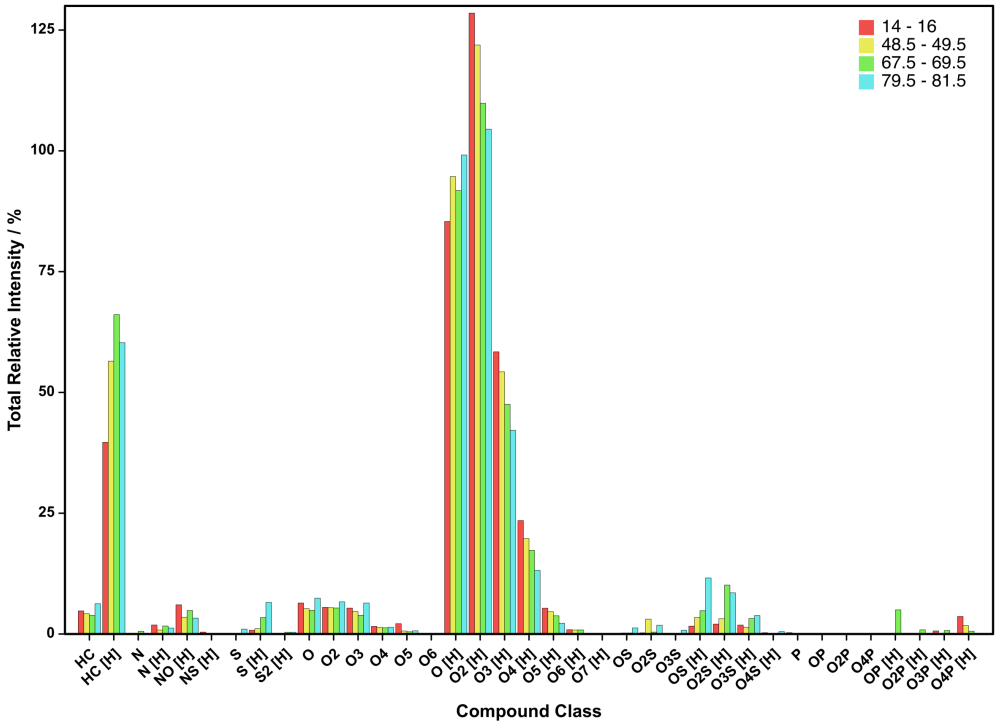

Figure 7.9 Compound class distribution from GC-APCI FTICR MS analysis of four sampling depths, summed over all retention time intervals

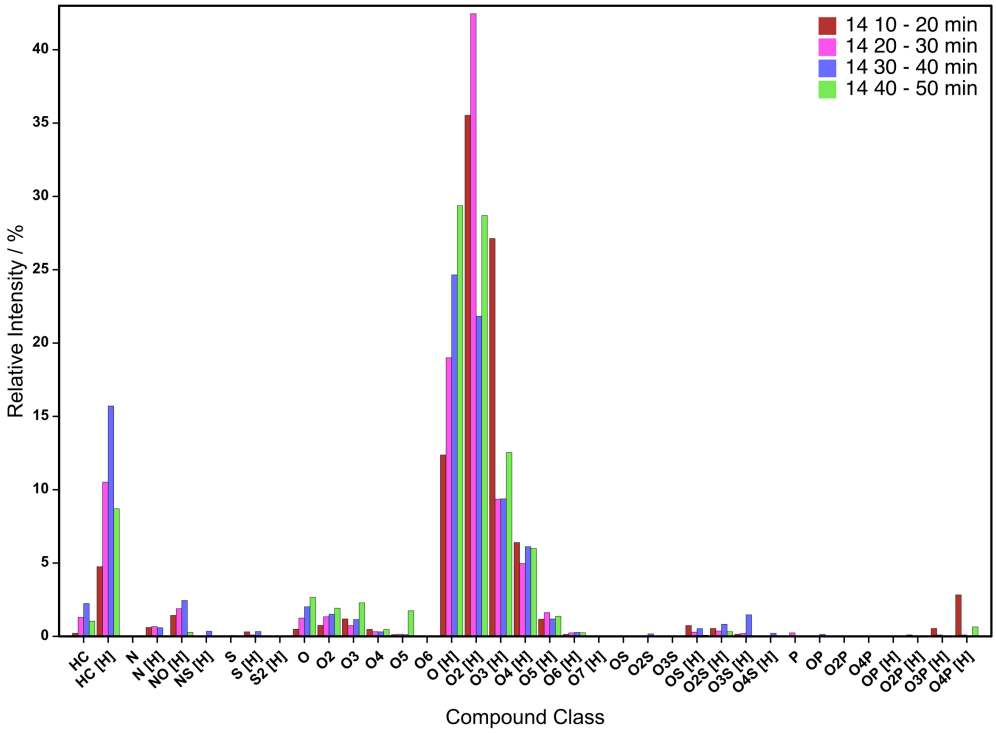

Figure 7.10 Change in compound class distribution over time from GC-APCI FTICR MS analysis of sampling depth 14 - 16 cm

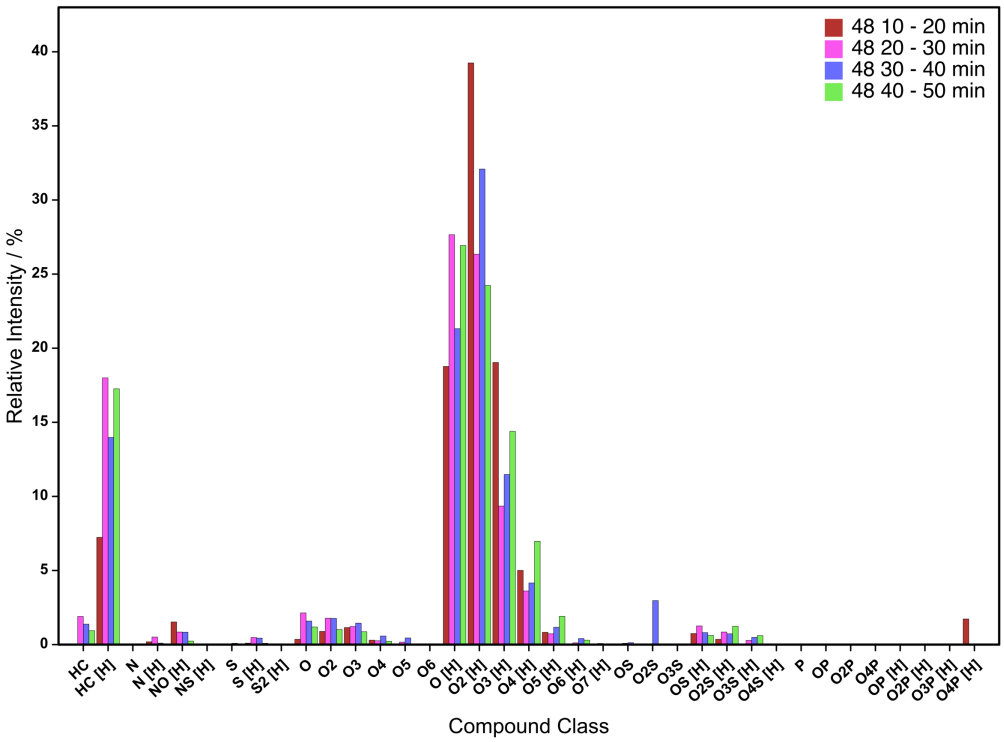

Figure 7.11 Change in compound class distribution over time from GC-APCI FTICR MS analysis of sampling depth 48.5 – 49.5 cm

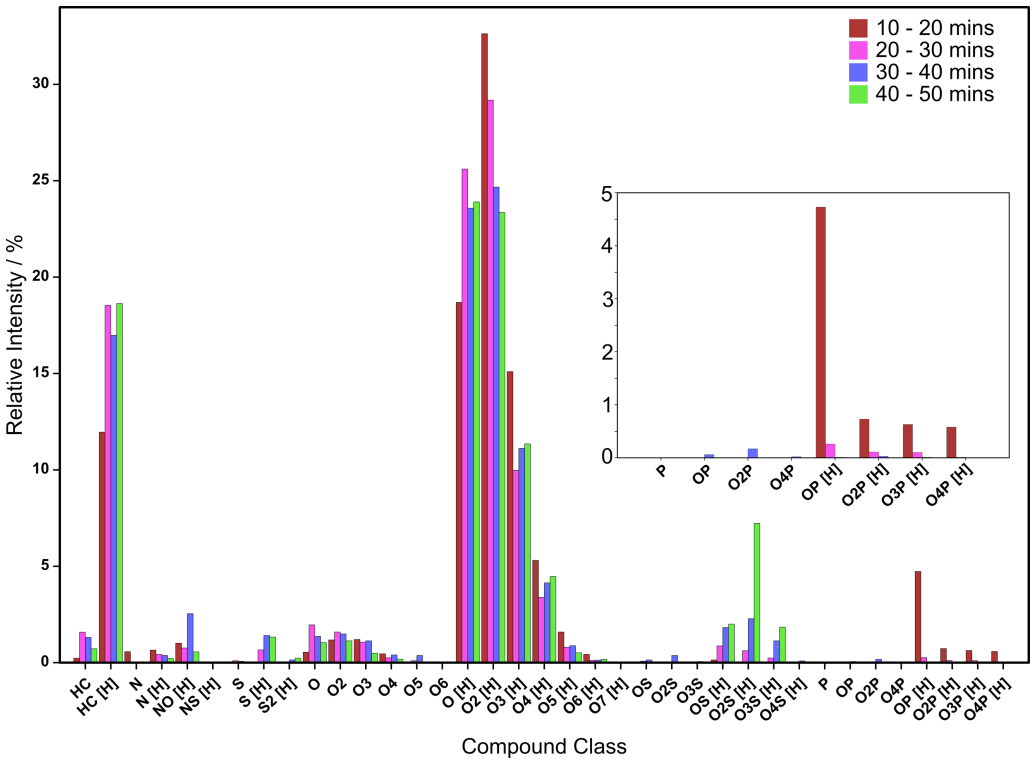

Figure 7.12 Change in compound class distribution over time from GC-APCI FTICR MS analysis of sampling depth 67.5 – 69.5 cm. An enlarged region showing contributions from the phosphorous containing classes is inset

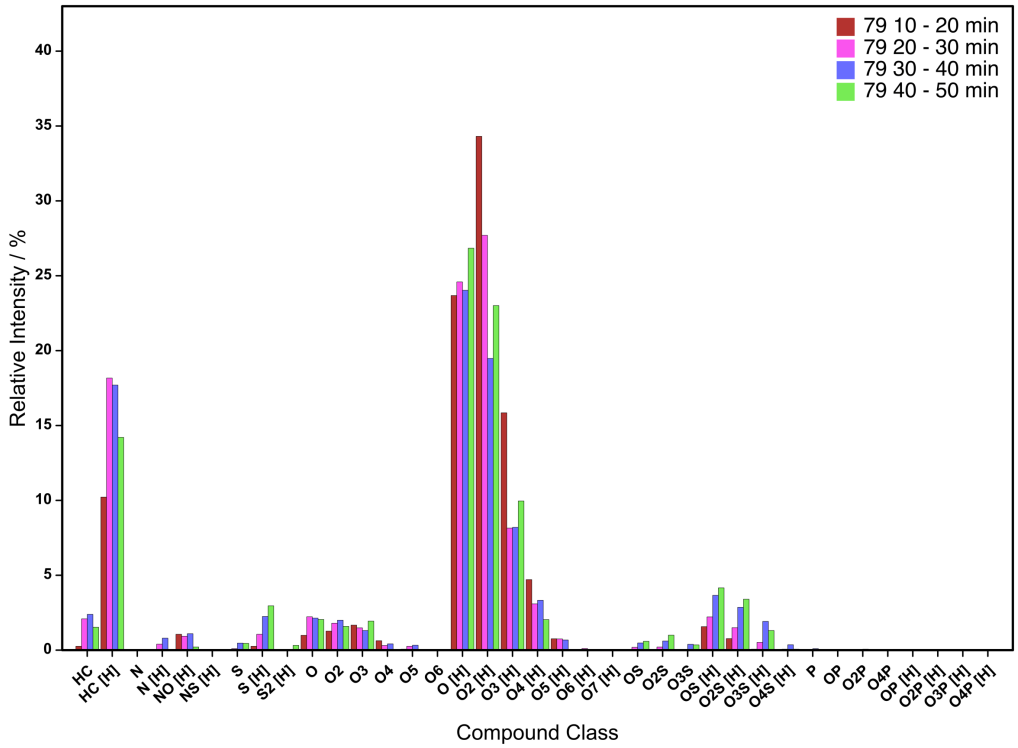

Figure 7.13 Change in compound class distribution over time from GC-APCI FTICR MS analysis of sampling depth 79.5– 81.5 cm

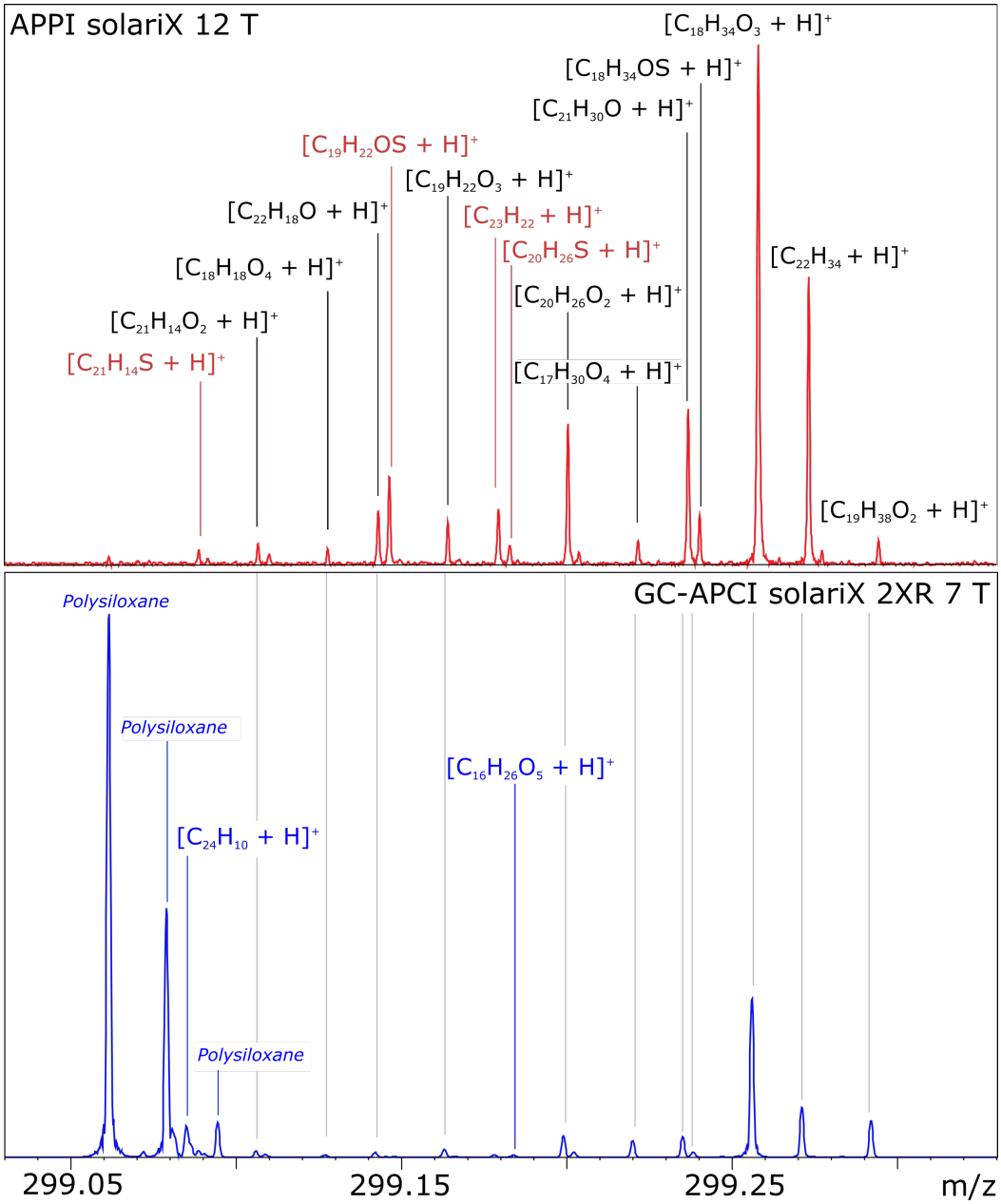

Figure 7.14 Enlarged 0.30 Da regions of the mass spectra obtained for the 67.5 – 69.5 cm sampling depth using a 12 T FTICR instrument equipped with an APPI ion source (top) and a 7 T FTICR instrument coupled with GC-APCI and implementing 2ω detection (bottom), with data shown for the retention time range of 40 - 50 min. Molecular compositions observed using both techniques are labelled in black, while those observed only using DI-APPI are shown in red and those observed only by GC-APCI are shown in blue. The polysiloxane peaks are not sample-related, instead originating from the GC column; these peaks correspond to an isotopologue of $[C_8H_{24}O_4Si_4 + H]^+$ and the monoisotopic peaks for $[C_7H_{22}O_5Si_4 + H]^+$ and $[C_{12}H_{22}O_3Si_3 + H]^+$

Notably, phosphorous-containing classes including $O_4P[H]$ also make a substantial contribution to the depths of 14 – 16 cm, 48.5 – 49.5 cm, and 67.5 - 69.5 cm (Figures 7.10 – 7.13), typically eluting early in the run. The $O_4P[H]$ class was also detected in DI-APPI FTICR MS experiments at 48.5 - 49.5 cm. Several possible sources of phosphorous contamination in the NY/NJ Estuary exist, including agricultural effluent, leaks from chemical plants and manufacturers, and leaching of materials dumped in the now closed Fresh Kills Landfill (Anon, 2001). Example phosphorous compounds detected by GC-APCI FTICR MS include $[C_8H_{19}O_4P + H]^+$ and $[C_{12}H_{27}O_4P + H]^+$ which may be dibutyl and tributyl phosphate, substances that are used in multiple industrial processes and, in the latter case, in fungicides and herbicides (Thomas et al., 1997). It is of particular note that, in the initial screening provided by Rock-Eval pyrolysis, the sampling depth of 67.5 – 69.5 cm appeared to contain relatively low levels of both free volatile hydrocarbons and bound polymeric hydrocarbons, as indicated in Figure 7.2, but that DI-APPI and GC-APCI analyses show that soil at this depth contains a range of substances that may have an anthropogenic source, including shipping activity, refineries, industrial and agricultural chemicals, landfill leachate, and sewage which suggests that the NY/NJ Estuary is continually affected by contamination. Natural interferences in the analysis of an environmental complex mixture cannot be ruled out completely, although the extraction in DCM limits the hydrophilic substances, such as natural organic matter (Hertkorn et al., 2008), carried forward for FTICR MS.

Several compound classes elute preferentially at specific times, for example the relative contributions from the $O_xS[H]$ classes generally increase with retention time. NO[H] and S[H] have the greatest relative intensity at 30 - 40 min at both the 14 - 16 cm and 67.5 – 69.5 cm sampling depths. The $O_xP[H]$ classes have the greatest relative intensity at the early elution times of 10 - 20 and 20 - 30 min. A lower relative intensity of the S class was seen for all samples by GC-APCI compared to DI-APPI, which may be associated with the greater ionization efficiency of more aromatic compounds by APPI. Figure 7.10 – 7.13 show a high relative contribution from the HC[H] class, which increases from the first time interval, and this corresponds to an increase in the number of data points as seen in the DBE plots shown in Figure 7.15a for the 67.5 – 69.5 cm sampling depth. Figure 7.15a also shows the DBE plots shifting to higher carbon number over time, with the highest mass species eluting later in the GC run. While there was an increase in absolute intensity for all DBE between 20 – 30 min and 40 – 50 min, Figure 7.15b shows the change in relative contribution from each DBE to the

overall HC[H] class intensity. DBE of 2.5 and below, and 6.5 and above, make a greater relative contribution at 40 – 50 min, while those between 2.5 and 5.5 inclusive make a greater contribution at 20 – 30 min, suggesting that they have a lower boiling point due to weaker intermolecular attractions, and elute earlier as a result. An ion with DBE of 6.5 in the HC[H] class (neutral DBE of 7) corresponds to the threshold for two, fused, 6-membered, aromatic rings. By comparison, an ion DBE of 9.5 (neutral DBE of 10) corresponds to the threshold for the cata-condensed structure incorporating three, 6-membered, aromatic rings. As an additional example, the DBE plots for the O[H] class of the 14 – 16 cm sampling depth show a similar increase in carbon number and DBE over time (Figure 7.16), but a more pronounced shift in the relative contribution from DBE of 6.5 and greater at 40 – 50 min compared to 20 - 30 min (Figure 7.16).

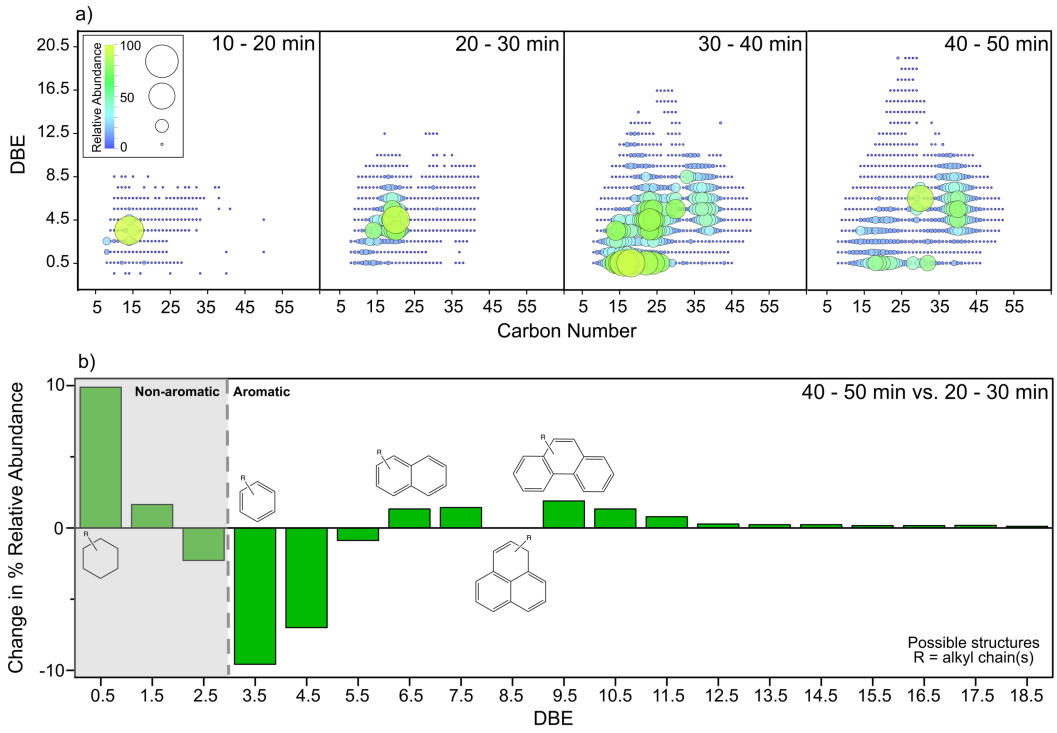

Figure 7.15 a) Plots of DBE against carbon number for the HC[H] class of sample depth 67.5 - 69.5 cm over 10 minute intervals of the GC-APCI FTICR MS experiment, where marker size scales with relative intensity and b) Change in relative abundance of each DBE comparing the 40 - 50 min to the 20 - 30 min interval. Possible structures are shown for selected DBE values, indicating where these specific structures would be found, if present

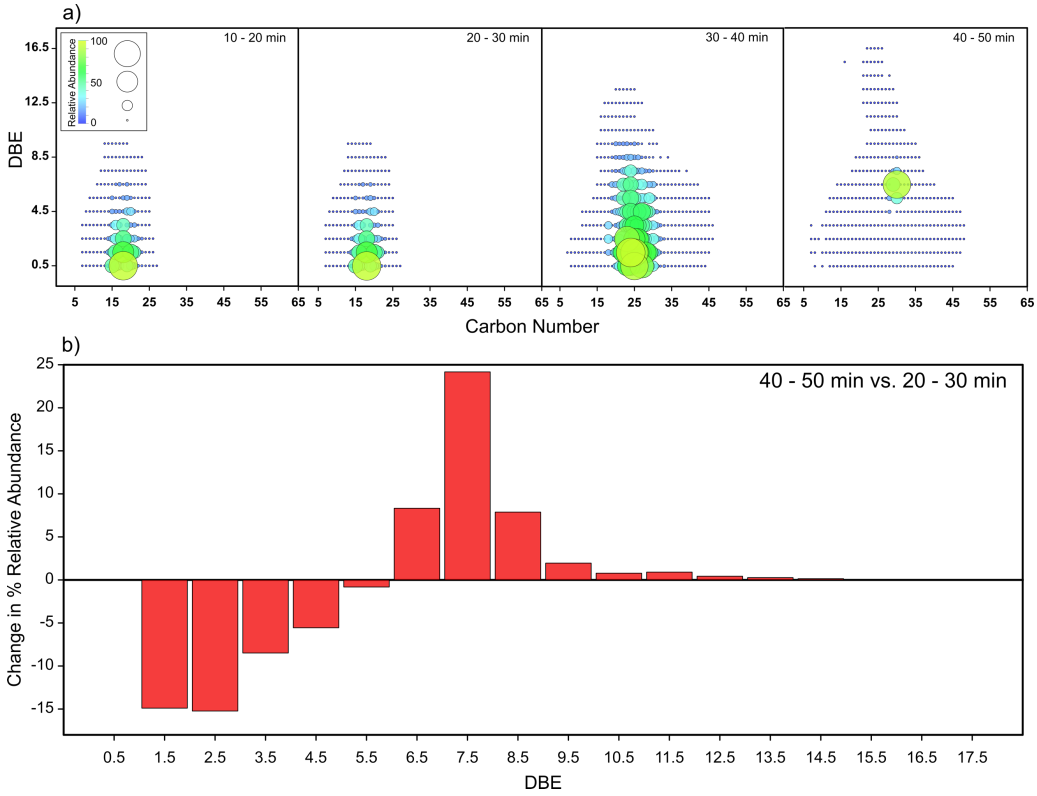

Figure 7.16 a) Plots of DBE against carbon number for the O[H] class of sample depth 14 - 16 cm over 10 minute intervals of the GC-APCI FTICR MS experiment and b) Change in relative abundance of each DBE comparing the 40 - 50 min to the 20 - 30 min interval

DI-APPI was able to access a greater DBE range for the HC[H] class than GC-APCI, with species detected up to a DBE of 25.5 (Figure 7.17). This can be explained by the preferential ionization of aromatic structures offered by APPI, allowing extensively condensed PAHs to be accessed more readily, as well as access to species with higher boiling points by DI. In contrast, species with higher carbon numbers were accessed at the later elution times of GC-APCI, including numerous assignments for carbon numbers in excess of 45.

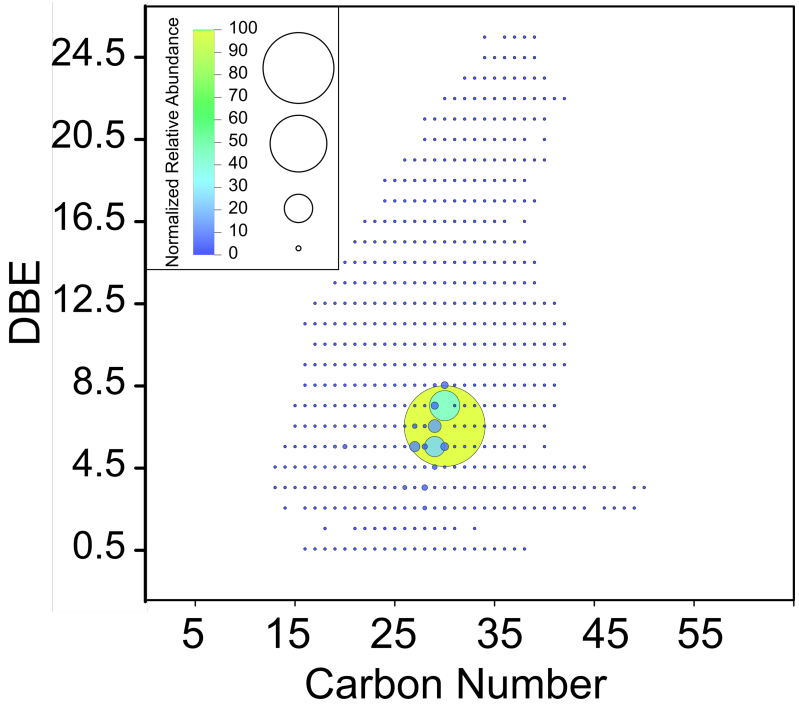

Figure 7.17 Plot of DBE against carbon number for the HC[H] class at 67.5 - 69.5 cm depth from DI-APPI data

Further adding to the complexity of the data, EICs can be used to visualise the number of isomers present for a single molecular composition (data point) within a DBE plot. Figure 7.18 shows EICs for three individual molecular formulae, represented by three points on the DBE plot of the O[H] class (Figure S7.19). Figure 7.18 shows the additional depth and complexity of data offered by the coupled GC-APCI FTICR MS technique, with each molecular ion peak representative of multiple isomeric compounds, and increasing complexity when increasing both carbon number and DBE. The EICs span two or more of the 10 minute intervals over which averaged spectra were produced, demonstrating that information in the time dimension was not lost during data processing. By combining GC with the ultra-high resolving power of the FTICR MS instrumentation, the EICs are selected for a given molecular composition in a narrow window of ± 0.0005 Da, which would not be possible for an instrument operating at lower resolution. For instance, if the resolution at m/z 300 were 30,000 FWHM, this would limit the mass difference resolvable to 0.01 m/z, and selecting a peak with this window would result in the EICs for multiple molecular formulae detected in the study overlapping. In practice, peaks can be resolved to less than a ± 0.01 Da range within a GC-APCI mass spectrum in this study and, as a result, the EICs would overlap if this selection tolerance was used (Figure 7.21).

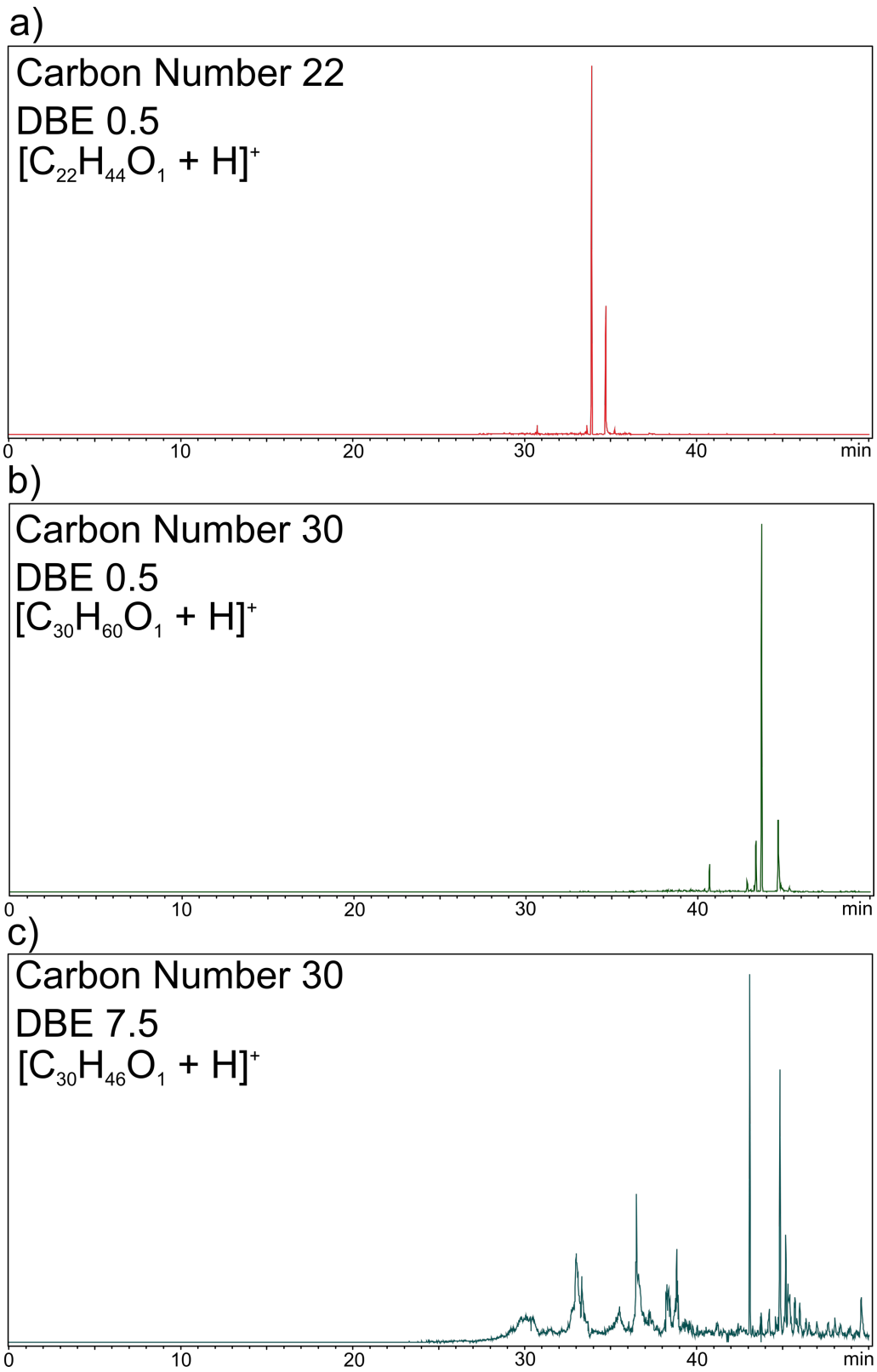

Figure 7.18 Extracted ion chromatograms for three individual molecular formulae from the O[H] class at 67.5 – 69.5 cm sampling depth, demonstrating increasing complexity with increasing carbon number and DBE (see Figure 7.19). b) represents an increase in carbon number from a), while c) represents an increase in DBE from b)

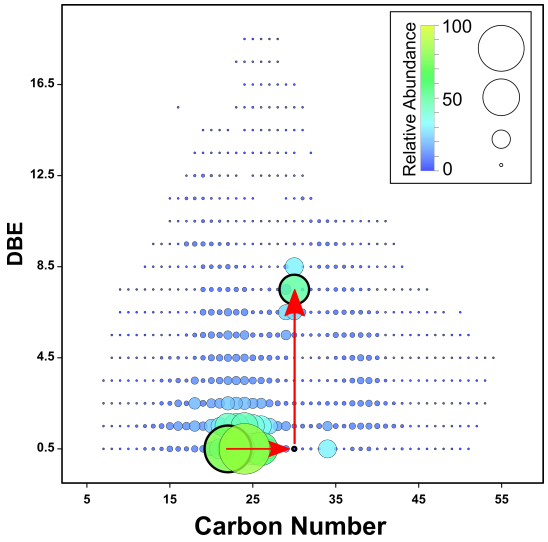

Figure 7.19 DBE plot for the O[H] class from the GC-APCI data for the 67.5 - 69.5 cm sampling depth at a retention time range of 30 – 40 min. The formulae selected for the EICs shown in Figure 7.19 are indicated by bold outline. Figure 7.18a) is represented by the first point selected, 7.18b) is represented by an increase in carbon number, and 7.18c) by a subsequent increase in DBE

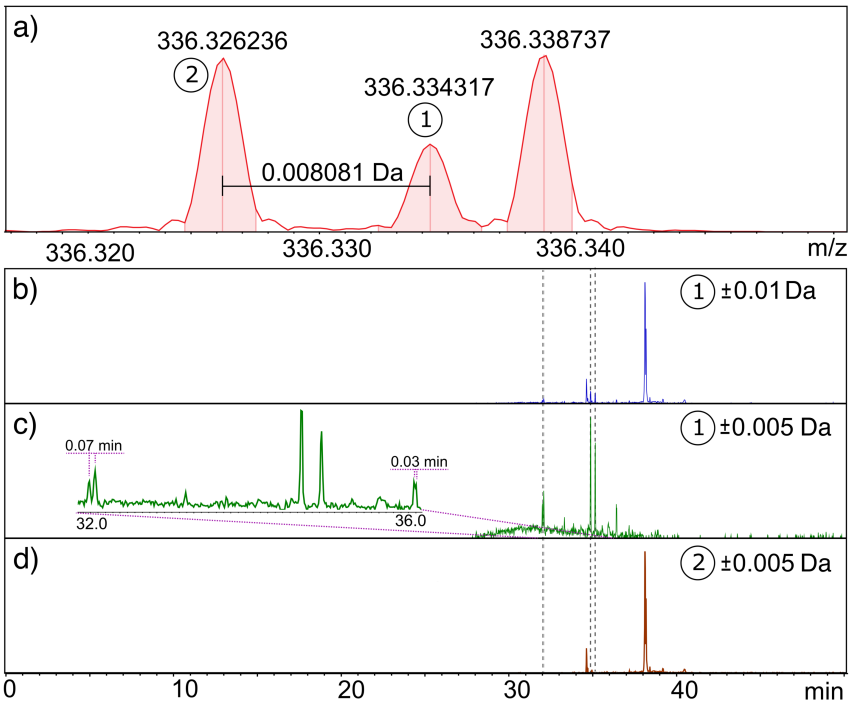

Figure 7.20 a) Enlarged region of GC-APCI FTICR mass spectrum for the 67.5 – 69.5 cm sampling depth showing two peaks within a narrow m/z range. b) When using a tolerance of ± 0.01 Da during data processing to generate EICs, the EICs for two peaks overlap. c) and d) Individual EICs can be properly resolved by using a narrower selection tolerance, where the instrument performance affords sufficiently high resolution

EICs can also be compared between sampling depths, providing an indication of the differences in isomeric complexity underlying relative class contributions and the range of structures possessing the same molecular formula (Figure 7.21). The EICs shown in Figures 7.18 and 7.21 demonstrate greater isomeric complexity for individual compositions than oil sands process water samples also studied by GC-APCI FTICR MS (Ortiz et al., 2014; Barrow et al., 2014), for example, although greater complexity may be determined utilising a chromatographic method not limited by boiling point, such as supercritical fluid chromatography (SFC) (Pereira and Martin, 2015) or high pressure liquid chromatography HPLC (Hawkes et al., 2018).

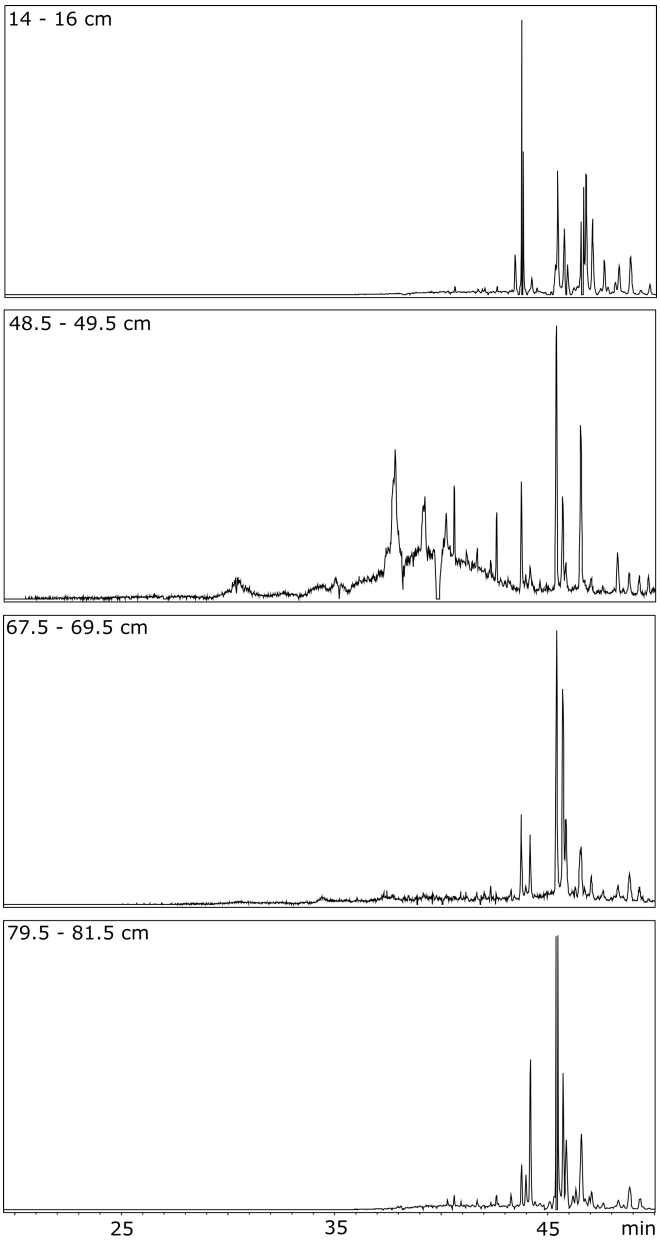

Figure 7.21 EICs for the molecular composition $[C_{30}H_{48} + H]^+$, demonstrating the differences in isomeric complexity and predominant retention times as a function of sampling depths

7.4 Conclusions

Several sampling depths with relatively high PI were identified by bulk Rock-Eval pyrolysis, with key sampling depths that may be linked to major spills in the NY/NJ Estuary carried forward for further analysis. A sample with a relatively low PI was also included, as well as a sample representative of topsoil. To complement the Rock-Eval data obtained for these soil depths, the selected samples were profiled more extensively by DI-APPI FTICR MS, plus GC-APCI FTICR MS equipped with 2ω detection. Several trends in the compositional profile were observed by DI-APPI FTICR MS, including relatively high HC and O_xS_y[H] contributions, at the sampling depths that corresponded to a spike in PI by Rock-Eval analysis. The range of oxygen- and sulfur-containing classes observed increased at these depths, which may be related to contamination from petroleum-related compounds.

GC-APCI FTICR analysis identified additional groups and provided complementary information to DI-APPI data. Phosphorous-containing compounds with low retention times were detected, which may indicate contamination from other anthropogenic sources, including agricultural effluent and industrial chemicals, in the NY/NJ Estuary area. The sample that was found to have a relatively low PI by Rock-Eval pyrolysis was observed to contain many hydrocarbon and phosphorous-containing compounds by DI-APPI and GC-APCI FTICR MS, suggesting that there may have been continuous pollution from anthropogenic sources such as shipping, agricultural activity, refineries, and other industrial activity in the NY/NJ Estuary.

The 7 T solariX 2xR instrument was shown to be capable of providing ultrahigh resolution data comparable to that obtained at the higher field of 12 T on sufficiently short timescales suitable for coupling with GC. Coupling GC with ultrahigh resolution mass spectrometry affords a unique capability to resolve a greater number of compounds, including co-eluting components, making it possible to resolve EICs fully and to detect isomeric components, even within highly complex mixtures. This provides greater analytical capabilities for complex mixture analysis and reduces the risk of loss of information which would result from coupling GC with lower resolution instruments. The viability of GC-APCI FTICR MS experiments on the 7 T 2xR instrument, using 2ω mode for increased performance, has been demonstrated as an emerging tool for the analysis of complex samples, including petroleum and environmental samples.

The detailed compositional profiling complements other analyses of the Staten Island site, which assess bulk metal and organic contamination. The adverse effects of multiple oil spill events on ecological health are confirmed, and it is noted that disturbing the sediment interval of 20-50 cm could release legacy contamination into the waterways (Vane et al., 2020). The FTICR MS analyses performed in this Chapter could be applied to the study of contaminants extracted from other environmental matrices, or be used to profile soil sampled at different time points, to provide an assessment of the effect repurposing of the site and the progress of remediation.

7.5 References

Alimi, H., Ertel, T., Schug, B., 2003. Fingerprinting of hydrocarbon fuel contaminants: Literature review. Environ. Forensics, 4:25-38.

Andrade, F. J., Shelley, J. T., Wetzel, W. C., Webb, M. R., Gamez, G., Ray, S. J., Hieftje, G. M., 2008. Atmospheric Pressure Chemical Ionization Source. 1. Ionization of Compounds in the Gas Phase. Anal. Chem., 80:2646-2653.

Anonymous, 2001. New York, New York - Fresh kills landfill closes. BioCycle, 42:22-23.

Atlas, R. M., 1981. Microbial-Degradation Of Petroleum-Hydrocarbons - An Environmental Perspective. Microbiol. Rev., 45:180-209.

Barrow, M. P., 2010. Petroleomics: study of the old and the new. Biofuels, 1:651-655.

Barrow, M. P., Peru, K. M., Headley, J. V., 2014. An Added Dimension: GC Atmospheric Pressure Chemical Ionization FTICR MS and the Athabasca Oil Sands. Anal. Chem., 86:8281-8288.

Barrow, M. P., Witt, M., Headley, J. V., Peru, K. M., 2010. Athabasca Oil Sands Process Water: Characterization by Atmospheric Pressure Photoionization and Electrospray Ionization Fourier Transform Ion Cyclotron Resonance Mass Spectrometry. Anal. Chem., 82:3727-3735.

Beens, J., Brinkman, U., 2000. The role of gas chromatography in compositional analyses in the petroleum industry. TrAC, Trends Anal. Chem., 19:260-275.

Benigni, P., DeBord, J., Thompson, C., Gardinali, P., Fernandez-Lima, F., 2016. Increasing Polyaromatic Hydrocarbon (PAH) Molecular Coverage during Fossil Oil Analysis by Combining Gas Chromatography and Atmospheric-Pressure Laser Ionization Fourier Transform Ion Cyclotron Resonance Mass Spectrometry (FT-ICR MS). Energy Fuels, 30:196-203.

Beriro, D. J., Vane, C. H., Cave, M. R., Nathanail, C. P., 2014. Effects of physical sample preparation on the concentrations of polycyclic aromatic hydrocarbons in gasworks contaminated soils. Chemosphere, 111:396-404.

Blomberg, J., Schoenmakers, P. J., Brinkman, U. A. T., 2002. Gas chromatographic methods for oil analysis. J. Chromatogr. A, 972:137-173.

Boldin, I. A., Nikolaev, E. N., 2011. FTICR cell with dynamic harmonization of the electric field in the whole volume by shaping of excitation and detection electrode assembly. Rapid Commun. Mass Spectrom., 25:122-126.

Cho, E., Witt, M., Hur, M., Jung, M.-J., Kim, S., 2017. Application of FT-ICR MS Equipped with Quadrupole Detection for Analysis of Crude Oil. Anal. Chem., 89:12101-12107.

Chen, H., Hou, A. X., Corilo, Y. E., Lin, Q. X., Lu, J., Mendelssohn, I. K., Zhang, R., Rodgers, R. P., McKenna, A. M., 2016. 4 Years after the Deepwater Horizon Spill: Molecular Transformation of Macondo Well Oil in Louisiana Salt Marsh Sediments Revealed by FT-ICR Mass Spectrometry. Environ. Sci. Technol., 50:9061-9069.

Cho, Y., Ahmed, A., Islam, A., Kim, S., 2015. Developments in FT-ICR MS instrumentation, ionization techniques, and data interpretation methods for petroleomics. Mass Spectrom. Rev., 34:248-263.

Cho Y., Mi J. J., Witt M., Birdwell J. E., Na J. G., Roh N. S., Kim, S., 2013. Comparing laser desorption ionization and atmospheric pressure photoionization coupled to Fourier transform ion cyclotron resonance mass spectrometry to characterize shale oils at the molecular level. Energy Fuels, 27:1830–1837.

Creary, X., Mehrsheikh-Mohammadi, M. E., McDonald, S., 1989. A Comparison of the Radical-Stabilizing Ability of Aromatic Groups. γ• Values for Aromatic Groups. J. Org. Chem., 54, 2904-2910.

da Silva, D. A. M., Bicego, M. C., 2010. Polycyclic aromatic hydrocarbons and petroleum biomarkers in Sao Sebastiao Channel, Brazil: Assessment of petroleum contamination. Mar. Environ. Res., 69:277-286.

Douglas, G. S., Bence, A. E., Prince, R. C., McMillen, S. J., Butler, E. L., 1996. Environmental stability of selected petroleum hydrocarbon source and weathering ratios. Environ. Sci. Technol., 30:2332-2339.

Fathalla., E. M., 2011. Products of Polycyclic Aromatic Sulfur Heterocycles in Oil Spill Photodegradation. Environ. Toxicol. Chem., 30:2004 - 2012.

Griffiths, M. T., Da Campo, R., O'Connor, P. B., Barrow, M. P., 2014. Throwing light on petroleum : simulated exposure of crude oil to sunlight and

characterization using atmospheric pressure photoionization fourier transform ion cyclotron resonance mass spectrometry. Anal. Chem., 86:527-534.

Gunster, D. G., Gillis, C. A.; Bommevie, N. L., Abel, T. B., Wenning, R. J., 1993. Petroleum and hazardous chemical spills in Newark Bay, New Jersey, USA from 1982 to 1991. Environ. Pollut., 82:245-253.

Hawkes, J. A., Patriarca, C., Sjöberg, P. J. R., Tranvik, L. J., Bergquist, J., 2018. Extreme isomeric complexity of dissolved organic matter found across aquatic environments. Limnol. Oceanogr. Lett., 3:21-30.

Headley, J. V., Barrow, M. P., Peru, K. M., Fahlman, B., Frank, R. A., Bickerton, G., McMaster, M. E., Parrott, J., Hewitt, L. M., 2011. Preliminary fingerprinting of Athabasca oil sands polar organics in environmental samples using electrospray ionization Fourier transform ion cyclotron resonance mass spectrometry. Rapid Commun. Mass Spectrom., 25:1899-1909.

Hegazi, A. H., Fathalla, E. M., Panda, S. K., Schrader, W., Andersson, J. T., 2012. High-molecular weight sulfur-containing aromatics refractory to weathering as determined by Fourier transform ion cyclotron resonance mass spectrometry. Chemosphere, 89:205-212

Hertkorn, N., Frommberger, M., Witt, M., Koch, B. P., Schmitt-Kopplin, P., Perdue, E. M., 2008. Natural organic matter and the event horizon of mass spectrometry. Anal. Chem., 80:8908-8919.

Hourani, N., Andersson, J. T., Möller, I., Amad, M., Witt, M., Sarathy, S. M., 2013. Atmospheric pressure chemical ionization Fourier transform ion cyclotron resonance mass spectrometry for complex thiophenic mixture analysis. Rapid Commun. Mass Spectrom., 27:2432–2438.

Hsu, C., Hendrickson, C., Rodgers, R., McKenna, A., Marshall, A., 2011. Petroleomics: advanced molecular probe for petroleum heavy ends. J. Mass Spectrom., 46:337-343.

Huba, A. K., Huba, K., Gardinali, P. R., 2016. Understanding the atmospheric pressure ionization of petroleum components: The effects of size, structure, and presence of heteroatoms. Sci. Total Environ., 568:1018-1025.

Jertz, R., Friedrich, J., Kriete, C., Nikolaev, E. N., Baykut, G., 2015. Tracking the Magnetron Motion in FT-ICR Mass Spectrometry, J. Am. Soc. Mass Spectrom., 26:1349-1366.

Lalli, P. M., Jarvis, J. M., Marshall, A. G., Rodgers, R. P., 2017. Functional Isomers in Petroleum Emulsion Interfacial Material Revealed by Ion Mobility Mass

Spectrometry and Collision-Induced Dissociation. Energy Fuels, 31:311-318.

Langston, W. J., O'Hara, S., Pope, N. D., Davey, M., Shortridge, E., Imamura, M., Harino, H., Kim, A. W., Vane C. H., 2012. Bioaccumulation surveillance in Milford Haven Waterway. Environ. Monit. Assess., 184:289-311.

Könitzer, S. F., Stephenson, M. H., Davies, J., Vane, C. H., Leng, M. J., 2016. Significance of sedimentary organic matter input for shale gas generation potential of Mississippian Mudstones, Widmerpool Gulf, UK. Rev. Palaeobot. Palynol., 224:146-148.

Marshall, A., Blakney, G., Beu, S., Hendrickson, C., McKenna, A., Purcell, J., Rodgers, R., Xian, F., 2010. Petroleomics: a test bed for ultra-high-resolution Fourier transform ion cyclotron resonance mass spectrometry. Eur. J. Mass Spectrom., 16:367-371.

Marshall, A., Rodgers, R., 2008. Petroleomics: Chemistry of the underworld. Proc. Natl. Acad. Sci. U. S. A., 105:18090-18095.

McLafferty, F. W., Turecek, F., 1993. Interpretation of Mass Spectra. 4 ed.; University Science Books: Mill Valley, CA.

Newell, A. J., Vane, C. H., Sorensen, J. P. R., Moss-Hayes, V., Gooddy, D. C., 2016. Long-term Holocene groundwater fluctuations in a chalk catchment: evidence from Rock-Eval pyrolysis of riparian peats. Hydrol. Processes, 30:4556-4567.

Oros, D. R., Ross, J. R. M., 2004. Polycyclic aromatic hydrocarbons in San Francisco Estuary sediments. Mar. Chem., 86:169-184.

Packer, D. B., 1991 NOAA Technical Memorandum NMFS-NE-167. Assessment of characterisation of salt marshes in the Arthur Kill (New York-New Jersey) replanted after a server oil spill. pp. 232.

Pan, Y., Ridge, D. P., Rockwood, A. L., 1988. Harmonic Signal Enhancement in ion-cyclotron resonance mass-spectrometry using Multiple Electrode Detection. Int. J. Mass Spectrom. Ion Processes, 84:293-304.

Panda, S. K., Schrader, W., al-Hajji, A., Andersson, J. T., 2007. Distribution of Polycyclic Aromatic Sulfur Heterocycles in Three Saudi Arabian Crude Oils as Determined by Fourier Transform Ion Cyclotron Resonance Mass Spectrometry. Energy Fuels, 21: 1071-1077.

Pereira, A. S., Martin, J. W., 2015. Exploring the complexity of oil sands process-affected water by high efficiency supercritical fluid chromatography/orbitrap mass spectrometry. Rapid Commun. Mass Spectrom., 29:735-744.

Pharaoh T. C., Gent, M. A., Hannis, S. D., Kirk, K. L., Monaghan, A. A., Quinn, M. F., Smith, N. J. P., Vane, C. H., Wakefiled, O., Waters, C. N., 2018. An overlooked play? Structure, stratigraphy and hydrocarbon prospectivity of the Carboniferous in the East Irish Sea-North Channel basin complex. Geol. Soc. Spec. Publ., 471.

Purcell, J. M., Hendrickson, C. L., Rodgers, R. P., Marshall, A. G., 2007a. Atmospheric Pressure Photoionization Proton Transfer for Complex Organic Mixtures Investigated by Fourier Transform Ion Cyclotron Resonance Mass Spectrometry. J. Am. Soc. Mass Spectrom., 18:1682-1689.

Purcell, J. M., Juyal, P., Kim, D.-G., Rodgers, R. P., Hendrickson, C. L., Marshall, A. G., 2007b. Sulfur Speciation in Petroleum: Atmospheric Pressure Photoionization or Chemical Derivatization and Electrospray Ionization Fourier Transform Ion Cyclotron Resonance Mass Spectrometry, Energy Fuels, 21:2869-2874.

Purcell, J. M., Rodgers, R. P., Hendrickson, C. L., Marshall, A. G., 2007c. Speciation of Nitrogen Containing Aromatics by Atmospheric Pressure Photoionization or Electrospray Ionization Fourier Transform Ion Cyclotron Resonance Mass Spectrometry. J. Am. Soc. Mass Spectrom., 18:1265-1273.

Richardson, S. D., Ternes, T. A., 2018. Water Analysis: Emerging Contaminants and Current Issues. Anal. Chem., 90:398-428.

Rowland, S. M., Robbins, W. K., Marshall, A. G., Rodgers, R. P., 2014. Characterization of Highly Oxygenated and Environmentally Weathered Crude Oils by Liquid Chromatography Fourier Transform Ion Cyclotron Mass Spectrometry (FT-ICR MS). International Oil Spill Conference Proceedings, 2014:300205.

Schweikhard, L., 1991. Theory of Quadrupole Detection Fourier transform ion cyclotron-resonance. Int. J. Mass Spectrom. Ion Processes, 107:281-292.

Schweikhard, L., Lindinger, M., Kluge, H. J., 1990. Quadrupole-detection FT-ICR mass-spectrometry. Int. J. Mass Spectrom. Ion Processes, 98:25-33.

Schwemer, T., Rüger, C. P., Sklorz, M., Zimmermann, R., 2015. Gas Chromatography Coupled to Atmospheric Pressure Chemical Ionization FT-ICR Mass Spectrometry for Improvement of Data Reliability. Anal. Chem., 87:11957-11961.

Slowakiewicz, M., Tucker, M. E., Vane, C. H., Harding, R., Collins, A., Pancost, R.D., 2015. Shale-gas potential of the mid-Carboniferous Bowland-Hodder unit in the Cleveland Basin (Yorkshire), Central Britain. J. Pet. Geol., 38:59-76.

Tessarolo, N. S., Silva, R. C., Vanini, G., Pinho, A., Romao, W., de Castro, E. V. R., Azevedo, D. A., 2014. Assessing the chemical composition of bio-oils using FT-ICR mass spectrometry and comprehensive two-dimensional gas chromatography with time-of-flight mass spectrometry. Microchem. J., 117:68-76.

Thomas, R. A. P., Morby, A. P., Macaskie, L. E. The biodegradation of tributyl phosphate by naturally occurring microbial isolates. FEMS Microbiol. Lett., 155:155-159.

Vane, C. H., Chenery, S. R., Harrison, I., Kim, A. W., Moss-Hayes, V., Jones, D. G., 2011. Chemical signatures of the Anthropocene in the Clyde Estuary, UK: Sediment hosted Pb, $^{207/206}$Pb, Polyaromatic Hydrocarbon (PAH) and Polychlorinated Biphenyl (PCB) pollution records. Philos. Trans. R. Soc., A, 369:1085-1111

Vane, C. H., Harrison, I., Kim, A. W., 2007. Polycyclic aromatic hydrocarbons (PAHs) and polychlorinated biphenyls (PCBs) in sediments from the Mersey Estuary, U.K. Sci. Total Environ., 374:112-126.

Vane, C. H., Harrison, I., Kim, A. W., Moss-Hayes, V., Vickers, B. P., Hong, K., 2009. Organic and Metal Contamination in Surface Mangrove Sediments of South China. Mar. Pollut. Bull., 58:134-144.

Vane, C. H., Harrison, I., Kim, A. W., Moss-Hayes, V., Vickers, B. P., Horton., B. P., 2008. Status of Organic Pollutants in Surface Sediments of Barnegat Bay-Little Egg Harbor Estuary, New Jersey, USA. Mar. Pollut. Bull., 56:1802-1808.

Vane, C. H., Kim, A. W. McGowan, S., Leng, M. J., Heaton, T. H. E. Coombs, P. Kendrick, C. P., Yang, H., Swann, G. E. A., 2010. Sedimentary record of sewage pollution using faecal marker compounds in contrasting peri-urban shallow lakes. Sci. Total Environ., 409: 345-356.

Vane CH, Kim AW, Moss-Hayes V, Turner G, Mills K, Chenery SR, et al. Organic pollutants, heavy metals and toxicity in oil spill impacted salt marsh sediment cores, Staten Island, New York City, USA. Marine Pollution Bulletin 2020; 151.

Vane, C. H., Moss-Hayes, V., Kim, A. W., Edgley, E., Bearcock, J., 2018. Mercury (Hg), *n*-alkane and unresolved complex mixture (UCM) hydrocarbon pollution in surface sediment across rural-urban-estuarine continuum of the Clyde, UK. Earth Environ. Sci. Trans. R. Soc. Edinburgh (accepted in-press).

Wang, Z., Fingas, M., 1997. Developments in the analysis of petroleum hydrocarbons in oils, petroleum products and oil-spill-related

environmental samples by gas chromatography. J. Chromatogr. A, 774:51-78.

Wang, Z. D., Fingas, M., Blenkinsopp, S., Sergy, G., Landriault, M., Sigouin, L., Foght, J., Semple, K., Westlake, D. W. S., 1998. Comparison of oil composition changes due to biodegradation and physical weathering in different oils. J. Chromatogr. A, 809:89-107.

White, H. K., Xu, L., Hartmann, P., Quinn, J. G., Reddy, C. M., 2013. Unresolved Complex Mixture (UCM) in Coastal Environments Is Derived from Fossil Sources. Environ. Sci. Technol., 47:726-731.

Zubair, A., Pappoe, M., James, L., Hawboldt, K., 2015. Development, optimization, validation and application of faster gas chromatography - flame ionization detector method for the analysis of total petroleum hydrocarbons in contaminated soils. J. Chromatogr. A, 1425:240-248.

8. Conclusions

This research carried out in this thesis: 'Advancing petroleomics methodologies and their application to crude and heavy fuel oils, asphaltenes, and the environment', developed and utilised new experimental and data analysis approaches, and applied them to a range of petrochemical and environmental sample types. In doing so, not only have challenging and novel samples and approaches been explored, but the importance of understanding what is being measured and how through varying experimental procedure has been highlighted.

Proof-of-concept Fourier transform ion cyclotron mass spectrometry (FTICR MS) analysis of marine heavy fuel oils (HFOs) showed that the most detailed compositional profiles could be accessed using atmospheric pressure photoionization (APPI), with electrospray ionization (ESI) better suited to the selective characterisation of highly polar and acidic species in samples with a high total acid number (TAN). Soxhlet extraction afforded optimised prior separation of the asphaltene fraction from HFOs, allowing the observed differences in bulk behaviour and responsiveness to additive chemistries to be better understood. Fragmentation experiments allowed greater structural information to be obtained, while combining novel means of visualization with statistical approaches afforded more rapid identification of compositional features that may underly asphaltene handling issues. Targeting such species may drive improvements in additive chemistries with the eventual development of simpler and more ubiquitous formulations.

Additive packages designed to limited oxidation in lubricant base oils, which is exacerbated in the presence of biodiesel, are also undergoing development. In addition to direct infusion (DI) FTICR MS, hyphenated gas chromatography (GC) analysis of oxidised base oil samples was performed, providing molecular-level, isomeric, and semi-quantitative information. In further studies, analyses of samples taken at earlier and more regular oxidation intervals could allow the disappearance and appearance of individual species to be tracked, such that those that could be targeted to curb oxidative degradation are identified. FTICR MS presents a viable tool to extend industry understanding of oxidation processes at the molecular level, furthering development of lubricant base oil additive packages.

The significant impact of experimental procedure, and the importance of carefully considering what is being measured and how, was demonstrated by studying crude oil in several solvent systems and at a range of flow rates. Sample pH was also found to be a significant factor when FTICR MS was applied to the analysis of oil-sands process affected water (OSPW). High sample injection flow rates and the use of high proton affinity cosolvents were found to attenuate overall signal response and to change the predominant molecular classes observed, and the O_2/O_4 ratio, previously proposed as a potential indicative tool in environmental forensics, was inverted in low pH transfer solvent. Varying experimental parameters demonstrated that their careful selection and control is required for comparing compositional profiles, including those associated with environmental contamination. Such findings are likely to be paralleled more generally across the analytical sciences, and are critical for improved assessment of the toxicity, fate and transport of environmental contaminants, and to make comparisons between data obtained for petroleum-related samples more robust.

Compositional depth profiling of the organic components of soil sampled at a range of depths on Staten Island, New York, complements ongoing studies into the legacy of anthropogenic contamination, including multiple oil spill events. DI-APPI-FTICR MS and GC coupled to atmospheric pressure chemical ionization (APCI) FTICR MS analyses were utilized, with the hyphenated approach allowing the isomeric complexity for unique molecular formulae to be compared between sampling depths. In addition to petroleum-related substances, such as polycyclic aromatic hydrocarbons (PAHs) and sulfur-containing compounds, species that may be linked to spills of industrial chemicals or agricultural effluent were also identified, demonstrating the versatility of petroleomics approaches. Petroleomic characterisation of organic compounds extracted from other environmental matrices, or profiles of substance sampled at a series of time points, could be used to assess the effects of repurposing and remediating contaminated sites.

Advancing petroleomics methodologies and their role as a viable tool in the study of a range of samples are established throughout this thesis, with insight that furthers the interests of industry and analytical and environmental sciences. Findings that aid and accelerate developments in industrially produced additive packages may drive forward wider suitability for marine HFO products, including those which have undergone desulfurization processes to meet modern

environmental regulations, and formulations for lubricant oils that can withstand oxidation imparted more rapidly and extensively by greener biodiesels.

Recently developed quadrupolar (2ω) detection on FTICR instrumentation was used to couple ultra-high-resolution MS to prior GC separation, identifying that tools for streamlined analysis of hyphenated data are vital for the next stage of petroleomics. Furthermore, the use of standard compounds may improve structural characterization, identification, and ultimately quantitation. Such approaches could then be further explored, for instance the use of standard compounds for quantitative characterisation of compounds of concern in contaminated soil, identifying and tracking the reaction of specific molecules in oxidation and ageing studies, and application to understanding the molecular transformation and potential impact of silent spills of lubricant oils in the local environment. Fragmentation of compounds of interest affords structural insight, and a combination of prior isomeric separation, followed by sufficiently narrow precursor isolation and fragmentation, would further such characterization. While databases of known structures, fragmentation patterns, and retention times remain unattainable due to various bulk conditions and presence of multiple matrix interferents, a comprehensive structural characterization combining a streamlined data analysis, interpretation, and visualization approach could eventually be developed. The importance of considering and carefully controlling experimental parameters has been demonstrated in the research presented, and eventual development of standardised methods and approaches may improve the robustness of advanced comparative analytical studies.